Regulation of mTOR signaling by amino acids and Rapamycin-FKBP complexes

Inaugural-Dissertation

zur

Erlangung des Doktorgrades

der Mathematisch-Naturwissenschaftlichen Fakultät

der Universität zu Köln

vorgelegt von

Nina Grützmacher

aus Villingen-Schwenningen

Köln, 2023

Berichterstatter (Gutachter):	Dr. Constantinos Demetriades Prof Dr. Jan Riemer
Vorsitzender der Prüfungskommission:	Prof. Dr. Marius Lemberg
Tag der mündlichen Prüfung:	21.09.2023

I've been here so long, I think that it's time to move

The winter's so cold, summer's over too soon

So let's pack our bags and settle down where palm trees grow.

- Rise Against (Swing Life Away)

Index

Abstract

The mechanistic target of Rapamycin (mTOR) serves as the central regulator of cell growth and metabolism, operating through two distinct complexes, mTORC1 and mTORC2. Abnormal mTORC1 activity is a common feature in various diseases including cancer, metabolic disorders, neurodegenerative conditions, as well as ageing. Therefore, it is crucial to understand the regulatory mechanisms of mTORC1 activity. In this work, I focused on elucidating the regulation of mTORC1 by amino acids as well as the small compound Rapamycin in complex with FKBPs.

Amino acids play a dominant role in the regulation of mTORC1 activity and recent discoveries revealed an amino acid sensing machinery centered around the Rag GTPases. Although mammalian cells express four different Rags, *RRAGA-D*, the Rag paralogs were considered functionally redundant until recently. Furthermore, Rapamycin, a naturally-occuring mTOR inhibitor, selectively targets mTORC1 by forming a tertiary complex with the small immunophilin FKBP12. However, potential mTOR-independent effects of Rapamycin prompted further investigation.

In the context of my PhD work, I demonstrated that there are indeed functional differences between RagA and RagB as well as RagC and RagD. Whereas RagA/B determines the response to amino acid depletion, RagC/D determines substrate specificity downstream of mTORC1. Moreover, I showed that Rapamycin selectively inhibits mTORC1 and that all observed effects can be attributed to mTOR inhibition. My data indicate that Rapamycin-treatment minimally alters the interactome of FKBPs, confirming its specificity towards mTOR. Additionally, I discovered a novel FKBP-interacting protein called PRR14L which may function as a transcriptional regulator with implications in cancer and vesicle exocytosis.

Collectively, my findings offer valuable insights into the regulation of mTORC1 by amino acids and the specificity of Rapamycin towards mTOR inhibition. A comprehensive understanding of mTOR regulation holds immense promise in advancing our knowledge about cellular physiology and provides a foundation for the development of innovative therapeutic strategies.

Abbreviations

General

ATP	adenosine triphosphate
CaM	calmodulin-binding
CASTOR1	cellular arginine sensor for mTORC1
CLEAR	coordinated lysosomal expression and regulation
ER	endoplasmic reticulum
FAT	Frap, ATM, TRRAP
FATC	C-terminal Frap, ATM, TRRAP
FRB	FKBP12-Rapamycin binding
GAP	GTPase activating protein
GATOR1	GAP activity towards the Rags 1
GATOR2	GAP activity towards the Rags 2
GEF	GTP exchange factors
HEAT	Huntington, EF3A, ATM, mTOR
HPA	hypothalamic-pituitary-adrenal
KI	kinase inhibitor
LAMTOR	late endosomal/lysosomal adaptor and MAPK and mTOR activator
mTORC1	mechanistic target of Rapamycin complex 1
mTORC2	mechanistic target of Rapamycin complex 2
PPIase	peptidyl-proline isomerase
PROTOR	protein associated with rictor
PTSD	post-traumatic stress disorder
RCC	renal cancer carcinoma
SAM	*S*-adenosylmethionine
SAMTOR	*S*-adenosylmethionine sensor upstream of mTORC1
TPR	tetratricopeptide repeat
TSC	tuberous sclerosis complex
TOS	TOR signaling

Protein names

4E-BP1	eIF4E Binding Protein 1
AMPK	AMP-activated protein kinase
ATF4	Activating Transcription Factor 4
ATG13	autophagy-related protein 13
ATG101	autophagy-related protein 101
Bcl-2	B-cell lymphoma 2
CAD	carbamoyl-phosphate synthetase
DEPDC5	DEP domain containing 5
DEPTOR	DEP domain containing mTOR-interacting protein
ERK	extracellular signal-regulated kinase

FIP200	200-kDa FAK family kinase-interacting protein
FKBP	FK506-binding protein
FLCN	folliculin
GR	glucocorticoid receptor
Hsp90	heat shock protein 90
IP3R	inositol 1,4,5 triphosphate receptor
LRS	leucyl-tRNA synthetase
mLST8	mammalian lethal with sec13
mSIN1	mammalian stress-activated protein kinase-interacting protein 1
MTHFD2	methylenetetrahydrofolate dehydrogenase 2
mTOR	mechanistic target of Rapamycin
NFAT	nuclear factor of activated cells
PDK1	3-phosphoinositide-dependent protein kinase 1
PI3K	phosphatidylinositol-3 kinase
PIKK	phosphatidylinositol-3 kinases-related kinase
PKB	protein kinase B
PRAS40	proline-rich Akt substrate of 40 kDa
RAPTOR	regulatory-associated protein of mTOR
RAS	rat sarcoma
REDD1	regulated in DNA damage and development 1
Rheb	ras homolog enriched in brain
RICTOR	raptor-independent companion of mTOR
RyR	ryanodine receptor
S6K1	p70 S6 Kinase 1
SLC38A9	solute carrier family 38 member 9
SREBP	sterol responsive element binding protein
TARS2	threonyl-tRNA synthetase
TFE3	transcription factor E3
TFEB	transcription factor EB
TGFβR1	type 1 receptors for TGF-β
TGFβR2	type 2 receptors for TGF-β
TOR	target of Rapamycin
ULK1	Unc-51 like autophagy activating kinase

List of Figures

1. General Introduction

1.1 mTORC1 is a central regulator of cell growth

Cells possess the capacity to detect the nutritional state of their environment and to synchronize effectively their growth with the availability of nutrients. Only when enough nutrients are present, do cells trigger the activation of growth and proliferation. The central hub for cell growth in mammals is mTOR (mechanistic target of Rapamycin), a highly conserved 289-kDa serine/threonine protein kinase that belongs to the PIKK (phosphatidylinositol-3 kinases-related kinase) family. It consists of an N-terminal as well as a middle HEAT (Huntington, EF3A, ATM, mTOR) repeat region, followed by a FAT (Frap, ATM, TRRAP) domain. HEAT repeats mediate protein-protein interactions (Grove *et al.*, 2008) while the FAT domain possibly serves as a scaffold or protein interaction domain (Bosotti *et al.*, 2000). Furthermore, mTOR contains an FRB (FKBP12-Rapamycin binding) domain, the catalytic kinase domain, and a FATC (C-terminal FAT) domain. mTOR controls cell growth and proliferation by integrating a diverse set of extra- and intracellular signals and upon activation triggers the promotion of anabolic processes while suppressing catabolism.

1.1.1 mTOR forms two distinct complexes

While yeast expresses two different *TOR* genes (Heitman *et al.*, 1991), higher eukaryotes, including mammals, possess only one *MTOR* gene but the resulting protein itself can be incorporated into two functionally and structurally distinct complexes: mTORC1 (mTOR complex 1) and mTORC2 (mTOR complex 2). A substantial milestone in deciphering the molecular architecture of both complexes was the discovery of RAPTOR (regulatory-associated protein of mTOR), a core component of mTORC1 (Kim *et al.*, 2002). RAPTOR is responsible for substrate recruitment towards mTORC1 by binding to a specific TOS (TOR signaling) motif present in the respective substrates (Nojima *et al.*, 2003). Besides RAPTOR, mLST8 (mammalian lethal with sec13 protein 8), DEPTOR (DEP domain containing mTOR-interacting protein), and PRAS40 (proline-rich Akt substrate of 40 kDa) bind to mTOR to form mTORC1 (Saxton and Sabatini, 2017). While mLST8 is suggested to stabilize the kinase domain (Yang *et al.*, 2013), PRAS40, as well as DEPTOR, are endogenous inhibitors of mTORC1 (Sancak *et al.*, 2007; Peterson *et al.*, 2009).

On the other hand, the identification of RICTOR (raptor-independent companion of mTOR) and mSIN1 (mammalian stress-activated protein kinase-interacting protein) affirmed the existence of mTORC2 (Sarbassov *et al.*, 2004; Wullschleger *et al.*, 2005). RICTOR acts as a scaffold protein while mSIN1 itself is important for the RICTOR-mTOR interaction and regulates AKT phosphorylation (Jacinto *et al.*, 2006). In addition to RICTOR and mSIN1, mTORC2 also contains mLST8, DEPTOR, and PROTOR1/2 (protein associated with rictor 1 or 2) (Wullschleger *et al.*, 2005). While mTORC1 is responsible for the regulation of cell growth and metabolism via the coordination of translation, transcription, and autophagy (Schmelzle and Hall, 2000), mTORC2 is responsible for the organization of the actin cytoskeleton and cell survival (Jacinto *et al.*, 2004; Sarbassov *et al.*, 2005).

1.1.2 mTORC1 pathway in disease and ageing

Aberrant mTORC1 activity is the underlying cause of many age-related diseases including cancer and neurodevelopmental disorders. In up to 80% of human cancers, mTOR signaling was shown to be hyperactive (Menon and Manning, 2008). Although mTOR itself is rarely mutated, mutations in other key regulators of the mTOR pathway were reported to cause abnormal cell growth. For example, RagC mutations can lead to follicular lymphoma (Okosun *et al.*, 2016) whereas mutations in FLCN (Folliculin) cause Birt-Hogg-Dubé syndrome (Nickerson *et al.*, 2002). Moreover, mutations in all three components of the GATOR1 (GAP activity towards the Rags 1) complex have been identified in glioblastomas (Bar-Peled *et al.*, 2013). Dysregulation of the mTORC1 pathway has also been implicated in several neurodevelopmental disorders. The best-studied case is TSC (tuberous sclerosis complex). Mutations in either TSC1 or TSC2 lead to constitutively active mTORC1 with patients showing growth of lesions that disrupt the laminar organization of the cortex resulting in epileptogenic foci (Hunold *et al.*, 2014). Moreover, several mTOR inhibitors are currently in clinical trials as anti-epileptic agents for the treatment of epilepsy and mTORopathies that are directly connected to mutations in the mTOR signaling pathway (Brandt *et al.*, 2018).

With a growing body of genetic and pharmacological evidence, mTORC1 activity is now widely accepted as a major driver of ageing (Weichhart, 2017). Inhibition of the mTORC1 pathway extends lifespan in various model organisms including yeast (Kaeberlein *et al.* 2005), nematodes (Vellai *et al.*, 2003), flies (Kapahi *et al.*, 2004), and mammals (Wu *et al.*, 2013).

Although slowing down ageing and potentially extending lifespan by chronic inhibition of mTORC1 activity can be advantageous, it is crucial to recognize potential side effects. In patients undergoing cancer therapy or organ transplantation, administration of regular doses of mTORC1 inhibitors led to the development of insulin resistance and immunosuppression (Yang *et al.*, 2012). However, it should be noted that these patients received intense, high-dose regimens, and far lower doses are likely required for anti-ageing benefits, based on what is known from studies in model organisms.

1.1.3 Several cues converge on mTORC1 to regulate cell growth and metabolism

Cell growth and subsequent cell proliferation can occur by promoting the synthesis of proteins, lipids, and nucleotides while at the same time suppressing catabolic processes such as autophagy and lysosomal biogenesis. mTORC1 plays a crucial role in all of these pathways making it a central hub for cell growth and metabolism. When external conditions are favorable for cell growth, mTORC1 is active and phosphorylates its downstream targets. Protein synthesis is mainly induced by the phosphorylation of S6K1 (p70S6 Kinase 1) and 4E-BP1 (eIF4E Binding Protein 1). While phosphorylation of S6K1 leads to its subsequent activation by PDK1 (3-phosphoinositide-dependent protein kinase 1) and further initiation of mRNA translation (Holz *et al.*, 2005), 4E-BP1 phosphorylation releases its inhibitory effect on eIF4E which subsequently allows 5' cap-dependent mRNA translation to occur (Brunn *et al.*, 1997).

Besides protein synthesis, growing cells also need sufficient lipids to form new membranes as well as nucleotides for DNA replication and ribosome biogenesis. mTORC1 induces lipid synthesis through SREBP1/2 (sterol regulatory element binding proteins 1 and 2) (Porstmann *et al.*, 2008). SREBPs are activated at the Golgi and translocate to the nucleus where they bind to sterol regulatory elements to induce gene expression involved in cholesterol and fatty acid biosynthesis (Rawson, 2003). Nucleotide synthesis is promoted by increasing ATF4-dependent expression of MTHFD2 (Ben-Sahra *et al.*, 2016) as well as regulating the direct mTORC1-downstream target S6K1 which in turn phosphorylates CAD (carbamoyl-phosphate synthetase) (Ben-Sahra *et al.*, 2013). CAD then catalyzes the first three steps of *de novo* pyrimidine synthesis leading to nucleotide synthesis.

Active mTORC1 does not only promote anabolic processes but also suppresses protein catabolism by inhibiting autophagy and lysosomal biogenesis. ULK1 (Unc-51 like autophagy activating kinase), a kinase that forms a complex with ATG13 (autophagy-related protein 13),

FIP200 (200-kDa FAK family kinase-interacting protein) and ATG101 (autophagy-related protein 101), is phosphorylated by mTORC1 in nutrient replete conditions which blocks its activating phosphorylation by AMPK (AMP-activated protein kinase) that is necessary for induction of autophagy (Kim *et al.*, 2011). Moreover, mTORC1 also phosphorylates and inhibits the nuclear relocalization of the MiTF/TFE transcription factors TFEB (transcription factor EB) and TFE3 (transcription factor E3) (Martina *et al.*, 2012). TFEB and TFE3 drive the expression of genes for the autophagy machinery and lysosomal biogenesis through the activation of the CLEAR (coordinated lysosomal expression and regulation) network of target genes (Martina *et al.*, 2014).

Various signaling cues including amino acids, growth factors, oxygen, and energy converge on mTORC1 to promote cell growth. Only if all of these conditions are favorable for cell growth, mTORC1 can be activated and phosphorylates its downstream targets. Amino acids are sensed through the heterodimeric Rag GTPases (Rag guanosine triphosphates) that are tethered to the lysosomal surface via the LAMTOR (also known as Ragulator) complex (Sancak *et al.*, 2008; Sancak *et al.*, 2010). LAMTOR is a pentameric late endosomal/lysosomal scaffold complex comprised of LAMTOR1 (p18; Nada *et al.*, 2009), LAMTOR2 (p14; Wunderlich *et al.*, 2001), LAMTOR3 (MP1; Schaeffer *et al.*, 1998), LAMTOR4 (C7orf59) and LAMTOR5 (HBXIP; Bar-Peled *et al.*, 2012). On the other hand, growth factors signal through the heterotrimeric TSC complex that consists of TSC1, TSC2, and TBC1D7 (Dibble *et al.*, 2012). The TSC complex acts as a GAP (GTPase activating protein) for the small GTPase Rheb (Ras homolog enriched in brain) catalyzing the conversion from the active GTP-bound to the inactive GDP-bound state (Inoki *et al.*, 2003).

In addition, intracellular and environmental stresses can affect cell growth such as low ATP levels or hypoxia. Low energy levels as for example during glucose deprivation, can activate AMPK which rapidly redirects metabolism towards increased catabolism and decreased anabolism. AMPK does so by inhibiting mTORC1 either directly through phosphorylation of RAPTOR or indirectly through phosphorylation and activation of TSC2 (Gwinn *et al.*, 2008). Low oxygen levels inhibit mTORC1 in a similar way, partially through AMPK activation but also through the induction of REDD1 (regulated in DNA damage and development 1) (Brugarolas *et al.*, 2004). REDD1 expression is highly induced in response to hypoxia and activates TSC by mediating the dissociation of the inhibitory 14-3-3 from TSC2 (DeYoung *et al.*, 2008).

1.1.4 Amino acids regulate mTORC1 via the Rag GTPases

The regulation of mTORC1 by nutrients is a complex process that is tightly regulated by various players including the small GTPases Rag and Rheb. Among the major nutrients, amino acids play a dominant role in regulating mTORC1 activity. The precise mechanism by which mTORC1 detects amino acids remained unknown until the identification of the Rag-GTPases (Sancak *et al.*, 2008; Kim *et al.*, 2008). Lower organisms including flies, worms, and yeast express one small and one large Rag (RagA and RagC) whereas non-mammal vertebrates (including fish and frogs) express another large Rag (RagD). In mammals, however, four distinct genes express four different Rag proteins (RagA-D) therefore the duplication of each Rag gene implies a more specialized function for each protein. The Rag GTPases form obligate heterodimers consisting of a small Rag, RagA or RagB, and a large Rag, RagC or RagD. To maintain proper functionality, the Rags rely on intersubunit communication to ensure that they are in either of two stable configurations. When activated, RagA/B is GTP- and RagC/D is GDP-loaded, while the opposite configuration occurs when they are in their inactive state (Shen *et al.*, 2017). In their active state, the Rags can interact with RAPTOR mediating the localization of mTORC1 to the lysosomal surface (Sancak *et al.*, 2008) where it is then activated by Rheb. The Rags themselves do not contain a lysosomal membrane-targeting sequence but are bound to lysosomes via the pentameric LAMTOR complex. Besides tethering the Rags to lysosomes, LAMTOR can also function as a GEF (GTP exchange factor) towards RagA/B (Bar-Peled *et al.*, 2012).

Over the past decade, various GAPs and GEFs were identified that affect the GTP/GDP loading state of the Rags and therefore, affect mTORC1 activity (**Figure 1**). The GATOR1 complex is the most direct regulator of the Rags. It catalyzes the hydrolysis of GTP to GDP in RagA/B when amino acid levels are decreasing resulting in mTORC1 inhibition (Shen *et al.*, 2018). GATOR1 itself is regulated indirectly by amino acid sensors such as Sestrin2 and SAR1B for leucine (Wolfson *et al.*, 2016; Chen *et al.*, 2021) and CASTOR1 (cellular arginine sensor for mTORC1) for cytosolic arginine (Saxton *et al.*, 2016). These sensors bind and inhibit GATOR2 which in turn inhibits GATOR1 in the absence of the respective amino acids. In addition to CASTOR1 which senses the cytosolic pool of arginine, a lysosomal arginine sensor was identified (Rebsamen *et al.*, 2015). SLC38A9 is a lysosomal transmembrane protein that can shuttle neutral amino acids out of the lysosomal lumen in an arginine-dependent manner (Wyant *et al.*, 2017).

In addition to GEFs that specifically target RagA/B, several GAPs have also been identified for RagC/D. The FLCN-FNIP2 complex acts as a GAP for RagC/D to sustain mTORC1 activity when amino acids are present (Tsun *et al.*, 2013). In addition, LRS (leucyl-tRNA synthetase) was shown to directly bind RagD and hydrolyze its GTP to GDP thus activating mTORC1 (Han *et al.*, 2012). More recently, TARS2 (threonyl-tRNA synthetase 2) was shown to affect mTORC1 activity. TARS2 binds inactive RagC and induces GTP-loading of RagA in the presence of threonine, thus activating mTORC1 activity (Kim *et al.*, 2021). Additionally, besides sensing amino acids directly, a sensor for the downstream metabolite of methionine metabolism SAM (*S*-adenosylmethionine) called SAMTOR was identified (Gu *et al.*, 2017). SAMTOR binds GATOR1 and inhibits mTORC1 activity in the absence of methionine.

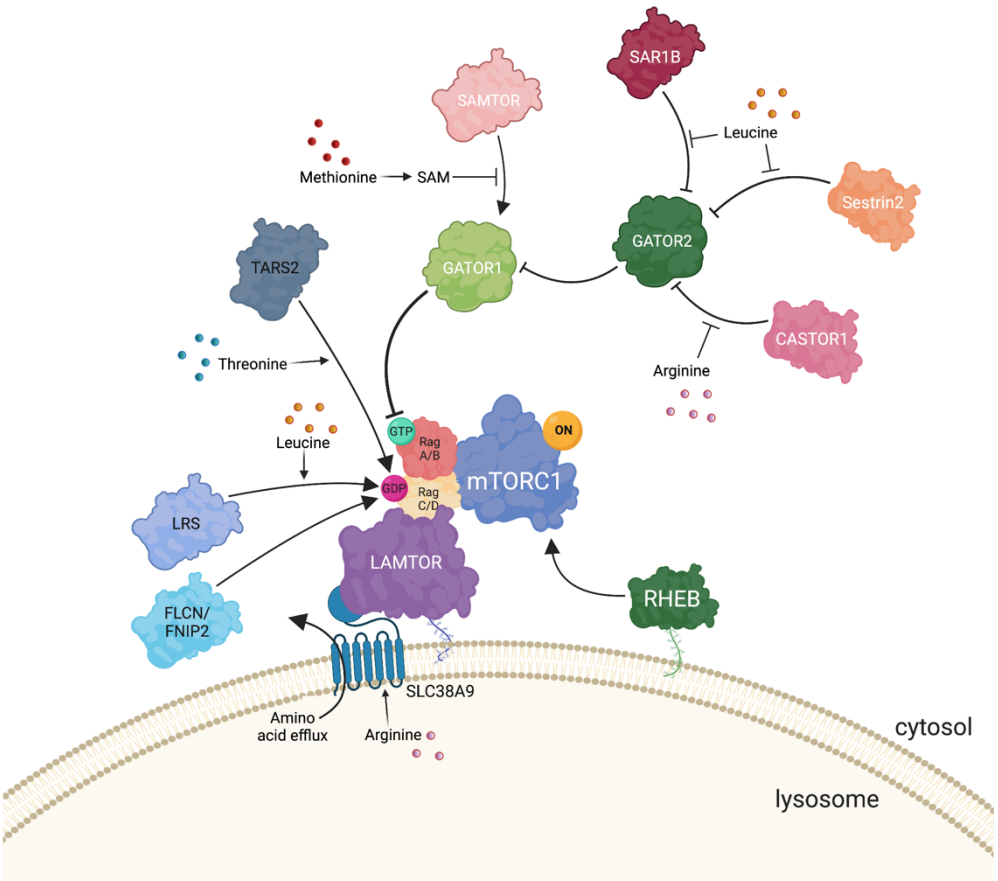

Figure 1. Amino acids regulate mTORC1 activity on the lysosomal surface. The heterodimeric Rag GTPases tether mTORC1 to lysosomes in the presence of amino acids where mTORC1 can be activated by the small GTPase Rheb. The Rags themselves are tethered to the lysosomal surface via the LAMTOR complex. Amino acids are sensed through various upstream sensors that either act on the GATOR complex which is a GEF for RagA/B, or directly act as a GAP for RagC/D. Created with BioRender.com.

1.2 Rapamycin is an allosteric inhibitor of mTORC1

1.2.1 History of Rapamycin

Rapamycin is an antifungal antibiotic that was discovered in the soil of Easter Islands (also known as Rapa Nui) where it is produced by *Streptomyces hygroscopicus*. At first, it was shown that Rapamycin inhibits the proliferation of the yeast *Candida albicans* but did not affect the growth of bacteria (Vézina *et al.*, 1975). Later studies showed that it also confers immunosuppressive properties in mammals (Martel *et al.*, 1977) and since then, it was used as a standard therapy to treat autoimmune disorders as well as to prevent graft rejection in transplant patients (Ingle *et al.*, 2000). However, the most interesting discovery was that Rapamycin also inhibits the growth and proliferation of solid tumors spurring an interest in identifying the mechanism behind it (Eng *et al.*, 1984). The discovery that Rapamycin is able to potently inhibit S6K1 activation (Chung *et al.*, 1992) led to the identification of TOR (target of Rapamycin) in yeast (Heitman *et al.*, 1991). Shortly after, the mammalian homolog mTOR was identified sharing 40% homology with the *Sacharomyces cerevisiae* TOR proteins (Brown *et al.*, 1994; Sabatini *et al.*, 1994) generating the field of mTOR research.

1.2.2 mTOR inhibitors and their use in the clinic

Due to the low solubility and pharmacokinetics of Rapamycin, Rapalogs (Rapamycin analogs) were developed for their application in clinical research (1st generation mTORC1 inhibitors; Figure 2a). Temsirolismus (Punt *et al.*, 2003) and Everolismus (Lebwohl *et al.*, 2013) are two water-soluble Rapalogs that are approved by the FDA (Food and Drug Administration) for the treatment of advanced RCC (renal cancer carcinoma). However, the effects of Rapalogs on major solid cancers were moderate due to negative feedback loops, activating upstream signaling pathways like PI3K-AKT signaling or the RAS-ERK pathway (Carracedo *et al.*, 2008). In addition to Rapamycin and its derivates, that act as allosteric inhibitors on mTOR, ATP-competitive kinase inhibitors (2nd generation mTOR inhibitors; mTOR-KIs) were developed to target the catalytic domain of mTOR (Benjamin *et al.*, 2011). One of the most potent ATP-competitive kinase inhibitors is Torin1 which became an important tool to inhibit both mTORC1 and mTORC2 activity (Liu *et al.*, 2010). Although Rapamycin is yet the most common mTOR inhibitor, only mTORC1 is highly Rapamycin-sensitive whereas mTORC2 is only inhibited by long-term exposure (Sarbassov *et al.*, 2006). Since mutations in the *MTOR* gene can

spontaneously occur rendering the patient insensitive to either Rapalogs or KIs, 3rd generation mTOR inhibitors were developed which are able to overcome drug-resistant mutations in either the FRB or the kinase domain. An example of such an inhibitor is RapaLink, which was developed by the Shokat lab. RapaLink has a Rapamycin-FRB binding element which is linked to a KI that selectively targets and inhibits the kinase domain of mTOR (Rodrik-Outmezguine *et al.*, 2016). This bivalent mTOR inhibitor is expected to suppress mTOR activity in patients with Rapamycin-resistant mutations since the KI binding site simultaneously targets the kinase domain. Similarly, in patients with mutations in the kinase domain, RapaLink is predicted to exhibit comparable potency by binding simultaneously to the FRB domain (Rodrik-Outmezguine *et al.*, 2016).

Besides the extension of lifespan caused by mTORC1 inhibition, Rapamycin was also shown to delay or reverse various age-associated diseases in mice including cognitive decline (Halloran *et al*., 2012), cardiac dysfunction (Flynn *et al*., 2013) and immunosenescence (Chen *et al*., 2009). Given the rapid growth of the ageing population in recent decades, the potential advantages of Rapamycin in addressing ageing and age-related diseases make it a promising tool for treating these conditions in humans and improving their quality of life.

1.2.3 Rapamycin's mode of action

The mechanism of action of Rapamycin was originally revealed in yeast and involves its binding to the immunophilin FKBP12 (FK506-binding protein 12). The formation of a binary gain-of-function complex of Rapamycin with FKBP12 leads to the binding and inhibition of mTORC1 (Sabers *et al.*, 1995, Figure 2b). More precisely, Rapamycin consists of two moieties, the TOR-binding and the FKBP12-binding region. Therefore, the hydrophobic drug can bind to both, the 11-kDa FRB domain of mTOR (Chen *et al*., 1995) as well as the hydrophobic pocket of FKBP12 forming a sandwich-like structure (Choi *et al*., 1996). The FRB domain only exists in TOR proteins explaining the high specificity of Rapamycin. By binding to the FRB domain, the FKBP12-Rapamycin complex inhibits mTORC1 by blocking the access of substrate molecules at the PIKK domain (Zheng *et al*., 1995; Oshiro *et al*., 2004) which is responsible for the kinase activity of TOR proteins (Keith and Schreiber, 1995). Furthermore, Oshiro *et al*. showed that binding of the FKBP12-Rapamycin complex to mTOR inhibits the association of RAPTOR with mTOR leading to decreased mTOR-catalyzed phosphorylation of RAPTOR-dependent substrates whereas mTOR autophosphorylation is not affected (Oshiro *et al*., 2004).

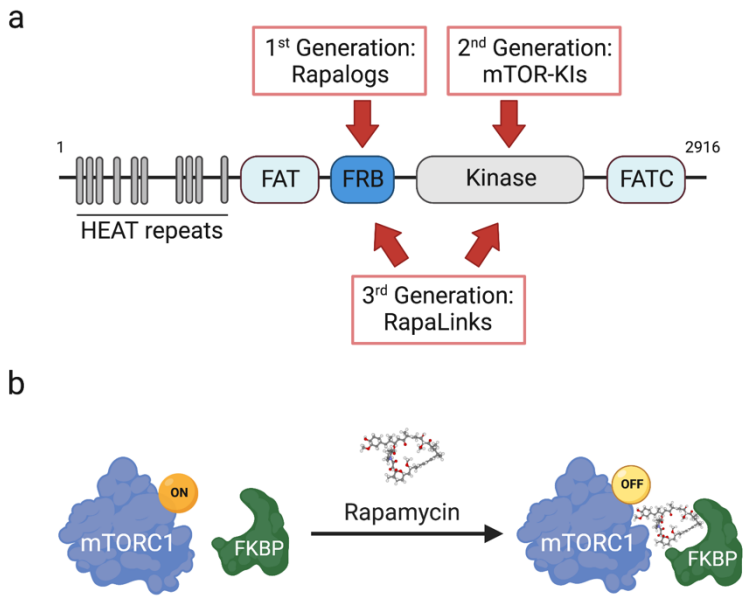

Figure 2. mTOR inhibition by different inhibitor generations (a) Domain structure of mTOR with binding sites of the different depicted mTOR inhibitor classes. (b) The FKBP-Rapamycin complex binds to mTORC1 and inhibits its activity by spatially blocking the access of substrate molecules to the kinase domain of mTOR. Created with BioRender.com.

1.3 FKBPs are immunophilins that bind FK506 and Rapamycin

1.3.1 The FKBP family consists of 15 proteins in humans

FKBPs belong to the large family of immunophilins and are characterized by their ability to bind and mediate the effects of the immunosuppressants FK506 and Rapamycin (Harikishore and Yoon, 2015). Although early experiments in *Saccharomyces cerevisiae* indicated that FKBPs are dispensable for cell viability (Dolinski *et al.*, 1997), an increasing amount of research has been conducted showing that FKBPs play various functional roles in many cellular pathways including protein folding (Wang *et al.*, 2007; Feng *et al.*, 2011), receptor signaling (Wang *et al.*, 1994; Wochnik *et al.*, 2005), apoptosis (Shirane *et al.*, 2003; Wang *et al.*, 2005) and transcription (Erlejman *et al.*, 2014). These diverse functions correlate with the increased number of FKBP family genes in higher organisms. While the yeast *Schizosaccharomyces pombe* has only 3 FKBPs and *E.coli* expresses 4 FKBP-like proteins (Galat, 2000), humans have been found to possess a total of 15 different FKBPs (Bonner and Boulianne, 2017).

The first FKBP identified as a FK506-binding protein was FKBP12 (*Harding et al.*, 1989; Siekierka *et al.*, 1989). It is the smallest member of the family and contains only one functional PPIase domain similar to the highly homologous FKBP12.6 (Arakawa *et al.*, 1994). Larger FKBPs

aquired additional PPIase domains and/or functionally independent motifs such as CaM (calmodulin-binding), Ca^{2+}-binding EF hand, TPR (tetratricopeptide repeat), and DNA binding motifs (Galat, 2013). Similar to the variable domain composition between the different FKBPs, also their subcellular localization can be different (**Figure 3a**). FKBP12 and FKBP12.6 localize to the cytosol whereas FKBP51 and FKBP52 can shuttle between the cytosol and nucleus (Galigniana *et al.*, 2001). Several FKBPs, including FKBP15, 22, 24, 25, 63 and 64, harbor an ER signal peptide, while FKBP38 contains a transmembrane sequence for the localization to mitochondria (Shirane and Nakayama, 2003). The variety in domains and subcellular localization patterns contribute to a wide functional variability among FKBPs, hence making them central players in a diverse range of cellular functions.

1.3.2 FKBPs have a variety of natural targets

Originally, FK506 was identified as the binding partner of FKBP12 (Harding *et al.*, 1989; Siekierka *et al.*, 1989). The binary complex consisting of FKBP12 and FK506 can interact with CaN (calcineurin), a Ca^{2+}-dependent serine/threonine phosphatase (Liu *et al.*, 1991). CaN normally dephosphorylates NFAT (nuclear factor of activated cells) which can then translocate to the nucleus to initiate a transcriptional cascade that ultimately leads to T-cell activation (Jain *et al.*, 1993). By binding of FKBP12-FK506 to CaN, NFAT can not be dephosphorylated and, therefore, resides in the cytosol leading to inhibition of T-cell activation.

However, FKBPs also have a variety of different natural target proteins. The PPIase domain of FKBPs is responsible for cis/trans isomerization of proline residues in proteins (Lang *et al.*, 1987; **Figure 3b**) and, therefore, FKBPs represent important players in protein folding. Furthermore, FKBP12 binds and regulates several receptors including RyR (ryanodine receptor) and IP3R (inositol 1,4,5 triphosphate receptor). Both receptors are responsible for calcium release from the ER or sarcoplasmic reticulum (Jayaraman *et al.*, 1992). The interaction between FKBP12 and the receptor is inhibited by FK506 and thus, removing FKBP12 leads to a leaky channel resulting in the depletion of ER calcium stores and disruption of calcium signaling (Timerman *et al.*, 1993). Moreover, FKBP12 binds directly to TGF-βR1 (type I receptors for TGF-β) blocking the phosphorylation by TGF-βR2 and trapping the receptors in their inactive state (Wang *et al.*, 1994).

Besides FKBP12 and FKBP12.6, which predominantly localize to the cytoplasm, larger FKBPs are able to localize to specific cell organelles. For example, FKBP38 localizes to the mitochondria due to a transmembrane sequence and interacts with the antiapoptotic protein Bcl-2 (Shirane and Nakayama, 2003). By recruiting Bcl-2 to the mitochondrial outer membrane, it can inhibit apoptosis (Choi et al., 2010). This interaction between FKBP38 and Bcl-2 is regulated by Rheb providing a link between nutrient status and apoptotic activity (Ma *et al.*, 2010). Additionally, large FKBPs are important in protein trafficking for example in the nuclear transport of steroid receptors (Wochnik *et al.*, 2005). FKBP52 binds Hsp90 (heat shock protein 90) and interacts with the dynein-dynactin complex to shuttle GR (glucocorticoid receptor) to the nucleus in response to hormone signals (Galigniana *et al.*, 2001). The highly-homologous FKBP51, however, plays an antagonistic role in this process and keeps the steroid receptor in the cytosol when no hormonal cue is present (Davies *et al.*, 2002). Therefore, both FKBPs are important in the interplay of steroid receptor activity and their deregulation can contribute to a variety of hormone-dependent diseases (Zgajnar *et al.*, 2019).

a

protein	localization
FKBP12	cytoplasm
FKBP12.6	
FKBP1C	
FKBP25	cytoplasm/nucleus
FKBP36	cytoplasm/nucleus
FKBP51	cytoplasm/nucleus
FKBP52	cytoplasm/nucleus
FKBP133	
FKBP15	Endoplasmic reticulum
FKBP22	Endoplasmic reticulum
FKBP24	Endoplasmic reticulum
FKBP25	Endoplasmic reticulum
FKBP63	Endoplasmic reticulum
FKBP64	Endoplasmic reticulum
FKBP38	Endoplasmic reticulum/mitochondria

b

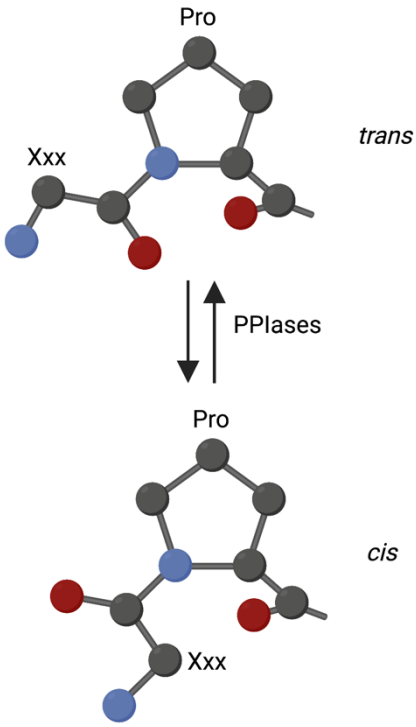

Figure 3. Overview of the human FKBPs. (a) Table of all 15 FKBPs identified in human cells with their respective protein name and subcellular localization. (b) FKBPs exert their PPIase activity towards proline residues in polypeptide chains and, therefore, play an important role in protein folding. Created with BioRender.com.

1.4 Research Aims

Given the numerous implications linked to impaired mTOR signaling and its associated diseases, it is crucial to gain a comprehensive understanding of this signaling pathway. mTORC1 plays a pivotal role in governing a diverse set of downstream targets that regulate a variety of cellular processes. This positioning of mTORC1 as a central hub for cell growth and metabolism underscores its significance. Therefore, the primary objective of this study was to investigate the regulation of the mTOR pathway by amino acids as well as by the small compound Rapamycin which forms a complex with FKBPs. Accordingly, I aimed to answer the two following key questions:

1.4.1 Are the Rag paralogs functionally redundant?

Gene duplication plays a critical role in evolution by providing a source of new genetic material that can lead to the emergence of novel traits and functions. RagA and RagB, referred to as the small Rags, share 90% of amino acid sequence homology. Similarly, the large Rags, RagC and RagD, share around 80% of amino acid sequence homology. This raises the question, whether the four paralogous Rag genes that are expressed in mammalian cells are indeed functionally redundant, or if they have acquired distinct functions throughout evolution. To address this question, I investigated how the different Rag heterodimers influence mTORC1 activity and localization in response to amino acids. By analyzing the differences between the supposedly redundant Rag paralogs, we can increase our understanding of mTORC1 regulation by amino acids, and gain deeper insights into how the lysosomal amino acid sensing machinery functions in cells.

1.4.2 Does Rapamycin exert its anti-proliferative effects only through mTOR?

Rapamycin has been used in a variety of applications in the clinic over the last decades as a specific mTOR inhibitor. Interestingly, however, its specificity and selectivity towards mTOR, although assumed, have not been tested experimentally until recently. In fact, hints in the literature suggest that it could also exert mTOR-independent functions (Goodman *et al.*, 2011). In order to fully characterize the physiological consequences of Rapamycin in cells and to gain a comprehensive understanding of the response mechanism to Rapamycin-treatment, I followed two independent but interconnected approaches:

- First, I generated a cell line that expresses a mutant mTOR protein harboring a point mutation in the FRB domain. In this cell line, Rapamycin is no longer able to bind to mTOR and therefore, any observed effects of Rapamycin-treatment would be due to mTOR-independent mechanisms. The physiological effects of Rapamycin were investigated by two different high-throughput approaches analyzing the cell transcriptome and the whole-cell proteome.
- Second, I analyzed the Rapamycin-dependent changes of the FKBP-interactome. Several FKBPs have been reported to bind Rapamycin and, consequently, inhibit mTORC1 activity. However, Rapamycin might also affect the interaction of FKBPs to additional client proteins. Therefore, an unbiased proteomic approach was performed to assess potential changes in these interactions and to identify potential novel interaction partners of FKBPs that may or may not be involved in mTOR signaling.

2. Results

Chapter 1. A Rag GTPase dimer code defines the regulation of mTORC1 by amino acids

Gollwitzer P*, Grützmacher N*, Wilhelm S, Kümmel D, Demetriades C.

*equal contribution

Published in Nature Cell Biology 24 (2022) 1394-1406. Reprint with submission from Gollwitzer, Grützmacher, *et al.*

Supplementary Material is provided after the publication.

Statement of contribution:

In this publication, I generated the data for most of the western blot experiments including all necessary replicates, and performed some of the cell culture treatments. I also performed the qPCR analysis (Fig 2c), several replicates for co-IP experiments (Fig 3e and 4f) as well as the Lyso-IP experiment (in collaboration with Peter Gollwitzer; Fig 3c). I was also responsible for most of the colocalization analysis of the confocal images and I performed the statistical tests and comparisons for all experiments in this publication. Additionally, I prepared most figure panels (except Fig 1a, 3g, 4a, 4b, 7a, 7f) and generated the final figures with help of Dr. Constantinos Demetriades. Finally, I gave my scientific input to the text that was written by Dr. Constantinos Demetriades.

ARTICLES
https://doi.org/10.1038/s41556-022-00976-y

nature cell biology

OPEN

A Rag GTPase dimer code defines the regulation of mTORC1 by amino acids

Peter Gollwitzer[1,4], Nina Grützmacher[1,4], Sabine Wilhelm[1], Daniel Kümmel[2] and Constantinos Demetriades[1,3] ✉

Amino acid availability controls mTORC1 activity via a heterodimeric Rag GTPase complex that functions as a scaffold at the lysosomal surface, bringing together mTORC1 with its activators and effectors. Mammalian cells express four Rag proteins (RagA–D) that form dimers composed of RagA/B bound to RagC/D. Traditionally, the Rag paralogue pairs (RagA/B and RagC/D) are referred to as functionally redundant, with the four dimer combinations used interchangeably in most studies. Here, by using genetically modified cell lines that express single Rag heterodimers, we uncover a Rag dimer code that determines how amino acids regulate mTORC1. First, RagC/D differentially define the substrate specificity downstream of mTORC1, with RagD promoting phosphorylation of its lysosomal substrates TFEB/TFE3, while both Rags are involved in the phosphorylation of non-lysosomal substrates such as S6K. Mechanistically, RagD recruits mTORC1 more potently to lysosomes through increased affinity to the anchoring LAMTOR complex. Furthermore, RagA/B specify the signalling response to amino acid removal, with RagB-expressing cells maintaining lysosomal and active mTORC1 even upon starvation. Overall, our findings reveal key qualitative differences between Rag paralogues in the regulation of mTORC1, and underscore Rag gene duplication and diversification as a potentially impactful event in mammalian evolution.

Nutrients are the building blocks for cells to grow and proliferate; hence, nutrient sensing mechanisms ensure that cells only grow when all necessary elements are available and conditions are optimal. The main nutrient sensor in cells is mechanistic target of rapamycin complex 1 (mTORC1), which is robustly regulated by amino acid (AA) availability[1–3], and—directly or indirectly—controls virtually all homoeostatic processes, including cell growth, metabolism and secretion[4–9].

A major site for mTORC1 activation is the lysosomal surface, where it is recruited by the heterodimeric Rag (ras-related GTP binding) GTPases, consisting—in mammalian cells—of RagA or RagB ('small' Rags) bound to RagC or RagD ('large' Rags). In AA sufficiency, an 'active' Rag dimer (containing GTP-bound RagA/B and GDP-bound RagC/D) recruits mTORC1 to lysosomes, where it is activated by another small GTPase, Rheb (ras homologue enriched in brain)[10–12]. In turn, active mTORC1 phosphorylates lysosomal (for example, transcription factor EB (TFEB) and transcription factor E3 (TFE3)) and non-lysosomal (for example, ribosomal protein S6 kinase (S6K)) substrates, to regulate various cellular processes such as lysosome biogenesis and protein synthesis[7,9]. In contrast, AA removal leads to inactivation of the Rag dimer and subsequent de-localization of mTORC1 away from lysosomes, which is part of its inactivation process[2,3,12,13]. Therefore, the Rags coordinate the cellular response to AA availability via the regulation of mTORC1 at the lysosomal surface.

Phenomena of gene duplication and divergence have driven evolution since the dawn of life and are generally considered a source of new protein functions[14,15]. Although paralogous genes usually code for proteins with similar structure and function, they often demonstrate specialized activities that contribute to the fine-tuning of key cellular processes[16–19]. Mammalian cells contain four Rag genes, designated *RRAGA–D*. With 90% AA sequence homology, the RagA and RagB proteins are very similar to each other[20], which is also the case for RagC and RagD, which are ~80% identical[11,21,22]. Consequently, the different Rag dimers have so far been used interchangeably to study AA signalling to mTORC1. Moreover, despite the apparent sequence diversification between RagA and RagB, and between RagC and RagD, they are traditionally referred to as functionally redundant and equivalent to each other[23–26]. However, scattered observations in the literature hint at the existence of non-overlapping functions between the Rag paralogues. For instance, we have previously reported that tuberous sclerosis complex 2 (TSC2), a key negative regulator of Rheb and mTORC1, demonstrates strong preference for RagA binding over the other Rags[2]. Another example is leucyl-tRNA synthetase (LARS), an enzyme that binds and regulates RagD—but not RagC—in response to leucine supplementation[27,28].

Driven by such observations, we hypothesized that the different Rags may be functionally divergent, and that the presence of two additional Rag paralogues in mammalian cells may be adding to the complexity of the regulation of mTORC1 by AAs. By using genetically modified cell lines that express only one of the four Rag dimer combinations, we now show that these are qualitatively different. We report two major dissimilarities: (1) whereas RagD-containing dimers are primarily responsible for the lysosomal recruitment and activation of mTORC1 (as seen by TFEB/TFE3 phosphorylation), both RagC and RagD can drive phosphorylation of its non-lysosomal targets (for example, S6K); (2) cells expressing RagA-containing dimers respond to AA withdrawal by robustly inactivating mTORC1, while RagB-containing dimers confer partial resistance to starvation. Furthermore, we provide a mechanistic explanation for the enhanced lysosomal tethering of RagD over RagC, characterize previously described, cancer-associated RagC mutants and identify regions in each Rag paralogue pair that are responsible for these functional differences.

[1]Max Planck Institute for Biology of Ageing (MPI-AGE), Cologne, Germany. [2]Institute of Biochemistry, University of Münster, Münster, Germany. [3]Cologne Excellence Cluster on Cellular Stress Responses in Aging-Associated Diseases (CECAD), University of Cologne, Cologne, Germany. [4]These authors contributed equally: Peter Gollwitzer, Nina Grützmacher. ✉e-mail: Demetriades@age.mpg.de

Results

The RagC and RagD paralogues differentially regulate mTORC1. Although mammalian cells express four Rag proteins (RagA–D) from four distinct genes (*RRAGA*, *RRAGB*, *RRAGC* and *RRAGD*), non-mammal vertebrates (for example, frogs and fishes) lack a second 'small' Rag gene, while lower organisms (for example, flies, worms and yeast) have only one 'small' and one 'large' Rag gene, primarily corresponding to the mammalian RagA and RagC (Fig. 1a). The duplication and sequence diversification of Rag genes in mammals suggest that RagB and RagD may have acquired distinct functions, compared with the ancestral RagA and RagC. Because the Rags function as obligate heterodimers, four possible Rag combinations exist. To investigate whether different Rag dimers have equivalent or diverse functions in the regulation of mTORC1 and AA signalling, we first generated a RagA–D quadruple knock-out (qKO) HEK293FT cell line, using clustered regularly interspaced short palindromic repeats (CRISPR)/Cas9 gene-editing methods (Extended Data Fig. 1a–d). Consistent with the well-known role of the Rags in recruiting mTOR to the lysosomal surface when AAs are abundant[2,9,12,29], two independent Rag qKO clones demonstrated diminished lysosomal mTOR accumulations (Extended Data Fig. 2a,b) and blunted mTORC1 re-activation upon AA re-supplementation, as assessed by phosphorylation of TFEB, TFE3, S6K, 4E-BP1 and ULK1, five direct mTORC1 substrates (Extended Data Fig. 2c).

We then reconstituted Rag expression in the qKO cells by stably re-expressing one Rag dimer at a time, thus generating the RagA/C, RagA/D, RagB/C and RagB/D cell lines, or a luciferase (Luc)-expressing line as a negative control. To assess the qualitative differences between the four Rag dimers, we selected monoclonal lines that show comparable Rag dimer expression (see also 'Stable cell line generation' in Methods), and tested the phosphorylation status of various mTORC1 substrates (Extended Data Fig. 2d). Strikingly, expression of the different Rag dimers differently affected mTORC1 activity towards its substrates in standard growth conditions: although all four dimers were able to restore S6K phosphorylation (albeit with RagA-containing dimers being slightly more potent than RagB-containing dimers), RagD-containing dimers (RagA/D and RagB/D) showed dramatically stronger phosphorylation of TFEB and TFE3 than RagC-containing dimers (Extended Data Fig. 2d). As the Rags are involved in AA signalling to mTORC1, we then tested the responsiveness of the RagA/C- and RagA/D-expressing cells to AA starvation and re-supplementation, using two independent clones each, and observed substantial differences (Fig. 1b–f and Extended Data Fig. 3a–e): RagA/D-expressing cells showed mTORC1 activity towards all substrates, and responded to AA starvation and re-supplementation similarly to wild-type (WT) cells; in contrast, phosphorylation of TFEB/TFE3 was barely detectable in RagA/C-expressing cells, whereas S6K phosphorylation was comparable to that observed in WT and RagA/D cells grown under nutrient-replete conditions.

Considering that TFEB/TFE3 are phosphorylated by active mTORC1 on the lysosomal surface, we reasoned that the observed signalling differences between RagA/C and RagA/D may be due to differential recruitment of mTORC1 to lysosomes. Indeed, we observed significantly stronger lysosomal accumulation of mTOR in RagA/D-expressing cells, whereas RagA/C-reconstituted cells were considerably less capable of rescuing mTOR localization (Fig. 1g,h and Extended Data Fig. 3f,g). Together, these data suggest that the different Rag dimers demonstrate distinct qualities in the regulation of mTORC1 activity and localization, with RagD-containing dimers favouring its lysosomal recruitment and the phosphorylation of its lysosomal substrates.

RagC and RagD differentially regulate lysosomal biogenesis. The TFEB/TFE3 transcription factors regulate lysosome biogenesis and autophagy via controlling gene expression in response to nutrient starvation and mTORC1 inhibition[30–32]. Their subcellular localization is controlled by mTORC1: under nutrient-replete conditions, TFEB/TFE3 are recruited to the lysosomal surface in a Rag-dependent manner[33], where they get phosphorylated by mTORC1, a modification that causes their cytoplasmic sequestration. In contrast, when mTORC1 is inactivated, dephosphorylation of TFEB/TFE3 leads to their re-localization to the nucleus where they promote target gene expression[34–36]. We therefore sought to investigate how TFEB/TFE3 function is influenced by expression of the RagA/C and RagA/D dimers. As expected, endogenous TFE3 showed predominantly nuclear localization in qKO cells, whereas it was mostly cytoplasmic in control cells (Fig. 2a). Consistent with the effects of the two Rag dimers in its phosphorylation, RagA/D expression in qKO cells was able to fully reverse TFE3 localization, whereas RagA/C only partially rescued the nuclear localization phenotype (Fig. 2a,b). The changes in TFE3 localization were further accompanied by changes in the expression of TFEB/TFE3 target genes, such as transmembrane glycoprotein NMB (*GPNMB*) and UDP-*N*-acetylhexosamine pyrophosphorylase-like protein 1 (*UAP1L1*) (refs. [30,37–42]) (Fig. 2c), and in lysosomal biogenesis, as indicated by LysoTracker staining (Fig. 2d,e): while the increases in gene expression and lysosomal signal observed in qKO cells were completely rescued in RagA/D-expressing cells, RagA/C was much less potent (Fig. 2c–e). In sum, the signalling differences between RagC and RagD in the regulation of mTORC1 translate into functional differences in gene expression and lysosome biogenesis in cells.

Enhanced association of RagD with lysosomes via p18/LAMTOR1. We then aimed to investigate the underlying cause for the functional differences between RagC- and RagD-containing dimers. The presence of RagC or RagD did not influence the stability of the Rag heterodimer as both 'large' Rags were equally capable of binding to RagA (Extended Data Fig. 4a), consistent with previous reports[43]. Next, driven by the observation that RagD is more potent than RagC in recruiting mTOR to lysosomes, we reasoned that the localization of these Rags themselves may also differ. Indeed, in co-localization/confocal microscopy experiments, RagD-containing dimers showed significantly stronger lysosomal localization than RagC-containing dimers (Fig. 3a,b). To independently confirm these findings, we developed a biochemical approach, which we named LysoRag IP, that is a modified version of the Lyso-IP method previously established by others[44]. Using the qKO cell lines that stably express haemagglutinin (HA)-tagged RagA/C or RagA/D (or an unrelated protein as control), we performed detergent-free cell lysis and co-immunoprecipitated intact lysosomes under native conditions with HA-tagged Rags as bait. With this method, the amount of lysosomes that is pulled down with the Rags is indicative of the relative affinity of each Rag dimer to the lysosomes. In agreement with our microscopy studies, RagD-containing dimers specifically co-purified more lysosomes, compared with RagC-containing dimers, as indicated by the lysosome-associated membrane glycoprotein 2 (LAMP2) and cathepsin D (CTSD) lysosomal markers (Fig. 3c,d). Accordingly, the lysosomal fraction from RagA/D samples also contained higher levels of mTORC1 components, that is, mTOR and Raptor, albeit the differences to the RagA/C samples were not as dramatic as those for lysosomal markers (Fig. 3c).

As the Rags are only indirectly tethered to the lysosomal surface, via binding to the LAMTOR complex, we then tested if the Rag–LAMTOR interaction is the underlying cause for the increased lysosomal tethering of RagD. Indeed, co-immunoprecipitation (co-IP) experiments with exogenously expressed FLAG-tagged p18/LAMTOR1 (or an unrelated FLAG-tagged protein as control) and HA-tagged RagA/C or RagA/D in qKO cells, showed that RagD bound much more strongly to p18 (Fig. 3e,f).

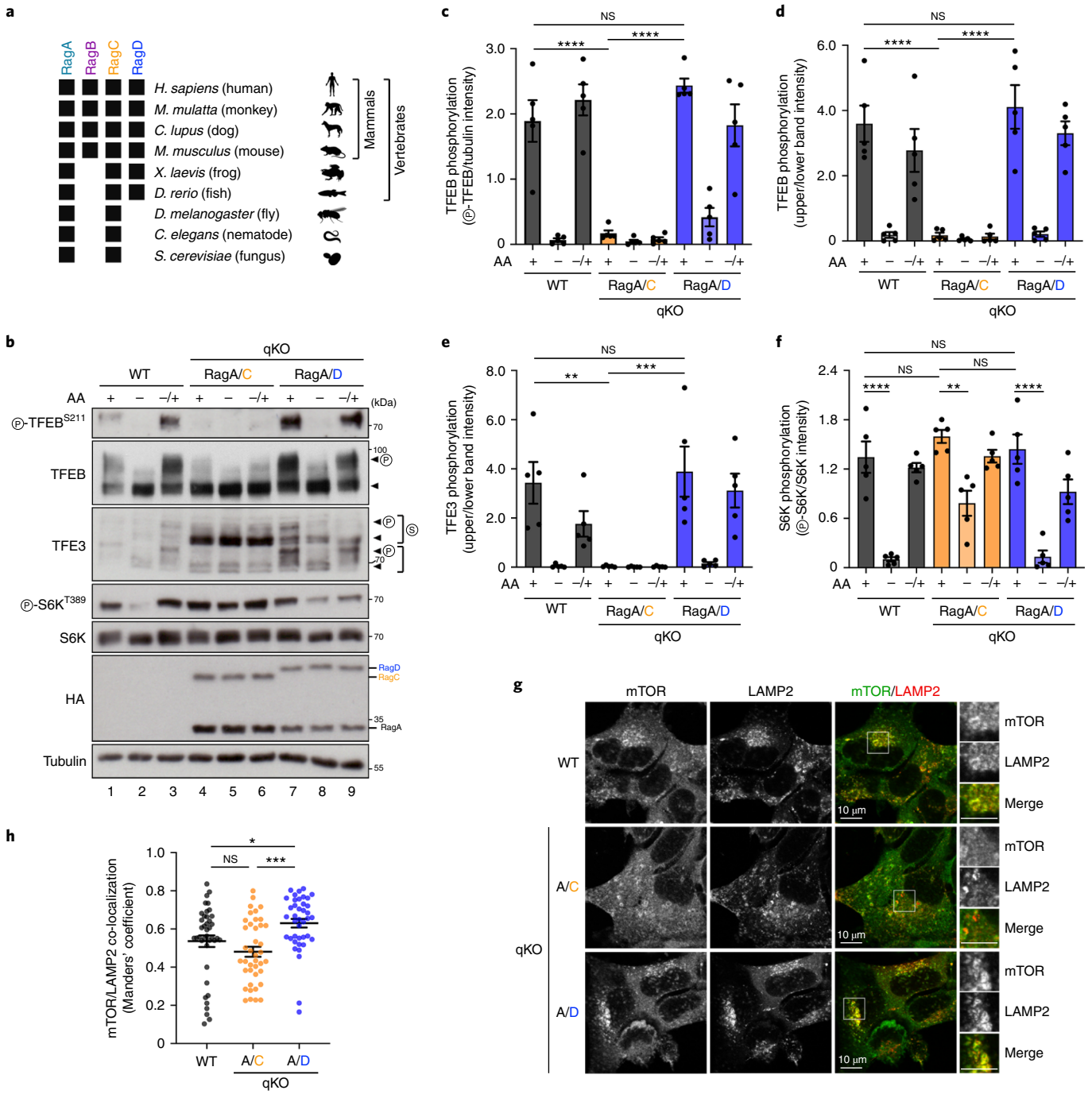

Fig. 1 | The RagC and RagD paralogues differentially regulate mTORC1. a, Schematic representation of the presence (black squares) or absence of the *RagA–D* genes in the genome of the indicated species. **b**, Immunoblots with lysates from HEK293FT WT, or qKO cells stably expressing HA-tagged RagA/C or RagA/D, treated with medium containing (+) or lacking (–) AA, in basal (+), starvation (–) or add-back (–/+) conditions, probed with the indicated antibodies. Arrowheads indicate bands corresponding to different protein forms, when multiple bands are present. P, phosphorylated form; S, SUMOylated form[60]. **c**–**f**, Quantification of TFEB (**c** and **d**), TFE3 (**e**) and S6K (**f**) phosphorylation from **b**. $n = 5$ independent experiments. **g**, Co-localization analysis of mTOR with LAMP2 (lysosomal marker) in HEK293FT WT, or qKO cells stably expressing RagA/C or RagA/D, using confocal microscopy. Magnified insets shown to the right. Scale bars, 10 μm. **h**, Quantification of mTOR/LAMP2 co-localization from $n = 40$ individual cells per condition from a representative experiment out of two independent replicates. Data in graphs shown as mean ± s.e.m. $^*P < 0.05$, $^{**}P < 0.01$, $^{***}P < 0.005$, $^{****}P < 0.001$. Source numerical data and unprocessed blots are available in source data.

consistent with a previous report[28]. Interestingly, their interaction with mTORC1 components (mTOR, Raptor), the lysosomal mTORC1 substrates (TFEB, TFE3) or the upstream RagC/D regulators (FLCN, LARS) was comparable between RagC- and RagD-containing dimers (Extended Data Fig. 4b–f), suggesting that the increased RagD-p18 binding is the primary cause for the enhanced mTORC1 recruitment to lysosomes and the phosphorylation of TFEB/TFE3 (Fig. 3g, right). In contrast, RagC-containing dimers localize less strongly to lysosomes, owing to weaker binding to p18, but are still capable of binding

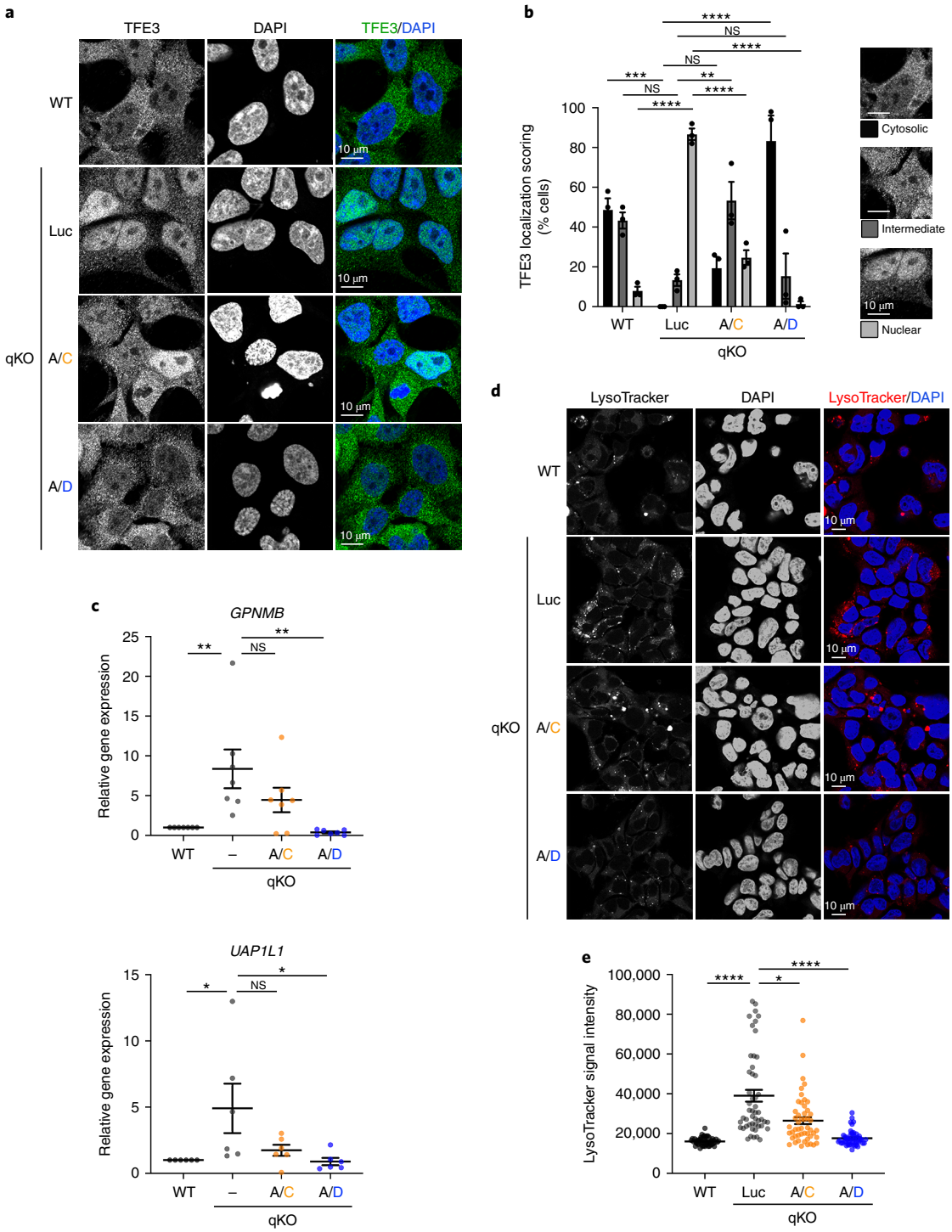

Fig. 2 | RagC and RagD differentially regulate TFE3 localization, target gene expression and lysosomal biogenesis. a, TFE3 localization analysis in HEK293FT WT or qKO cells, stably expressing HA-tagged RagA/C, RagA/D or Luc as a negative control, using confocal microscopy. Nuclei stained with DAPI. Magnified insets shown to the right. Scale bars, 10 μm. $n = 3$ independent experiments. **b**, Scoring of TFE3 localization from **a**. Individual cells were scored for nuclear, intermediate or cytoplasmic TFE3 localization, as indicated in the example images. Scale bars, 10 μm. $n = 3$ independent experiments. **c**, Expression analysis of the TFE3 target genes *GPNMB* and *UAP1L1* in HEK293FT WT, qKO cells or qKOs stably expressing HA-tagged RagA/C or RagA/D. $n_{GPNMB} = 7$ independent experiments; $n_{UAP1L1} = 6$ independent experiments. **d**, LysoTracker staining in HEK293FT WT, qKO cells or qKOs stably expressing HA-tagged RagA/C or RagA/D. **e**, Quantification of LysoTracker signal intensity from $n = 50$ individual cells per condition from a representative experiment out of three independent replicates. Data in graphs shown as mean ± s.e.m. $^*P < 0.05$, $^{**}P < 0.01$, $^{***}P < 0.005$, $^{****}P < 0.001$. Source numerical data are available in source data.

mTORC1 and inducing the phosphorylation of cytoplasmic substrates, such as S6K (Fig. 3g, left). These data favour a model where RagC and RagD are qualitatively different from each other and define substrate specificity downstream of mTORC1, thereby differentially regulating mTORC1 functions such as lysosome biogenesis.

The RagC/D terminal regions define their distinct properties. The RagC and RagD paralogues share ~80% AA sequence identity[21], with the majority of differences between the two proteins localizing to the unstructured N- and C-terminal regions (Extended Data Fig. 5a). To investigate which are the responsible parts for the functional differences between RagC and RagD, we first modelled RagD by introducing substitutions in the RagC structure resolved previously (PDBID: 6S6D)[45]. Of note, this 'core' structure does not include the disordered, variable N- and C-terminal tails of RagC (residues 1–58 and 370–399, respectively). As expected from their AA sequence alignment (Extended Data Fig. 5a), a surface representation of the variable positions between the RagC and RagD cores (as heterodimers with RagA) showed minimal surface residue differences (Extended Data Fig. 5b), none of which localizes at the Rag dimer interface with the LAMTOR complex (PDBID: 6EHP)[46] (Extended Data Fig. 5c). Accordingly, superposition of the core structure of RagC with the respective RagD model showed very high similarity between the two structures (Fig. 4a).

To experimentally test if the N- and C-terminal unstructured tails of RagC and RagD are the cause of their functional differences, we then generated qKO cells stably expressing a 'RagDCD' chimaeric protein, in which the N-terminal 60 AA and the C-terminal 30 AA of RagC were replaced by the respective RagD tails (Fig. 4b). Notably, despite containing the complete core region of RagC, the RagDCD chimaera closely resembled the properties of RagD, showing elevated TFEB/TFE3 phosphorylation (Fig. 4c–e) and enhanced binding to exogenously expressed FLAG-tagged p18 in co-IP experiments (Fig. 4f,g). These structural and biochemical analyses suggest that the differences in the N- and C-terminal RagD regions are responsible for its differential behaviour, compared with RagC.

Cancer-associated RagC mutants upregulate lysosomal mTORC1. Genetic analyses have previously identified activating mutations in *RRAGC* in patients with follicular lymphoma[45,47,48], highlighting the importance of the dysregulation of RagC activity in human disease. Two such mutants, RagC^{T90N} and RagC^{W115R}, were previously described to enhance mTORC1 activity when overexpressed in HEK293T cells (assessed by S6K phosphorylation)[47]. Given that WT RagC shows very weak activation of mTORC1 towards TFEB/TFE3, we wondered if the oncogenicity of these mutants also involves aberrant activation of this pathway. Indeed, compared with RagC^{WT}-expressing cells, qKO cells stably expressing each activating RagC mutant (Fig. 5a) showed strongly elevated TFEB/TFE3—but not S6K—phosphorylation (Fig. 5b–f), accompanied by enhanced lysosomal recruitment of mTOR (Fig. 5g,h), largely resembling the behaviour of RagD. Accordingly, the RagC mutant proteins localized more strongly to lysosomes (Extended Data Fig. 6a,b), probably due to increased affinity to p18 (Extended Data Fig. 6c).

The RagA/B paralogues differently control mTORC1 in starvation. RagB is a mammal-specific paralogue of RagA (Fig. 1a), with the two Rags showing very high AA sequence identity (90%). Our initial analysis of mTORC1 activity in the Rag-dimer-reconstituted qKO lines grown under basal, nutrient-replete culture conditions did not show robust differences between RagA- and RagB-containing dimers (Extended Data Fig. 2d). To investigate if RagB is functionally divergent from RagA under different nutritional conditions, we compared mTORC1 activity in qKO cells stably expressing RagA or RagB in complex with RagD (instead of RagC, to be able to also assess effects on TFEB/TFE3 phosphorylation), cultured under basal, starvation or AA re-addition conditions. These experiments, analysing two independent clones for each Rag combination, revealed that mTORC1 activity in RagA/D-expressing cells responds to AA withdrawal and re-supplementation similarly to WT cells (Figs. 1b and 6a–e and Extended Data Fig. 7a–e). Intriguingly, RagB/D expression caused attenuated response to starvation (Fig. 6a–e and Extended Data Fig. 7a–e), as assessed by phosphorylation of TFEB/TFE3 (Fig. 6a–d and Extended Data Fig. 7a–d) and—to a much lesser extent—S6K (Fig. 6a,e and Extended Data Fig. 7a,e). The incomplete mTORC1 inactivation in RagB/D-expressing cells was also reflected in the lysosomal localization of mTOR: whereas it readily de-localized away from lysosomes upon starvation in WT and RagA/D-expressing cells, RagB/D-expressing cells maintained substantial amounts of lysosomal mTOR (Fig. 6f,g and Extended Data Fig. 7f,g).

Structure–function analysis of RagA/B in AA starvation. The AA sequence differences between the RagA/B paralogues map to two regions: the RagB-specific disordered N-terminal tail, spanning 33 AA; and five AA substitutions in the folded RagA/B 'body' (Fig. 7a and Extended Data Fig. 8a). To look into the structural differences between RagA and RagB that may explain their functional divergence, we used the active RagA/RagC dimer structure (PDBID: 6S6D)[45] and introduced residue substitutions to model the respective RagB/RagD dimer. The few RagA/B differences predicted no structural changes between the RagA structure and the RagB model, both as dimers with RagD (Extended Data Fig. 8b–d). The same was true when comparing the two 'small' Rags in their inactive conformation (based on PDBID: 6ULG) (Extended Data Fig. 8e). Therefore, the structural comparison between RagA and RagB suggests that functional differences are probably encoded by the variable, unstructured N-terminal tail of RagB.

We then generated qKO cell lines, stably expressing RagB mutants that resemble the RagA structural characteristics, either by removing the N-terminal RagB tail ('RagBΔN') or by substituting the five variable residues in the RagB 'body' with those of RagA ('RagB^{AQVHS}'), as HA-tagged proteins (Fig. 7a), together with RagD. Both mutants were described previously[2]. Whereas cells expressing RagBΔN responded to AA starvation similarly to WT or RagA/D-expressing cells, RagB^{AQVHS} expression resembled

Fig. 3 | RagD shows higher affinity to p18 and associates with lysosomes more strongly than RagC. a, Co-localization analysis of stably expressed HA-tagged RagA/C or RagA/D dimers with LAMP2 (lysosomal marker) in HEK293FT qKO cells, using confocal microscopy. Magnified insets shown to the right. Scale bars, 10 µm. **b**, Quantification of HA/LAMP2 co-localization from $n = 40$ individual cells per condition from a representative experiment out of three independent replicates. **c**, LysoRag IP experiments in HEK293FT qKO cells stably expressing HA-tagged RagA/C, RagA/D or Luc as a negative control. Intact lysosomes were immunopurified by HA–Rag IPs under native conditions and the presence of LAMP2, CTSD, mTOR and Raptor proteins in the lysosomal fractions was analysed by immunoblotting. **d**, Quantification of relative Rag–lysosome affinity. $n = 3$ independent experiments. **e**, p18/LAMTOR1 binds more strongly to RagD, compared with RagC. Co-IP experiments in HEK293FT qKO cells, transiently expressing FLAG-tagged p18 or Luc as negative control, and HA-tagged RagA with RagC or RagD. Binding of the Rags to p18 was analysed by immunoblotting. **f**, Quantification of relative Rag-p18 binding. $n = 3$ independent experiments. **g**, Working model for the differential regulation of mTORC1 by RagC- or RagD-containing dimers. RagD-containing dimers show stronger binding to p18/LAMTOR1, lysosomal localization, lysosomal recruitment of mTORC1, and phosphorylation of the TFE3/TFEB mTORC1 substrates. In contrast, RagC-containing dimers bind much less to p18, localize less to lysosomes and are less potent in recruiting mTORC1 to lysosomes to phosphorylate TFE3/TFEB. Both complexes are similarly capable of driving S6K phosphorylation. See main text for details. Created with BioRender.com. Data in graphs shown as mean ± s.e.m. $^{**}P < 0.01$. Source numerical data and unprocessed blots are available in source data.

more closely the partial insensitivity to AA removal observed with full-length, RagB^{WT}-containing dimers, in terms of both mTORC1 activity (Fig. 7b,c) and lysosomal localization (Fig. 7d,e). These data confirm that the RagB-specific N-terminal tail is responsible for the incomplete response of mTORC1 to AA starvation.

In sum, the findings presented here underscore the functional divergence between the RagA and RagB paralogues, with the former responding fully to AA removal to dynamically regulate mTORC1 localization and activity, and the latter retaining lysosomal and active mTORC1 even in starved cells (Fig. 7f).

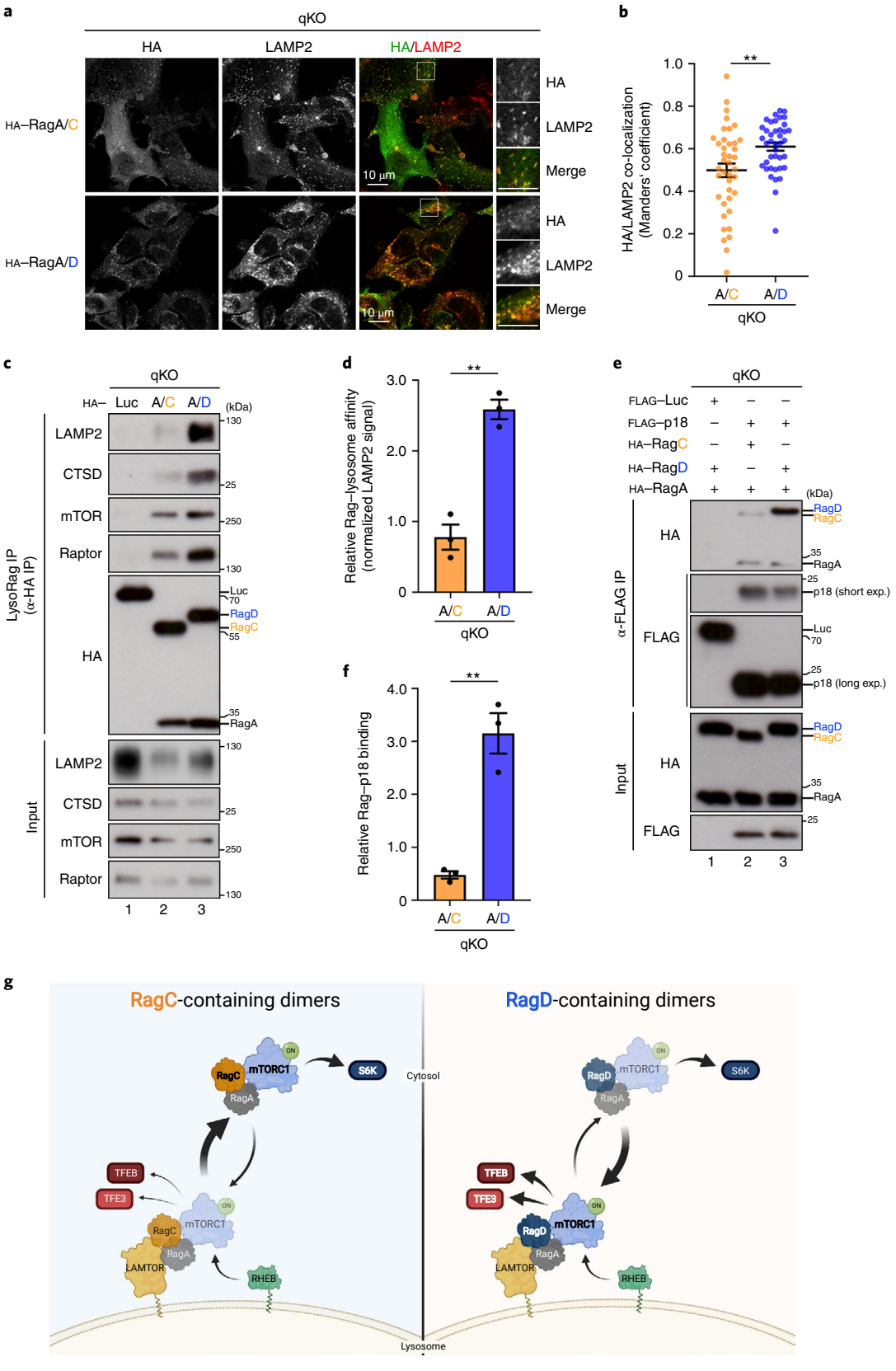

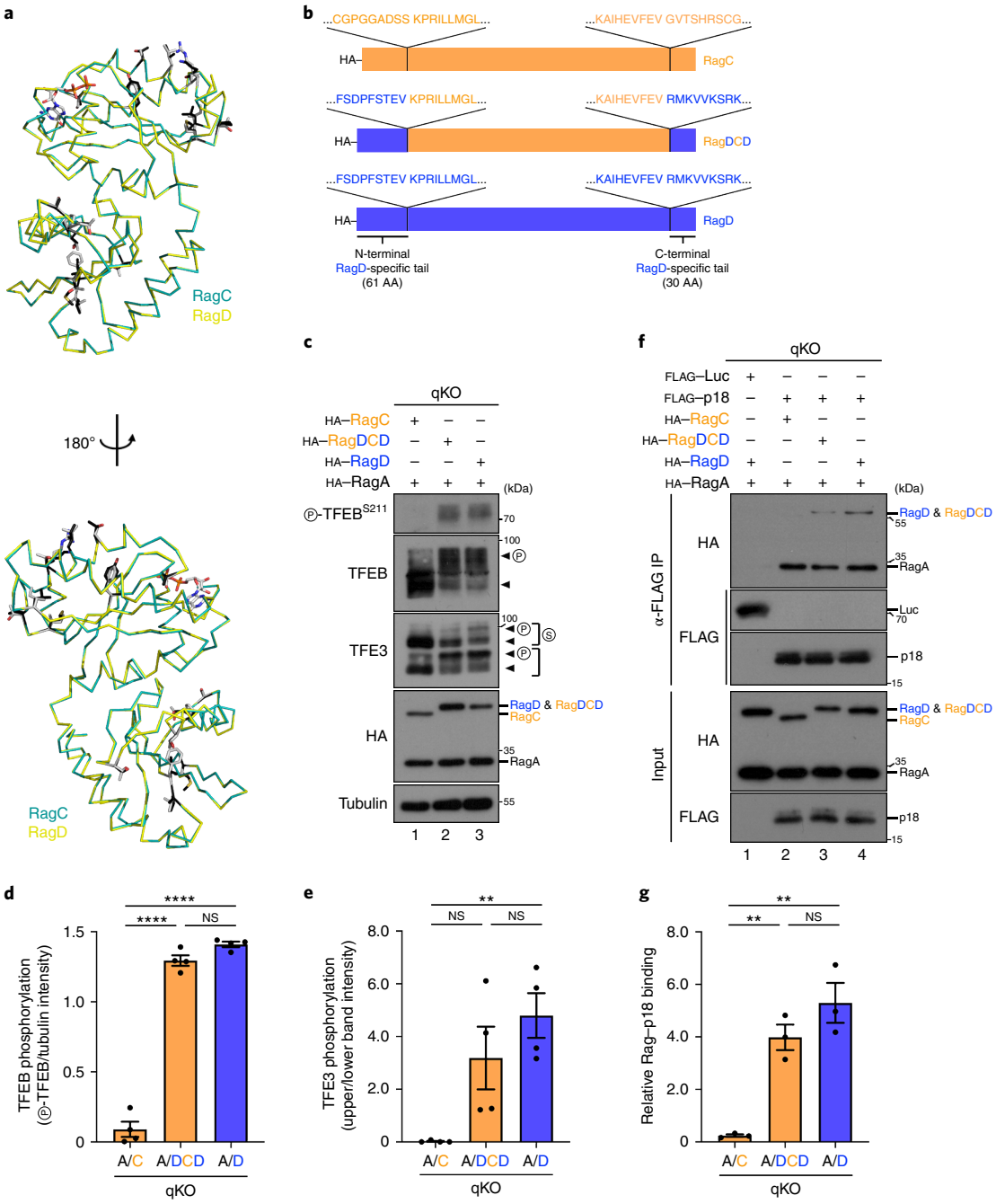

Fig. 4 | Differences in the N- and C-terminal RagD regions are responsible for its differential behaviour, compared with RagC. a, Superposition of the structure of RagC (from PDBID: 6S6D; shown in cyan) with RagD (modelled; shown in yellow) shows high structural similarity between the two structures. Side chains of variable positions shown as dark grey (RagC) or light grey (RagD) sticks. **b**, Schematic representation of HA-tagged RagC, RagD and the RagDCD chimaera, in which the N- and C-terminal tails of RagC were replaced with those of RagD. The AA sequences around the fusion points are shown as insets. **c**, Immunoblots with lysates from HEK293FT qKO cells stably expressing HA-tagged RagA with RagC, RagD or the RagDCD chimaera, probed with the indicated antibodies. Arrowheads indicate bands corresponding to different protein forms, when multiple bands are present. P, phosphorylated form; S, SUMOylated form. **d**,**e**, Quantification of TFEB (**d**) and TFE3 (**e**) phosphorylation. $n = 4$ independent experiments. **f**, Co-IP experiments in HEK293FT qKO cells transiently expressing FLAG-tagged p18 or Luc as control, and HA-tagged RagA with RagC, RagD or the RagDCD chimaera. Binding of p18 to the Rags was analysed by immunoblotting. **g**, Quantification of relative Rag-p18 binding. $n = 3$ independent experiments. Data in graphs shown as mean ± s.e.m. $^{**}P < 0.01$, $^{****}P < 0.001$. Source numerical data and unprocessed blots are available in source data.

Discussion

In most studies, the RagA/B and the RagC/D paralogues are referred to as functionally redundant, despite lack of experimental evidence that supports this statement. On the contrary, several hints in the literature imply that Rag paralogues may possess gene-specific functions. A recent study identified the mTORC1-mediated phosphorylation of RagC on Ser21 as part of an autoregulatory mechanism that fine-tunes mTORC1 activity towards S6K and 4E-BP1 in response to growth factor and AA signalling[49]. Notably, none of the other Rags was found to be phosphorylated under the same

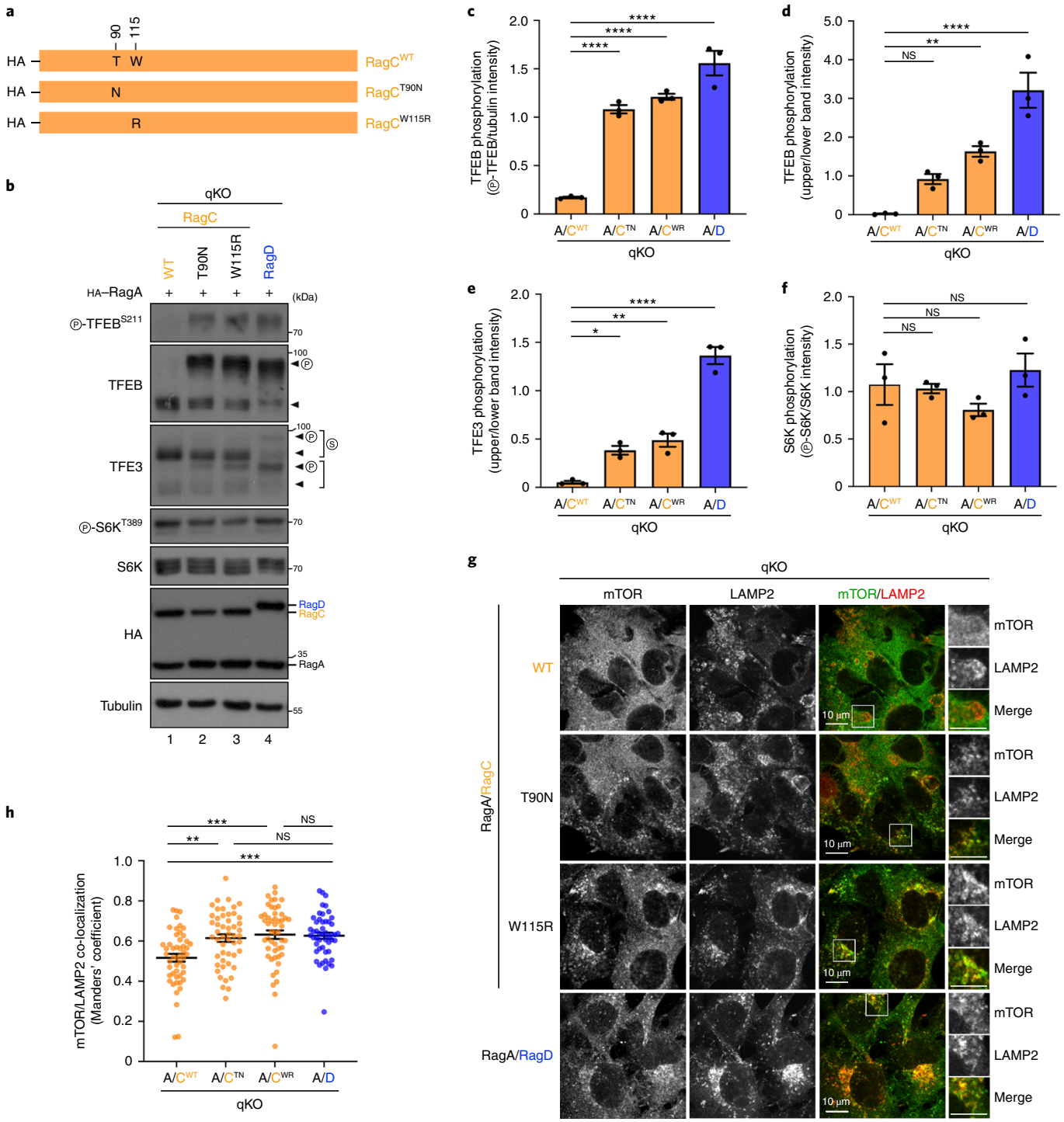

Fig. 5 | Cancer-associated RagC mutations enhance TFE3/TFEB phosphorylation and mTOR lysosomal recruitment. a, Schematic representation of HA-tagged WT RagC and the cancer-related T90N, W115R RagC point mutants. **b**, Immunoblots with lysates from HEK293FT qKO cells stably expressing HA-tagged RagA with WT RagC or RagD, or the T90N, W115R RagC mutants, probed with the indicated antibodies. Arrowheads indicate bands corresponding to different protein forms, when multiple bands are present. P, phosphorylated form; S, SUMOylated form. **c**–**f**, Quantification of TFEB (**c** and **d**), TFE3 (**e**) and S6K (**f**) phosphorylation from **b**. $n = 3$ independent experiments. **g**, Co-localization analysis of mTOR with LAMP2 (lysosomal marker) in HEK293FT qKO cells stably expressing HA-tagged RagA with the RagC proteins shown in **a** or RagD, using confocal microscopy. Magnified insets shown to the right. Scale bars, 10 μm. **h**, Quantification of mTOR/LAMP2 co-localization from $n = 50$ individual cells per condition from a representative experiment out of three independent replicates. Data in graphs shown as mean ± s.e.m. $^*P < 0.05$, $^{**}P < 0.01$, $^{***}P < 0.005$, $^{****}P < 0.001$. Source numerical data and unprocessed blots are available in source data.

conditions[49], and this RagC phospho-residue is not conserved in the N-terminus of RagD, suggesting that RagC may not be a biological equivalent to RagD. As mentioned above, the LARS GTPase-activating protein (GAP) was shown in another study to bind and regulate RagD—but not RagC—despite their high sequence homology[27,28]. Similarly, the lysosomally

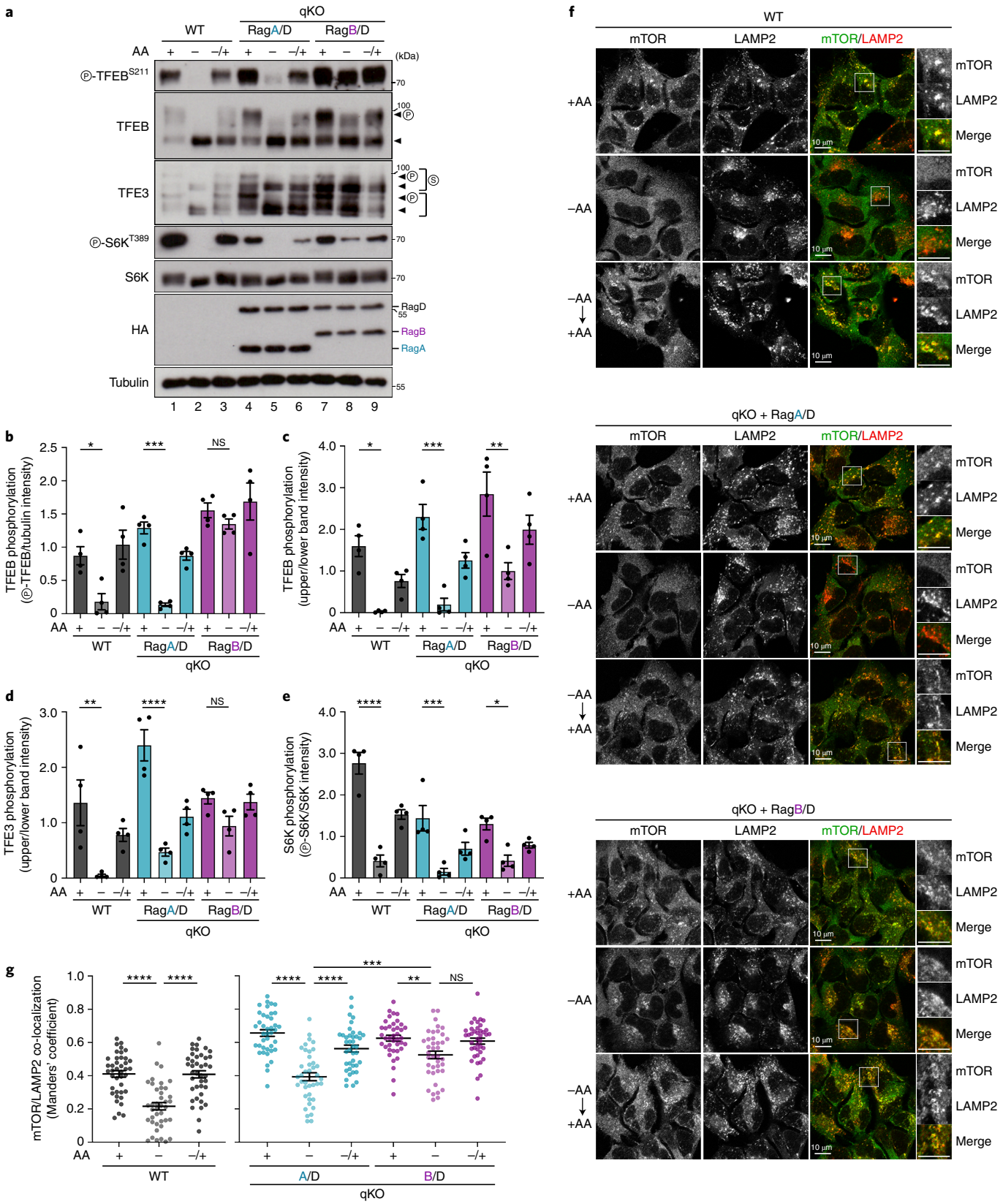

localized GATOR1 complex components nitrogen permease regulator 2-like protein (NPRL2) and NPRL3 preferentially bind to RagD—over RagC—in an AA- and GTP/GDP-loading-dependent manner[50], whereas the mitochondrial threonyl-tRNA synthetase 2 (TARS2) interacts primarily with RagC—but not RagD—in response to threonine availability[51]. Finally, looking into the mechanistic details of the lysosomal recruitment of TSC upon AA starvation, we have previously described strong binding preference of TSC2 to RagA, compared with all other Rags[2]. These experimental observations are in accordance with the classical evolutionary theory of

Fig. 6 | The RagA and RagB paralogues differentially control mTORC1 activity upon AA starvation. a, Immunoblots with lysates from HEK293FT WT, or qKO cells stably expressing RagA/D or RagB/D, treated with medium containing (+) or lacking (–) AA, in basal (+), starvation (–) or add-back (–/+) conditions, probed with the indicated antibodies. Arrowheads indicate bands corresponding to different protein forms, when multiple bands are present. P, phosphorylated form; S, SUMOylated form. **b**–**e**, Quantification of TFEB (**b** and **c**), TFE3 (**d**) and S6K (**e**) phosphorylation from the blots shown in **a**. $n = 4$ independent experiments. **f**, Co-localization analysis of mTOR with LAMP2 (lysosomal marker) in HEK293FT WT or qKO cells stably expressing RagA/D or RagB/D, using confocal microscopy. Magnified insets shown to the right. Scale bars, 10 μm. **g**, Quantification of mTOR/LAMP2 co-localization from $n = 40$ individual cells per condition from a representative experiment out of two independent replicates. Data in graphs shown as mean ± s.e.m. $^{*}P < 0.05$, $^{**}P < 0.01$, $^{***}P < 0.005$, $^{****}P < 0.001$. Source numerical data and unprocessed blots are available in source data.

gene duplication and diversification, based on which paralogous genes often participate in distinct regulatory networks and acquire specialized functions[14,15].

We report here that a Rag dimer code defines the substrate specificity downstream of mTORC1, and its responsiveness to starvation. In particular, RagD appears to be responsible for the regulation of mTORC1 on lysosomes, where it phosphorylates the TFEB/TFE3 transcription factors to control lysosomal biogenesis and autophagy, whereas RagC seems to be more loosely connected to the lysosomal LAMTOR tethering complex and presumably more relevant for the phosphorylation of non-lysosomal mTORC1 substrates like S6K. Although the Rags are traditionally viewed as lysosomal proteins, our data suggest that their relative affinity to lysosomes is variable. Interestingly, early work that identified the LAMTOR–Rag interaction showed that the binding between LAMTOR subunits and a RagA/C dimer is weakened upon AA re-supplementation[23], suggesting that the lysosomal localization of RagC-containing dimers may dynamically respond to AA availability. Indeed, a more recent study revealed that RagC-containing dimers cycle between the lysosomal surface and the cytosol, with nutrients enhancing its re-localization by weakening the association of the Rags with the lysosomally bound LAMTOR complex[43]. Of note, the cancer-related RagC mutants—that we show here increase TFEB phosphorylation and lysosomal localization of mTOR—were also found to stabilize the RagC–LAMTOR association and reduce cycling of a RagB/C dimer[43]. In sum, we here identify RagC/RagD as substrate- and location-specific regulators of mTORC1. The search for ways to selectively modify their activities will probably provide tools to perturb specific pathways downstream of mTORC1, and dissect the relative contribution of these pathways in conditions where mTOR is dysregulated.

According to the publicly available protein and mRNA expression data (summarized in the Human Protein Atlas webpage; www.proteinatlas.org), no tissues that express exclusively RagA or RagB exist, with RagA generally being expressed at higher levels in most tissues. Therefore, RagA- and RagB-containing dimers probably co-exist in cells, where they may differentially regulate how subpopulations of mTORC1 respond to starvation. While the more abundant RagA-containing dimers would ensure a proper inactivation of mTORC1 when AA levels drop, RagB-containing dimers may be responsible for maintaining a baseline mTORC1 activity tone, to support essential physiological processes even upon starvation. Consistent with such a model, AA-starved cells do not completely shut off protein synthesis or gene expression. For instance, mitochondrial protein synthesis has been reported to actually increase upon starvation[52]. Moreover, the ATF4 transcription factor lies downstream of both mTORC1 and GCN2 signalling and upregulates the expression of specific genes as part of the cellular stress/starvation response[53,54]. Finally, autophagosome and lysosome biogenesis, two processes that require massive upregulation of the constituent proteins—many of which are produced in an mTORC1-activity-dependent manner—are also known to be induced in starved cells. Whether mTORC1 complexes that stay active by binding to RagB-containing dimers on lysosomes contribute to such starvation-induced cellular processes will be important to investigate in the future.

At the molecular level, we show that functional differences between RagA versus RagB and RagC versus RagD are encoded by their variable termini. These regions are unstructured and unlikely to directly influence their GTPase cycle. However, they may provide sites for post-translational modifications or interaction motifs for regulatory proteins, as we report here for p18 preferentially binding to RagD. Accordingly, in an accompanying paper, Figlia et al. reveal that RagB isoforms maintain active mTORC1 in starved neurons or various tumours by inhibiting GATOR1, the RagA/B GTPase activating protein complex[55].

In addition to mediating the binding of mTORC1 to the lysosomal surface, the Rag GTPases are also necessary for the recruitment of the TFEB/TFE3 transcription factors to lysosomes, where they are phosphorylated by mTORC1. Consequently, Rag- or LAMTOR-mutant cells have non-phosphorylated and constitutively nuclear TFEB/TFE3 (refs. [32,33,56]). Therefore, the differential behaviour of RagC and RagD towards the regulation of TFEB/TFE3 phosphorylation and localization could be explained by differences in their ability to either recruit and activate the kinase (that is, mTORC1) or function as a lysosomal tether for the substrates (that is, TFEB/TFE3). Our data show that overexpressed RagC- and RagD-containing dimers have similar affinities for TFEB, TFE3, mTOR and Raptor (Extended Data Fig. 4b–f), with the primary difference being the strongly enhanced binding of RagD to p18/LAMTOR1 (Fig. 3e,f), which is the likely cause for their functional divergence.

The TFEB/TFE3 transcription factors are master regulators of a starvation-induced transcriptional programme that controls

Fig. 7 | The RagB-specific N-terminal tail is responsible for its differential effect towards mTORC1 upon AA starvation, compared with RagA. **a**, Schematic representation of HA-tagged WT RagA, WT RagB and the RagBΔN, RagB^{AQVHS} chimaeras. **b**, Immunoblots with lysates from HEK293FT qKO cells stably expressing the proteins shown in **a** as dimers with HA-tagged RagD, probed with the indicated antibodies. Arrowheads indicate bands corresponding to different protein forms, when multiple bands are present. P, phosphorylated form. **c**, Quantification of TFEB phosphorylation. $n = 3$ independent experiments. **d**, Co-localization analysis of mTOR with LAMP2 (lysosomal marker) in HEK293FT qKO cells stably expressing HA-tagged RagBΔN or RagB^{AQVHS} as dimers with RagD, treated with medium containing (+) or lacking (–) AA, using confocal microscopy. Magnified insets shown to the right. Scale bars, 10 μm. **e**, Quantification of mTOR/LAMP2 co-localization from $n = 50$ individual cells per condition from a representative experiment out of three independent replicates. **f**, Working model for the differential regulation of mTORC1 by RagA- or RagB-containing dimers, in basal or AA starvation conditions. Whereas RagA-containing dimers allow for mTORC1 de-localization away from lysosomes and for its inactivation upon AA starvation, RagB-containing dimers retain lysosomal and active mTORC1 even in AA starvation conditions. See main text for details. Created with BioRender.com. Data in graphs shown as mean ± s.e.m. $^{*}P < 0.05$, $^{**}P < 0.01$, $^{***}P < 0.005$, $^{****}P < 0.001$. Source numerical data and unprocessed blots are available in source data.

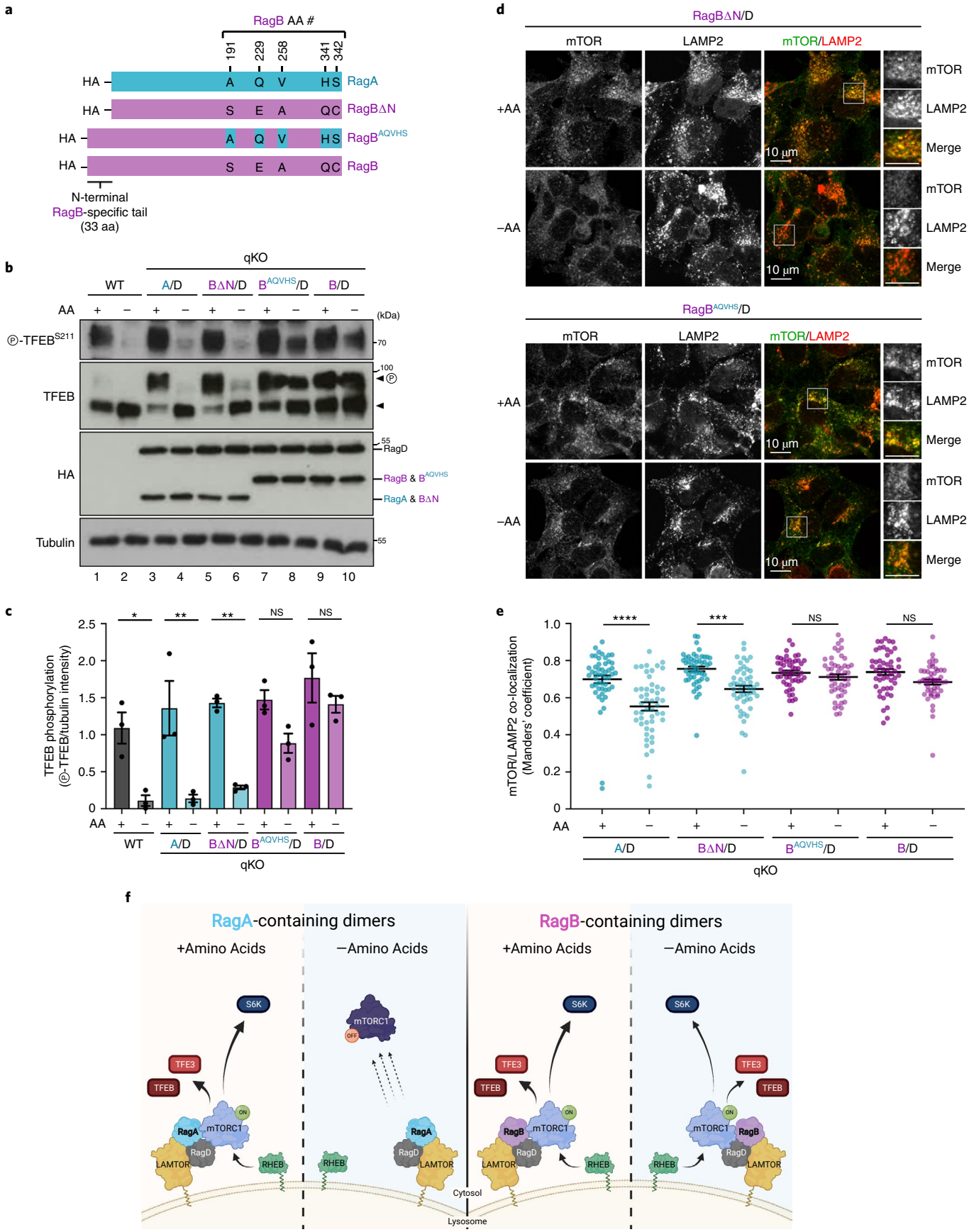
a
RagB AA #
191
229
258
341
342
HA
A Q V H S
RagA
S E A Q C
RagBΔN
RagB^AQVHS
RagB
N-terminal
RagB-specific tail
(33 aa)
b
qKO
WT
A/D
BΔN/D
B^AQVHS/D
B/D
AA
(kDa)
Ⓟ-TFEB^S211
TFEB
HA
Tubulin
70
100
55
RagD
RagB & B^AQVHS
RagA & BΔN
1 2 3 4 5 6 7 8 9 10
c
TFEB phosphorylation
(Ⓟ-TFEB/tubulin intensity)
* ** ** NS NS
WT
A/D
BΔN/D
B^AQVHS/D
B/D
qKO
d
RagBΔN/D
mTOR
LAMP2
mTOR/LAMP2
+AA
–AA
10 μm
Merge
RagB^AQVHS/D
e
mTOR/LAMP2 co-localization
(Manders' coefficient)
**** *** NS NS
f
RagA-containing dimers
RagB-containing dimers
+Amino Acids
–Amino Acids
S6K
TFE3
TFEB
mTORC1
OFF
ON
RagA
RagB
RagD
LAMTOR
RHEB
Cytosol
Lysosome

lysosome biogenesis and autophagy. The importance of this process is underscored by the existence of autoregulatory feedback mechanisms that ensure proper fine-tuning of the Rag–mTORC1–TFEB/TFE3 signalling hub. For instance, TFEB expression was previously shown to be induced by starvation via a positive feedback loop that involves direct TFEB binding to its own promoter[57]. Moreover, TFEB and TFE3 control lysosomal recruitment and activity of mTORC1 by robustly upregulating RagD expression, whereas RagC expression is much less affected[58,59]. Our data expand this model further, showing that the TFEB/TFE3 target, RagD, is—in turn—the key regulator of their phosphorylation, subcellular localization and activity, thus establishing a negative feedback loop to facilitate rapid and robust re-phosphorylation and inactivation of TFEB/TFE3 when AAs are available again, following starvation.

In sum, our work identifies the mammalian Rag GTPases as a unique example of functionally divergent paralogues in the core AA sensing/mTOR signalling pathway. Through evolution, duplication of the ancestral *RRAGA* and *RRAGC* genes and functional diversification of the additional copies has led to four mammalian Rags that form distinct Rag dimers with specialized functions in the regulation of mTORC1 by AAs. Hence, our findings support the existence of a Rag dimer code that adds to the complexity of metabolic signalling in mammalian cells.

Online content

Any methods, additional references, Nature Research reporting summaries, source data, extended data, supplementary information, acknowledgements, peer review information; details of author contributions and competing interests; and statements of data and code availability are available at https://doi.org/10.1038/s41556-022-00976-y.

Received: 2 August 2021; Accepted: 13 July 2022;
Published online: 12 September 2022

References

1. Hara, K. et al. Amino acid sufficiency and mTOR regulate p70 S6 kinase and eIF-4E BP1 through a common effector mechanism. *J. Biol. Chem.* **273**, 14484–14494 (1998).
2. Demetriades, C., Doumpas, N. & Teleman, A. A. Regulation of TORC1 in response to amino acid starvation via lysosomal recruitment of TSC2. *Cell* **156**, 786–799 (2014).
3. Carroll, B. et al. Control of TSC2–Rheb signaling axis by arginine regulates mTORC1 activity. *eLife* **5**, e11058 (2016).
4. Kennedy, B. K. & Lamming, D. W. The mechanistic target of rapamycin: the grand ConducTOR of metabolism and aging. *Cell Metab.* **23**, 990–1003 (2016).
5. Gonzalez, A. & Hall, M. N. Nutrient sensing and TOR signaling in yeast and mammals. *EMBO J.* **36**, 397–408 (2017).
6. Liu, G. Y. & Sabatini, D. M. mTOR at the nexus of nutrition, growth, ageing and disease. *Nat. Rev. Mol. Cell Biol.* **21**, 183–203 (2020).
7. Rabanal-Ruiz, Y. & Korolchuk, V. I. mTORC1 and nutrient homeostasis: the central role of the lysosome. *Int. J. Mol. Sci.* **19**, 818 (2018).
8. Nuchel, J. et al. An mTORC1-GRASP55 signaling axis controls unconventional secretion to reshape the extracellular proteome upon stress. *Mol. Cell* **81**, 3275–3293 (2021).
9. Fernandes, S. A. & Demetriades, C. The multifaceted role of nutrient sensing and mTORC1 signaling in physiology and aging. *Front. Aging* **2**, 707372 (2021).
10. Sancak, Y. et al. The Rag GTPases bind raptor and mediate amino acid signaling to mTORC1. *Science* **320**, 1496–1501 (2008).
11. Kim, E., Goraksha-Hicks, P., Li, L., Neufeld, T. P. & Guan, K. L. Regulation of TORC1 by Rag GTPases in nutrient response. *Nat. Cell Biol.* **10**, 935–945 (2008).
12. Sancak, Y. et al. Ragulator–Rag complex targets mTORC1 to the lysosomal surface and is necessary for its activation by amino acids. *Cell* **141**, 290–303 (2010).
13. Demetriades, C., Plescher, M. & Teleman, A. A. Lysosomal recruitment of TSC2 is a universal response to cellular stress. *Nat. Commun.* **7**, 10662 (2016).
14. Taylor, J. S. & Raes, J. Duplication and divergence: the evolution of new genes and old ideas. *Annu Rev. Genet* **38**, 615–643 (2004).
15. Copley, S. D. Evolution of new enzymes by gene duplication and divergence. *FEBS J.* **287**, 1262–1283 (2020).
16. Izzo, A. et al. The genomic landscape of the somatic linker histone subtypes H1.1 to H1.5 in human cells. *Cell Rep.* **3**, 2142–2154 (2013).
17. Sweadner, K. J. et al. Genotype-structure-phenotype relationships diverge in paralogs ATP1A1, ATP1A2, and ATP1A3. *Neurol. Genet* **5**, e303 (2019).
18. Harvey, K. L., Jarocki, V. M., Charles, I. G. & Djordjevic, S. P. The diverse functional roles of elongation factor Tu (EF-Tu) in microbial pathogenesis. *Front. Microbiol.* **10**, 2351 (2019).
19. Storz, J. F., Opazo, J. C. & Hoffmann, F. G. Gene duplication, genome duplication, and the functional diversification of vertebrate globins. *Mol. Phylogenet. Evol.* **66**, 469–478 (2013).
20. Schurmann, A., Brauers, A., Massmann, S., Becker, W. & Joost, H. G. Cloning of a novel family of mammalian GTP-binding proteins (RagA, RagBs, RagB1) with remote similarity to the Ras-related GTPases. *J. Biol. Chem.* **270**, 28982–28988 (1995).
21. Sekiguchi, T., Hirose, E., Nakashima, N., Ii, M. & Nishimoto, T. Novel G proteins, Rag C and Rag D, interact with GTP-binding proteins, Rag A and Rag B. *J. Biol. Chem.* **276**, 7246–7257 (2001).
22. Powis, K. & De Virgilio, C. Conserved regulators of Rag GTPases orchestrate amino acid-dependent TORC1 signaling. *Cell Disco.* **2**, 15049 (2016).
23. Bar-Peled, L., Schweitzer, L. D., Zoncu, R. & Sabatini, D. M. Ragulator is a GEF for the rag GTPases that signal amino acid levels to mTORC1. *Cell* **150**, 1196–1208 (2012).
24. Brady, O. A., Diab, H. I. & Puertollano, R. Rags to riches: amino acid sensing by the Rag GTPases in health and disease. *Small GTPases* **7**, 197–206 (2016).
25. Fromm, S. A., Lawrence, R. E. & Hurley, J. H. Structural mechanism for amino acid-dependent Rag GTPase nucleotide state switching by SLC38A9. *Nat. Struct. Mol. Biol.* **27**, 1017–1023 (2020).
26. Peng, W. & Jewell, J. L. Amino acid sensing: architecture of mTORC1 on the lysosome surface. *Curr. Biol.* **30**, R89–R91 (2020).
27. Han, J. M. et al. Leucyl-tRNA synthetase is an intracellular leucine sensor for the mTORC1-signaling pathway. *Cell* **149**, 410–424 (2012).
28. Lee, M. et al. Coordination of the leucine-sensing Rag GTPase cycle by leucyl-tRNA synthetase in the mTORC1 signaling pathway. *Proc. Natl Acad. Sci. USA* **115**, E5279–E5288 (2018).
29. Jewell, J. L. et al. Metabolism. Differential regulation of mTORC1 by leucine and glutamine. *Science* **347**, 194–198 (2015).
30. Sardiello, M. et al. A gene network regulating lysosomal biogenesis and function. *Science* **325**, 473–477 (2009).
31. Settembre, C. et al. TFEB links autophagy to lysosomal biogenesis. *Science* **332**, 1429–1433 (2011).
32. Martina, J. A. et al. The nutrient-responsive transcription factor TFE3 promotes autophagy, lysosomal biogenesis, and clearance of cellular debris. *Sci. Signal* **7**, ra9 (2014).
33. Martina, J. A. & Puertollano, R. Rag GTPases mediate amino acid-dependent recruitment of TFEB and MITF to lysosomes. *J. Cell Biol.* **200**, 475–491 (2013).
34. Settembre, C. et al. A lysosome-to-nucleus signalling mechanism senses and regulates the lysosome via mTOR and TFEB. *EMBO J.* **31**, 1095–1108 (2012).
35. Martina, J. A., Chen, Y., Gucek, M. & Puertollano, R. MTORC1 functions as a transcriptional regulator of autophagy by preventing nuclear transport of TFEB. *Autophagy* **8**, 903–914 (2012).
36. Puertollano, R., Ferguson, S. M., Brugarolas, J. & Ballabio, A. The complex relationship between TFEB transcription factor phosphorylation and subcellular localization. *EMBO J.* **37**, e98804 (2018).
37. Baba, M. et al. TFE3 Xp11.2 translocation renal cell carcinoma mouse model reveals novel therapeutic targets and identifies GPNMB as a diagnostic marker for human disease. *Mol. Cancer Res.* **17**, 1613–1626 (2019).
38. Taniguchi, M. et al. TFE3 is a bHLH-ZIP-type transcription factor that regulates the mammalian Golgi stress response. *Cell Struct. Funct.* **40**, 13–30 (2015).
39. Alesi, N. et al. TSC2 regulates lysosome biogenesis via a non-canonical RAGC and TFEB-dependent mechanism. *Nat. Commun.* **12**, 4245 (2021).
40. Hong, S. B. et al. Inactivation of the FLCN tumor suppressor gene induces TFE3 transcriptional activity by increasing its nuclear localization. *PLoS ONE* **5**, e15793 (2010).
41. Kobos, R. et al. Combining integrated genomics and functional genomics to dissect the biology of a cancer-associated, aberrant transcription factor, the ASPSCR1–TFE3 fusion oncoprotein. *J. Pathol.* **229**, 743–754 (2013).
42. Goodwin, J. M. et al. GABARAP sequesters the FLCN–FNIP tumor suppressor complex to couple autophagy with lysosomal biogenesis. *Sci. Adv.* **7**, eabj2485 (2021).
43. Lawrence, R. E. et al. A nutrient-induced affinity switch controls mTORC1 activation by its Rag GTPase–Ragulator lysosomal scaffold. *Nat. Cell Biol.* **20**, 1052–1063 (2018).
44. Abu-Remaileh, M. et al. Lysosomal metabolomics reveals V-ATPase- and mTOR-dependent regulation of amino acid efflux from lysosomes. *Science* **358**, 807–813 (2017).

45. Anandapadamanaban, M. et al. Architecture of human Rag GTPase heterodimers and their complex with mTORC1. *Science* **366**, 203–210 (2019).
46. de Araujo, M. E. G. et al. Crystal structure of the human lysosomal mTORC1 scaffold complex and its impact on signaling. *Science* **358**, 377–381 (2017).
47. Okosun, J. et al. Recurrent mTORC1-activating RRAGC mutations in follicular lymphoma. *Nat. Genet.* **48**, 183–188 (2016).
48. Ying, Z. X. et al. Recurrent mutations in the MTOR regulator RRAGC in follicular lymphoma. *Clin. Cancer Res.* **22**, 5383–5393 (2016).
49. Yang, G. et al. RagC phosphorylation autoregulates mTOR complex 1. *EMBO J.* **38**, e99548 (2019).
50. Kwak, S. S. et al. Amino acid-dependent NPRL2 interaction with Raptor determines mTOR complex 1 activation. *Cell Signal* **28**, 32–41 (2016).
51. Kim, S. H. et al. Mitochondrial threonyl-tRNA synthetase TARS2 is required for threonine-sensitive mTORC1 activation. *Mol. Cell* **81**, 398–407 e394 (2021).
52. Johnson, M. A. et al. Amino acid starvation has opposite effects on mitochondrial and cytosolic protein synthesis. *PLoS ONE* **9**, e93597 (2014).
53. Harding, H. P. et al. Regulated translation initiation controls stress-induced gene expression in mammalian cells. *Mol. Cell* **6**, 1099–1108 (2000).
54. Park, Y., Reyna-Neyra, A., Philippe, L. & Thoreen, C. C. mTORC1 balances cellular amino acid supply with demand for protein synthesis through post-transcriptional control of ATF4. *Cell Rep.* **19**, 1083–1090 (2017).
55. Figlia et al. Brain-enriched RagB isoforms regulate the dynamics of mTORC1 activity through GATOR1 inhibition. *Nat. Cell Biol.* https://doi.org/10.1038/s41556-022-00977-x (2022).
56. Villegas, F. et al. Lysosomal signaling licenses embryonic stem cell differentiation via inactivation of Tfe3. *Cell Stem Cell* **24**, 257–270 e258 (2019).
57. Settembre, C. et al. TFEB controls cellular lipid metabolism through a starvation-induced autoregulatory loop. *Nat. Cell Biol.* **15**, 647–658 (2013).
58. Di Malta, C. et al. Transcriptional activation of RagD GTPase controls mTORC1 and promotes cancer growth. *Science* **356**, 1188–1192 (2017).
59. Napolitano, G. et al. A substrate-specific mTORC1 pathway underlies Birt–Hogg–Dube syndrome. *Nature* **585**, 597–602 (2020).
60. Miller, A. J., Levy, C., Davis, I. J., Razin, E. & Fisher, D. E. Sumoylation of MITF and its related family members TFE3 and TFEB. *J. Biol. Chem.* **280**, 146–155 (2005).

Methods

Cell culture and treatments. All cell lines were grown at 37 °C, 5% CO_2. Human female embryonic kidney HEK293FT cells (#R70007, Invitrogen; RRID: CVCL_6911) and the resulting genetically modified cell lines were cultured in high-glucose DMEM (#41965039, Thermo Fisher Scientific), containing 10% foetal bovine serum (FBS) and 1% penicillin–streptomycin. The parental HEK293FT cells were purchased from Invitrogen before the initiation of the project. Their identity was validated by the Multiplex human Cell Line Authentication test (Multiplexion GmbH), which uses a single-nucleotide polymorphism typing approach, and was performed as described at www.multiplexion.de. All cell lines were regularly tested for *Mycoplasma* contamination using a PCR-based approach and were confirmed to be *Mycoplasma* free.

AA starvation experiments were performed as described previously[13]. In brief, custom-made starvation media were formulated according to the Gibco recipe for high-glucose DMEM, specifically omitting the AAs. The media were filtered through a 0.22-µm filter device and tested for proper pH and osmolality before use. For the respective AA-replete (+AA) treatment media, commercially available high-glucose DMEM was used (#41965039, Thermo Fisher Scientific). All treatment media were supplemented with 10% dialysed FBS. For this purpose, FBS was dialysed against 1× PBS through 3,500 MWCO dialysis tubing. For basal (+AA) conditions, the culture media were replaced with +AA treatment media 60–90 min before lysis or fixation. For AA starvation, culture media were replaced with starvation media for 1 h. For AA add-back experiments, cells were first starved as described above and then starvation media were replaced with +AA treatment media for 30 min.

Antibodies. Antibodies against phospho-TFEB (Ser211) (#37681), TFEB (#4240), TFE3 (#14779), phospho-S6K (Thr389) (#9205), S6K (#9202), 4E-BP1 (#9452), phospho-4E-BP1 (Thr37/46) (#9459), phospho-4E-BP1 (Ser65) (9451), ULK1 (#8054), phospho-ULK1 (Ser757) (#14202), DYKDDDDK (FLAG) tag (#2368), mTOR (#2983), RagA (#4357), RagB (#8150), RagC (#9480), RagD (#4470), FLCN (#3697) and CTSD (#2284) proteins were purchased from Cell Signaling Technology. Anti-Raptor (#20984-1-AP) and anti-LARS (#21146-1-AP) antibodies were purchased from Proteintech. A monoclonal antibody recognizing human and mouse α-tubulin (#T9026) was purchased from Sigma, and the anti-HA (3F10; #11867423001) antibody was purchased from Roche. The anti-LAMP2 monoclonal antibody (DSHB Hybridoma Product H4B4) was purchased from Developmental Studies Hybridoma Bank (DSHB) and was deposited to the DSHB by August, J.T./Hildreth, J.E.K. For immunoprecipitation (IP) experiments, FLAG-tagged proteins were pulled down using anti-FLAG M2 affinity gel (#A2220, Sigma). For immunoblotting, all primary antibodies were used 1:1,000 in PBS-T, 5% BSA, except for anti-FLAG, for which 1:3,000 was used. Peroxidase-conjugated AffiniPure anti-rabbit, anti-mouse and anti-rat secondary antibodies (#711-035-152, #715-035-151 and #712-035-153, respectively; all from Jackson ImmunoResearch) were used 1:10,000 in PBS-T (1× PBS and 0.1% Tween-20), 5% powdered milk. For immunofluorescence (IF), all primary antibodies were used 1:200 in BBT solution (1× PBS, 0.1% Tween-20 and 0.1% BSA). Anti-mouse rhodamine (TRITC)-conjugated (#715-025-150, Jackson ImmunoResearch) and anti-rabbit fluorescein (FITC)-conjugated AffiniPure secondary antibodies (#711-095-152, Jackson ImmunoResearch) were used 1:100 in BBT, whereas anti-rabbit Alexa Fluor 488-conjugated (#711-545-152, Jackson ImmunoResearch) and anti-rat Alexa Fluor 647-conjugated AffiniPure secondary antibodies (#712-605-153, Jackson ImmunoResearch) were used 1:500 in BBT.

Plasmid constructs. Expression plasmids for FLAG- and HA-tagged RagA and RagC, as well as for FLAG–Luc, were described previously[2]. The respective expression vectors for RagB and RagD were PCR amplified from pRK5–HA–GST plasmids (described in ref. [2]) and cloned in pcDNA3-HA and pcDNA3-FLAG vectors as EcoRI/NotI inserts. For the pcDNA3-FLAG-p18 expression construct, p18 was PCR-amplified from cDNA using appropriate primers, and cloned into the EcoRI/NotI sites of pcDNA3-FLAG. The pcDNA3–HA–RagC T90N and W115R point mutants were generated by site-directed mutagenesis using appropriate primers. The RagA/B chimaeric constructs were described previously[2]. The RagDCD chimaera was generated by first constructing a RagDC plasmid (containing the RagD N-terminal tail) using a two-step overlap PCR and appropriate primers to amplify parts of RagD and RagC. The end product was cloned into the pcDNA3-HA vector as NdeI/NotI fragment. Then a GeneArt string (Thermo Fisher Scientific) was used to introduce the C-terminal RagD part as a HpaI/NotI fragment in the RagDC plasmid, generating the RagDCD expression vector.

For the cell lines stably expressing HA-tagged Rag GTPase dimers (WT, mutants and chimaeras), the respective pcDNA3-puro vectors were generated by replacing the EcoRI/ClaI pcDNA3 fragment, containing the neomycin cassette, with the StuI/BstBI fragment of the MCSV-puro plasmid (Addgene #68469, RRID:Addgene_68469; described in ref. [61]), containing the PGK-puro cassette. The backbone and insert fragment ends were blunt before ligation.

All restriction enzymes were purchased from Fermentas/Thermo Scientific. The integrity of all constructs was verified by sequencing. Sequences of all cloning primers are provided in Supplementary Table 1.

Generation of KO cell lines. HEK293FT knock-out (KO) cell lines were generated using the CRISPR/Cas9 system developed by the Zhang lab[62]. Double-stranded DNA oligos that encode single guide RNAs (sgRNAs) against target genes were designed using online tools. For RagB, RagC and RagD, two sgRNAs were designed per gene targeting the 5′ coding sequence or untranslated region and the 3′ coding sequence or untranslated region, respectively (Supplementary Fig. 1). RagA was efficiently knocked out using a single sgRNA. Each sgRNA was cloned into the BbsI restriction sites of the PX459 vector. The oligo sequences for all sgRNAs are provided in Supplementary Table 1.

In brief, cells were seeded in six-well plates and transfected on the following day with the respective sgRNA-expressing vectors using Effectene reagent (QIAGEN), according to the manufacturer's instructions. Forty-eight hours post-transfection, cells were selected with 3 µg ml^{-1} puromycin (#A1113803, Thermo Fisher Scientific) for 3 days. Single-cell clones were picked by single-cell dilution, and KO clones were validated by genomic DNA PCR/sequencing (Extended Data Fig. 1) and immunoblotting using specific antibodies.

Transient DNA transfection. Plasmid DNA transfections were performed using Effectene (QIAGEN), according to the manufacturer's instructions.

Stable cell line generation. For the generation of monoclonal stable lines expressing HA-tagged Rag GTPases (WT, mutants and chimaeras), HEK293FT qKO cells were transfected using the indicated Rag dimer expression vectors. Forty-eight hours post-transfection, cells were selected with 2 µg ml^{-1} puromycin for 2 days and then propagated in maintenance selection media containing the same puromycin concentration. To specifically assess the qualitative differences between the various Rag GTPase paralogues, single-cell clones that express comparable Rag levels were selected for functional characterization experiments. For the RagA versus RagB comparison, RagB expression is lower than RagA, resembling the endogenous RagA/B expression differences. Rag expression levels were validated by immunoblotting.

Despite the complications that generating monoclonal stable cell lines may introduce to a study (for example, due to clonal propagation and interclonal variability), and the fact that this is a tedious and lengthy process, this proved to be the best and only way that allows for a direct comparison between different Rag dimers and the functional characterization of their qualitative properties in the regulation of mTORC1 by AAs: while transiently overexpressing Rags could show the differences in interactions between RagC/D and other proteins in co-IP experiments, it largely masked the qualitative effects towards mTORC1 activity. This was probably due to overexpression artefacts, as Rag levels were massively higher in transiently transfected cells, compared with stable cell lines. Moreover, cells expressing such high Rag levels showed non-physiological localization patterns, with the majority of cells showing non-lysosomal Rag localization, regardless of the dimer expressed. Although polyclonal stable cell lines performed much better in maintaining the physiological regulation of mTORC1 by the Rags, they were still not appropriate for this study: because individual cells in the polyclonal population express uneven/variable Rag levels, some cells demonstrated almost undetectable Rag expression, while others had massive Rag overexpression. This led to large cell-to-cell variability, especially in microscopy studies, where we assessed mTOR or Rag localization at the single-cell level. In sum, monoclonal cell lines that express comparable Rag levels for the different Rag dimers and show low cell-to-cell variability were the only way to reliably investigate the Rag dimer code that defines the mTORC1 response to AAs.

Immunoblotting. For immunoblotting analyses, cells were washed once in-well with serum-free DMEM, to remove FBS, and lysed in 250 µl Triton lysis buffer (50 mM Tris pH 7.5, 1% Triton X-100, 150 mM NaCl, 50 mM NaF, 2 mM Na-vanadate, 0.011 g ml^{-1} β-glycerophosphate, 1× PhosSTOP phosphatase inhibitors and 1× Complete protease inhibitors) for 10 min on ice. Samples were clarified by centrifugation (14,000*g*, 15 min, 4 °C), and supernatants were transferred to new tubes. Protein concentration was measured using the Protein Assay Dye Reagent (#5000006, Bio-Rad).

Protein samples were subjected to electrophoretic separation on SDS–PAGE and analysed by standard western blotting techniques. In brief, proteins were transferred to nitrocellulose membranes (#10600002, Amersham) and stained with 0.2% Ponceau solution (Serva) to confirm equal loading. Membranes were blocked with 5% powdered milk in PBS-T (1× PBS and 0.1% Tween-20) for 1 h at room temperature, washed three times for 10 min with PBS-T and incubated with primary antibodies (1:1,000 in PBS-T, 5% BSA) rotating overnight at 4 °C. The next day, membranes were washed three times for 10 min with PBS-T and incubated with appropriate HRP-conjugated secondary antibodies (1:10,000 in PBS-T, 5% milk) for 1 h at room temperature. Signals were detected by enhanced chemiluminescence, using the ECL Western Blotting Substrate (#W1015, Promega), or SuperSignal West Pico PLUS (#34577, Thermo Scientific) and SuperSignal West Femto Substrate (#34095, Thermo Scientific) for weaker signals. Immunoblot images were captured on film (#28906835, GE Healthcare) and quantified using the GelAnalyzer software (v19.1; www.gelanalyzer.com).

Co-IP. For co-IP experiments, 1×10^6 cells were transiently transfected with the indicated plasmids and lysed 40–48 h post-transfection in IP lysis buffer (50 mM Tris pH 7.5, 0.3% CHAPS, 150 mM NaCl, 50 mM NaF, 2 mM Na-vanadate, 0.011 g ml^{-1} β-glycerophosphate, 1× PhosSTOP phosphatase inhibitors and 1× Complete protease inhibitors). FLAG-tagged proteins were incubated with 30 µl pre-washed anti-FLAG M2 affinity gel (Sigma, #A2220) for 3 h at 4 °C and washed four times with IP wash buffer (50 mM Tris pH 7.5, 0.3% CHAPS, 150 mM NaCl and 50 mM NaF). Samples were then boiled for 6 min in 2× Laemmli sample buffer and analysed by immunoblotting using appropriate antibodies.

LysoRag IP. To purify Rag-bound lysosomes, we developed the LysoRag IP method, a modified version of the Lyso-IP method that was previously described by the Sabatini lab[44]. This method allows for the purification of intact lysosomes, using HA-tagged Rags as bait. As a result, Rag dimers that bind to lysosomes more strongly pull down larger amounts of lysosomal material. HEK293FT qKO monoclonal cell lines, stably expressing HA-tagged RagC or RagD as dimers with RagA, were used to compare the relative affinities of RagC and RagD to lysosomes. In brief, 2×10^7 cells were seeded in a 15 cm dish and allowed to settle for 24 h. On the next day, cells were washed once with ice-cold PBS and scraped in 1 ml of ice-cold PBS containing 1× PhosSTOP phosphatase inhibitors (#04906837001, Roche) and 1× Complete protease inhibitors (#11697498001, Roche). Cells were then pelleted by centrifugation (1,000*g*, 2 min, 4 °C) and resuspended in 1 ml of 1× ice-cold PBS with inhibitors. For input samples, 25 µl of the suspension was transferred in a new tube and lysed by the addition of 125 µl CHAPS lysis buffer (50 mM Tris pH 7.5, 0.3% CHAPS, 150 mM NaCl, 50 mM NaF, 2 mM Na-vanadate, 0.011 g ml^{-1} β-glycerophosphate, 1× PhosSTOP phosphatase inhibitors and 1× Complete protease inhibitors) on ice for 10 min. Lysed input samples were then cleared by centrifugation (14,000*g*, 15 min, 4 °C), and the supernatant was transferred to new tubes containing 37.5 µl of 6× Laemmli and boiled for 6 min.

For the lysosomal fractions, the remaining cell suspension was homogenized with 20 strokes in pre-chilled 2 ml hand Dounce homogenizers kept on ice. The homogenate was cleared by centrifugation (1,000*g*, 2 min, 4 °C) and incubated with 100 µl pre-washed Pierce anti-HA magnetic beads (#88837, Thermo Fisher Scientific) on a nutating mixer for 3 min at room temperature, followed by three washes with ice-cold PBS, containing phosphatase and protease inhibitors, on a DynaMag spin magnet (#12320D, Invitrogen). After the last wash, lysosomes were eluted from the beads by addition of 60 µl 2× Laemmli sample buffer and boiling for 6 min.

IF and confocal microscopy. IF/confocal microscopy experiments and quantification of co-localization were performed as previously described[13]. In brief, cells were seeded on fibronectin-coated coverslips and treated as indicated in each experiment. After treatments, cells were fixed for 10 min at room temperature with 4% PFA in PBS. Samples were washed/permeabilized with PBT solution (1× PBS and 0.1% Tween-20), and blocked with BBT solution (1× PBS, 0.1% Tween-20 and 0.1% BSA). Staining was performed with the indicated primary antibodies in BBT (1:200 dilution) and then with appropriate highly cross-adsorbed secondary fluorescent antibodies (1:100 in BBT for FITC- or TRITC-conjugated antibodies; 1:500 in BBT for Alexa Fluor-conjugated antibodies). Finally, nuclei were stained with DAPI and cells mounted on slides using Fluoromount-G (#00-4958-02, Invitrogen). Images from single-channel captures are shown in greyscale. For the merged images, FITC, Alexa 647 (for anti-HA IFs), and Alexa 488 (for anti-TFE3 IFs) are shown in green, TRITC in red and DAPI in blue. Images were captured using a 40× objective lens on an SP8 Leica confocal microscope.

To quantify co-localization of mTOR or HA signal with the lysosomal marker LAMP2, the Fiji software (version 2.1.0/1.53c)[63] was used to define regions of interest corresponding to individual cells, excluding the nucleus. Forty to 50 individual cells from approximately ten independent fields were selected per experiment for the analysis. The Coloc2 plugin was used to calculate the Manders' co-localization coefficient, using automatic Costes thresholding[64,65]. The Manders' co-localization coefficient yields the fraction of the signal of interest (mTOR or HA-Rag in this study) that overlaps with a second signal (in our case, lysosomes).

Subcellular localization of TFE3 was analysed by scoring cells on the basis of the signal distribution of TFE3, as shown in the example images in Fig. 2b. Signal was scored as nuclear (more TFE3 signal in the nucleus), cytoplasmic (more TFE3 signal in the cytoplasm) or intermediate (similar TFE3 signal between nucleus and cytoplasm). Approximately 50 individual cells were scored per genotype for each experiment.

Gene expression analysis (RT–qPCR). For gene expression analysis, RNA was isolated with TRIzol (#15596018, Thermo Fisher Scientific) and reverse transcription was performed using the RevertAid H Minus Reverse Transcriptase kit (#EP0451, Thermo Fisher Scientific). The cDNAs were diluted 1:10 in nuclease-free H_2O and 4 µl of diluted cDNA was used per reaction, along with 5 µl of 2× Maxima SYBR Green/ROX qPCR master mix (#K0223, Thermo Fisher Scientific) and 1 µl of primer mix (2.5 µM of forward and reverse primers). For each replicate experiment, reactions were set in technical triplicates in a StepOnePlus Real-Time PCR system (Applied Biosystems) and analysed with the StepOne software (v2.2.2; Applied Biosystems). Relative gene expression levels were calculated with the $2^{-\Delta\Delta Ct}$ method. *RPL13a* expression was used for normalization as internal control.

LysoTracker staining. For LysoTracker staining experiments, cells were seeded in fibronectin-coated coverslips and grown until they reached 80–90% confluency. Lysosomes were stained by the addition of 100 nM LysoTracker Red DND-99 (#L7528, Invitrogen) in complete medium for 1.5 h in standard culturing conditions. Cells were then fixed with 4% PFA in PBS for 10 min at room temperature, washed and permeabilized with PBT solution (1× PBS and 0.1% Tween-20), and nuclei stained with DAPI (1:2,000 in PBT) for 10 min. Coverslips were mounted on slides using Fluoromount-G (#00-4958-02, Invitrogen). Images were captured using a 40× objective lens on an SP8 Leica confocal microscope, using the Leica Application Suite X software (v3.5.7.23225). LysoTracker signal intensity was measured from 50 individual cells per genotype for each experiment using Fiji (version 2.1.0/1.53c)[63].

Phylogenetic analysis. Rag orthologues were identified by performing a blastp search (blastp suite) against the NCBI Reference proteins (refseq_protein; version 2021-07) database, using the AA sequences of human RRAGA (Uniprot ID: Q7L523), RRAGB (Uniprot ID: Q5VZM2-2), RRAGC (Uniprot ID: Q9HB90) and RRAGD (Uniprot ID: Q9NQL2-1) as query proteins, filtering for each of the organisms shown in Fig. 1a (*H. sapiens*, taxid: 9606; *M. mulatta*, taxid: 9544; *C. lupus*, taxid: 9615; *M. musculus*, taxid: 10090; *X. laevis*, taxid: 8355; *D. rerio*, taxid: 7955; *D. melanogaster*, taxid: 7227; *C. elegans*, taxid: 6239; *S. cerevisiae*, taxid: 4932). The expect threshold for identified proteins was set at 1×10^{-30}; with a maximum of 100 target sequences; disabled low-complexity region filtering; using the BLOSUM62 matrix; a word size of 6; and gap existence and extension costs of 11 and 1, respectively.

Sequence alignment and structure modelling. Structure-based sequence alignments of RagA and RagB or RagC and RagD were prepared with Clustal Omega[66] and ESPript[67]. To generate a model of the RagA/RagC/LAMTOR complex, we superposed the crystal structure of the active RagA–Q66L–GTP/RagC–S75N–GDP heterodimer (PDBID: 6S6D)[45] with the complex structure of LAMTOR with the dimerization domains of RagA and RagC (PDBID: 6EHR)[46]. To model the active RagB or RagD GTPases, we introduced AA substitution in the RagA or RagC GTPases (PDBID: 6S6D), respectively, in Coot[68], followed by structure idealization using refmac5[69]. The inactive RagB/RagD dimer conformation was modelled accordingly on the basis of the cryo-EM structure of the inactive RagA/RagC dimer bound to the FLCN–FNIP2 complex (PDBID: 6ULG)[70].

Statistics and reproducibility. Statistical analysis and data presentation in graphs was performed using the GraphPad Prism software (v9.1.0). For all quantifications, data in the graphs are shown as mean ± standard error of the mean (s.e.m.). Normal distribution was tested using the Shapiro–Wilk or the Kolmogorov–Smirnov tests, and correction for multiple comparisons was performed using the Tukey test. Significance was calculated using unpaired two-tailed *t*-test (for pairwise comparisons, see Fig. 3b,d,f and Extended Data Figs. 3b–e,g and 4c–f) or one-way analysis of variance (for multiple comparisons, see Figs. 1c–f,h, 2b,c, 4d,e,g, 5c–f,h, 6b–e,g and 7c,e and Extended Data Figs. 2b, 6b and 7b–e,g) for normally distributed data, or the Kruskal–Wallis test for non-normally distributed data (Fig. 2e). *P* values are described in the figures and figure legends ($^*P < 0.05$, $^{**}P < 0.01$, $^{***}P < 0.005$, $^{****}P < 0.001$; NS, non-significant). Statistics source data are provided in the numerical source data table.

All findings were reproducible over multiple independent experiments, within a reasonable degree of variability between replicates. The number of replicate experiments for each assay is provided in the respective figure legends. No statistical method was used to pre-determine sample size, which was determined in accordance with standard practices in the field. No data were excluded from the analyses. The experiments were not randomized, and the investigators were not blinded to allocation during experiments and outcome assessment.

Reporting summary. Further information on research design is available in the Nature Research Reporting Summary linked to this article.

Data availability

Uncropped immunoblots and statistics source data are provided as image source data or numerical source data files, respectively, alongside the paper. All other data supporting the findings of this study are available from the corresponding author upon reasonable request. Source data are provided with this paper.

Code availability

No code was generated in this study.

References

61. Akama-Garren, E. H. et al. A modular assembly platform for rapid generation of DNA constructs. *Sci. Rep.* **6**, 16836 (2016).

62. Ran, F. A. et al. Genome engineering using the CRISPR–Cas9 system. *Nat. Protoc.* **8**, 2281–2308 (2013).
63. Schindelin, J. et al. Fiji: an open-source platform for biological-image analysis. *Nat. Methods* **9**, 676–682 (2012).
64. Manders, E. M. M., Verbeek, F. J. & Aten, J. A. Measurement of co-localization of objects in dual-colour confocal images. *J. Microsc.* **169**, 375–382 (1993).
65. Costes, S. V. et al. Automatic and quantitative measurement of protein–protein colocalization in live cells. *Biophys. J.* **86**, 3993–4003 (2004).
66. Sievers, F. et al. Fast, scalable generation of high-quality protein multiple sequence alignments using Clustal Omega. *Mol. Syst. Biol.* **7**, 539 (2011).
67. Robert, X. & Gouet, P. Deciphering key features in protein structures with the new ENDscript server. *Nucleic Acids Res.* **42**, W320–W324 (2014).
68. Emsley, P., Lohkamp, B., Scott, W. G. & Cowtan, K. Features and development of Coot. *Acta Crystallogr. D* **66**, 486–501 (2010).
69. Murshudov, G. N., Vagin, A. A. & Dodson, E. J. Refinement of macromolecular structures by the maximum-likelihood method. *Acta Crystallogr. D* **53**, 240–255 (1997).
70. Shen, K. et al. Cryo-EM structure of the human FLCN–FNIP2–Rag–Ragulator complex. *Cell* **179**, 1319–1329 e1318 (2019).

Acknowledgements

We thank all members of the Demetriades lab for valuable discussions and feedback on the project; and the MPI-AGE FACS & Imaging Core Facility for support with confocal microscopy. C.D. is funded by the European Research Council (ERC) under the European Union's Horizon 2020 research and innovation programme (grant agreement number 757729) and by the Max Planck Society.

Author contributions

Experimental work: P.G. and N.G., assisted by S.W.; data analysis: P.G., N.G. and C.D.; structure analysis: D.K.; project design and supervision: C.D.; funding acquisition: C.D.; figure preparation: N.G. and C.D.; manuscript draft: C.D. All authors approved the final version of the manuscript and agree on the content and conclusions.

Funding

Open access funding provided by the Max Planck Society.

Competing interests

The authors declare no competing interests.

Additional information

Extended data is available for this paper at https://doi.org/10.1038/s41556-022-00976-y.

Supplementary information The online version contains supplementary material available at https://doi.org/10.1038/s41556-022-00976-y.

Correspondence and requests for materials should be addressed to Constantinos Demetriades.

Peer review information *Nature Cell Biology* thanks the anonymous reviewers for their contribution to the peer review of this work.

Reprints and permissions information is available at www.nature.com/reprints.

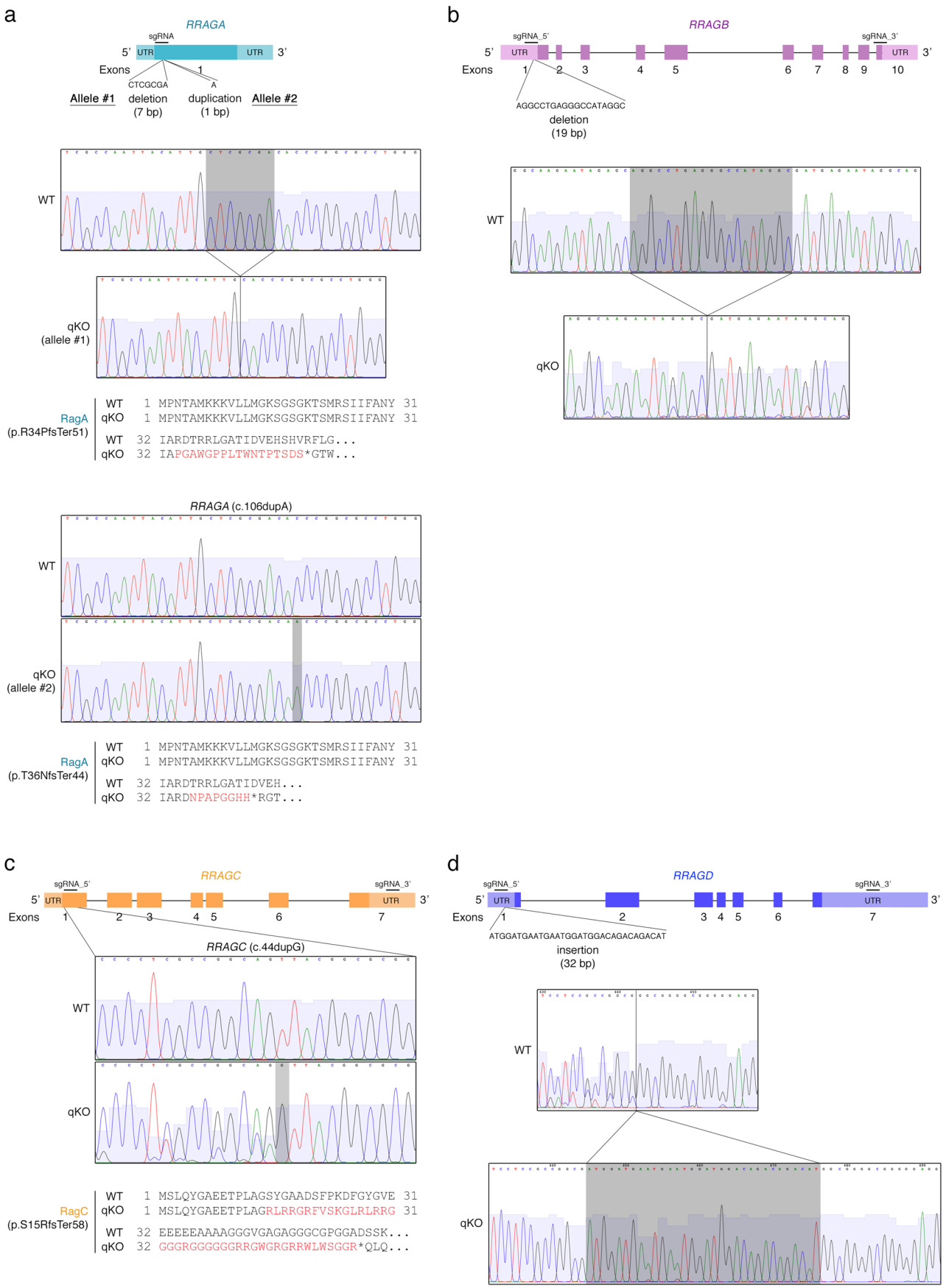

Extended Data Fig. 1 | See next page for caption.

Extended Data Fig. 1 | Characterization of the *Rag* genomic alterations in qKO HEK293FT cells. (a) CRISPR/Cas9-mediated knockout of *RRAGA*. The associated genomic changes in the two *RRAGA* alleles and the resulting changes in the RagA protein are shown. **(b)** CRISPR/Cas9-mediated knockout of *RRAGB*. The associated genomic changes in *RRAGB* are shown. **(c)** CRISPR/Cas9-mediated knockout of *RRAGC*. The associated genomic changes in *RRAGC* and the resulting changes in the RagC protein are shown. **(d)** CRISPR/Cas9-mediated knockout of *RRAGD*. The associated genomic changes in *RRAGD* are shown.

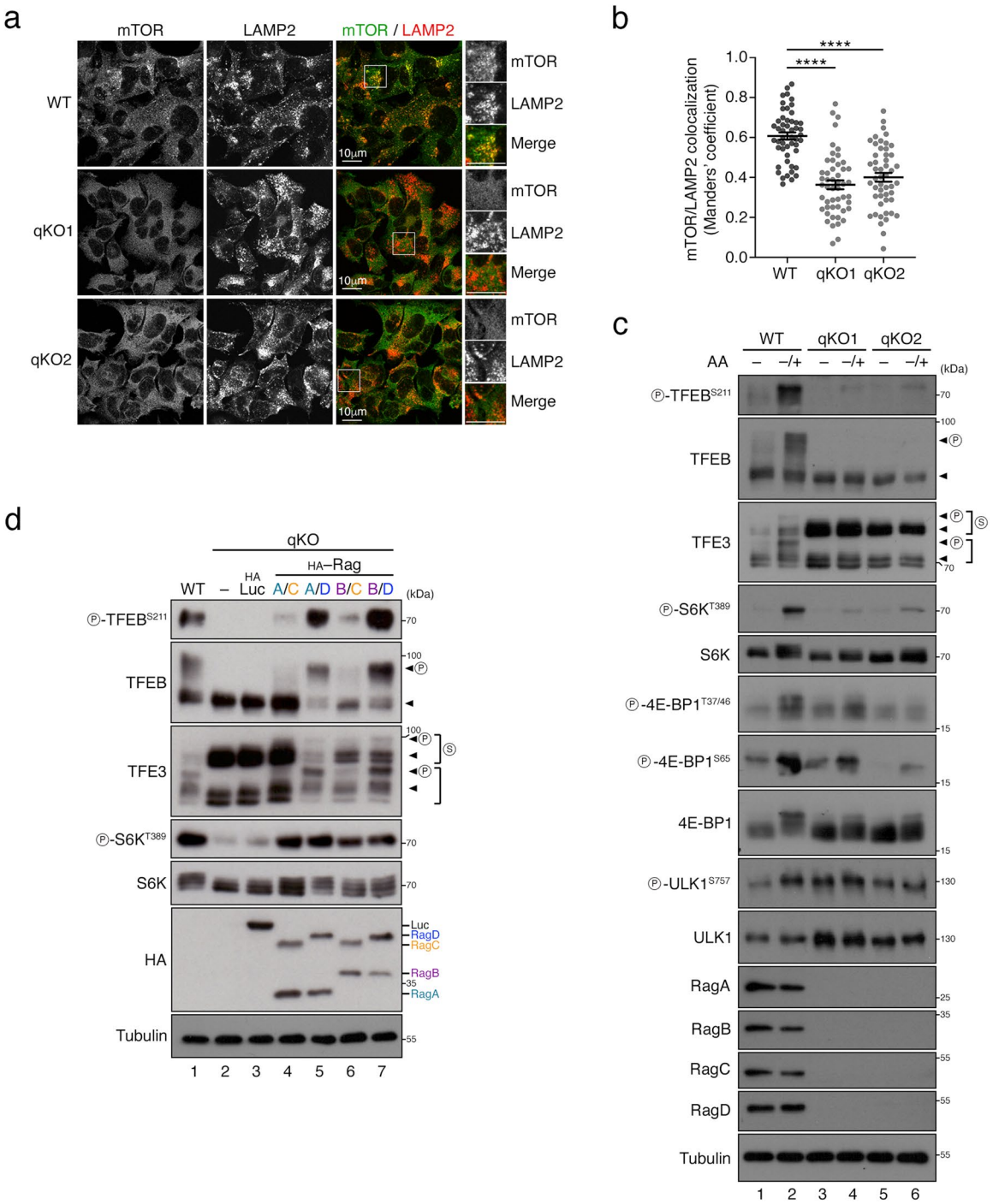

Extended Data Fig. 2 | Characterization of the HEK293FT qKO and Rag dimer reconstituted cell lines. (a-b) Two independent quadruple RagA-D knockout (qKO) HEK293FT clones show no lysosomal accumulations of mTOR. Colocalization analysis of mTOR with LAMP2 (lysosomal marker) in WT and qKO cells (clones qKO1, qKO2), using confocal microscopy. Magnified insets shown to the right. Scale bars = 10 μm (a). Quantification of mTOR/LAMP2 colocalization from n = 50 individual cells per condition from a representative experiment out of 2 independent replicates is shown in (b). Data shown as mean ± SEM. **** $p<0.001$. **(c)** Genetic ablation of all four Rags blunts mTORC1 reactivation by amino acids. Immunoblots with lysates from HEK293FT WT and qKO cells (clones qKO1, qKO2), treated with media containing or lacking AA, in starvation (–) or add-back (–/+) conditions, probed with the indicated antibodies. Arrowheads indicate bands corresponding to different protein forms, when multiple bands are present. P: phosphorylated form; S: SUMOylated form. n = 2 independent experiments. **(d)** Reconstitution of qKO cells with different Rag dimers reveals qualitative differences in the regulation of mTORC1. Immunoblots with the indicated antibodies using lysates from HEK293FT WT and qKO cells stably expressing comparable amounts of the four different Rag dimer combinations, or Luciferase (Luc) as a negative control, as HA-tagged proteins. Arrowheads indicate bands corresponding to different protein forms, when multiple bands are present. P: phosphorylated form; S: SUMOylated form. n = 3 independent experiments. Source numerical data and unprocessed blots are available in Source Data.

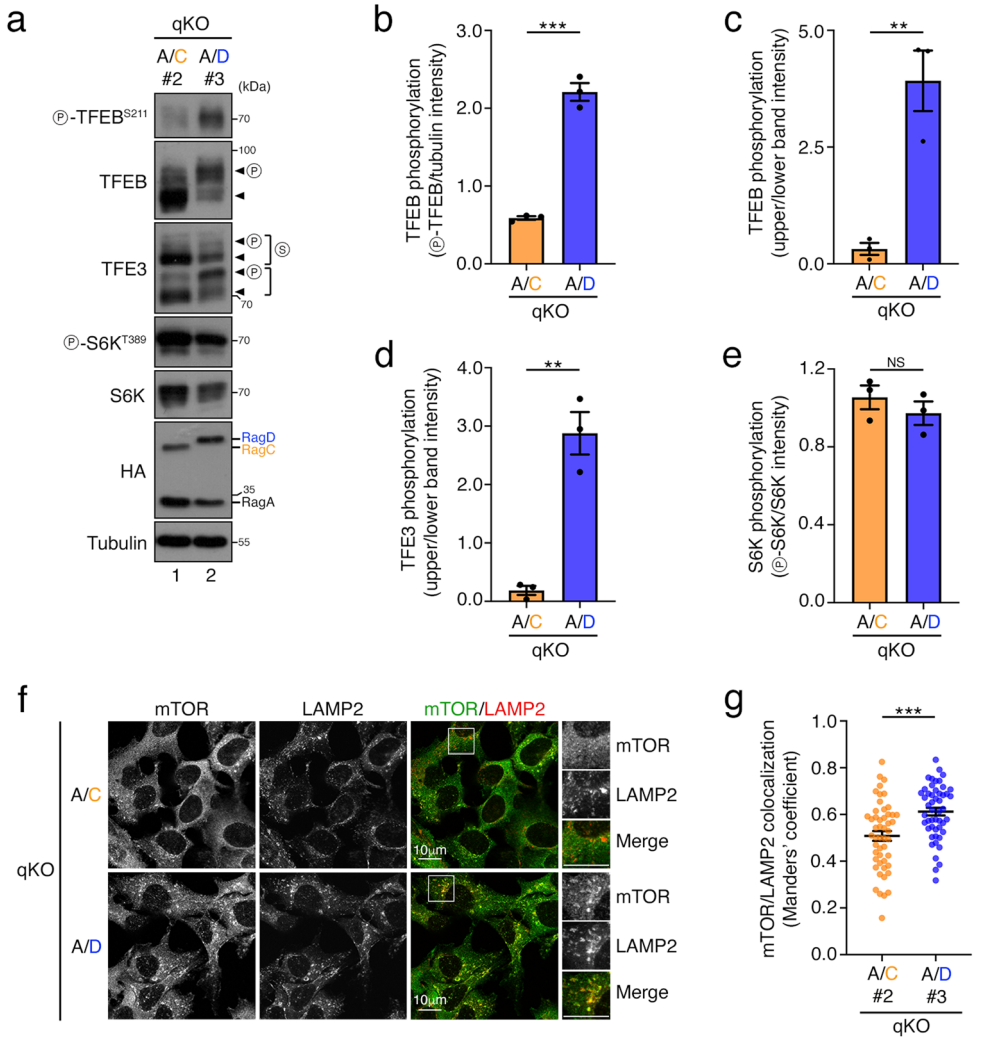

Extended Data Fig. 3 | Analysis of independent RagA/C- and RagA/D-expressing clones. (a-e) Immunoblots with lysates from qKO HEK293FT cells stably expressing HA-tagged RagA/C or RagA/D, grown under basal, AA-replete culture conditions, probed with the indicated antibodies. Arrowheads indicate bands corresponding to different protein forms, when multiple bands are present. P: phosphorylated form; S: SUMOylated form (a). Quantification of TFEB, TFE3 and S6K phosphorylation from (a), shown in (b-c), (d) and (e), respectively. Data in graphs shown as mean ± SEM. ** p<0.01, *** p<0.005. n = 3 independent experiments. **(f-g)** Colocalization analysis of mTOR with LAMP2 (lysosomal marker) in qKO HEK293FT cells stably expressing RagA/C or RagA/D, grown under basal, AA-replete culture conditions, using confocal microscopy. Magnified insets shown to the right. Scale bars = 10 μm (f). Quantification of mTOR/LAMP2 colocalization from n = 50 individual cells per condition from a representative experiment out of 3 independent replicates is shown in (g). Source numerical data and unprocessed blots are available in Source Data.

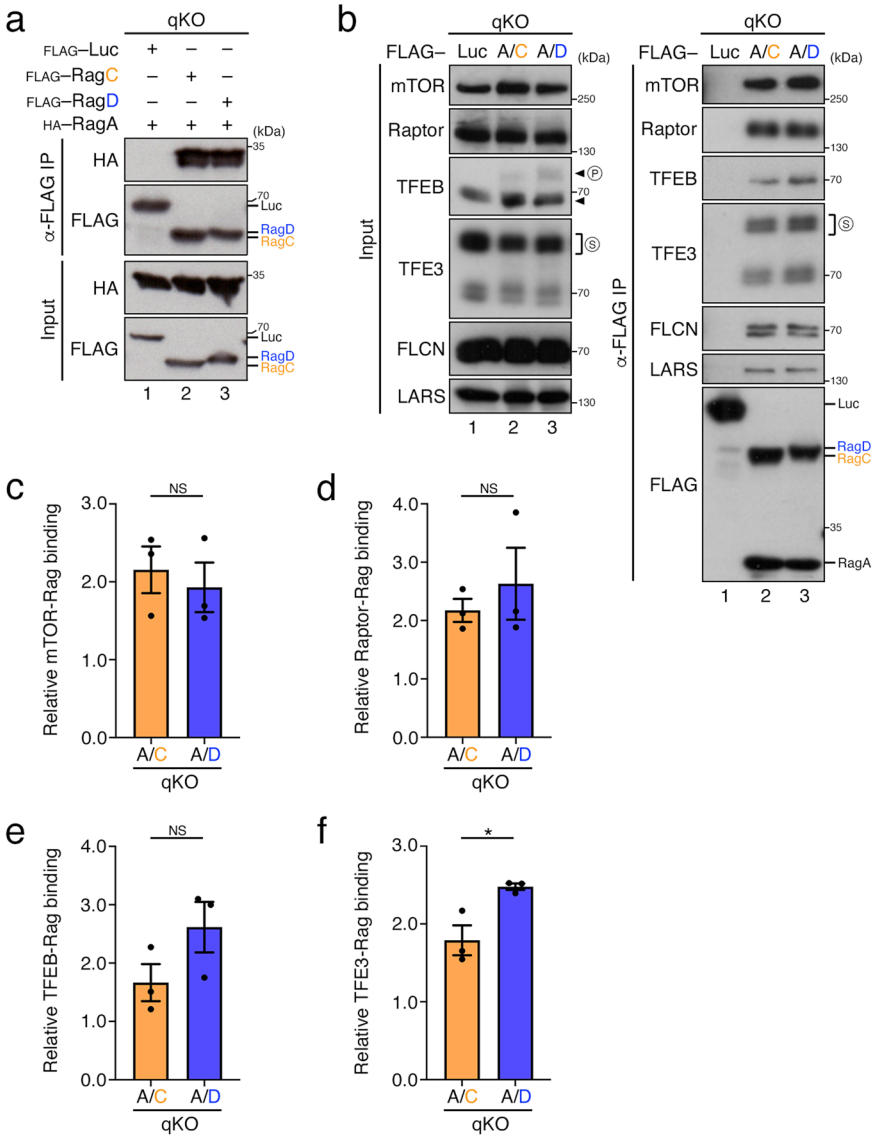

Extended Data Fig. 4 | Interaction properties of RagC- and RagD-containing dimers. (a) RagC and RagD bind similarly to RagA. Co-immunoprecipitation experiments in HEK293FT qKO cells, transiently expressing HA-tagged RagA with FLAG-tagged RagC, RagD, or Luciferase (Luc) as negative control. Binding of RagA to RagC or RagD was analyzed by immunoblotting as indicated. n = 2 independent experiments. **(b-f)** Co-immunoprecipitation experiments in HEK293FT qKO cells transiently expressing FLAG-tagged RagA/C, RagA/D, or Luciferase (Luc) as a negative control. Binding of the Rags to the indicated proteins was analyzed by immunoblotting. P: phosphorylated protein form; S: SUMOylated protein form(s) (b). Quantification of Rag binding to mTOR, Raptor, TFEB, and TFE3, shown in (c), (d), (e), (f), respectively. n = 3 independent experiments. Data in graphs shown as mean ± SEM. * $p<0.05$. Source numerical data and unprocessed blots are available in Source Data.

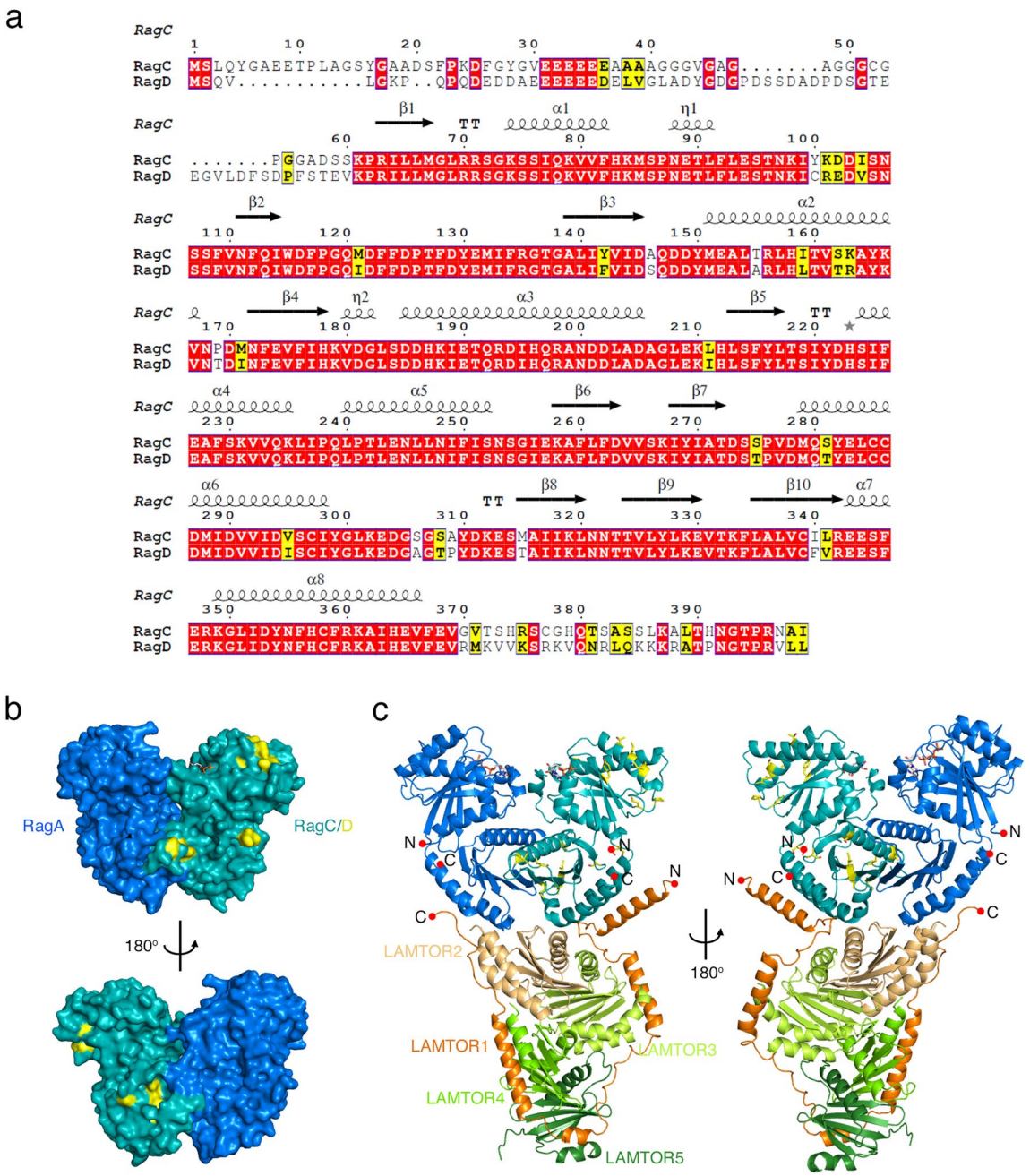

Extended Data Fig. 5 | Structural comparison between RagC and RagD suggests main differences localize to the unstructured N- and C-terminal tails. **(a)** Structure-based sequence alignment of RagC and RagD prepared with ESPript. Similar and identical residues are marked by yellow and red boxes, respectively. Secondary structure assignment is based on PDBID: 6S6D. **(b)** Minimal surface residue differences between RagC and RagD. Surface representation of the RagA (blue) / RagC (cyan) heterodimer (PDBID: 6S6D). Variable positions between RagC and RagD are coloured yellow. **(c)** No residue differences between the RagC and RagD structures localize at the Rag dimer / LAMTOR complex interface. Model of the RagA (blue) / RagC (cyan) heterodimer in the active conformation (PDBID: 6S6D) bound to the pentameric LAMTOR1-5 complex (PDBID: 6EHP). Variable positions between RagC and RagD are shown as yellow sticks. The ultimate residues that could be modelled at the N- and C-termini of the RagA, RagC and LAMTOR1 in the published structures are also labelled (N, C).

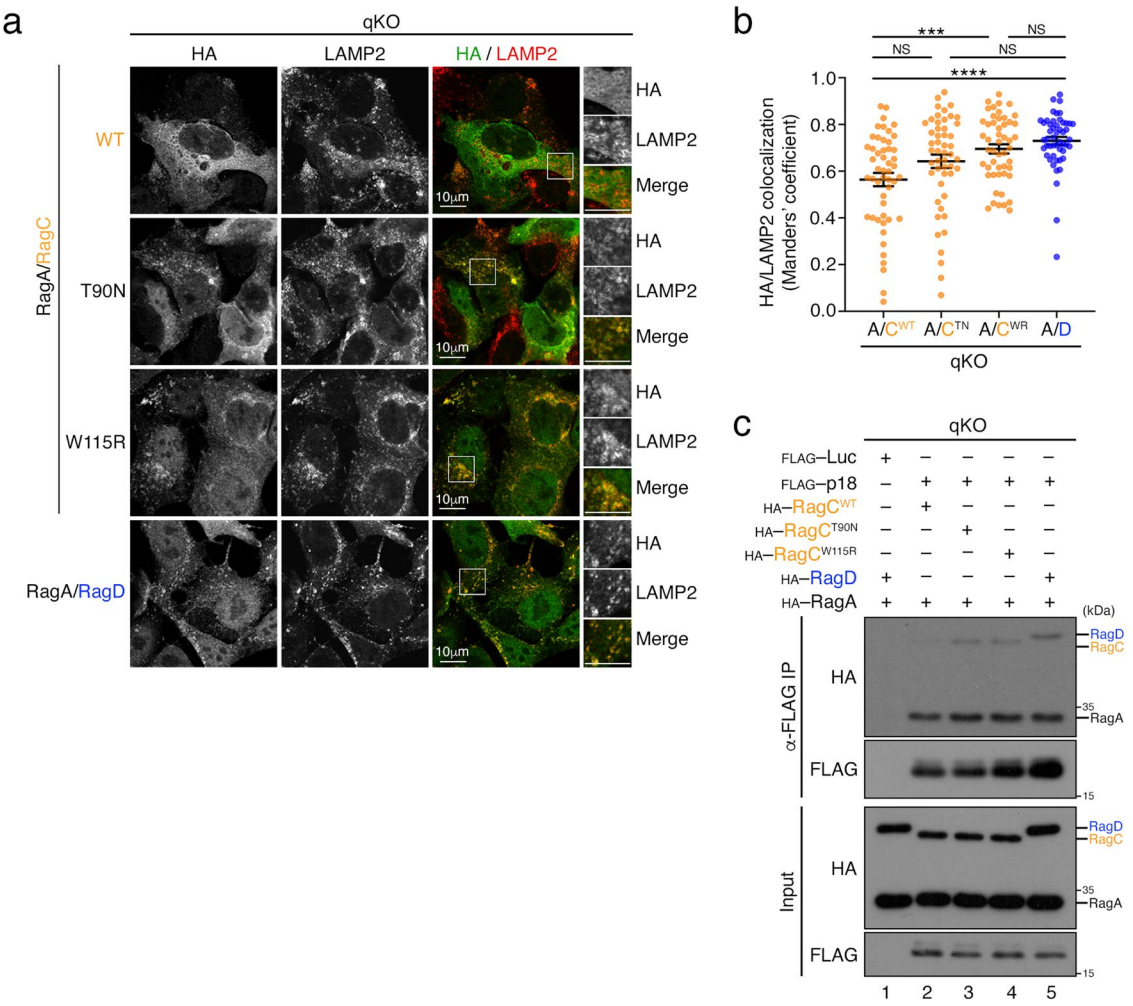

Extended Data Fig. 6 | Cancer-associated RagC mutations show increased lysosomal localization and p18 binding. (a-b) Colocalization analysis between the Rags and LAMP2 (lysosomal marker) in HEK293FT qKO cells stably expressing HA-tagged RagA with WT RagC, RagD, or the T90N and W115R RagC mutants, using confocal microscopy. Magnified insets shown to the right. Scale bars = 10 μm (a). Quantification of HA/LAMP2 colocalization from n = 50 individual cells per condition from a representative experiment out of 2 independent replicates is shown in (b). Data shown as mean ± SEM. *** p<0.005, **** p<0.001. **(c)** The cancer-associated RagC mutants bind more strongly to p18/LAMTOR1, compared to wild-type RagC. Co-immunoprecipitation experiments in HEK293FT qKO cells, transiently expressing FLAG-tagged p18 or Luciferase (Luc) as negative control, and HA-tagged RagA with WT RagC, RagD, or the T90N and W115R RagC mutants. Binding of the Rags to p18 was analyzed by immunoblotting as indicated. n = 2 independent experiments. Source numerical data and unprocessed blots are available in Source Data.

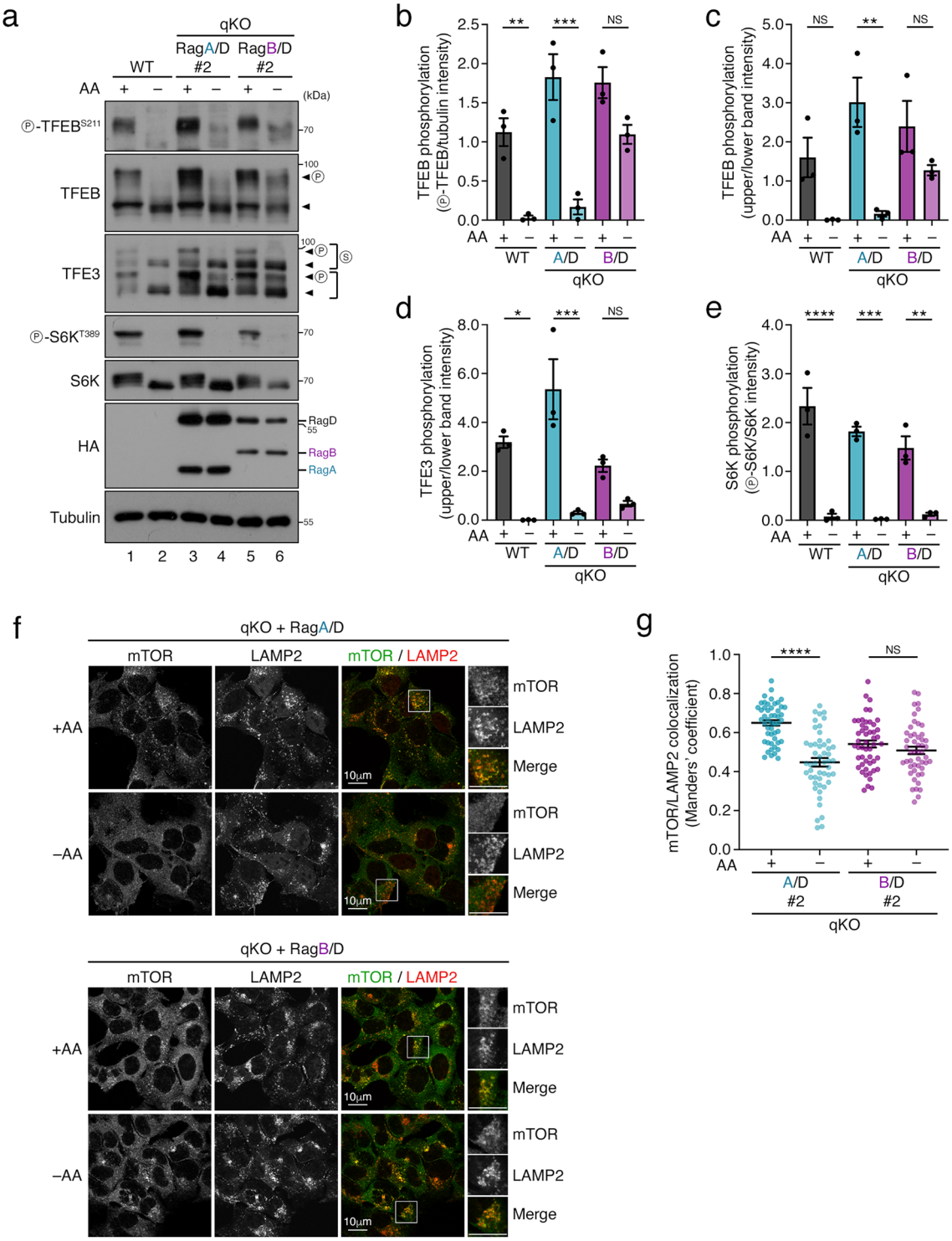

Extended Data Fig. 7 | Analysis of independent RagA/D- and RagB/D-expressing clones. (a-e) Immunoblots with lysates from HEK293FT WT or qKO cells stably expressing RagA/D or RagB/D, treated with media containing (+) or lacking (–) AA, probed with the indicated antibodies. Arrowheads indicate bands corresponding to different protein forms, when multiple bands are present. P: phosphorylated form; S: SUMOylated form (a). Quantification of TFEB, TFE3 and S6K phosphorylation from the blots in (a), shown in (b-c), (d), and (e), respectively. n = 3 independent experiments. **(f-g)** Colocalization analysis of mTOR with LAMP2 (lysosomal marker) in HEK293FT WT or qKO cells stably expressing RagA/D or RagB/D, using confocal microscopy. Magnified insets shown to the right. Scale bars = 10 μm (f). Quantification of mTOR/LAMP2 colocalization from n = 50 individual cells per condition from a representative experiment out of 3 independent replicates is shown in (g). Data in all graphs shown as mean ± SEM. * p<0.05, ** p<0.01, *** p<0.005, **** p<0.001. Source numerical data and unprocessed blots are available in Source Data.

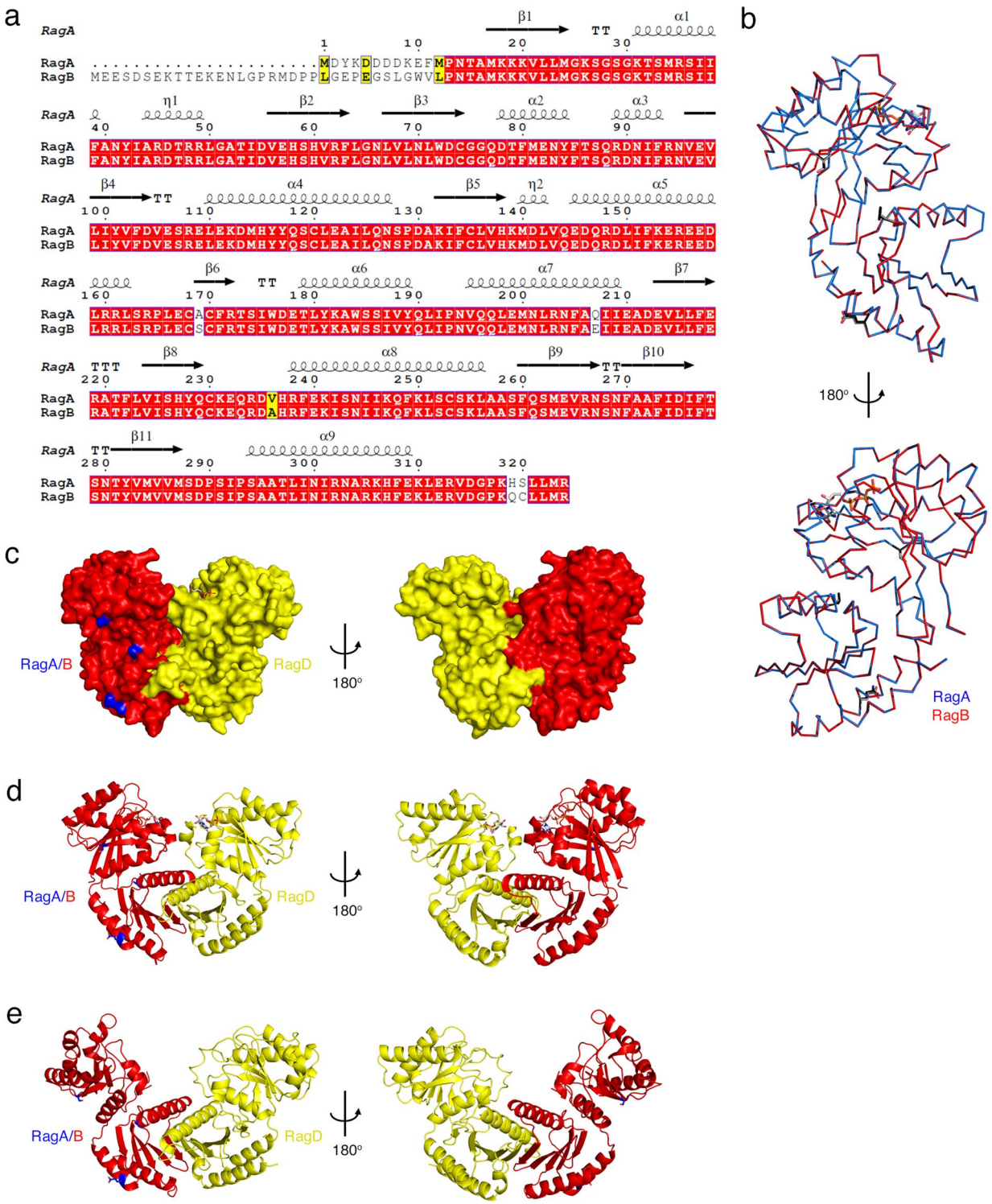

Extended Data Fig. 8 | Structural comparison between RagA and RagB suggests main differences localize to the unstructured N-terminal tail. (a) Structure-based sequence alignment of RagA and RagB prepared with ESPript. Similar and identical residues are marked by yellow and red boxes, respectively. Secondary structure assignment is based on PDBID: 6S6D. **(b)** Residue differences in the structures of RagA and RagB are not predicted to cause overall structural changes. Superposition of the structure of RagA (from PDBID: 6S6D; shown in blue) with RagB (modelled; shown in red) shows high structural similarity between the two structures. Side chains of variable positions shown as dark grey (RagA) or light grey (RagB) sticks. **(c)** Minimal surface residue differences between RagA and RagB. Surface representation of the model of RagB (red) / RagD (yellow) heterodimer in the active conformation (modelled based on PDBID: 6S6D). Variable positions between RagA and RagB are coloured blue. **(d)** Ribbon representation of the model of the RagB (red) / RagD (yellow) heterodimer in the active conformation (modelled based on PDBID: 6S6D). Variable positions between RagA and RagB are coloured blue and side chains are shown as sticks. **(e)** Same as in (d), but for the inactive RagB/D dimer (modelled based on PDBID: 6ULG).

nature portfolio

Corresponding author(s): Dr Constantinos Demetriades

Last updated by author(s): Jun 24, 2022

Reporting Summary

Nature Portfolio wishes to improve the reproducibility of the work that we publish. This form provides structure for consistency and transparency in reporting. For further information on Nature Portfolio policies, see our Editorial Policies and the Editorial Policy Checklist.

Statistics

For all statistical analyses, confirm that the following items are present in the figure legend, table legend, main text, or Methods section.

n/a	Confirmed
☐	☒ The exact sample size (*n*) for each experimental group/condition, given as a discrete number and unit of measurement
☐	☒ A statement on whether measurements were taken from distinct samples or whether the same sample was measured repeatedly
☐	☒ The statistical test(s) used AND whether they are one- or two-sided *Only common tests should be described solely by name; describe more complex techniques in the Methods section.*
☒	☐ A description of all covariates tested
☐	☒ A description of any assumptions or corrections, such as tests of normality and adjustment for multiple comparisons
☐	☒ A full description of the statistical parameters including central tendency (e.g. means) or other basic estimates (e.g. regression coefficient) AND variation (e.g. standard deviation) or associated estimates of uncertainty (e.g. confidence intervals)
☐	☒ For null hypothesis testing, the test statistic (e.g. *F*, *t*, *r*) with confidence intervals, effect sizes, degrees of freedom and *P* value noted *Give P values as exact values whenever suitable.*
☒	☐ For Bayesian analysis, information on the choice of priors and Markov chain Monte Carlo settings
☒	☐ For hierarchical and complex designs, identification of the appropriate level for tests and full reporting of outcomes
☒	☐ Estimates of effect sizes (e.g. Cohen's *d*, Pearson's *r*), indicating how they were calculated

Our web collection on statistics for biologists contains articles on many of the points above.

Software and code

Policy information about availability of computer code

Data collection	No code for data collection was generated in this study. Commercial software packages from other developers used in this study are: Confocal microscopy: Leica Application Suite X 3.5.7.23225; https://www.leica-microsystems.com/products/microscope-software/p/leica-las-x-ls/ qPCR data acquisition: StepOne software, Applied Biosystems, Version 2.2.2; https://www.thermofisher.com/de/de/home/technical-resources/software-downloads/StepOne-and-StepOnePlus-Real-Time-PCR-System.html
Data analysis	No code for data analysis was generated in this study. Commercial software packages from other developers used in this study are: Statistical analysis and graph preparation: GraphPad Prism 9.1.0 (216); https://www.graphpad.com/ Quantification of colocalization: Fiji Version 2.1.0 / 1.53c; https://imagej.net/software/fiji/ Quantification of immunoblots: GelAnalyzer 19.1; http://www.gelanalyzer.com/ Sequence alignment: Clustal Omega (https://www.ebi.ac.uk/Tools/msa/clustalo/); ESPript 3.0 (https://espript.ibcp.fr/ESPript/ESPript/) Modelling of Rag structure: WinCoot 0.8.9 and Refmac5; https://www.ccp4.ac.uk/download/

For manuscripts utilizing custom algorithms or software that are central to the research but not yet described in published literature, software must be made available to editors and reviewers. We strongly encourage code deposition in a community repository (e.g. GitHub). See the Nature Portfolio guidelines for submitting code & software for further information.

Data

Policy information about availability of data

All manuscripts must include a data availability statement. This statement should provide the following information, where applicable:

- Accession codes, unique identifiers, or web links for publicly available datasets
- A description of any restrictions on data availability
- For clinical datasets or third party data, please ensure that the statement adheres to our policy

Uncropped immunoblots and statistics source data are provided as Image Source Data or Numerical Source Data files, respectively, alongside the paper. All other data supporting the findings of this study are available from the corresponding author upon reasonable request. Structure modelling was performed using published structures as described in the 'Structure alignment and Structure modelling' part of the Methods section.

Field-specific reporting

Please select the one below that is the best fit for your research. If you are not sure, read the appropriate sections before making your selection.

☒ Life sciences ☐ Behavioural & social sciences ☐ Ecological, evolutionary & environmental sciences

For a reference copy of the document with all sections, see nature.com/documents/nr-reporting-summary-flat.pdf

Life sciences study design

All studies must disclose on these points even when the disclosure is negative.

Sample size	No statistical methods were used for sample size determination, which was determined in accordance with standard practices in the field and based on our long-standing experience in this type of experimental approaches (e.g., PMIDs 26868506, 33497611, 33974911). For colocalization analysis, 40-50 cells from multiple independent fields were quantified per condition per experiment. For qPCR gene expression analysis, data from 6-7 independent experiments are shown, with 3 technical replicates per experiment.
Data exclusions	No data were excluded from the analyses.
Replication	All findings were reproducible over multiple independent experiments, within a reasonable degree of variability between replicates. The numbers of replicate experiments are provided in the respective figure legends.
Randomization	Sample randomization was not performed for the experiments described in this study, as the order of analysis does not influence the experimental outcomes.
Blinding	No blinding was included in the data collection or analysis, as the method of quantification over multiple replicates and individual cells (for microscopy experiments) ensures unbiased processing.

Reporting for specific materials, systems and methods

We require information from authors about some types of materials, experimental systems and methods used in many studies. Here, indicate whether each material, system or method listed is relevant to your study. If you are not sure if a list item applies to your research, read the appropriate section before selecting a response.

Materials & experimental systems

n/a	Involved in the study
☐	☒ Antibodies
☐	☒ Eukaryotic cell lines
☒	☐ Palaeontology and archaeology
☒	☐ Animals and other organisms
☒	☐ Human research participants
☒	☐ Clinical data
☒	☐ Dual use research of concern

Methods

n/a	Involved in the study
☒	☐ ChIP-seq
☒	☐ Flow cytometry
☒	☐ MRI-based neuroimaging

Antibodies

Antibodies used

Primary antibodies
Rabbit, monoclonal, anti-phospho-TFEB (Ser211), clone E9S8N, #37681, Cell Signaling Technology, Lot #2
Rabbit, polyclonal, ant-TFEB, #4240, Cell Signaling Technology, Lot #3
Rabbit, polyclonal, anti-TFE3, #14779, Cell Signaling Technology, Lot #1
Rabbit, monoclonal, anti-phospho-S6K (Thr389), clone 108D2, #9234, Cell Signaling Technology, Lot #12

Rabbit, polyclonal, anti-S6K, #9202, Cell Signaling Technology, Lot #20
Rabbit, polyclonal, anti-4E-BP1, #9452, Cell Signaling Technology, Lot #12
Rabbit, polyclonal, ant-phospho-4E-BP1 (Thr37/46), #9459, Cell Signaling Technology, Lot #10
Rabbit, polyclonal, ant-phospho-4E-BP1 (Ser65), #9451, Cell Signaling Technology, Lot #16
Rabbit, monoclonal, anti-ULK1, clone D8H5, #8054, Cell Signaling Technology, Lot #7
Rabbit, monoclonal, anti-phospho-ULK1 (Ser757), clone D7O6U, #14202, Cell Signaling Technology, Lot #5
Rabbit, polyclonal, anti-DYKDDDDK Tag, #2368, Cell Signaling Technology, Lot #12
Rabbit, monoclonal, anti-mTOR, clone 7C10, #2983, Cell Signaling Technology, Lot #19
Rabbit, monoclonal, anti-RagA, clone D8B5, #4357, Cell Signaling Technology, Lot #3
Rabbit, monoclonal, anti-RagB, clone D18F3, #8150, Cell Signaling Technology, Lot #1
Rabbit, monoclonal, anti-RagC, clone D8H5, #9480, Cell Signaling Technology, Lot #2
Rabbit, polyclonal, anti-RagD, #4470, Cell Signaling Technology, Lot #2
Rabbit, monoclonal, anti-FLCN, clone D14G9, #3697, Cell Signaling Technology, Lot #3
Rabbit, polyclonal, anti-Cathepsin D, #2284, Cell Signaling Technology, Lot #2
Rabbit, polyclonal, anti-Raptor, #20984-1-AP, Proteintech
Rabbit, polyclonal, anti-LARS, #21146-1-AP, Proteintech
Mouse, monoclonal, anti-alpha-tubulin, clone DM1A, #T9026, Sigma
Rat, monoclonal, anti-HA, clone 3F10, #11867423001, Roche
Mouse, monoclonal, anti-LAMP2, clone H4B4, Developmental Studies Hybridoma Bank

Secondary antibodies
Peroxidase-conjugated AffiniPure donkey anti-rabbit IgG (H+L), polyclonal, #711-035-152, Jackson ImmunoResearch
Peroxidase-conjugated AffiniPure donkey anti-mouse IgG (H+L), polyclonal, #715-035-151, Jackson ImmunoResearch
Peroxidase-conjugated AffiniPure donkey anti-rat IgG (H+L), polyclonal, #712-035-153, Jackson ImmunoResearch
Rhodamine (TRITC)-conjugated AffiniPure donkey anti-mouse IgG (H+L), polyclonal, #715-025-150, Jackson ImmunoResearch
Fluorescein (FITC)-conjugated AffiniPure donkey anti-rabbit IgG (H+L), polyclonal, #711-095-152, Jackson ImmunoResearch
Alexa Fluor 488-conjugated AffiniPure donkey anti-rabbit IgG (H+L), polyclonal, #711-545-152, Jackson ImmunoResearch
Alexa Fluor 647-conjugated AffiniPure donkey anti-rat IgG (H+L) polyclonal, #712-605-153, Jackson ImmunoResearch

Validation

Specificity of phospho-antibodies extensively verified in this study and in the context of other projects in the Demetriades lab, using inhibitors for the respective kinases or starvation media.
Specificity of total protein antibodies extensively verified in this study and in the context of other projects in the Demetriades lab, using knock-out cell lines, or knock-down and overexpression experiments.

Additional information for all antibodies used in this study can be found in the manufacturer's website for each product:

anti-phospho-TFEB (Ser211), #37681, Cell Signaling Technology, validated for Western Blotting, relevant citations can be found on the manufacturer's website (https://www.cellsignal.com/products/primary-antibodies/phospho-tfeb-ser211-e9s8n-rabbit-mab/37681)

anti-TFEB, #4240, Cell Signaling Technology, validated for Western Blotting and Immunoprecipitation, relevant citations can be found on the manufacturer's website (https://www.cellsignal.com/products/primary-antibodies/tfeb-antibody/4240)

anti-TFE3, #14779, Cell Signaling Technology, validated for Western Blotting, relevant citations can be found on the manufacturer's website (https://www.cellsignal.com/products/primary-antibodies/tfe3-antibody/14779)

anti-phospho-S6K (Thr389), #9234, Cell Signaling Technology, validated for Western Blotting, relevant citations can be found on the manufacturer's website (https://www.cellsignal.com/products/primary-antibodies/phospho-p70-s6-kinase-thr389-108d2-rabbit-mab/9234)

anti-S6K, #9202, Cell Signaling Technology, validated for Western Blotting and Immunoprecipitation, relevant citations can be found on the manufacturer's website (https://www.cellsignal.com/products/primary-antibodies/p70-s6-kinase-antibody/9202)

anti-4E-BP1, #9452, Cell Signaling Technology, validated for Western Blotting, relevant citations can be found on the manufacture's website (https://www.cellsignal.com/products/primary-antibodies/4e-bp1-antibody/9452)

anti-phospho-4E-BP1 (Thr37/46), #9459, Cell Signaling Technology, validated for Western Blotting, relevant citations can be found on the manufacture's website (https://www.cellsignal.com/products/primary-antibodies/phospho-4e-bp1-thr37-46-antibody/9459)

anti-phospho-4E-BP1 (Ser65), #9451, Cell Signaling Technology, validated for Western Blotting, relevant citations can be found on the manufacture's website (https://www.cellsignal.com/products/primary-antibodies/phospho-4e-bp1-ser65-antibody/9451)

anti-ULK1, #8054, Cell Signaling Technology, validated for Western Blotting, relevant citations can be found on the manufacture's website
(https://www.cellsignal.com/products/primary-antibodies/ulk1-d8h5-rabbit-mab/8054)

anti-phospho-ULK1 (Ser757), #14202, Cell Signaling Technology, validated for Western Blotting, relevant citations can be found on the manufacture's website
(https://www.cellsignal.com/products/primary-antibodies/phospho-ulk1-ser757-d7o6u-rabbit-mab/14202)

anti-DYKDDDDK Tag, #2368, Cell Signaling Technology, validated for Western Blotting, Immunoprecipitation and Flow Cytometry, relevant citations can be found on the manufacturer's website (https://www.cellsignal.com/products/primary-antibodies/dykddddk-tag-antibody-binds-to-same-epitope-as-sigma-s-anti-flag-m2-antibody/2368)

anti-mTOR, #2983, Cell Signaling Technology, validated for Western Blotting, Immunohistochemistry, Immunofluorescence and Flow Cytometry, relevant citations can be found on the manufacturer's website (https://www.cellsignal.com/products/primary-antibodies/

mtor-7c10-rabbit-mab/2983)

anti-RagA, #4357, Cell Signaling Technology, validated for Western Blotting and Immunoprecipitation, relevant citations can be found on the manufacturer's website (https://www.cellsignal.com/products/primary-antibodies/raga-d8b5-rabbit-mab/4357)

anti-RagB, #8150, Cell Signaling Technology, validated for Western Blotting and Immunoprecipitation, relevant citations can be found on the manufacturer's website (https://www.cellsignal.com/products/primary-antibodies/ragb-d18f3-rabbit-mab/8150)

anti-RagC, #9480, Cell Signaling Technology, validated for Western Blotting, Immunoprecipitation, Immunofluorescence and Flow Cytometry, relevant citations can be found on the manufacturer's website (https://www.cellsignal.com/products/primary-antibodies/ragc-d8h5-rabbit-mab/9480)

anti-RagD, #4470, Cell Signaling Technology, validated for Western Blotting, relevant citations can be found on the manufacturer's website (https://www.cellsignal.com/products/primary-antibodies/ragd-antibody/4470)

anti-FLCN, #3697, Cell Signaling Technology, validated for Western Blotting and Immunoprecipitation, relevant citations can be found on the manufacturer's website (https://www.cellsignal.com/products/primary-antibodies/flcn-d14g9-rabbit-mab/3697)

anti-Cathepsin D, #2284, Cell Signaling Technology, validated for Western Blotting and Immunohistochemistry, relevant citations can be found on the manufacturer's website (https://www.cellsignal.com/products/primary-antibodies/cathepsin-d-antibody/2284)

anti-Raptor, #20984-1-AP, proteintech, validated for Western Blotting, Immunoprecipitation, Immunohistochemistry and Immunofluorescence, relevant citations can be found on the manufacturer's website (https://www.ptglab.com/products/RPTOR-Antibody-20984-1-AP.htm#tested-applications)

anti-LARS, #21146-1-AP, proteintech, validated for Western Blotting, Immunoprecipitation, Immunohistochemistry and Immunofluorescence, relevant citations can be found on the manufacturer's website (https://www.ptglab.com/products/LARS-Antibody-21146-1-AP.htm)

anti-alpha-tubulin, #T9026, Sigma, validated for Western Blotting and Immunofluorescence, relevant citations can be found on the manufacturer's website (https://www.sigmaaldrich.com/DE/en/product/sigma/t9026)

anti-HA, #11867423001, Roche, validated for Western Blotting, Dot Blots, ELISA, Immunocytochemistry and Immunoprecipitation, relevant citations can be found on the manufacturer's website (https://www.sigmaaldrich.com/DE/en/product/roche/roahaha)

anti-LAMP2, clone H4B4, Developmental Studies Hybridoma Bank, validated for Western Blotting, FACS, Function Blocking, Immunofluorescence, Immunohistochemistry and Immunoprecipitation, relevant citations can be found on the manufacturer's website (https://dshb.biology.uiowa.edu/H4B4)

Eukaryotic cell lines

Policy information about cell lines

Cell line source(s)	The parental HEK293FT cells were purchased from Invitrogen before the initiation of the project.
Authentication	The identity of the parental HEK293FT cells was validated by the Multiplex human Cell Line Authentication test (Multiplexion GmbH), which uses a single nucleotide polymorphism (SNP) typing approach, and was performed as described at www.multiplexion.de.
Mycoplasma contamination	All cell lines were regularly tested for Mycoplasma contamination, using a PCR-based approach and were confirmed to be Mycoplasma-free.
Commonly misidentified lines (See ICLAC register)	No commonly misidentified lines were used in this study.

nature portfolio

https://doi.org/10.1038/s41556-022-00976-y

Supplementary information

A Rag GTPase dimer code defines the regulation of mTORC1 by amino acids

In the format provided by the authors and unedited

Supplementary Figures 1-7

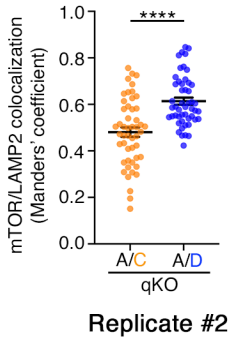

Suppl. Fig. 1. Replicate of experiment in Fig. 1g-h. Quantification of mTOR/LAMP2 colocalization in RagA/C and RagA/D expressing cells, showing higher lysosomal localization of mTOR in the latter. Fifty individual cells were analysed per condition. Data shown as mean ± SEM. **** p<0.001. Source numerical data are available in Source Data.

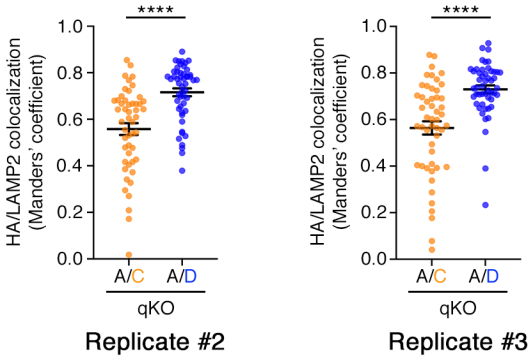

Suppl. Fig. 2. Replicates of experiment in Fig. 3a-b. Quantification of HA/LAMP2 colocalization in RagA/C and RagA/D expressing cells, showing higher lysosomal localization of RagD-containing dimers. The data shown in the right panel were also used in the graph in Ext. Data Fig. 5b. Fifty individual cells were analysed per condition. Data shown as mean ± SEM. **** p<0.001. Source numerical data are available in Source Data.

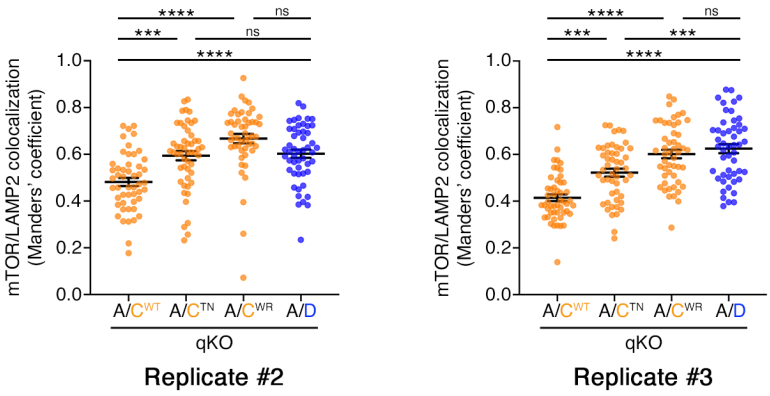

Suppl. Fig. 3. Replicates of experiment in Fig. 5g-h. Quantification of mTOR/LAMP2 colocalization in cells expressing wild-type RagA/C, RagA/D, or cancer-associated RagC mutants, showing higher lysosomal localization of mTOR in the RagC mutants (C^{TN}, C^{WR}), compared to WT RagC (C^{WT}). Fifty individual cells were analysed per condition. Data shown as mean ± SEM. *** p<0.005, **** p<0.001. Source numerical data are available in Source Data.

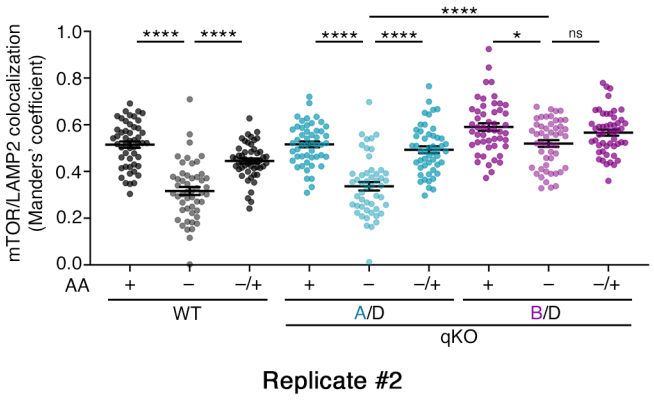

Suppl. Fig. 4. Replicate of experiment in Fig. 6f-g. Quantification of mTOR/LAMP2 colocalization in WT, RagA/D, and RagB/D expressing cells, showing compromised AA starvation response and incomplete delocalization of mTOR from lysosomes in the latter. Fifty individual cells were analysed per condition. Data shown as mean ± SEM. * p<0.05, **** p<0.001. Source numerical data are available in Source Data.

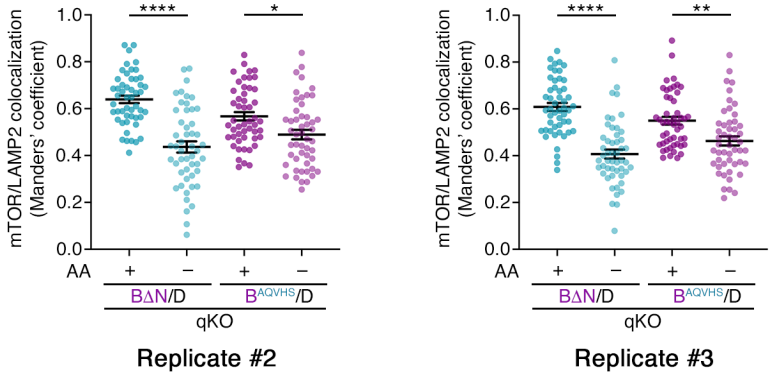

Suppl. Fig. 5. Replicates of experiment in Fig. 7d-e. Quantification of mTOR/LAMP2 colocalization in WT, RagA/C and RagB/D expressing cells, showing compromised AA starvation response and incomplete delocalization of mTOR from lysosomes in the latter. Fifty individual cells were analysed per condition. Data shown as mean ± SEM. * p<0.05, ** p<0.01, **** p<0.001. Source numerical data are available in Source Data.

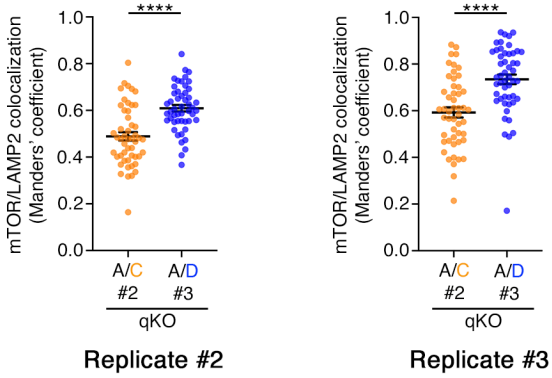

Suppl. Fig. 6. Replicates of experiment in Ext. Data Fig. 3f-g. Quantification of mTOR/LAMP2 colocalization in RagA/C and RagA/D expressing cells (additional clones #2), showing higher lysosomal localization of mTOR in the latter. Fifty individual cells were analysed per condition. Data shown as mean ± SEM. **** p<0.001. Source numerical data are available in Source Data.

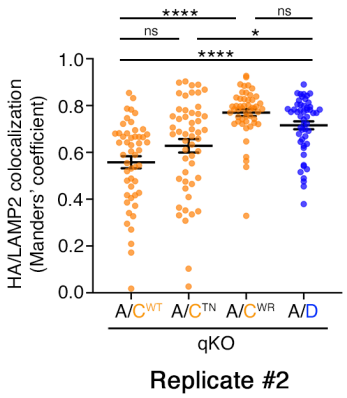

Suppl. Fig. 7. Replicate of experiment in Ext. Data Fig. 6a-b. Quantification of HA/LAMP2 colocalization in cells expressing wild-type RagA/C, RagA/D, or cancer-associated RagC mutants, showing higher lysosomal localization of the RagC mutants (C^{TN}, C^{WR}), compared to WT RagC (C^{WT}). Fifty individual cells were analysed per condition. Data shown as mean ± SEM. * p<0.05, ** p<0.01, *** p<0.005, **** p<0.001. Source numerical data are available in Source Data.

Chapter 2. Unbiased Evaluation of Rapamycin's Specificity as an mTOR inhibitor

Artoni F, **Grützmacher N**, Demetriades C.

Published in Aging Cell (2023) e13888. Reprint with submission from Artoni *et al.*
Supplementary Material is provided after the publication.

Statement of contribution:
In this publication, I designed the CRISPR-Cas9 genome editing vector to generate the mutant cell line with the necessary guide RNAs and donor oligos to insert the respective point mutation in the *MTOR* gene. Furthermore, I generated several of the western blot experiments including replicates (Fig 1c-f) as well as performed the co-IP experiments with all necessary replicates (Fig 1b). Finally, I gave my scientific input to the text that was written by Filippo Artoni and Dr. Constantinos Demetriades.

Received: 22 December 2022 | Revised: 2 May 2023 | Accepted: 7 May 2023

DOI: 10.1111/acel.13888

Aging Cell WILEY

RESEARCH ARTICLE

Unbiased evaluation of rapamycin's specificity as an mTOR inhibitor

Filippo Artoni[1,2] | Nina Grützmacher[1] | Constantinos Demetriades[1,2,3]

[1]Max Planck Institute for Biology of Ageing (MPI-AGE), Cologne, Germany

[2]Cologne Graduate School of Ageing Research (CGA), Cologne, Germany

[3]Cologne Excellence Cluster on Cellular Stress Responses in Aging-Associated Diseases (CECAD), University of Cologne, Cologne, Germany

Correspondence
Constantinos Demetriades, Max Planck Institute for Biology of Ageing (MPI-AGE), 50931 Cologne, Germany.
Email: demetriades@age.mpg.de

Funding information
H2020 European Research Council, Grant/Award Number: 757729; Max-Planck-Gesellschaft

Abstract

Rapamycin is a macrolide antibiotic that functions as an immunosuppressive and anti-cancer agent, and displays robust anti-ageing effects in multiple organisms including humans. Importantly, rapamycin analogues (rapalogs) are of clinical importance against certain cancer types and neurodevelopmental diseases. Although rapamycin is widely perceived as an allosteric inhibitor of mTOR (mechanistic target of rapamycin), the master regulator of cellular and organismal physiology, its specificity has not been thoroughly evaluated so far. In fact, previous studies in cells and in mice hinted that rapamycin may be also acting independently from mTOR to influence various cellular processes. Here, we generated a gene-edited cell line that expresses a rapamycin-resistant mTOR mutant ($mTOR^{RR}$) and assessed the effects of rapamycin treatment on the transcriptome and proteome of control or $mTOR^{RR}$-expressing cells. Our data reveal a striking specificity of rapamycin towards mTOR, demonstrated by virtually no changes in mRNA or protein levels in rapamycin-treated $mTOR^{RR}$ cells, even following prolonged drug treatment. Overall, this study provides the first unbiased and conclusive assessment of rapamycin's specificity, with potential implications for ageing research and human therapeutics.

KEYWORDS
ageing, mTORC1, proteomics, rapamycin, sirolimus

1 | INTRODUCTION

Rapamycin (also known as sirolimus) is a naturally occurring macrolide compound which was originally isolated from soil bacteria on Easter Island (Rapa Nui) in 1972 (Arriola Apelo & Lamming, 2016; Benjamin et al., 2011; Li et al., 2014). Rapamycin was primarily used in the clinic as an anti-fungal agent until 1999 when it was approved by the FDA for the prevention of kidney transplant rejection and later for the treatment of advanced kidney cell carcinoma. Its immunosuppressive and anti-proliferative properties are thought to be largely mediated by inhibition of mTOR, a serine/threonine kinase that functions as the master regulator of most cellular functions, including immune cell activation and cell growth control (Arriola Apelo & Lamming, 2016; Benjamin et al., 2011; Fernandes & Demetriades, 2021; Li et al., 2014). At the molecular level, rapamycin inhibits mTORC1 (mTOR complex 1) activity as a complex with the cytosolic immunophilin FKBP12 (FK506-binding protein 12). Binding of this drug-protein complex to mTOR blocks access to its catalytic site and prevents the phosphorylation of key substrates like S6K (ribosomal protein S6 kinase) (Chung et al., 1992). Additional

Abbreviations: Cas9, CRISPR-associated protein 9; CRISPR, Clustered Regularly Interspaced Short Palindromic Repeats; EMA, European Medicine Agency; FDA, Federal Food and Drug Administration; TGFβ, Transforming Growth Factor beta; TRP channel, transient receptor potential channel.

immunophilins such as FKBP12.6, FKBP51, and FKBP52 have also been reported to bind and shape the pharmacology of rapamycin (März et al., 2013).

Over the last two decades, rapamycin has gained renewed interest after multiple studies uncovered its powerful anti-ageing properties (Arriola Apelo & Lamming, 2016; Benjamin et al., 2011; Fernandes & Demetriades, 2021; Li et al., 2014). Rapamycin has been repeatedly shown to extend lifespan and/or healthspan in worms (Robida-Stubbs et al., 2012), flies (Bjedov et al., 2010; Castillo-Quan et al., 2019; Schinaman et al., 2019), and mice (Bitto et al., 2016; Fok et al., 2014; Harrison et al., 2009). It extends chronological age in yeast (Powers et al., 2006) and reduces markers of senescence in cultured cells (Wang et al., 2017). More recently, studies conducted on marmoset monkeys have demonstrated rapamycin to have a good safety and tolerability profile (Lelegren et al., 2016; Tardif et al., 2015) thus paving the way for human trials. Currently, trials are underway both on companion dogs (Creevy et al., 2022) and humans (NCT04488601) with preliminary evidence suggesting improvement in cardiac function in middle-aged dogs who received rapamycin for 10 weeks (Urfer et al., 2017). Furthermore, RAD001/everolimus, a rapamycin analogue, was shown to improve immune function and the response to influenza vaccination in elderly humans (Kennedy & Pennypacker, 2015; Mannick et al., 2014). Notably, rapamycin extends lifespan at doses much lower than the ones used to achieve immunosuppression in transplant patients thus minimizing potential side effects. Finally, even transient, intermittent, or late-life rapamycin administration has been shown to extend lifespan in flies and mice thus making rapamycin an attractive option for human use as an anti-ageing compound (Bitto et al., 2016; Harrison et al., 2009; Partridge et al., 2020).

The target specificity of rapamycin has recently been debated. On one hand, *in vitro* kinase activity assays showed other serine/threonine kinases, besides mTOR, to be largely insensitive to rapamycin up to concentrations at the micromolar range. Likewise, receptor-binding assays indicated that many ligand-receptor interactions remain unaffected by rapamycin, with the possible exception of histamine I binding (EMA, 2005). On the other hand, accumulating evidence in the literature suggest that rapamycin may exert some of its effects via mTOR-independent mechanisms. This is also supported by the fact that most kinase inhibitors demonstrate very low target selectivity (Hantschel, 2015; Hantschel et al., 2012; Karaman et al., 2008). For instance, rapamycin was suggested to block the exercise-induced accumulation of ribosomal RNA (rRNA) in the skeletal muscle of both wild-type mice and mice containing a rapamycin-resistant mTOR allele (Goodman et al., 2011). Moreover, rapamycin and other rapalogs were shown to directly bind and activate the lysosomal mucolipin TRP channel (TRPML1; also known as MCOLN1) independently of mTOR inhibition (Zhang et al., 2019). Finally, since FKBPs serve as chaperones for proper folding of several proteins (Bonner & Boulianne, 2017; Bultynck et al., 2001; Galfre et al., 2012; Vervliet et al., 2015; Wang et al., 1996), it can be speculated that their binding to rapamycin may be influencing cellular physiology via altering the interaction of FKBPs to their client proteins.

Here, to conclusively address this important unresolved issue, we generated a rapamycin-resistant cell line by editing a single base in the *MTOR* gene at its endogenous locus (Choi et al., 1996; Hosoi et al., 1999; Lorenz & Heitman, 1995) and assessed how rapamycin affects the cellular transcriptome and proteome in an unbiased manner. These experiments unraveled an impressive specificity of rapamycin towards mTOR, with the rapamycin effects on gene expression and protein levels being virtually non-existent in the mTOR-mutant cells.

2 | RESULTS

2.1 | Generation and characterization of a gene-edited cell line that expresses rapamycin-resistant mTOR

Mutations in the mTOR FRB (FKBP-rapamycin-binding) domain that disrupt its interaction with FKBP12 and confer rapamycin resistance to mTOR have been described almost 30 years ago (Brown et al., 1995; Chen et al., 1995; Choi et al., 1996; Hara et al., 1997; Hosoi et al., 1999; Lorenz & Heitman, 1995). Although such mTOR mutants have been used in previous studies, usually expressed exogenously in cells or via transgenic expression in mouse tissues, the presence of endogenous wild-type mTOR has complicated the interpretation of these results (Ge et al., 2009; Goodman et al., 2011; Luo et al., 2015; Zhang et al., 2000). Moreover, a thorough analysis of rapamycin's effects in such cellular models, beyond single readouts, is lacking. Therefore, to probe whether rapamycin also acts through mTOR-independent mechanisms or exclusively via mTOR inhibition, we used CRISPR/Cas9-mediated gene editing to generate a HEK293FT cell line that expresses a Ser2035Thr mTOR mutant (Figure 1a, Figure S1) that was previously described to be rapamycin-resistant (Brown et al., 1995; Chen et al., 1995; Choi et al., 1996; Hara et al., 1997; Hosoi et al., 1999; Lorenz & Heitman, 1995). Intuitively, we named this mutant and the associated cell line, mTOR^{RR} (mTOR rapamycin-resistant). Importantly, as we mutated *MTOR* in the endogenous locus, no wild-type mTOR is expressed in these cells, verified by genomic DNA sequencing (Figure S1). Consistent with previous reports, the rapamycin-induced interaction of FLAG-tagged FKBP12 with wild-type mTOR, was completely abrogated in mTOR^{RR} (Figure 1b). Of note, the catalytic activity of mTORC1 containing mTOR^{RR}, as assessed by the phosphorylation of its direct substrate S6K, was indistinguishable from that in control cells and was diminished by treatment with Torin1, an ATP-competitive mTOR inhibitor (Figure 1c). In contrast, mTOR^{RR} demonstrated complete resistance to rapamycin even when cells were treated with this compound at micromolar concentrations (Figure 1c), or when the treatment was extended to 24 or 48 h (Figure 1d). Similar to rapamycin, mTOR^{RR} also exhibited full resistance to other rapalogs like everolimus and temsirolimus (Figure 1e), but responded properly to amino acid (AA) starvation, showing that the regulation of mTORC1 by other inhibitory stimuli

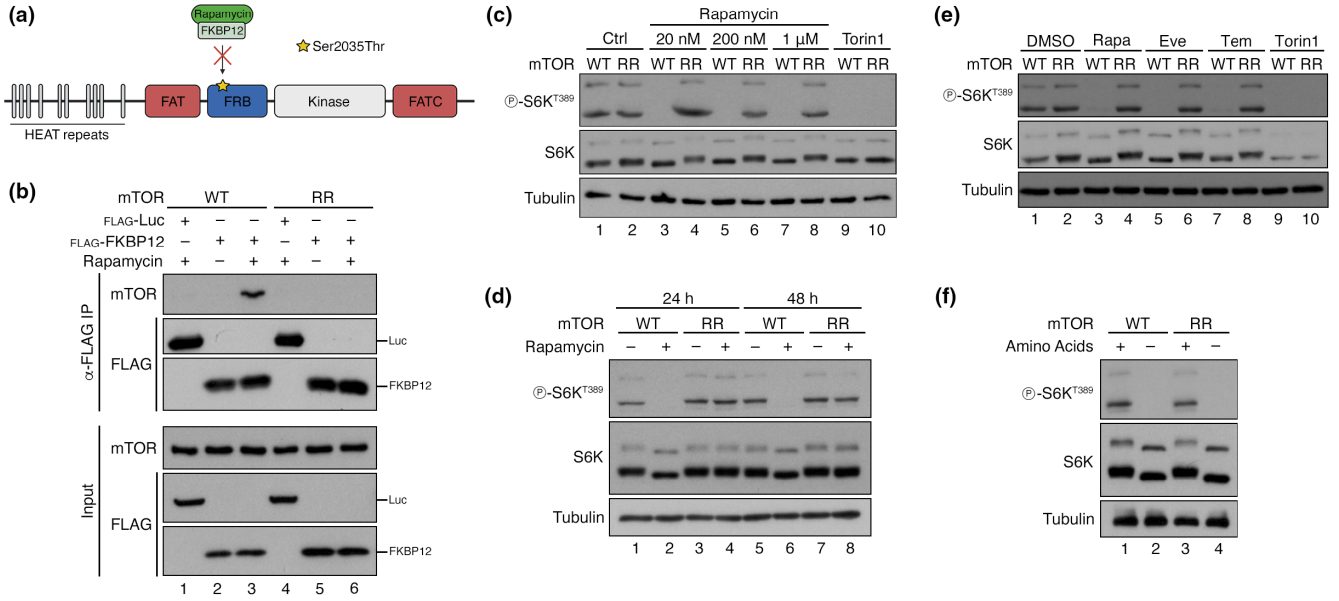

FIGURE 1 Generation and characterization of a gene-edited cell line that expresses rapamycin-resistant mTOR. (a) Schematic model of the mTOR protein depicting key domains and the location of the Ser2035Thr substitution in the FRB domain that prevents its inhibition by rapamycin/FKBP12. (b) Diminished binding of FKBP12 to the mTOR^{RR} mutant protein. Co-immunoprecipitation experiments in control (WT) or mTOR^{RR} HEK293FT cells, transiently expressing FLAG-tagged FKBP12 or Luciferase (Luc) as negative control, treated with rapamycin (20 nM, 1 h) or DMSO. Binding of mTOR to FKBP12 was analysed by immunoblotting as indicated. (c) mTOR^{RR} does not respond to rapamycin even at extremely high concentrations. Immunoblots with lysates from HEK293FT WT and mTOR^{RR} cells treated for 1 h with 20 nM to 1 μM rapamycin as indicated, 250 nM Torin1, or DMSO as control. mTORC1 activity was assessed by S6K phosphorylation. (d) mTOR^{RR} is resistant to long-term rapamycin treatment. Immunoblots with lysates from HEK293FT WT and mTOR^{RR} cells treated with DMSO or rapamycin (20 nM) for 24 or 48 h, probed with the indicated antibodies. (e) mTOR^{RR} shows resistance to multiple rapalogs. Immunoblots with lysates from HEK293FT WT and mTOR^{RR} cells treated with DMSO, rapamycin (Rapa; 20 nM), everolimus (Eve; 20 nM), temsirolimus (Tem; 20 nM), or Torin1 (250 nM) for 1 h, probed with the indicated antibodies. (f) Cell expressing mTOR^{RR} have active mTORC1 that responds properly to AA starvation. Immunoblots with lysates from HEK293FT WT and mTOR^{RR} cells treated with control (+) or AA-free media (–) for 1 h, probed with the indicated antibodies.

is unperturbed in mTOR^{RR} cells (Figure 1f). In sum, the mTOR^{RR} HEK293FT cell line is a 'clean', reliable and robust model to investigate rapamycin's specificity towards mTOR.

2.2 | Rapamycin alters gene expression exclusively via mTOR inhibition

Having validated our experimental model, we then treated control (WT) and mTOR^{RR} cells with rapamycin for 24 h and performed RNA-seq experiments to investigate its effects on global gene expression. In line with mTOR—directly or indirectly—regulating the activity of several transcription factors (Hardwick et al., 1999; Laplante & Sabatini, 2013), we detected more than 5000 genes whose expression changed significantly in WT cells upon rapamycin treatment (Figure 2a,b, Table S1). Our analysis identified several genes that are known to be affected by mTOR inhibition (e.g., HMOX1, RHOB, MYC) (Bayeva et al., 2012; Gordon et al., 2015; Jin et al., 2013; Sun et al., 2022; Visner et al., 2003) (Figure 2b) thus validating our experimental setup. Similarly, rapamycin decreased the expression of AA transporters like SLC7A5 and SLC7A11, which are known to be regulated downstream of an mTORC1-ATF4 axis (Torrence et al., 2021) (Figure 2b, Tables S1 and S2).

Gene ontology (GO) term enrichment analysis, using the differentially regulated genes that are strongly down- or up-regulated by rapamycin ($Log_2FC < -0.75$ and $Log_2FC > +0.8$, respectively; and adjusted p-value <0.05), revealed a strong enrichment of ribosome-related Biological Process (BP) and Cellular Component (CC) terms (e.g., BP:GO:0042254 ~ ribosome biogenesis; CC:GO:0030684 ~ preribosome) (Figure 2c,d, Table S2). Confirming the well-known role of mTOR in promoting ribosome biogenesis and positively regulating rRNA expression (Mayer & Grummt, 2006; Powers & Walter, 1999), all genes that fall under these terms (e.g., RRP12, RRP9, RRS1, RRP1, RPF2, NOP16, NOL6, DDX21, MRTO4, MRM1) were found to be downregulated by rapamycin (Figure 2c,d, Table S2). Interestingly, we also observed a strong enrichment of terms related to mitochondria-resident proteins (e.g., CC:GO:0005739 ~ mitochondrion; CC:GO:0005759 ~ mitochondrial matrix) and associated mitochondrial functions (e.g., BP:GO:0019752 ~ carboxylic acid metabolic process) among the genes that are differentially regulated by rapamycin (Figure 2c,d, Table S2). Similar results were obtained when performing the GO analysis with more relaxed criteria including all significantly down- and upregulated genes, instead of setting cut-offs for those that change robustly upon rapamycin (Figure S2a,b, Table S3). Strikingly, unlike the pervasive transcriptional effects of rapamycin in control

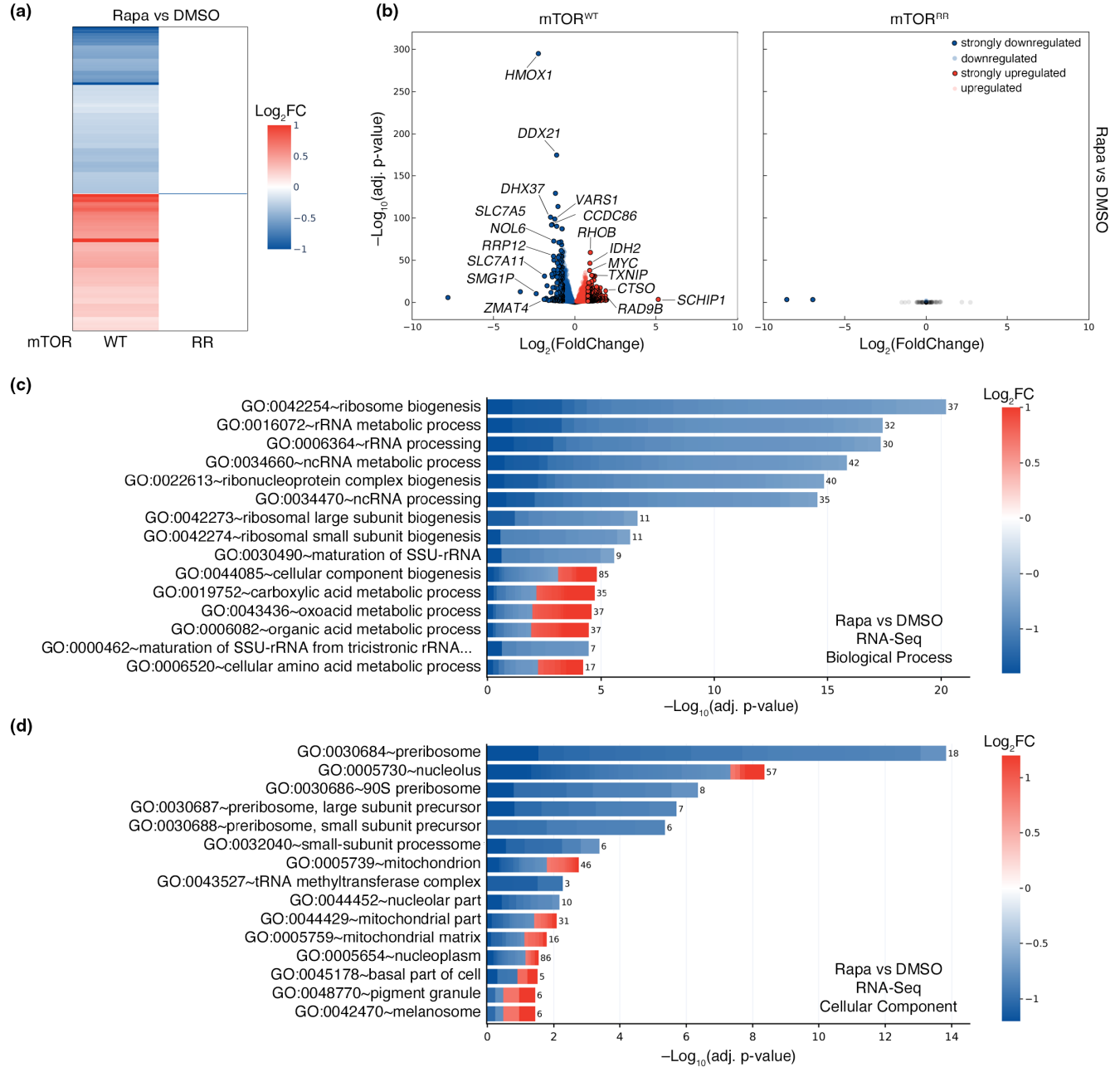

FIGURE 2 Rapamycin alters gene expression exclusively via mTOR inhibition. (a) Heatmap depicting the rapamycin-induced changes in gene expression in HEK293FT WT and mTOR^{RR} cells. RNA-seq data from cells treated with rapamycin (20 nM, 24 h) expressed as log-transformed fold change (Log$_2$FC). Only statistically-significant changes (adj. *p*-value <0.05) are shown. (b) Volcano plots showing the rapamycin-induced changes in gene expression in HEK293FT WT (left) and mTOR^{RR} (right) cells from the RNA-seq experiment described in (a). Genes that are significantly (adj. *p*-value <0.05) down- or upregulated by rapamycin are shown in blue or red respectively. Strongly down- (Log$_2$FC < −0.75) or upregulated (Log$_2$FC > +0.8) genes are shown with black outline. Unaffected genes (adj. *p*-value >0.05) shown as grey dots. Selected genes are marked in the plot. (c) Biological process (BP) GO term analysis using the genes that are strongly down- (blue) or upregulated (red) by rapamycin in WT cells as described in (b). The colour of each box in the cell plot represents log-transformed fold change values for each gene in rapamycin- vs DMSO-treated cells. The number of genes in the selected dataset for each GO term is shown on the right side of each bar. (d) As in (c), but for Cellular Component (CC) GO term analysis.

cells, we found only two genes (*UPK3BL1*, *AC007326.4*) whose expression was altered in mTOR^{RR} cells treated with rapamycin, based on the same selection criteria (Figure 2a,b, Table S1). These data indicate that rapamycin practically regulates transcription exclusively via its direct inhibitory effect on mTOR.

2.3 | Rapamycin alters the cellular proteome exclusively through mTOR

In addition to their involvement in transcriptional regulation, the best-described role of rapamycin and mTORC1 is in the control of

de novo protein synthesis via regulating the phosphorylation and activity of—direct or indirect—mTORC1 targets like S6K, 4E-BP1, and S6, with only certain 4E-BP1 phospho-sites being rapamycin-sensitive (Thoreen et al., 2009, 2012). Therefore, we next sought to investigate the rapamycin-induced changes in the cellular proteome and explore the extent to which this happens because of mTOR inhibition.

To this end, we treated control and mTOR^{RR} cells with rapamycin for 24 or 48 h and performed whole-proteome quantitative mass spectrometry experiments. Out of a total of approximately 7500 proteins that were detected and quantified, the levels of more than 2500 and 2300 proteins changed significantly in WT cells treated with rapamycin for 24 or 48 h, respectively (Figure 3a–c, Table S4). Similar to what we observed in transcriptomic analyses, these hits include multiple proteins belonging to pathways that have been previously described to be regulated by rapamycin and mTOR (e.g., PDCD4, RHOB, HMOX1, SQSTM1, PRELID1, SCD, SESN2) (Bayeva et al., 2012; Dorrello et al., 2006; Gordon et al., 2015; Jin et al., 2013; Ko et al., 2017; Mauvoisin et al., 2007; Sun et al., 2022; Visner et al., 2003; Wall et al., 2008; Zhu et al., 2020) as well as several amino acid transporters (SLC7A11, SLC38A10, SLC3A2, SLC7A5) (Graber et al., 2017; Nachef et al., 2021; Torrence et al., 2021; Zhang et al., 2021) (Figure 3b,c, Table S4). Remarkably, however, none of the 7574 detected proteins were differentially regulated in rapamycin-treated mTOR^{RR} cells, even after prolonged drug treatment (Figure 3a–c, Table S4), again showing complete absence of mTOR-independent effects of rapamycin.

Consistent with our observations from RNA-seq experiments, GO analysis using all proteins that are significantly down- or upregulated (adj. *p*-value <0.05) upon 24-h rapamycin treatment in WT cells showed strong enrichment of terms related to ribosomes and translation (e.g., BP:GO:0022613 ~ ribonucleoprotein complex biogenesis; BP:GO:0042254 ~ ribosome biogenesis; BP:GO:0006412 ~ translation) (Figure 3d, Table S5) with the majority of proteins that belong to this category being downregulated (e.g., CDC123, LTV1, RRN3, EIF1AD, SESN2, GNL3L, CCDC86, WDR74, NUFIP1, CDK4) (Figure 3b,d, Tables S4 and S5). Another prominent group of GO terms that is enriched in the proteomic analysis includes terms related to the cell cycle (e.g., BP:GO:0007049 ~ cell cycle, BP:GO:0000278 ~ mitotic cell cycle) (Figure 3d, Tables S4 and S5) with proteins being either down- or upregulated upon rapamycin treatment (e.g., CDC123, CDC6, ASNS, ECD, CEP72, PDCD4, RHOB, DHFR, TRIOBP, H1F0) (Figure 3d). Of note, this is in line with the well-established role of rapamycin and mTOR in the regulation of cell proliferation (Dowling et al., 2010). Similar results were obtained when analyzing the respective dataset (all significantly-regulated proteins; adj. *p*-value <0.05) from 48-h rapamycin treatment in WT cells (Figure 3a,c, Figure S3, Table S6).

Furthermore, in line with the robust expression changes in genes related to mitochondria (Figure 2c,d), we observed similar effects in the levels of mitochondrial proteins, as shown by the strong enrichment of related GO terms (e.g., CC:GO:0005739 ~ mitochondrion; CC:GO:0005759 ~ mitochondrial matrix) (Figure 3e, Tables S4 and S5). Interestingly, when performing the GO term analysis using only the strongly up- or downregulated proteins, the enrichment of terms related to mitochondrial proteins became even more prominent (Figure S4, Table S7) with most mitochondria-related proteins being upregulated by rapamycin (e.g., BNIP3, BNIP3L, CPS1, TXNRD2, SDSL, ACSF2, BPHL, HMGCL, HSD17B8, SFN) (Figure S4, Tables S4 and S7).

Finally, although a connection between mTOR activity and cell adhesion has been described before, the underlying mechanisms are less clear (Asrani et al., 2017; Chen et al., 2015). Interestingly, our proteomic analysis showed that rapamycin treatment led to significant changes in the levels of a large number of proteins that are related to adherens and anchoring junctions (CC:GO:0005912 ~ adherens junction; CC:GO:0070161 ~ anchoring junction), most of which are downregulated under these conditions (e.g., GJA1, SLC3A2, RANGAP1, DSP, FASN, APC, EEF2, TNKS1BP1, EHD4, CNN3) (Figure 3b,e, Tables S4 and S7). This suggests that some of the effects of rapamycin/mTOR on cell adhesion may stem from changes in the junctional proteome.

In sum, our unbiased interrogation of rapamycin's effects in cells reveals an extraordinary specificity of this compound towards mTOR, and—at the same time—provides a thorough evaluation of its role on the cellular transcriptome and proteome.

3 | DISCUSSION

According to previous studies, the majority of inhibitory compounds that are used in research or in therapeutics demonstrate off-target effects, influencing the activity of additional signaling molecules that can also be structurally-unrelated to their presumed targets. Sometimes, inhibitors even show higher potency towards off-targets compared to on-target effects (Bain et al., 2003, 2007; Davies et al., 2000; Davis et al., 2011; Fedorov et al., 2007). In fact, very few FDA-approved kinase inhibitors have demonstrated high target selectivity, whereas the majority influences the activity of 10–100 off-target kinases (Hantschel, 2015; Hantschel et al., 2012; Karaman et al., 2008). Importantly, the low specificity and selectivity of most kinase inhibitors greatly complicates the interpretation of data originating from their use and has important implications for their applicability in both research and therapeutics.

Surprisingly, although rapamycin has been used as an mTOR inhibitor for more than three decades, its specificity towards this key signaling hub has not been thoroughly evaluated so far. In fact, previous studies have hinted at the existence of mTOR-independent functions of rapamycin in cells and in transgenic mouse models, thus underscoring the need for a detailed evaluation of its specificity. In transgenic mice overexpressing a rapamycin-resistant mTOR mutant in skeletal muscles, rapamycin was still able to partially suppress mechanical-loading-induced ribosome biogenesis (Goodman et al., 2011). It is worth noting however, that these transgenic mice were maintained as hemizygotes with the mTOR^{RR} allele expressed on top of endogenous wild-type mTOR (Ge et al., 2009;

Goodman et al., 2011), which does not allow for definitive conclusions to be drawn from such experiments. Indeed, the observed rapamycin effects that were previously interpreted as mTOR-independent can also be ascribed to the inhibition of endogenous wild-type mTOR molecules. This is also supported by our findings, using a gene-edited cell line that expresses rapamycin-resistant mTOR from the endogenous *MTOR* locus, while lacking expression of wild-type mTOR: unlike the previously described mTOR^{RR} transgenic mice, our mTOR^{RR} cells are fully resistant to rapamycin, which is demonstrated by unaffected mTORC1 activity, abrogated

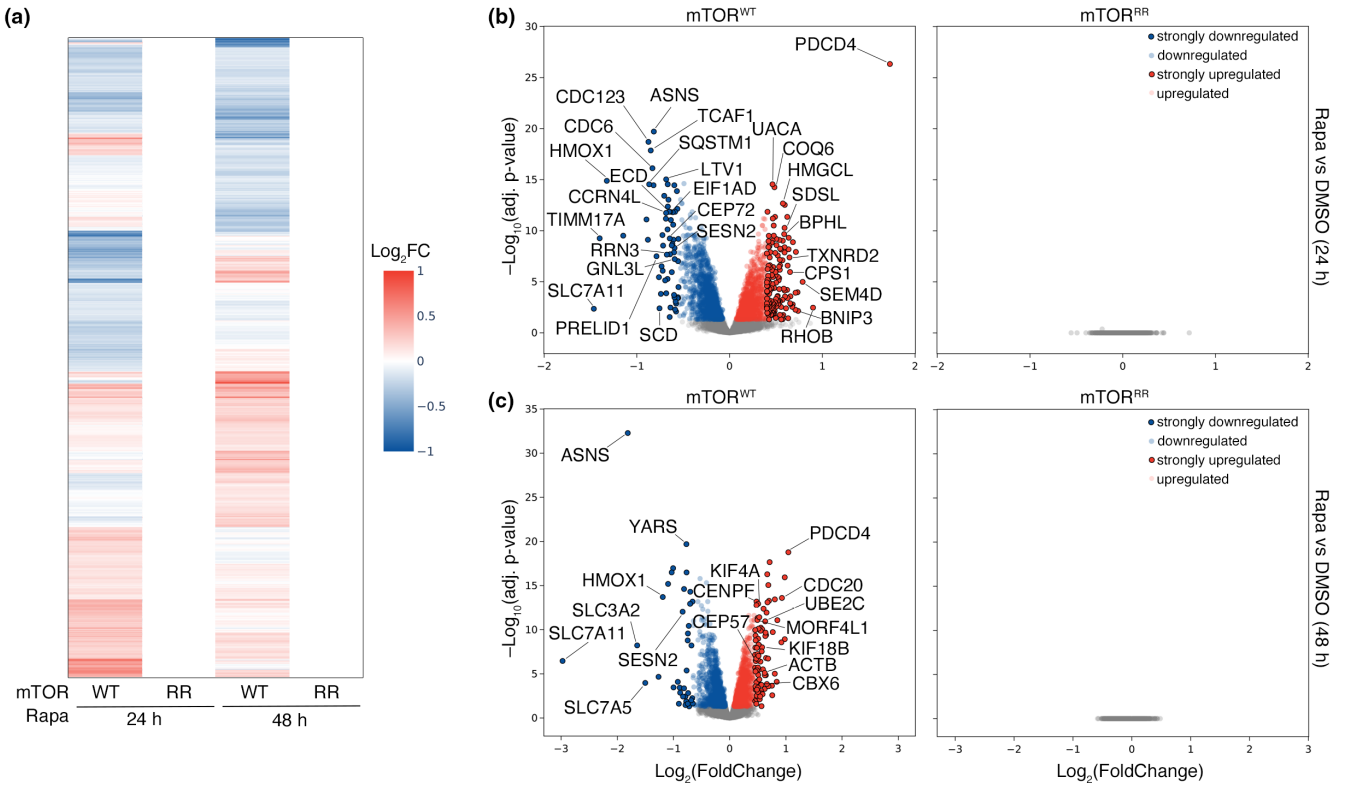

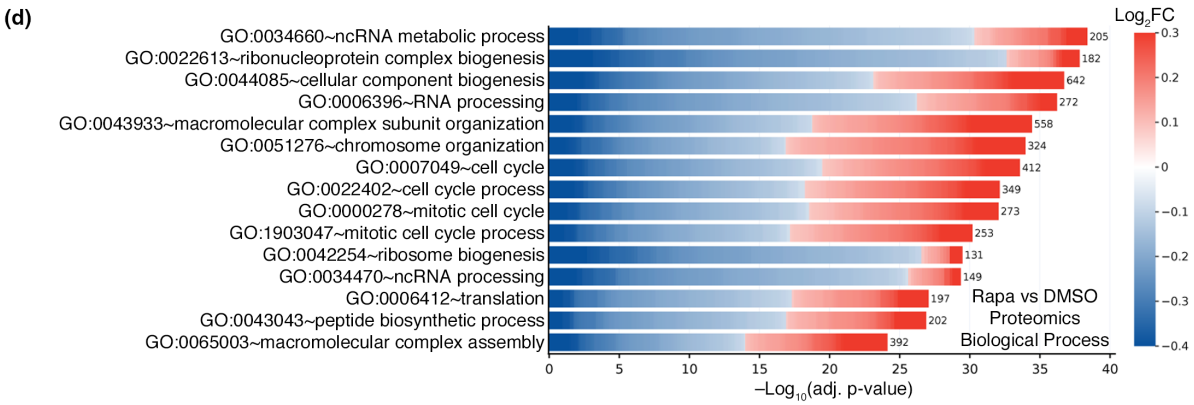

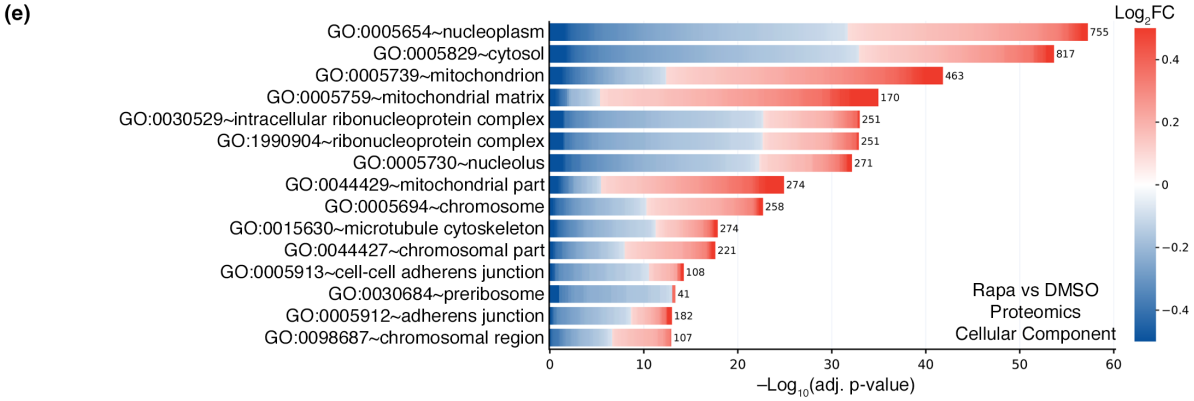

FIGURE 3 Rapamycin alters the cellular proteome exclusively via mTOR inhibition. (a) Heatmap depicting the rapamycin-induced changes in the proteome of HEK293FT WT and $mTOR^{RR}$ cells. Shown are whole-proteome quantitative mass-spectrometry data from cells treated with rapamycin (20 nM) for 24 or 48 h expressed as log-transformed fold change (Log_2FC). Only statistically-significant changes (adj. *p*-value <0.05) are shown. (b) Volcano plots showing the rapamycin-induced proteomic changes in HEK293FT WT (left) and $mTOR^{RR}$ (right) cells from the mass-spectrometry experiment described in (a). Proteins that are significantly (adj. *p*-value <0.05) down- or upregulated by rapamycin (20 nM, 24 h) are shown in blue or red respectively. Most strongly down- (Log_2FC <−0.55) or upregulated (Log_2FC > +0.4) proteins are shown with black outline. Unaffected proteins (adj. *p*-value >0.05) shown as grey dots. Selected proteins are marked in the plot. (c) As in (b), but for cells treated with 20 nM rapamycin (or DMSO) for 48 h. Strongly down- (Log_2FC <−0.65) or upregulated (Log_2FC >+0.45) proteins are shown with black outline. (d) Biological process (BP) GO term analysis using the proteins that are significantly down- (blue) or upregulated (red) by 24 h rapamycin in WT cells as described in (b). The color of each box in the cell plot represents log-transformed fold change values for each protein in rapamycin- vs DMSO-treated cells. The number of proteins in the selected dataset for each GO term is shown on the right side of each bar. (e) As in (d), but for Cellular Component (CC) GO term analysis.

FKBP12-mTOR binding, and complete lack of transcriptional or proteomic changes in response to rapamycin treatment.

A more recent study reported that micromolar concentrations of rapamycin (or of other rapalogs like everolimus and temsirolimus) can directly bind to TRPML1/MCOLN1, the primary lysosomal calcium release channel, and enhance its activity in an mTOR-independent manner (Zhang et al., 2019). Although rapalogs may indeed act on additional substrates at such concentrations, these are two to three orders of magnitude higher than those classically used in cell culture experiments (2–20 nM; like those we used for the transcriptomic and proteomic analyses described here) or—most importantly—those that are detected in the blood of patients that take rapamycin. More specifically, whole-blood concentrations (WBC) of rapamycin/sirolimus are in the 10–20 nM range in renal transplant patients to prevent graft rejection (Meier-Kriesche & Kaplan, 2000). In patients treated with everolimus against metastatic renal cell carcinoma, the median WBC is approximately 15 nM (Takasaki et al., 2019), while plasma concentrations of temsirolimus for relapsed/refractory multiple myeloma average around 9 nM (Farag et al., 2009). Higher doses of temsirolimus have only been used as a last resort in clinical trials against aggressive forms of lymphoma with WBC values reaching 500–600 nM (Hudes et al., 2007), which is still more than 25 times lower than the rapamycin concentration required to half-maximally activate TRPML1 (Zhang et al., 2019). Thus, the rapamycin-mediated TRPML1 activation, while observed *in vitro*, is not likely to be physiologically relevant for research and therapeutics. Furthermore, rapamycin doses aimed at slowing or reversing ageing are generally even lower than those used for immunosuppression and cancer treatment (Bitto et al., 2016; Bjedov et al., 2010; Castillo-Quan et al., 2019; Fok et al., 2014; Harrison et al., 2009; Robida-Stubbs et al., 2012; Schinaman et al., 2019), further suggesting that TRPML1 activation is unlikely to be involved in rapamycin-mediated lifespan extension.

Rapamycin acts as an allosteric mTOR inhibitor in complex with FKBP12 and other FKBP family members (Chung et al., 1992; Marz et al., 2013). Most FKBPs possess peptidyl-prolyl isomerase (PPIase) activity, hence functioning as protein folding chaperones for a variety of different proteins (Harrar et al., 2001; Kolos et al., 2018). For instance, FKBP12 and FKBP12.6 have been shown to bind and modulate the activity of ryanodine receptors (RyRs) and inositol 1,4,5-trisphosphate receptors (IP3Rs) (Bultynck et al., 2001; Galfre et al., 2012; Vervliet et al., 2015), which are channels involved in intracellular calcium release. FKBP12 has also been shown to inhibit TGFβ family type I receptors (Wang et al., 1996). Likewise, the larger FKBP51 and FKBP52 chaperones control glucocorticoid receptor (GR) localization and activity (Fries et al., 2017) as well as the protein levels of Argonaute 2 (AGO2) (Martinez et al., 2013), an essential component of the RNA-induced silencing complex (RISC). Hence, it would be reasonable to speculate that binding of rapamycin to different FKBP proteins may influence the folding—and thus function—of client proteins beyond mTOR inhibition. Because any changes in receptor or signaling pathway activities, organelle function, metabolism, or other cellular processes are eventually translated to changes in gene or protein expression, we here analyzed the cellular transcriptome and proteome to interrogate the effects of rapamycin treatment in an unbiased manner. These experiments revealed a striking dependence of rapamycin on mTOR inhibition to influence cells, with $mTOR^{RR}$-expressing cells demonstrating virtually no effects upon treatment with this drug. In sum, although rapamycin could—in theory—affect cells also independently from mTOR inhibition (via TRPML1 or through FKBP-dependent mechanisms), this is not the case, at least for rapamycin concentrations that are within the nanomolar range used in research or found in the blood of patients treated with this drug or its analogues. One possible reason for this phenomenal specificity and selectivity of rapamycin towards mTOR may be the fact that, unlike ATP-competitive kinase inhibitors that bind directly to their target, this compound inhibits mTOR activity in complex with FKBP12: only when the drug-protein holocomplex interacts with the FRB domain of mTOR, it blocks access of its substrates to its catalytic site and prevents their phosphorylation (Chung et al., 1992).

In addition to assessing rapamycin's specificity towards mTOR, we here also investigated how it influences gene expression and whole-cell protein levels in control cells that express wild-type mTOR. Consistent with the role of mTORC1 in regulating cap-dependent translation (Fonseca et al., 2014; Holz et al., 2005; Liu & Sabatini, 2020; Ma & Blenis, 2009; Thoreen et al., 2012) and with rapamycin's ability to repress both global and specific translation of key subsets of transcripts (Dickinson et al., 2011; Huo et al., 2011; Nandagopal & Roux, 2015; Tsukumo et al., 2016; Wang et al., 2007), these transcriptomics and proteomics datasets identified several thousands of genes and proteins whose expression changes in rapamycin-treated cells. For instance, highlighting the

well-described role of rapamycin/mTOR on ribosome biogenesis, rapamycin treatment strongly downregulated the expression of genes encoding for ribosomal proteins, tRNA synthetases (Kim et al., 2017; Lee et al., 2012) and other accessory proteins involved in this process (Mayer & Grummt, 2006; Powers & Walter, 1999) (Figure 2, Figure S2). Accordingly, we observed a strong enrichment of proteins related to non-coding RNA metabolic processes and ribonucleoprotein complex biogenesis among those downregulated by rapamycin (Figure 3, Figure S3). Furthermore, both our RNA-seq and proteomics data also confirm previous studies about rapamycin's role in regulating mitochondrial function (Morita et al., 2017; Ramanathan & Schreiber, 2009; Rosario et al., 2019; Schieke et al., 2006; Villa-Cuesta et al., 2014) (Figures 2 and 3, Figures S2 and S3). Interestingly, we find that proteins that are associated with adherens/anchoring junctions are enriched among those downregulated by rapamycin, which may suggest a role for mTOR in the regulation of cell–cell and cell-matrix contacts (Figure 3e and Figure S3b). Finally, we observe an enrichment of terms associated with the cell cycle and mitosis in the rapamycin-dependent proteome, possibly reflecting the anti-proliferative effects of rapamycin (Zaragoza et al., 1998) and the role of mTOR in cell proliferation (Dowling et al., 2010).

Overall, we here provide an unbiased evaluation of rapamycin's specificity towards mTOR in mammalian cells in unprecedented depth. Given the immense potential that rapamycin and its analogues have as anti-ageing compounds or in therapeutics, these findings provide important insight for both basic and translational research and aim at improving the applicability and specificity of its use in humans. Future studies using analogous $mTOR^{RR}$ animal models (e.g., *Drosophila* or mice) that express rapamycin-resistant mTOR from the endogenous locus will be important to assess whether rapamycin exhibits similar extraordinary selectivity and specificity towards mTOR also at the organismal level and in individual tissues.

4 | METHODS

4.1 | Cell culture

All cell lines were grown at 37°C, 5% CO_2. Human female embryonic kidney HEK293FT cells (#R70007; Invitrogen; RRID: CVCL_6911) were cultured in high-glucose Dulbecco's Modified Eagle Medium (DMEM) (#41965–039; Gibco) supplemented with 10% fetal bovine serum (FBS) (#F7524; Sigma, or #S1810; Biowest) and 1% Penicillin–Streptomycin (#15140–122; Gibco).

HEK293FT cells were purchased from Invitrogen. The identity of the HEK293FT cells was validated by the Multiplex human Cell Line Authentication test (Multiplexion GmbH), which uses a single nucleotide polymorphism (SNP) typing approach, and was performed as described at www.multiplexion.de. All parental and edited cell lines were regularly tested for *Mycoplasma* contamination using a PCR-based approach and were confirmed to be *Mycoplasma*-free.

4.2 | Cell culture treatments

To allosterically inhibit mTOR, rapamycin (#S1039; Selleckchem), everolimus (#S1120; Selleckchem) or temsirolimus (# S1044; Selleckchem) were dissolved in DMSO and added directly into full cell culture media at a final concentration of 20 nM unless otherwise indicated in the figure legends. Treatments were performed for the times described in the figure legends. DMSO was used as a negative control for all treatments. Torin1 (#4247; Tocris) was used as an ATP-competitive mTOR inhibitor and added in the culture media at a final concentration of 250 nM for 1 h.

Amino acid (AA) starvation experiments were performed as described previously (Demetriades et al., 2014; Tsokanos et al., 2016). In brief, custom-made starvation media were formulated according to the Gibco recipe for high-glucose DMEM specifically omitting all AAs. The media were filtered through a 0.22-μm filter device and tested for proper pH and osmolarity before use. For the respective AA-replete (+AA) treatment media, commercially available high-glucose DMEM was used (#41965039; Thermo Fisher Scientific). All treatment media were supplemented with 10% dialyzed FBS (dFBS) and 1x Penicillin–Streptomycin (#15140–122; Gibco). For this purpose, FBS was dialysed against 1× PBS through 3500 MWCO dialysis tubing. For basal (+AA) conditions, the culture media were replaced with +AA treatment media 1 h before lysis. For amino-acid starvation (−AA), culture media were replaced with starvation media for 1 h.

4.3 | Antibodies

Antibodies against phospho-p70 S6K (Thr389) (#9205), p70 S6K (#9202 for Figure 1c,e; #97596 for Figure 1d,f), FLAG (#2368) and mTOR (#2983) were purchased from Cell Signaling Technology. The anti-human tubulin (#T9026) antibody was purchased from Sigma.

4.4 | Plasmid DNA transfections

Plasmid DNA transfections in HEK293FT cells were performed using Effectene transfection reagent (#301425; Qiagen) according to the manufacturer's instructions.

4.5 | Generation of the gene-edited $mTOR^{RR}$ cell line

The rapamycin-resistant mTOR ($mTOR^{RR}$) HEK293FT cell line was generated by gene-editing using the pX459-based CRISPR/Cas9 system (Ran et al., 2013). The Ser2035Thr amino acid substitution was introduced by homology-directed repair (HDR) using a single-stranded DNA oligo as donor template (Paquet et al., 2016). The respective nucleotide change in the MTOR cDNA (NM_004958.4) is c.6103 T > A (Figure S1b). To target the *MTOR*

gene locus, a sgRNA expression vector was generated by cloning appropriate DNA oligonucleotides (Table S8) in the BbsI restriction sites of pX459 (#62988; Addgene). The resulting plasmid was co-transfected together with 1 μL of a donor DNA oligo (100 μM) containing the Ser2035Thr (TCT > ACT) substitution (Table S8) in HEK293FT cells. Transfected cells were selected with 3 μg/mL puromycin (#A11138-03; Thermo Fisher Scientific) 36–48 h post-transfection. Single-cell clones were generated by FACS sorting and individual mutant clones were validated by genomic DNA sequencing and functional assays to assess the responsiveness of mTORC1 to rapamycin (and other rapalogs).

4.6 | Gene expression analysis (RNA-seq)

To analyze gene expression changes via RNA-seq experiments, total mRNA was isolated using QIAshredder columns (#79656; Qiagen) and the RNeasy Plus Mini Kit (#74034; Qiagen) according to the manufacturer's instructions. RNA-seq experiments were performed by the Max Planck Genome Centre (MPGC) Cologne, Germany (https://mpgc.mpipz.mpg.de/home/). RNA quality was assessed with an Agilent Bioanalyzer (Nanochip). Library preparation was done according to NEBNext Ultra™ II Directional RNA Library Prep Kit for Illumina (#E7760L; New England Biolabs) including polyA enrichment and addition of ERCC RNA spike-ins. Libraries were quality controlled by Agilent TapeStation or LabChip GX or GX Touch (PerkinElmer). Sequencing-by-synthesis was performed on a HiSeq 3000 (Illumina) with single read mode 1 × 150 bp. Data from one representative RNA-seq experiment, out of two independent replicates, are shown in this manuscript. Each experiment was performed from 3 independent biological replicates. The raw data from both RNA-seq experiments are available in the NCBI Sequence Read Archive (see also the *Data Availability Statement* section).

4.7 | Cell lysis and immunoblotting

For standard SDS-PAGE and immunoblotting experiments, cells from a well of a 12-well plate were treated as indicated in the figures and lysed in 250 μL of ice-cold Triton lysis buffer (50 mM Tris pH 7.5, 1% Triton X-100, 150 mM NaCl, 50 mM NaF, 2 mM Na-vanadate, 0.011 gr/mL beta-glycerophosphate) supplemented with 1x PhosSTOP phosphatase inhibitors (#4906837001; Roche) and 1× complete protease inhibitors (#11836153001; Roche) for 10 min on ice. Samples were clarified by centrifugation (~22,000 *g*, 10 min, 4°C) and supernatants were boiled in 1x SDS sample buffer (5× SDS sample buffer: 350 mM Tris–HCl pH 6.8, 30% glycerol, 600 mM DTT, 12.8% SDS, 0.12% bromophenol blue). Protein samples were subjected to electrophoretic separation on SDS-PAGE and analysed by standard Western blotting techniques. In brief, proteins were transferred to nitrocellulose membranes (#10600002 or #10600001; Amersham) and stained with 0.2% Ponceau solution (#33427-01; Serva) to confirm equal loading. Membranes were blocked with 5% skim milk powder (#42590; Serva) in PBS-T [1× PBS, 0.1% Tween-20 (#A1389; AppliChem)] for 1 h at room temperature, washed three times for 10 min with PBS-T and incubated with primary antibodies [1:1000 in PBS-T, 5% bovine serum albumin (BSA; #10735086001; Roche)] rotating overnight at 4°C. The next day, membranes were washed three times for 10 min with PBS-T and incubated with appropriate HRP-conjugated secondary antibodies (1:10000 in PBS-T, 5% milk) for 1 h at room temperature. Signals were detected by enhanced chemiluminescence (ECL) using the ECL Western Blotting Substrate (#W1015; Promega) or SuperSignal West Pico PLUS (#34577; Thermo Scientific) and SuperSignal West Femto Substrate (#34095; Thermo Scientific) for weaker signals. Immunoblot images were captured on films (#28906835; GE Healthcare, #4741019289; Fujifilm).

4.8 | Co-immunoprecipitation (co-IP)

For co-IP experiments, 1.5×10^6 cells were transiently transfected with the indicated plasmids and lysed 36 h post-transfection in IP lysis buffer (50 mM Tris pH 7.5, 0.3% CHAPS, 150 mM NaCl, 50 mM NaF, 2 mM Na-vanadate, 0.011 g/mL β-glycerophosphate, 1× PhosSTOP phosphatase inhibitors and 1× complete protease inhibitors). FLAG-tagged proteins were incubated with 30 μL pre-washed anti-FLAG M2 affinity gel (Sigma; #A2220) for 3 h at 4°C and washed four times with IP wash buffer (50 mM Tris pH 7.5, 0.3% CHAPS, 150 mM NaCl and 50 mM NaF). Samples were then boiled for 6 min in 1× SDS sample buffer and analysed by immunoblotting using appropriate antibodies.

4.9 | Quantitative whole-cell proteomics

For mass-spectrometry experiments, HEK293FT cells were cultured in 10 cm dishes in 10 mL of complete culture media as described above. Rapamycin (or DMSO as negative control) were added directly in the culture media for 24 or 48 h. Experiments were performed with 5 independent biological replicates per condition (1 × 10 cm dish per replicate). In brief, cells were scraped, collected in 1.5 mL tubes on ice, washed in serum-free media, pelleted by centrifugation (500 *g*, 3 min), and cell pellets were snap-frozen in liquid nitrogen and stored at −80°C.

4.9.1 | Sample preparation

For sample preparation for quantitative proteomic analysis, cell pellets were lysed in 6 M guanidinium chloride (GdmCl) supplemented with 2.5 mM TCEP (tris(2-carboxyethyl)phosphine), 10 mM CAA (chloroacetamide) and 100 mM Tris–HCl at room temperature. Samples were boiled at 95°C for 10 min and sonicated for 30s

for 10 cycles, with 30 s breaks on high-performance mode with Bioruptor Plus (#B01020001; Diagenode). Samples were centrifuged at 20,000*g* for 20 min at RT, supernatants were diluted 10 times with 20 mM Tris and protein concentration was measured using Nanodrop 2000 (#ND-2000; Thermo Fischer Scientific). Three hundred micrograms of each sample were diluted 10 times with 20 mM Tris and digested with 1.5 µL of Mass Spectrometry Grade Trypsin Gold (#V5280; Promega) at 37°C overnight. Digestion was stopped by adding 50% FA to the reaction at a final concentration of 1%. Samples were centrifuged at 20,000*g* for 10 min at RT and supernatants were collected. C-18-SD StageTips were washed and equilibrated sequentially with 200 µL methanol, 200 µL 40% ACN (acetonitrile)/0.1% FA (formic acid) and 200 µL 0.1% FA by centrifugation, each step for 1 min at RT. Samples were diluted with 0.1% FA, loaded in StageTips and centrifuged for 1–2 min at RT. StageTips were then washed twice with 200 µL 0.1% FA. Tryptic peptides were eluted from StageTips with 100 µL 40% acetonitrile (ACN)/0.1% formic acid (FA) by centrifugation (300*g*, 4 min, RT). Eluates were dried in a Speed-Vac at 45°C for 40–45 min and resuspended in 20 µL 0.1% FA. Four micrograms of the peptides were dried in a Speed-Vac and stored at −20°C.

4.9.2 | TMT10plex labelling

The dried tryptic peptides were reconstituted in 9 µL of 0.1 M TEAB (triethylammonium bicarbonate). Tandem mass tag (TMT10plex, #90110; Thermo Fisher Scientific) labelling was carried out according to the manufacturer's instructions with the following changes: 0.8 mg of TMT10plex reagent was re-suspended with 70 µL anhydrous ACN. Seven microliters of TMT10plex reagent in ACN were added to 9 µL of clean peptide in 0.1 M TEAB. The final ACN concentration was 43.75% and the ratio of peptides to TMT10plex reagent was 1:20. After 60 min incubation, the reaction was quenched with 2 µL 5% hydroxylamine. Labelled peptides were pooled, dried, re-suspended in 200 µL 0.1% FA, split in two equal parts and desalted using home-made STAGE tips (Li et al., 2021).

4.9.3 | Fractionation of TMT10plex-labelled peptide mixture

One of the two parts was fractionated on a 1 mm × 150 mm ACQUITY column, packed with 130 Å, 1.7 µm C18 particles (#186006935; Waters) using an Ultimate 3000 UHPLC (Thermo Fisher Scientific). Peptides were separated at a flow of 30 µL/min with an 88 min segmented gradient from 1% to 50% buffer B for 85 min and from 50% to 95% buffer B for 3 min; buffer A was 5% ACN, 10 mM ammonium bicarbonate, buffer B was 80% ACN, 10 mM ammonium bicarbonate. Fractions were collected every 3 min, pooled in two passes (fraction 1 + 17, fraction 2 + 18, …, etc.) and dried in a vacuum centrifuge (Eppendorf).

4.9.4 | LC–MS/MS analysis

Dried fractions were re-suspended in 0.1% FA, separated on a 50 cm, 75 µm Acclaim PepMap column (#164942; Thermo Fisher Scientific) and analysed on a Orbitrap Lumos Tribrid mass spectrometer (Thermo Fisher Scientific) equipped with a FAIMS device (Thermo Fisher Scientific). The FAIMS device was operated in two compensation voltages, −50 V and −70 V. Synchronous precursor selection based MS3 was used for the acquisition of the TMT10plex reporter ion signals. Peptide separations were performed on an EASY-nLC1200 using a 90 min linear gradient from 6% to 31% buffer; buffer A was 0.1% FA, buffer B was 0.1% FA, 80% ACN. The analytical column was operated at 50°C. Raw files were split based on the FAIMS compensation voltage using FreeStyle (Thermo Fisher Scientific).

4.9.5 | Data analysis

Proteomics data was analysed using MaxQuant, version 1.6.17.0 (Cox & Mann, 2008). The isotope purity correction factors, provided by the manufacturer, were included in the analysis. Differential expression analysis was performed using limma, version 3.34.9 (Ritchie et al., 2015) in R, version 3.4.3 (R Core Team, 2017).

4.10 | Gene ontology analysis and data presentation

Gene Ontology (GO) term enrichment analysis was performed using the Database for Annotation, Visualization and Integrated Discovery (DAVID) tool (Huang da et al., 2009a, 2009b) of the Flaski toolbox (Iqbal et al., 2021) (https://flaski.age.mpg.de, developed and provided by the MPI-AGE Bioinformatics core facility). For the RNA-seq experiments, either all significantly changing genes (adjusted *p*-value <0.05) or selected genes whose expression levels change significantly between rapamycin- and DMSO-treated cells with Log_2-transformed fold change (Log_2FC) values lower than −0.75 (downregulated by rapamycin treatment) or higher than +0.8 (upregulated by rapamycin treatment), roughly corresponding to the top and bottom 5% of the dataset, were used for the DAVID GO analysis (for GOTERM_CC_FAT, GOTERM_BP_FAT). The selection criteria for each analysis are described in the respective figure legends.

For the DAVID GO analysis of quantitative proteomics experiments, either all significantly changing proteins (adjusted *p*-value <0.05) or selected proteins whose intensity changes significantly between rapamycin- and DMSO-treated cells with $Log_2FC < -0.55$ and $Log_2FC > +0.4$ (24 h treatments) or $Log_2FC < -0.65$ and $Log_2FC > +0.45$ (48 h treatments) were used (for GOTERM_CC_FAT, GOTERM_BP_FAT). Cut-offs were selected based on the distribution of the ranked Log_2FC values in each dataset to include only proteins whose levels change robustly in response to rapamycin treatment in control cells. The human proteome was used as reference list for all analyses.

Cell plots were generated using the DAVID and Cell plot apps in Flaski and include the 15 most significant GO terms from each analysis. The full list of genes/proteins that were detected in each experiment was used for generating the Volcano plots. The respective graphs were prepared using the Scatter plot app in Flaski and labelled in Adobe Photoshop (v. 23.4.2). Significantly changing genes/proteins are represented by blue (downregulated by rapamycin) or red (upregulated by rapamycin) dots. Proteins/genes whose levels change strongly upon rapamycin treatment (based on the selection criteria described above for each experiment) are shown as blue or red dots with black outline.

Heatmaps were generated using the homonymous app in Flaski, and hierarchical clustering was performed using Euclidean distance and Ward's method (Iqbal et al., 2021).

AUTHOR CONTRIBUTIONS

Experimental work: FA, NG; data analysis: FA, CD; project design & conceptualization: CD; project supervision: CD; funding acquisition: CD; figure preparation: FA, NG, CD; manuscript draft: FA, CD. All authors approved the final version of the manuscript and agree on the content and conclusions.

ACKNOWLEDGEMENTS

We thank all members of the Demetriades lab for critical discussions; Sabine Wilhelm for technical support with sample preparation for proteomics; Ilian Athanasov and Xinping Li from the MPI-AGE Proteomics Core Facility for performing the quantitative proteomics experiments described in this study; the Max Planck Genome Centre (MPGC) Cologne (http://mpgc.mpipz.mpg.de/home/) for performing the RNA-seq experiments described in this study; Franziska Metge and Jorge Boucas from the MPI-AGE Bioinformatics Core for initial RNA-seq analysis; and the MPI-AGE FACS & Imaging Core Facility for support with cell sorting experiments. FA received support by the Cologne Graduate School of Ageing Research (CGA). CD is funded by the European Research Council (ERC) under the European Union's Horizon 2020 research and innovation programme (grant agreement No 757729) and by the Max Planck Society. Illustrations in figures created with BioRender.com. Open Access funding enabled and organized by Projekt DEAL.

CONFLICT OF INTEREST STATEMENT

The authors declare no competing interests.

DATA AVAILABILITY STATEMENT

The data that support the findings of this study (uncropped immunoblots) or any additional information required to reanalyse the data reported in this paper are available from the corresponding author upon reasonable request. Other datasets that are produced in this study are available in the following databases:

- RNA-seq data: NCBI Sequence Read Archive (SRA) PRJNA872474 (www.ncbi.nlm.nih.gov/sra/PRJNA872474).
- Mass spectrometry proteomics: PRIDE (Perez-Riverol et al., 2022) PXD038051 (www.ebi.ac.uk/pride/archive/projects/PXD038051).

CODE AVAILABILITY

No code was generated in this study.

ORCID

Filippo Artoni https://orcid.org/0000-0003-3902-9217
Constantinos Demetriades https://orcid.org/0000-0001-7813-7726

REFERENCES

Arriola Apelo, S. I., & Lamming, D. W. (2016). Rapamycin: An InhibiTOR of aging emerges from the soil of Easter Island. *The Journals of Gerontology. Series A, Biological Sciences and Medical Sciences*, *71*(7), 841–849. https://doi.org/10.1093/gerona/glw090

Asrani, K., Sood, A., Torres, A., Georgess, D., Phatak, P., Kaur, H., Dubin, A., Talbot, C. C., Elhelu, L., Ewald, A. J., Xiao, B., Worley, P., & Lotan, T. L. (2017). mTORC1 loss impairs epidermal adhesion via TGF-beta/rho kinase activation. *The Journal of Clinical Investigation*, *127*(11), 4001–4017. https://doi.org/10.1172/JCI92893

Bain, J., McLauchlan, H., Elliott, M., & Cohen, P. (2003). The specificities of protein kinase inhibitors: An update. *The Biochemical Journal*, *371*(Pt 1), 199–204. https://doi.org/10.1042/BJ20021535

Bain, J., Plater, L., Elliott, M., Shpiro, N., Hastie, C. J., McLauchlan, H., Klevernic, I., Arthur, J. S., Alessi, D. R., & Cohen, P. (2007). The selectivity of protein kinase inhibitors: A further update. *The Biochemical Journal*, *408*(3), 297–315. https://doi.org/10.1042/BJ20070797

Bayeva, M., Khechaduri, A., Puig, S., Chang, H. C., Patial, S., Blackshear, P. J., & Ardehali, H. (2012). mTOR regulates cellular iron homeostasis through tristetraprolin. *Cell Metabolism*, *16*(5), 645–657. https://doi.org/10.1016/j.cmet.2012.10.001

Benjamin, D., Colombi, M., Moroni, C., & Hall, M. N. (2011). Rapamycin passes the torch: A new generation of mTOR inhibitors. *Nature Reviews. Drug Discovery*, *10*(11), 868–880. https://doi.org/10.1038/nrd3531

Bitto, A., Ito, T. K., Pineda, V. V., LeTexier, N. J., Huang, H. Z., Sutlief, E., Tung, H., Vizzini, N., Chen, B., Smith, K., Meza, D., Yajima, M., Beyer, R. P., Kerr, K. F., Davis, D. J., Gillespie, C. H., Snyder, J. M., Treuting, P. M., & Kaeberlein, M. (2016). Transient rapamycin treatment can increase lifespan and healthspan in middle-aged mice. *eLife*, *5*, e16351. https://doi.org/10.7554/eLife.16351

Bjedov, I., Toivonen, J. M., Kerr, F., Slack, C., Jacobson, J., Foley, A., & Partridge, L. (2010). Mechanisms of life span extension by rapamycin in the fruit fly Drosophila melanogaster. *Cell Metabolism*, *11*(1), 35–46. https://doi.org/10.1016/j.cmet.2009.11.010

Bonner, J. M., & Boulianne, G. L. (2017). Diverse structures, functions and uses of FK506 binding proteins. *Cellular Signalling*, *38*, 97–105. https://doi.org/10.1016/j.cellsig.2017.06.013

Brown, E. J., Beal, P. A., Keith, C. T., Chen, J., Shin, T. B., & Schreiber, S. L. (1995). Control of p70 s6 kinase by kinase activity of FRAP in vivo. *Nature*, *377*(6548), 441–446. https://doi.org/10.1038/377441a0

Bultynck, G., de Smet, P., Rossi, D., Callewaert, G., Missiaen, L., Sorrentino, V., de Smedt, H., & Parys, J. B. (2001). Characterization and mapping of the 12 kDa FK506-binding protein (FKBP12)-binding site on different isoforms of the ryanodine receptor and of the inositol 1,4,5-trisphosphate receptor. *The Biochemical Journal*, *354*(Pt 2), 413–422.

Castillo-Quan, J. I., Tain, L. S., Kinghorn, K. J., Li, L., Grönke, S., Hinze, Y., Blackwell, T. K., Bjedov, I., & Partridge, L. (2019). A triple drug combination targeting components of the nutrient-sensing network maximizes longevity. *Proceedings of the National Academy of Sciences of the United States of America*, *116*(42), 20817–20819. https://doi.org/10.1073/pnas.1913212116

Chen, J., Zheng, X. F., Brown, E. J., & Schreiber, S. L. (1995). Identification of an 11-kDa FKBP12-rapamycin-binding domain within the

289-kDa FKBP12-rapamycin-associated protein and characterization of a critical serine residue. *Proceedings of the National Academy of Sciences of the United States of America*, *92*(11), 4947–4951. https://doi.org/10.1073/pnas.92.11.4947

Chen, L., Xu, B., Liu, L., Liu, C., Luo, Y., Chen, X., Barzegar, M., Chung, J., & Huang, S. (2015). Both mTORC1 and mTORC2 are involved in the regulation of cell adhesion. *Oncotarget*, *6*(9), 7136–7150. https://doi.org/10.18632/oncotarget.3044

Choi, J., Chen, J., Schreiber, S. L., & Clardy, J. (1996). Structure of the FKBP12-rapamycin complex interacting with the binding domain of human FRAP. *Science*, *273*(5272), 239–242. https://doi.org/10.1126/science.273.5272.239

Chung, J., Kuo, C. J., Crabtree, G. R., & Blenis, J. (1992). Rapamycin-FKBP specifically blocks growth-dependent activation of and signaling by the 70 kd S6 protein kinases. *Cell*, *69*(7), 1227–1236. https://doi.org/10.1016/0092-8674(92)90643-q

Cox, J., & Mann, M. (2008). MaxQuant enables high peptide identification rates, individualized p.p.b.-range mass accuracies and proteome-wide protein quantification. *Nature Biotechnology*, *26*(12), 1367–1372. https://doi.org/10.1038/nbt.1511

Creevy, K. E., Akey, J. M., Kaeberlein, M., Promislow, D. E. L., & Dog Aging Project, C. (2022). An open science study of ageing in companion dogs. *Nature*, *602*(7895), 51–57. https://doi.org/10.1038/s41586-021-04282-9

Davies, S. P., Reddy, H., Caivano, M., & Cohen, P. (2000). Specificity and mechanism of action of some commonly used protein kinase inhibitors. *The Biochemical Journal*, *351*(Pt 1), 95–105. https://doi.org/10.1042/0264-6021:3510095

Davis, M. I., Hunt, J. P., Herrgard, S., Ciceri, P., Wodicka, L. M., Pallares, G., & Zarrinkar, P. P. (2011). Comprehensive analysis of kinase inhibitor selectivity. *Nature Biotechnology*, *29*(11), 1046–1051. https://doi.org/10.1038/nbt.1990

Demetriades, C., Doumpas, N., & Teleman, A. A. (2014). Regulation of TORC1 in response to amino acid starvation via lysosomal recruitment of TSC2. *Cell*, *156*(4), 786–799. https://doi.org/10.1016/j.cell.2014.01.024

Dickinson, J. M., Fry, C. S., Drummond, M. J., Gundermann, D. M., Walker, D. K., Glynn, E. L., Timmerman, K. L., Dhanani, S., Volpi, E., & Rasmussen, B. B. (2011). Mammalian target of rapamycin complex 1 activation is required for the stimulation of human skeletal muscle protein synthesis by essential amino acids. *The Journal of Nutrition*, *141*(5), 856–862. https://doi.org/10.3945/jn.111.139485

Dorrello, N. V., Peschiaroli, A., Guardavaccaro, D., Colburn, N. H., Sherman, N. E., & Pagano, M. (2006). S6K1- and betaTRCP-mediated degradation of PDCD4 promotes protein translation and cell growth. *Science*, *314*(5798), 467–471. https://doi.org/10.1126/science.1130276

Dowling, R. J., Topisirovic, I., Alain, T., Bidinosti, M., Fonseca, B. D., Petroulakis, E., Wang, X., Larsson, O., Selvaraj, A., Liu, Y., Kozma, S. C., Thomas, G., & Sonenberg, N. (2010). mTORC1-mediated cell proliferation, but not cell growth, controlled by the 4E-BPs. *Science*, *328*(5982), 1172–1176. https://doi.org/10.1126/science.1187532

EMA. (2005). *Rapamune: EPAR – scientific discussion*. https://www.ema.europa.eu/en/documents/scientific-discussion/rapamune-epar-scientific-discussion_en.pdf.

Farag, S. S., Zhang, S., Jansak, B. S., Wang, X., Kraut, E., Chan, K., Dancey, J. E., & Grever, M. R. (2009). Phase II trial of temsirolimus in patients with relapsed or refractory multiple myeloma. *Leukemia Research*, *33*(11), 1475–1480. https://doi.org/10.1016/j.leukres.2009.01.039

Fedorov, O., Marsden, B., Pogacic, V., Rellos, P., Müller, S., Bullock, A. N., Schwaller, J., Sundström, M., & Knapp, S. (2007). A systematic interaction map of validated kinase inhibitors with ser/Thr kinases. *Proceedings of the National Academy of Sciences of the United States of America*, *104*(51), 20523–20528. https://doi.org/10.1073/pnas.0708800104

Fernandes, S. A., & Demetriades, C. (2021). The multifaceted role of nutrient sensing and mTORC1 signaling in physiology and aging. *Front Aging*, *2*, 707372. https://doi.org/10.3389/fragi.2021.707372

Fok, W. C., Chen, Y., Bokov, A., Zhang, Y., Salmon, A. B., Diaz, V., Javors, M., Wood, W. H., Zhang, Y., Becker, K. G., Pérez, V. I., & Richardson, A. (2014). Mice fed rapamycin have an increase in lifespan associated with major changes in the liver transcriptome. *PLoS One*, *9*(1), e83988. https://doi.org/10.1371/journal.pone.0083988

Fonseca, B. D., Smith, E. M., Yelle, N., Alain, T., Bushell, M., & Pause, A. (2014). The ever-evolving role of mTOR in translation. *Seminars in Cell & Developmental Biology*, *36*, 102–112. https://doi.org/10.1016/j.semcdb.2014.09.014

Fries, G. R., Gassen, N. C., & Rein, T. (2017). The FKBP51 glucocorticoid receptor co-chaperone: Regulation, function, and implications in health and disease. *International Journal of Molecular Sciences*, *18*(12), 2614. https://doi.org/10.3390/ijms18122614

Galfré, E., Pitt, S. J., Venturi, E., Sitsapesan, M., Zaccai, N. R., Tsaneva-Atanasova, K., O'Neill, S., & Sitsapesan, R. (2012). FKBP12 activates the cardiac ryanodine receptor Ca^{2+}–release channel and is antagonised by FKBP12.6. *PLoS One*, *7*(2), e31956. https://doi.org/10.1371/journal.pone.0031956

Ge, Y., Wu, A. L., Warnes, C., Liu, J., Zhang, C., Kawasome, H., Terada, N., Boppart, M. D., Schoenherr, C. J., & Chen, J. (2009). mTOR regulates skeletal muscle regeneration in vivo through kinase-dependent and kinase-independent mechanisms. *American Journal of Physiology. Cell Physiology*, *297*(6), C1434–C1444. https://doi.org/10.1152/ajpcell.00248.2009

Goodman, C. A., Frey, J. W., Mabrey, D. M., Jacobs, B. L., Lincoln, H. C., You, J. S., & Hornberger, T. A. (2011). The role of skeletal muscle mTOR in the regulation of mechanical load-induced growth. *The Journal of Physiology*, *589*(Pt 22), 5485–5501. https://doi.org/10.1113/jphysiol.2011.218255

Gordon, E. B., Hart, G. T., Tran, T. M., Waisberg, M., Akkaya, M., Skinner, J., Zinöcker, S., Pena, M., Yazew, T., Qi, C. F., Miller, L. H., & Pierce, S. K. (2015). Inhibiting the mammalian target of rapamycin blocks the development of experimental cerebral malaria. *mBio*, *6*(3), e00725. https://doi.org/10.1128/mBio.00725-15

Graber, T. G., Borack, M. S., Reidy, P. T., Volpi, E., & Rasmussen, B. B. (2017). Essential amino acid ingestion alters expression of genes associated with amino acid sensing, transport, and mTORC1 regulation in human skeletal muscle. *Nutrition & Metabolism (London)*, *14*, 35. https://doi.org/10.1186/s12986-017-0187-1

Hantschel, O. (2015). Unexpected off-targets and paradoxical pathway activation by kinase inhibitors. *ACS Chemical Biology*, *10*(1), 234–245. https://doi.org/10.1021/cb500886n

Hantschel, O., Grebien, F., & Superti-Furga, G. (2012). The growing arsenal of ATP-competitive and allosteric inhibitors of BCR-ABL. *Cancer Research*, *72*(19), 4890–4895. https://doi.org/10.1158/0008-5472.CAN-12-1276

Hara, K., Yonezawa, K., Kozlowski, M. T., Sugimoto, T., Andrabi, K., Weng, Q. P., & Avruch, J. (1997). Regulation of eIF-4E BP1 phosphorylation by mTOR. *The Journal of Biological Chemistry*, *272*(42), 26457–26463. https://doi.org/10.1074/jbc.272.42.26457

Hardwick, J. S., Kuruvilla, F. G., Tong, J. K., Shamji, A. F., & Schreiber, S. L. (1999). Rapamycin-modulated transcription defines the subset of nutrient-sensitive signaling pathways directly controlled by the tor proteins. *Proceedings of the National Academy of Sciences of the United States of America*, *96*(26), 14866–14870. https://doi.org/10.1073/pnas.96.26.14866

Harrar, Y., Bellini, C., & Faure, J. D. (2001). FKBPs: at the crossroads of folding and transduction. *Trends in Plant Science*, *6*(9), 426–431. https://doi.org/10.1016/s1360-1385(01)02044-1

Harrison, D. E., Strong, R., Sharp, Z. D., Nelson, J. F., Astle, C. M., Flurkey, K., Nadon, N. L., Wilkinson, J. E., Frenkel, K., Carter, C. S., Pahor, M., Javors, M. A., Fernandez, E., & Miller, R. A. (2009). Rapamycin fed late in life extends lifespan in genetically heterogeneous

mice. *Nature*, *460*(7253), 392–395. https://doi.org/10.1038/nature08221

Holz, M. K., Ballif, B. A., Gygi, S. P., & Blenis, J. (2005). mTOR and S6K1 mediate assembly of the translation preinitiation complex through dynamic protein interchange and ordered phosphorylation events. *Cell*, *123*(4), 569–580. https://doi.org/10.1016/j.cell.2005.10.024

Hosoi, H., Dilling, M. B., Shikata, T., Liu, L. N., Shu, L., Ashmun, R. A., Germain, G. S., Abraham, R. T., & Houghton, P. J. (1999). Rapamycin causes poorly reversible inhibition of mTOR and induces p53-independent apoptosis in human rhabdomyosarcoma cells. *Cancer Research*, *59*(4), 886–894.

Huang da, W., Sherman, B. T., & Lempicki, R. A. (2009a). Bioinformatics enrichment tools: Paths toward the comprehensive functional analysis of large gene lists. *Nucleic Acids Research*, *37*(1), 1–13. https://doi.org/10.1093/nar/gkn923

Huang da, W., Sherman, B. T., & Lempicki, R. A. (2009b). Systematic and integrative analysis of large gene lists using DAVID bioinformatics resources. *Nature Protocols*, *4*(1), 44–57. https://doi.org/10.1038/nprot.2008.211

Hudes, G., Carducci, M., Tomczak, P., Dutcher, J., Figlin, R., Kapoor, A., Staroslawska, E., Sosman, J., McDermott, D., Bodrogi, I., Kovacevic, Z., Lesovoy, V., Schmidt-Wolf, I. G. H., Barbarash, O., Gokmen, E., O'Toole, T., Lustgarten, S., Moore, L., Motzer, R. J., & Global ARCC Trail. (2007). Temsirolimus, interferon alfa, or both for advanced renal-cell carcinoma. *The New England Journal of Medicine*, *356*(22), 2271–2281. https://doi.org/10.1056/NEJMoa066838

Huo, Y., Iadevaia, V., & Proud, C. G. (2011). Differing effects of rapamycin and mTOR kinase inhibitors on protein synthesis. *Biochemical Society Transactions*, *39*(2), 446–450. https://doi.org/10.1042/BST0390446

Iqbal, A., Duitama, C., Metge, F., Rosskopp, D., & Boucas, J. (2021). Flaski (2.0.0). *Zenodo*. https://doi.org/10.5281/zenodo.4849516

Jin, C., Zhao, Y., Yu, L., Xu, S., & Fu, G. (2013). MicroRNA-21 mediates the rapamycin-induced suppression of endothelial proliferation and migration. *FEBS Letters*, *587*(4), 378–385. https://doi.org/10.1016/j.febslet.2012.12.021

Karaman, M. W., Herrgard, S., Treiber, D. K., Gallant, P., Atteridge, C. E., Campbell, B. T., & Zarrinkar, P. P. (2008). A quantitative analysis of kinase inhibitor selectivity. *Nature Biotechnology*, *26*(1), 127–132. https://doi.org/10.1038/nbt1358

Kennedy, B. K., & Pennypacker, J. K. (2015). Aging interventions get human. *Oncotarget*, *6*(2), 590–591. https://doi.org/10.18632/oncotarget.3173

Kim, J. H., Lee, C., Lee, M., Wang, H., Kim, K., Park, S. J., Yoon, I., Jang, J., Zhao, H., Kim, H. K., Kwon, N. H., Jeong, S. J., Yoo, H. C., Kim, J. H., Yang, J. S., Lee, M. Y., Lee, C. W., Yun, J., Oh, S. J., … Kim, S. (2017). Control of leucine-dependent mTORC1 pathway through chemical intervention of leucyl-tRNA synthetase and RagD interaction. *Nature Communications*, *8*(1), 732. https://doi.org/10.1038/s41467-017-00785-0

Ko, J. H., Yoon, S. O., Lee, H. J., & Oh, J. Y. (2017). Rapamycin regulates macrophage activation by inhibiting NLRP3 inflammasome-p38 MAPK-NFkappaB pathways in autophagy- and p62-dependent manners. *Oncotarget*, *8*(25), 40817–40831. https://doi.org/10.18632/oncotarget.17256

Kolos, J. M., Voll, A. M., Bauder, M., & Hausch, F. (2018). FKBP ligands-where we are and where to go? *Frontiers in Pharmacology*, *9*, 1425. https://doi.org/10.3389/fphar.2018.01425

Laplante, M., & Sabatini, D. M. (2013). Regulation of mTORC1 and its impact on gene expression at a glance. *Journal of Cell Science*, *126*(Pt 8), 1713–1719. https://doi.org/10.1242/jcs.125773

Lee, J., Moir, R. D., McIntosh, K. B., & Willis, I. M. (2012). TOR signaling regulates ribosome and tRNA synthesis via LAMMER/Clk and GSK-3 family kinases. *Molecular Cell*, *45*(6), 836–843. https://doi.org/10.1016/j.molcel.2012.01.018

Lelegren, M., Liu, Y., Ross, C., Tardif, S., & Salmon, A. B. (2016). Pharmaceutical inhibition of mTOR in the common marmoset: Effect of rapamycin on regulators of proteostasis in a non-human primate. *Pathobiology of Aging & Age-related Diseases*, *6*, 31793. https://doi.org/10.3402/pba.v6.31793

Li, J., Kim, S. G., & Blenis, J. (2014). Rapamycin: One drug, many effects. *Cell Metabolism*, *19*(3), 373–379. https://doi.org/10.1016/j.cmet.2014.01.001

Li, X., Franz, T., Atanassov, I., & Colby, T. (2021). Step-by-step sample preparation of proteins for mass spectrometric analysis. *Methods in Molecular Biology*, *2261*, 13–23. https://doi.org/10.1007/978-1-0716-1186-9_2

Liu, G. Y., & Sabatini, D. M. (2020). mTOR at the nexus of nutrition, growth, ageing and disease. *Nature Reviews. Molecular Cell Biology*, *21*(4), 183–203. https://doi.org/10.1038/s41580-019-0199-y

Lorenz, M. C., & Heitman, J. (1995). TOR mutations confer rapamycin resistance by preventing interaction with FKBP12-rapamycin. *The Journal of Biological Chemistry*, *270*(46), 27531–27537. https://doi.org/10.1074/jbc.270.46.27531

Luo, Y., Liu, L., Wu, Y., Singh, K., Su, B., Zhang, N., Liu, X., Shen, Y., & Huang, S. (2015). Rapamycin inhibits mSin1 phosphorylation independently of mTORC1 and mTORC2. *Oncotarget*, *6*(6), 4286–4298. https://doi.org/10.18632/oncotarget.3006

Ma, X. M., & Blenis, J. (2009). Molecular mechanisms of mTOR-mediated translational control. *Nature Reviews. Molecular Cell Biology*, *10*(5), 307–318. https://doi.org/10.1038/nrm2672

Mannick, J. B., del Giudice, G., Lattanzi, M., Valiante, N. M., Praestgaard, J., Huang, B., Lonetto, M. A., Maecker, H. T., Kovarik, J., Carson, S., Glass, D. J., & Klickstein, L. B. (2014). mTOR inhibition improves immune function in the elderly. *Science Translational Medicine*, *6*(268), 179. https://doi.org/10.1126/scitranslmed.3009892

Martinez, N. J., Chang, H. M., Borrajo Jde, R., & Gregory, R. I. (2013). The co-chaperones Fkbp4/5 control Argonaute2 expression and facilitate RISC assembly. *RNA*, *19*(11), 1583–1593. https://doi.org/10.1261/rna.040790.113

März, A. M., Fabian, A. K., Kozany, C., Bracher, A., & Hausch, F. (2013). Large FK506-binding proteins shape the pharmacology of rapamycin. *Molecular and Cellular Biology*, *33*(7), 1357–1367. https://doi.org/10.1128/MCB.00678-12

Mauvoisin, D., Rocque, G., Arfa, O., Radenne, A., Boissier, P., & Mounier, C. (2007). Role of the PI3-kinase/mTor pathway in the regulation of the stearoyl CoA desaturase (SCD1) gene expression by insulin in liver. *Journal of Cell Communication and Signaling*, *1*(2), 113–125. https://doi.org/10.1007/s12079-007-0011-1

Mayer, C., & Grummt, I. (2006). Ribosome biogenesis and cell growth: mTOR coordinates transcription by all three classes of nuclear RNA polymerases. *Oncogene*, *25*(48), 6384–6391. https://doi.org/10.1038/sj.onc.1209883

Meier-Kriesche, H. U., & Kaplan, B. (2000). Toxicity and efficacy of sirolimus: Relationship to whole-blood concentrations. *Clinical Therapeutics*, *22 Suppl B*, B93–B100. https://doi.org/10.1016/s0149-2918(00)89026-8

Morita, M., Prudent, J., Basu, K., Goyon, V., Katsumura, S., Hulea, L., Pearl, D., Siddiqui, N., Strack, S., McGuirk, S., St-Pierre, J., Larsson, O., Topisirovic, I., Vali, H., McBride, H., Bergeron, J. J., & Sonenberg, N. (2017). mTOR controls mitochondrial dynamics and cell survival via MTFP1. *Molecular Cell*, *67*(6), 922–935 e925. https://doi.org/10.1016/j.molcel.2017.08.013

Nachef, M., Ali, A. K., Almutairi, S. M., & Lee, S. H. (2021). Targeting SLC1A5 and SLC3A2/SLC7A5 as a potential strategy to strengthen anti-tumor immunity in the tumor microenvironment. *Frontiers in Immunology*, *12*, 624324. https://doi.org/10.3389/fimmu.2021.624324

Nandagopal, N., & Roux, P. P. (2015). Regulation of global and specific mRNA translation by the mTOR signaling pathway. *Translation (Austin)*, *3*(1), e983402. https://doi.org/10.4161/21690731.2014.983402

Paquet, D., Kwart, D., Chen, A., Sproul, A., Jacob, S., Teo, S., Olsen, K. M., Gregg, A., Noggle, S., & Tessier-Lavigne, M. (2016). Efficient

introduction of specific homozygous and heterozygous mutations using CRISPR/Cas9. *Nature*, *533*(7601), 125–129. https://doi.org/10.1038/nature17664

Partridge, L., Fuentealba, M., & Kennedy, B. K. (2020). The quest to slow ageing through drug discovery. *Nature Reviews. Drug Discovery*, *19*(8), 513–532. https://doi.org/10.1038/s41573-020-0067-7

Perez-Riverol, Y., Bai, J., Bandla, C., García-Seisdedos, D., Hewapathirana, S., Kamatchinathan, S., Kundu, D. J., Prakash, A., Frericks-Zipper, A., Eisenacher, M., Walzer, M., Wang, S., Brazma, A., & Vizcaíno, J. A. (2022). The PRIDE database resources in 2022: A hub for mass spectrometry-based proteomics evidences. *Nucleic Acids Research*, *50*(D1), D543–D552. https://doi.org/10.1093/nar/gkab1038

Powers, R. W., 3rd, Kaeberlein, M., Caldwell, S. D., Kennedy, B. K., & Fields, S. (2006). Extension of chronological life span in yeast by decreased TOR pathway signaling. *Genes & Development*, *20*(2), 174–184. https://doi.org/10.1101/gad.1381406

Powers, T., & Walter, P. (1999). Regulation of ribosome biogenesis by the rapamycin-sensitive TOR-signaling pathway in Saccharomyces cerevisiae. *Molecular Biology of the Cell*, *10*(4), 987–1000. https://doi.org/10.1091/mbc.10.4.987

R Core Team. (2017). *R: A language and environment for statistical computing*. R Foundation for Statistical Computing.

Ramanathan, A., & Schreiber, S. L. (2009). Direct control of mitochondrial function by mTOR. *Proceedings of the National Academy of Sciences of the United States of America*, *106*(52), 22229–22232. https://doi.org/10.1073/pnas.0912074106

Ran, F. A., Hsu, P. D., Wright, J., Agarwala, V., Scott, D. A., & Zhang, F. (2013). Genome engineering using the CRISPR-Cas9 system. *Nature Protocols*, *8*(11), 2281–2308. https://doi.org/10.1038/nprot.2013.143

Ritchie, M. E., Phipson, B., Wu, D., Hu, Y., Law, C. W., Shi, W., & Smyth, G. K. (2015). Limma powers differential expression analyses for RNA-sequencing and microarray studies. *Nucleic Acids Research*, *43*(7), e47. https://doi.org/10.1093/nar/gkv007

Robida-Stubbs, S., Glover-Cutter, K., Lamming, D. W., Mizunuma, M., Narasimhan, S. D., Neumann-Haefelin, E., Sabatini, D. M., & Blackwell, T. K. (2012). TOR signaling and rapamycin influence longevity by regulating SKN-1/Nrf and DAF-16/FoxO. *Cell Metabolism*, *15*(5), 713–724. https://doi.org/10.1016/j.cmet.2012.04.007

Rosario, F. J., Gupta, M. B., Myatt, L., Powell, T. L., Glenn, J. P., Cox, L., & Jansson, T. (2019). Mechanistic target of rapamycin complex 1 promotes the expression of genes encoding electron transport chain proteins and stimulates oxidative phosphorylation in primary human trophoblast cells by regulating mitochondrial biogenesis. *Scientific Reports*, *9*(1), 246. https://doi.org/10.1038/s41598-018-36265-8

Schieke, S. M., Phillips, D., McCoy, J. P., Jr., Aponte, A. M., Shen, R. F., Balaban, R. S., & Finkel, T. (2006). The mammalian target of rapamycin (mTOR) pathway regulates mitochondrial oxygen consumption and oxidative capacity. *The Journal of Biological Chemistry*, *281*(37), 27643–27652. https://doi.org/10.1074/jbc.M603536200

Schinaman, J. M., Rana, A., Ja, W. W., Clark, R. I., & Walker, D. W. (2019). Rapamycin modulates tissue aging and lifespan independently of the gut microbiota in drosophila. *Scientific Reports*, *9*(1), 7824. https://doi.org/10.1038/s41598-019-44106-5

Sun, L., Yan, Y., Lv, H., Li, J., Wang, Z., Wang, K., Wang, L., Li, Y., Jiang, H., & Zhang, Y. (2022). Rapamycin targets STAT3 and impacts c-Myc to suppress tumor growth. *Cell Chemistry & Biology*, *29*(3), 373–385. https://doi.org/10.1016/j.chembiol.2021.10.006

Takasaki, S., Yamaguchi, H., Kawasaki, Y., Kikuchi, M., Tanaka, M., Ito, A., & Mano, N. (2019). Long-term relationship between everolimus blood concentration and clinical outcomes in Japanese patients with metastatic renal cell carcinoma: A prospective study. *Journal of Pharmaceutical Health Care and Sciences*, *5*, 6. https://doi.org/10.1186/s40780-019-0135-5

Tardif, S., Ross, C., Bergman, P., Fernandez, E., Javors, M., Salmon, A., Spross, J., Strong, R., & Richardson, A. (2015). Testing efficacy of administration of the antiaging drug rapamycin in a nonhuman primate, the common marmoset. *The Journals of Gerontology. Series A, Biological Sciences and Medical Sciences*, *70*(5), 577–587. https://doi.org/10.1093/gerona/glu101

Thoreen, C. C., Chantranupong, L., Keys, H. R., Wang, T., Gray, N. S., & Sabatini, D. M. (2012). A unifying model for mTORC1-mediated regulation of mRNA translation. *Nature*, *485*(7396), 109–113. https://doi.org/10.1038/nature11083

Thoreen, C. C., Kang, S. A., Chang, J. W., Liu, Q., Zhang, J., Gao, Y., Reichling, L. J., Sim, T., Sabatini, D. M., & Gray, N. S. (2009). An ATP-competitive mammalian target of rapamycin inhibitor reveals rapamycin-resistant functions of mTORC1. *The Journal of Biological Chemistry*, *284*(12), 8023–8032. https://doi.org/10.1074/jbc.M900301200

Torrence, M. E., MacArthur, M. R., Hosios, A. M., Valvezan, A. J., Asara, J. M., Mitchell, J. R., & Manning, B. D. (2021). The mTORC1-mediated activation of ATF4 promotes protein and glutathione synthesis downstream of growth signals. *eLife*, *10*, e63326. https://doi.org/10.7554/eLife.63326

Tsokanos, F. F., Albert, M. A., Demetriades, C., Spirohn, K., Boutros, M., & Teleman, A. A. (2016). eIF4A inactivates TORC1 in response to amino acid starvation. *The EMBO Journal*, *35*(10), 1058–1076. https://doi.org/10.15252/embj.201593118

Tsukumo, Y., Alain, T., Fonseca, B. D., Nadon, R., & Sonenberg, N. (2016). Translation control during prolonged mTORC1 inhibition mediated by 4E-BP3. *Nature Communications*, *7*, 11776. https://doi.org/10.1038/ncomms11776

Urfer, S. R., Kaeberlein, T. L., Mailheau, S., Bergman, P. J., Creevy, K. E., Promislow, D. E. L., & Kaeberlein, M. (2017). A randomized controlled trial to establish effects of short-term rapamycin treatment in 24 middle-aged companion dogs. *Geroscience*, *39*(2), 117–127. https://doi.org/10.1007/s11357-017-9972-z

Vervliet, T., Parys, J. B., & Bultynck, G. (2015). Bcl-2 and FKBP12 bind to IP3 and ryanodine receptors at overlapping sites: The complexity of protein-protein interactions for channel regulation. *Biochemical Society Transactions*, *43*(3), 396–404. https://doi.org/10.1042/BST20140298

Villa-Cuesta, E., Holmbeck, M. A., & Rand, D. M. (2014). Rapamycin increases mitochondrial efficiency by mtDNA-dependent reprogramming of mitochondrial metabolism in drosophila. *Journal of Cell Science*, *127*(Pt 10), 2282–2290. https://doi.org/10.1242/jcs.142026

Visner, G. A., Lu, F., Zhou, H., Liu, J., Kazemfar, K., & Agarwal, A. (2003). Rapamycin induces heme oxygenase-1 in human pulmonary vascular cells: Implications in the antiproliferative response to rapamycin. *Circulation*, *107*(6), 911–916. https://doi.org/10.1161/01.cir.0000048191.75585.60

Wall, M., Poortinga, G., Hannan, K. M., Pearson, R. B., Hannan, R. D., & McArthur, G. A. (2008). Translational control of c-MYC by rapamycin promotes terminal myeloid differentiation. *Blood*, *112*(6), 2305–2317. https://doi.org/10.1182/blood-2007-09-111856

Wang, R., Yu, Z., Sunchu, B., Shoaf, J., Dang, I., Zhao, S., Caples, K., Bradley, L., Beaver, L. M., Ho, E., Löhr, C. V., & Perez, V. I. (2017). Rapamycin inhibits the secretory phenotype of senescent cells by a Nrf2-independent mechanism. *Aging Cell*, *16*(3), 564–574. https://doi.org/10.1111/acel.12587

Wang, T., Li, B. Y., Danielson, P. D., Shah, P. C., Rockwell, S., Lechleider, R. J., Martin, J., Manganaro, T., & Donahoe, P. K. (1996). The immunophilin FKBP12 functions as a common inhibitor of the TGF beta family type I receptors. *Cell*, *86*(3), 435–444.

Wang, X., Yue, P., Chan, C. B., Ye, K., Ueda, T., Watanabe-Fukunaga, R., Fukunaga, R., Fu, H., Khuri, F. R., & Sun, S. Y. (2007). Inhibition of mammalian target of rapamycin induces phosphatidylinositol 3-kinase-dependent and Mnk-mediated eukaryotic translation initiation factor 4E phosphorylation. *Molecular and Cellular Biology*, *27*(21), 7405–7413. https://doi.org/10.1128/MCB.00760-07

Zaragoza, D., Ghavidel, A., Heitman, J., & Schultz, M. C. (1998). Rapamycin induces the G0 program of transcriptional repression in yeast by interfering with the TOR signaling pathway. *Molecular and Cellular Biology*, *18*(8), 4463–4470. https://doi.org/10.1128/MCB.18.8.4463

Zhang, H., Stallock, J. P., Ng, J. C., Reinhard, C., & Neufeld, T. P. (2000). Regulation of cellular growth by the drosophila target of rapamycin dTOR. *Genes & Development*, *14*(21), 2712–2724. https://doi.org/10.1101/gad.835000

Zhang, X., Chen, W., Gao, Q., Yang, J., Yan, X., Zhao, H., Su, L., Yang, M., Gao, C., Yao, Y., Inoki, K., Li, D., Shao, R., Wang, S., Sahoo, N., Kudo, F., Eguchi, T., Ruan, B., & Xu, H. (2019). Rapamycin directly activates lysosomal mucolipin TRP channels independent of mTOR. *PLoS Biology*, *17*(5), e3000252. https://doi.org/10.1371/journal.pbio.3000252

Zhang, Y., Swanda, R. V., Nie, L., Liu, X., Wang, C., Lee, H., Lei, G., Mao, C., Koppula, P., Cheng, W., Zhang, J., Xiao, Z., Zhuang, L., Fang, B., Chen, J., Qian, S. B., & Gan, B. (2021). mTORC1 couples cyst(e)ine availability with GPX4 protein synthesis and ferroptosis regulation. *Nature Communications*, *12*(1), 1589. https://doi.org/10.1038/s41467-021-21841-w

Zhu, Y., Zou, R., Sha, H., Lu, Y., Zhang, Y., Wu, J., Feng, J., & Wang, D. (2020). Lipid metabolism-related proteins of relevant evolutionary and lymphoid interest (PRELI) domain containing family proteins in cancer. *American Journal of Translational Research*, *12*(10), 6015–6026.

SUPPORTING INFORMATION

Additional supporting information can be found online in the Supporting Information section at the end of this article.

How to cite this article: Artoni, F., Grützmacher, N., & Demetriades, C. (2023). Unbiased evaluation of rapamycin's specificity as an mTOR inhibitor. *Aging Cell*, *00*, e13888. https://doi.org/10.1111/acel.13888

Supplementary Information

Figures S1-S4 and Tables S1-S8

Supplementary Tables

Table S1. Differential gene expression analysis in control (WT) and mTOR^{RR} HEK293FT cells upon rapamycin treatment.

Table S2. List of genes used for the GO analysis and associated GO terms from the RNA-seq analysis in Rapa- vs DMSO-treated WT cells (only strongly affected genes).

Table S3. List of genes used for the GO analysis and associated GO terms from the RNA-seq analysis in Rapa- vs DMSO-treated WT cells (all significantly changing genes).

Table S4. Differential protein expression analysis in control (WT) and mTOR^{RR} HEK293FT cells upon rapamycin treatment.

Table S5. List of proteins used for the GO analysis and associated GO terms from the proteomic analysis in 24 h Rapa- vs DMSO-treated WT cells (all significantly changing proteins).

Table S6. List of proteins used for the GO analysis and associated GO terms from the proteomic analysis in 48 h Rapa- vs DMSO-treated WT cells (all significantly changing proteins).

Table S7. List of proteins used for the GO analysis and associated GO terms from the proteomic analysis in 24 h Rapa- vs DMSO-treated WT cells (only strongly affected proteins).

Table S8. List of DNA oligonucleotides used in this study.

Supplementary Figures

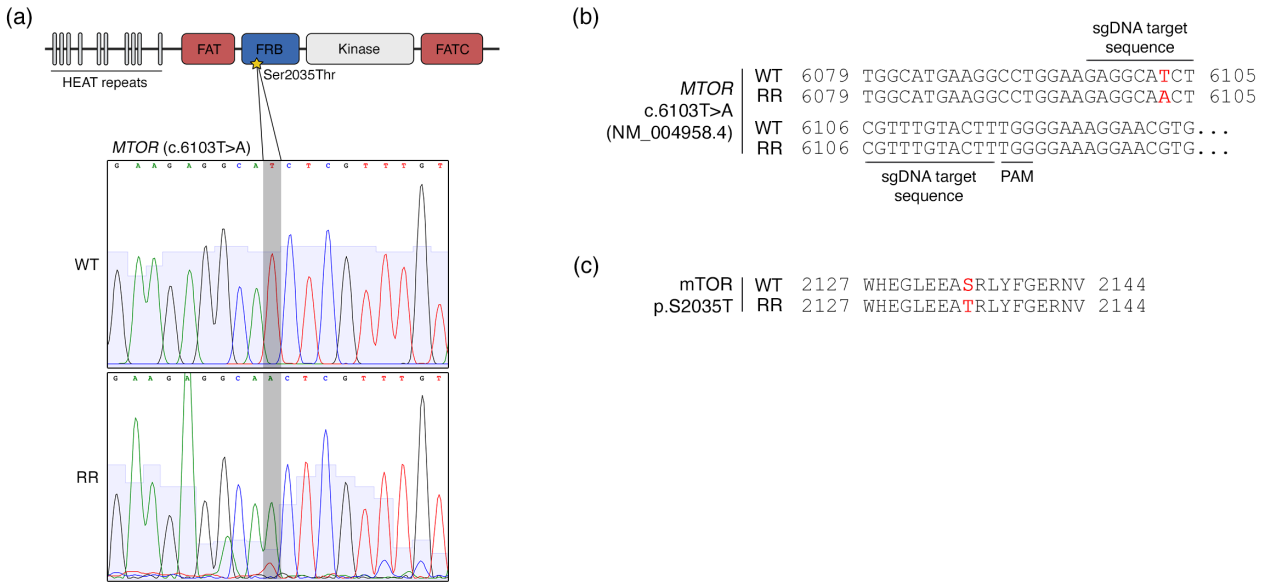

Figure S1. Characterization of the *MTOR* genomic alterations in the mTOR^{RR} HEK293FT cells.

(a-c) CRISPR/Cas9-mediated gene-editing of *MTOR*. The associated genomic changes in *MTOR* were validated by Sanger sequencing (a). The resulting changes in the mTOR cDNA (c.6103T>A) and protein sequence (p.S2035T) are shown in (b) and (c), respectively. The sgDNA target sequence and PAM site are marked on the *MTOR* sequence in (b). The position of the modified nucleotide / amino acid residue is shown in red.

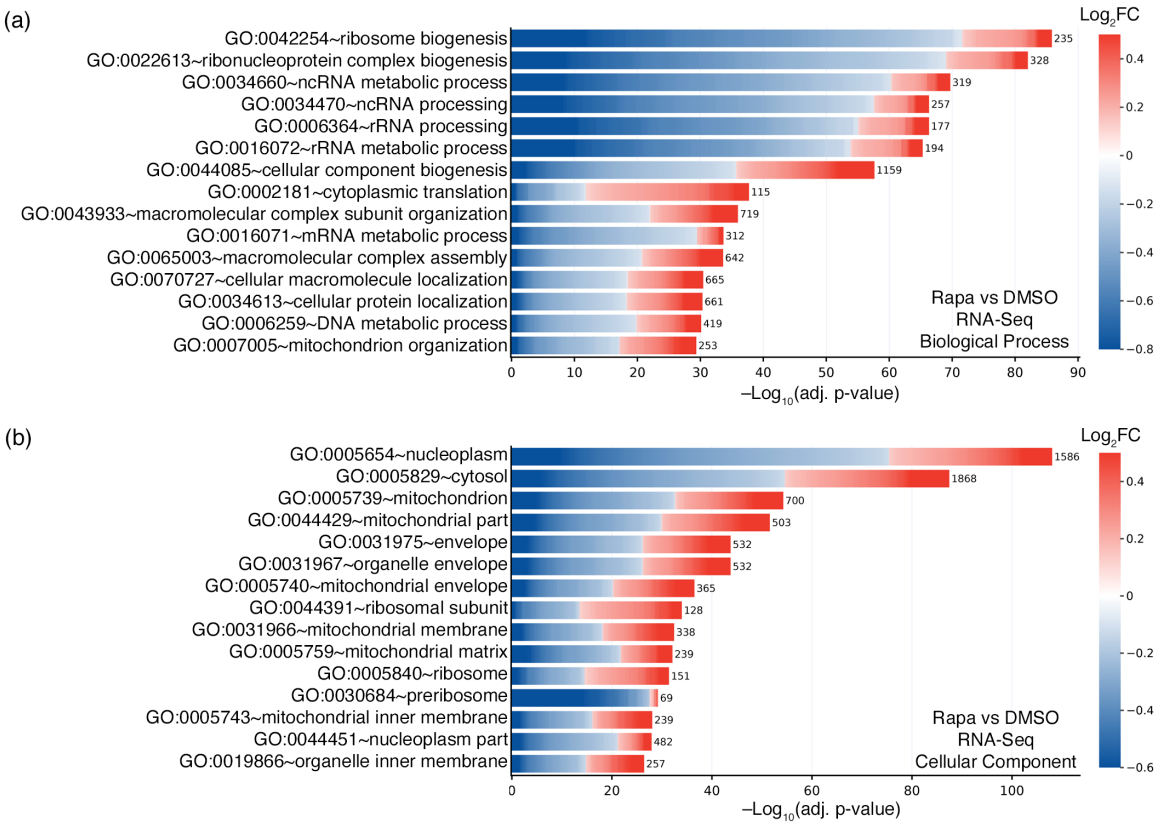

Figure S2. GO analysis of the rapamycin-induced changes in the transcriptome of WT HEK293FT cells.

(a) Biological process (BP) GO term analysis using all genes that are significantly (adj. p-value < 0.05) down- (blue) or upregulated (red) by rapamycin in WT cells, as described in Fig. 2b. The color of each box in the cell plot represents log-transformed fold change values for each gene in rapamycin- vs DMSO-treated cells. The number of genes in the selected dataset for each GO term is shown on the right side of each bar.

(b) As in (a), but for Cellular Component (CC) GO term analysis.

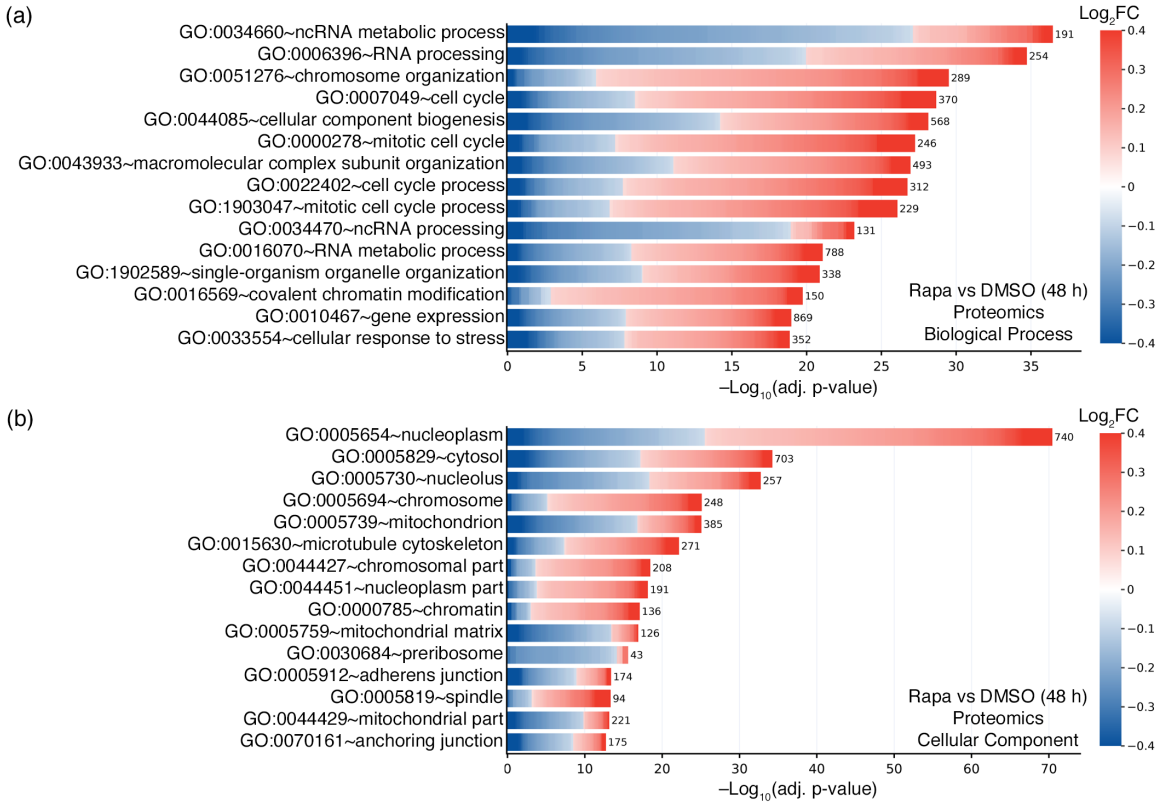

Figure S3. GO analysis of the rapamycin-induced changes (48 h) in the proteome of WT HEK293FT cells.

(a) Biological process (BP) GO term analysis using all proteins that are significantly down- (blue) or upregulated (red) by rapamycin (48 h) in WT cells, as described in Fig. 3c. The color of each box in the cell plot represents log-transformed fold change values for each protein in rapamycin- vs DMSO-treated cells. The number of proteins in the selected dataset for each GO term is shown on the right side of each bar.

(b) As in (a), but for Cellular Component (CC) GO term analysis.

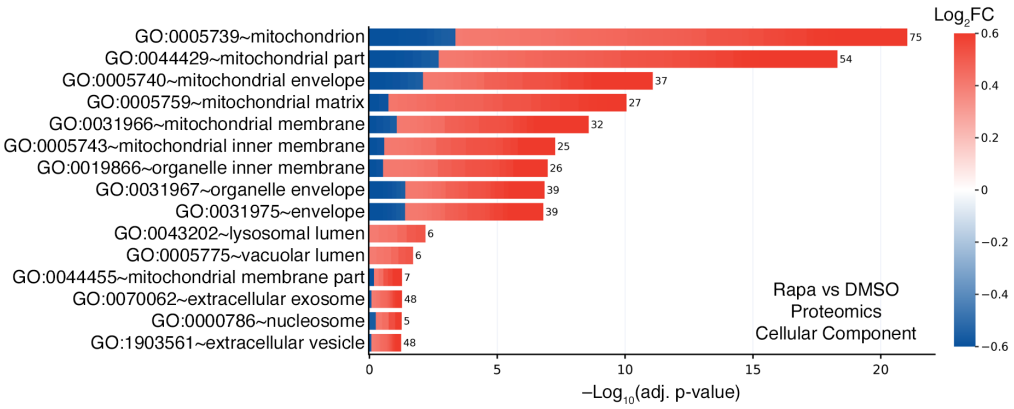

Figure S4. GO analysis of the robust rapamycin-induced changes (24 h) in the proteome of WT HEK293FT cells.

Cellular Component (CC) GO term analysis using only the proteins that are strongly down- (blue) or upregulated (red) by rapamycin (24 h) in WT cells, as described in Fig. 3b. The color of each box in the cell plot represents log-transformed fold change values for each protein in rapamycin- vs DMSO-treated cells. The number of proteins in the selected dataset for each GO term is shown on the right side of each bar.

Chapter 3. PRR14L is a novel transcriptional regulator of genes related to the vesicle exocytosis machinery

Grützmacher N, Demetriades C.

Manuscript in preparation.

Supplementary Material is provided after the manuscript.

PRR14L is a novel transcriptional regulator of genes related to the vesicle exocytosis machinery

Nina Grützmacher[1], Constantinos Demetriades[1,2,§]

[1]Max Planck Institute for Biology of Ageing (MPI-AGE), 50931 Cologne, Germany

[2]University of Cologne, Cologne Excellence Cluster on Cellular Stress Response in Aging-Associated Diseases (CECAD), 50931 Cologne, Germany

[§]Correspondence: Demetriades@age.mpg.de (C.D.)

Abstract

FK506-binding proteins (FKBPs) are immunophilins that are characterized by their PPIase activity and play an important role in protein folding. High molecular weight immunophilins have additional tetratricopeptide repeats that mediate binding to Hsp90, and FKBPs in complex with Hsp90 contribute to the regulation of the biological functions of several client proteins. Here, we have identified PRR14L, a so far largely uncharacterized protein, as a novel interaction partner of FKBP51 and FKBP52. PRR14L shows nuclear localization which is partially affected by loss of FKBP52. Furthermore, APEX2-proximome analysis revealed that PRR14L interacts with multiple chromatin and transcriptional regulators suggesting a potential role in regulating gene expression. Accordingly, knock-down of PRR14L causes significant changes in the gene expression of some of the core components of the synaptic vesicle exocytosis machinery. Taken together, our data reveal a novel FKBP-interacting protein that binds to chromatin and regulates transcription of genes implicated in the synaptic vesicle cycle.

Keywords

PRR14L, FKBP51, FKBP52, transcription, vesicles, exocytosis

Introduction

FKBPs (FK506-binding proteins) are immunophilins that can bind FK506 or Rapamycin, and are able to inhibit T-cell activation and proliferation by forming a binary complex with their respective immunosuppressants (Harikishore and Yoon, 2015). Currently, a total of 15 FKBP proteins have been identified in humans with different subcellular localization patterns, domain structures, and functions (Bonner and Boulianne, 2017). One well-known role of some FKBPs is the binding to Rapamycin and subsequent inhibition of mTORC1 (mechanistic target of Rapamycin complex 1) (Heitman *et al.*, 1991; Brown *et al.*, 1994). While FKBP12 is the smallest and archetypical member of the FKBP family, many more FKBPs were reported over the last years to be able to bind Rapamycin and therefore, exert its inhibitory effect on mTORC1, including FKBP12.6, FKBP51 and FKBP52 (Lam *et al.*, 1995; März *et al.*, 2013). FKBPs play a critical role as folding chaperones for various targets through their PPIase (peptidylprolyl cis/trans isomerase) activity (Galat and Metcalfe, 1995). However, although some FKBPs display a very similar structure, they can differ regarding their specific physiological roles. As a result of the diversification of their sequences and the variations in their domain structures, it is believed that FKBPs have undergone adaptations to accommodate the increasing number and diversity of cellular targets throughout evolution. While FKBP12 and FKBP12.6 possess only a single functional PPIase domain (Arakawa *et al*., 1994), larger FKBPs have additional domains and/or duplicated their PPIase domain. FKBP51 and FKBP52 both contain three TPR (tetratricopeptide repeat) motifs that are responsible for protein-protein interaction with Hsp90 resulting in co-chaperone activity that modifies SHR (steroid hormone receptor) activity (Pirkl and Buchner, 2001). Although FKBP51 and FKBP52 share 60% amino acid sequence identity, they function in distinct ways which is largely attributed to differences in their functional PPIase domain and the proline-rich loop (Pirkl and Buchner, 2001). While FKBP52 positively regulates the glucocorticoid receptor (Riggs *et al*., 2003), progesterone

receptor (Tranguch *et al*., 2005) and androgen receptor (Cheung-Flynn *et al*., 2005), FKBP51 negatively regulates SHR activity (Storer *et al*., 2011). Furthermore, overexpression of FKBP51 leads to a decreased regulation of SHR by FKBP52 due to the competitive binding of the FKBPs to the SHR complex (Riggs *et al*., 2003).

Rapamycin binds to FKBPs through their PPIase domain (Van Duyne *et al.*, 1991). Since FKBPs have several client proteins and exert a variety of physiological effects in cells (Tong and Jiang, 2016), we investigated if Rapamycin has any significant effects on the interactions of FKBPs to their substrates and, therefore, if Rapamycin exerts any functions that are independent of mTORC1 inhibition. To study the effect of Rapamycin on the interaction of FKBPs to their respective client proteins, we performed co-IP (co-immunoprecipitation)/MS (mass spectrometry) experiments with HEK293FT cells stably expressing FLAG-tagged FKBP proteins and treated these cells with Rapamycin. Although these experiments did not identify potential mTOR-independent effects of Rapamycin, they highlighted PRR14L as a novel interaction partner of FKBP51 and FKBP52. PRR14L is a protein with unclear function, and so far, its involvement has only been suggested in cell division (Chase *et al.*, 2019). Given the diverse functions of FKBP51 and FKBP52 (Hähle *et al.*, 2019; Davies and Sánchez, 2005), we aimed to functionally characterize PRR14L and investigate the potential role of FKBP-PRR14L interaction in PRR14L function.

Results

FKBP51 and FKBP52 bind PRR14L through their TPR domains

Whereas FKBP12 is the archetypical member of the FKBP family, to date there have been several FKBPs identified that are able to bind Rapamycin, such as FKBP12.6, FKBP51 and FKBP52 (Lam *et al.*, 1995; März *et al.*, 2013). In order to identify proteins that bind to these FKBPs, we performed co-IP/MS experiments. In addition, we investigated if Rapamycin influences these interactions and by doing so, if Rapamycin can exert mTOR-independent functions. We generated stable HEK293FT cell lines expressing FLAG-tagged FKBPs and subsequently treated these cells with 20 nM Rapamycin for 1 hour. Co-IP experiments were performed to immunoprecipitate FLAG-FKBPs, and MS analysis identified interacting proteins of the respective FKBPs. Our data showed that FLAG-FKBP12 interacts only with mTOR and mLST8, both subunits of mTORC1 and mTORC2, upon Rapamycin-treatment demonstrating the specificity of Rapamycin towards mTOR (Fig. S1A). Furthermore, FLAG-FKBP12.6 was shown to bind to GLMN (Glomulin) (Fig. S1B), a known interactor of FKBPs, which is responsible for priming proteins for proteasomal degradation (Hähle *et al.*, 2019). Interestingly, no proteins changed their binding affinity to FLAG-FKBP52 significantly upon Rapamycin-treatment (Fig. S1D) although it was shown before that FKBP52 can bind mTOR upon Rapamycin-treatment (März *et al.*, 2013). On the other hand, for FLAG-FKBP51, we observed mild effects of Rapamycin in its interaction with a limited set of proteins involved in transcriptional regulation, mRNA processing and filament structure during cell division (Fig. S1C). However, via an independent approach that we developed in parallel, we showed that Rapamycin acts exclusively via mTOR (Artoni *et al.*, 2023). This was demonstrated by experiments using a cell line that expressed Rapamycin-resistant mTOR ($mTOR^{RR}$). The findings indicated that Rapamycin-treatment did not lead to any alterations in mRNA or protein levels in $mTOR^{RR}$ cells. This suggests that even if Rapamycin affects some of the interactions

of FKBP51 with the identified interacting proteins, they would not be expected to have any physiological effects in cells. Therefore, we turned our attention to proteins that interact with FKBPs, independently of whether these interactions are influenced by Rapamycin or not.

We analyzed the interactome of FLAG-tagged FKBP51 and FKBP52 compared to an unrelated negative control protein, and identified several known interactors including GLMN (Hähle *et al.*, 2019), AGO1 (Argonaute-1) and AGO2 (Martinez *et al.*, 2013), NR3C1 (glucocorticoid receptor) (Wochnik *et al.*, 2005), as well as POLE (DNA polymerase epsilon) and POLR2B (RNA polymerase II subunit B) (Riggs *et al.*, 2003). Among the top hits, we also identified a poorly characterized protein called PRR14L (proline rich 14-like) that binds to both large FKBPs (Fig. 1A and 1B). By analyzing the data of Rapamycin-treated cells stably expressing FLAG-FKBP51 or FLAG-FKBP52 compared to DMSO-treated cells expressing an unrelated negative control protein, we also identified PRR14L as one of the top hits. This finding indicates that the interaction of PRR14L to FKBP51 and FKBP52 remains intact even in the presence of Rapamycin (Fig. S2E and S2F).

To validate the binding of PRR14L to FKBP51 and FKBP52, we performed co-IP experiments with exogenously expressed FLAG-tagged FKBPs or FLAG-Luc as negative control (Fig. 1C). Full-length FKBP51 and FKBP52 pulled down PRR14L confirming the binding between PRR14L and FKBPs (Fig. 1D). In contrast to FKBP12 and FKBP12.6, larger FKBPs have three TPR domains that are responsible for protein-protein interactions with Hsp90 (Pirkl and Buchner, 2001) (Fig. 1C). We generated ΔTPR-truncated FKBP51 and FKBP52, respectively, and by performing co-IP experiments, we showed that the binding of PRR14L to FKBPs was abolished (Fig. 1D) providing evidence that the protein-protein interaction specifically occurs through the TPR domains. Additionally, the lack of these TPR domains in the smaller FKBPs, FKBP12 and FKP12.6, explains why PRR14L did not show up as an interacting protein in their MS analysis (Fig. S2A-D).

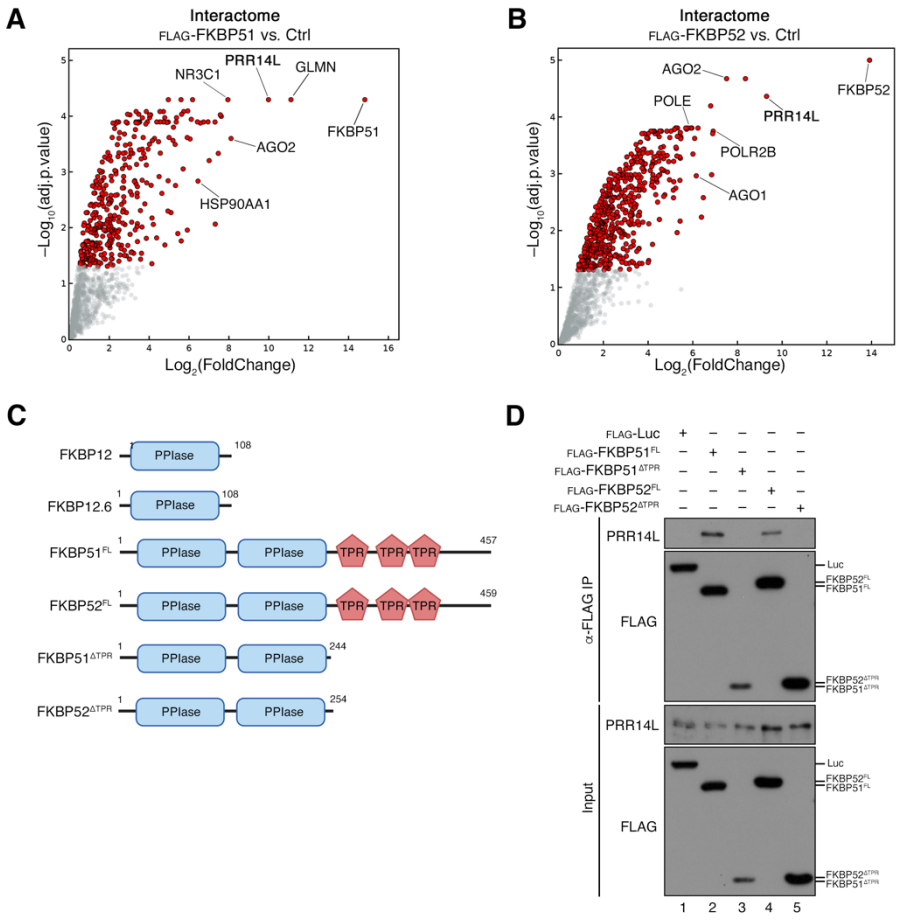

Figure 1. PRR14L is a novel binding partner of FKBP51 and FKBP52. (A) Interactome of FKBP51 in HEK293FT WT cells, stably expressing FLAG-tagged FKBP51 compared to cells expressing an unrelated control protein. Proteins that specifically interact with FKBP51 are shown in red. Proteins that don't significantly bind to FKBP51 are shown as grey dots. **(B)** Interactome of FKBP52 in HEK293FT WT cells, stably expressing FLAG-tagged FKBP52 compared to cells expressing an unrelated control protein. Proteins that specifically interact with FKBP52 are shown in red. Proteins that don't significantly bind to FKBP52 are shown as grey dots **(C)** Schematic model of the different FKBPs depicting key domains as well as FKBP51 and FKBP52 truncations used in (D). FL = full length. **(D)** Diminished binding of PRR14L to the truncated FKBP proteins. Co-immunoprecipitation experiments in HEK293FT cells, transiently expressing FLAG-tagged FKBPs constructs or Luciferase (Luc) as negative control. Binding of PRR14L to FKBPs was analyzed by immunoblotting as indicated. FL = full length.

PRR14L localizes to the nucleus

Apart from a 49 amino acid region of homology with PRR14 and the *Drosophila melanogaster* protein tant (tantalus), no other recognized domains have been identified in PRR14L (Dietrich *et al*., 2001). The cellular role of this tantalus-like domain is largely unknown and it might confer tissue-specific functions involved in the regulation of development in metazoans (Dietrich *et al*., 2001). Moreover, the physiological function of PRR14L remains unclear with the only published study suggesting a role in cell division (Chase *et al.*, 2019).

Previously, it was shown that PRR14L has two predicted NLS (nuclear localization signals) (Chase *et al.*, 2019) (Fig. 2A). Therefore, we investigated the subcellular localization of PRR14L by transiently transfecting HEK293FT cells with FLAG-tagged PRR14L constructs (Fig. 2A). As expected, full-length PRR14L showed predominantly nuclear localization whereas it was completely cytosolic when both NLS were truncated (Fig. 2B). Moreover, removing only the C-terminal NLS resulted in a mostly cytosolic localization pattern with some cells still displaying nuclear and intermediate localization (Fig. 2C). The reason for the presence of two NLS domains in PRR14L as well as their relative contribution to its localization is not clear and is worth exploring in the future.

Since PRR14L binds to FKBP51 and FKBP52, we investigated if its localization is affected by the loss of either one or both FKBPs. We generated KO (knock-out) cell lines using CRISPR-Cas9 genome editing to remove FKBP51 or FKBP52, alone or in combination. PRR14L localizes predominantly to the nucleus in control cells as expected (Fig. 2D). However, its localization was affected by the loss of FKBP52 resulting in a 50% delocalization of PRR14L to the cytosol (Fig. 2D and 2E). In contrast, loss of FKBP51 did not affect PRR14L localization suggesting a differential role of FKBP51 and FKBP52 in PRR14L localization. Interestingly, the removal of FKBP51 in addition to FKBP52 reversed the effect of FKBP52 loss on PRR14L localization suggesting that both FKBPs play a role in its localization. Whether the loss of

FKBP52 partially blocks the nuclear import or induces an active nuclear export of PRR14L to the cytosol, and which role FKBP51 plays in PRR14L localization has yet to be investigated.

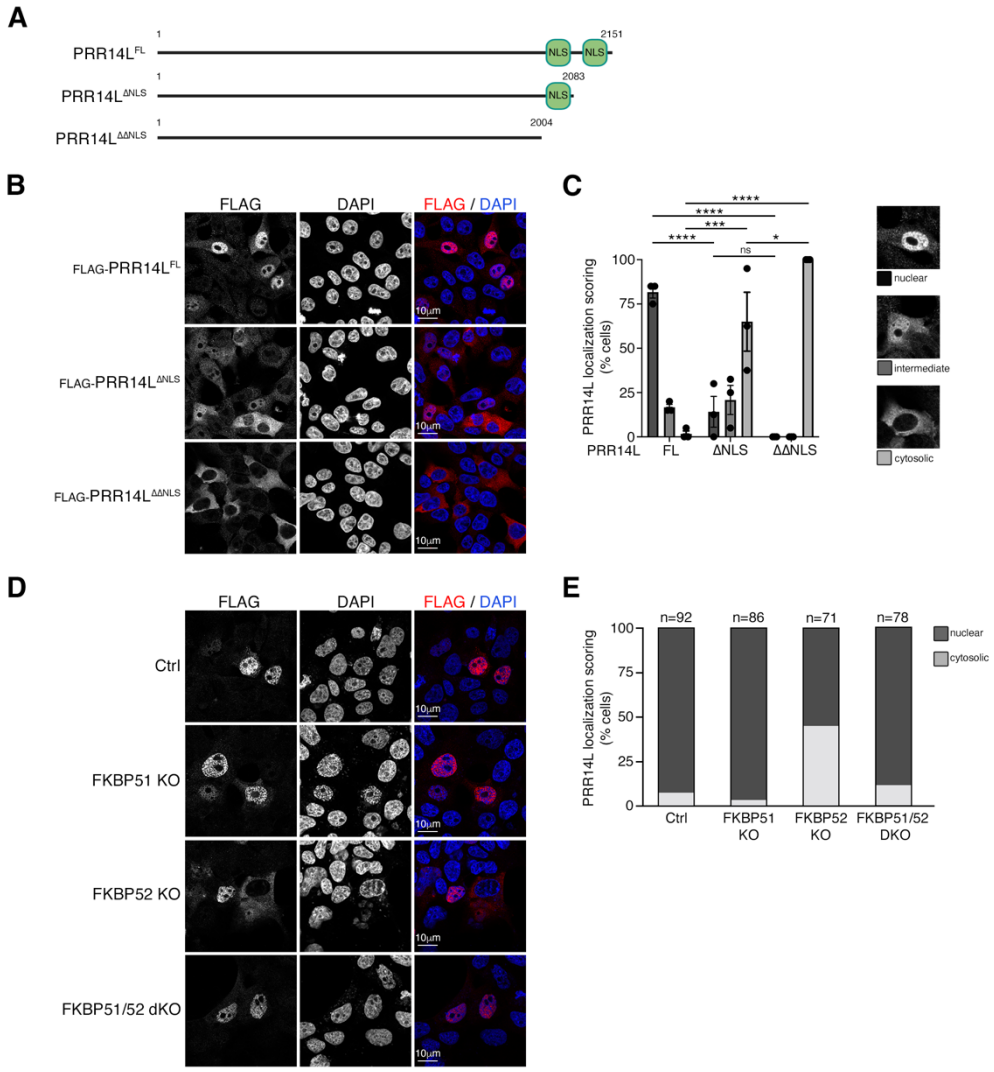

Figure 2. PRR14L localizes to the nucleus. (A) Schematic model of PRR14L with two predicted nuclear localization signals (NLS). **(B)** PRR14L localization analysis in HEK293FT WT cells, transiently expressing FLAG-tagged PRR14L constructs shown in (A), using confocal microscopy. Nuclei stained with DAPI. Scale bars, 10 µm. *n* = 3 independent experiments. **(C)** Scoring of PRR14L localization from (B). Individual cells were scored for nuclear, intermediate or cytoplasmic PRR14L localization, as indicated in the example images. *n* = 3 independent experiments. **(D)** PRR14L localization analysis in control, FKBP51 KO, FKBP52 KO or FKBP51/52 dKO cells, transiently expressing FLAG-tagged PRR14L, using confocal microscopy. Nuclei stained with DAPI. Scale bars, 10 µm. *n* = 3 independent experiments. **(E)** Scoring of PRR14L localization from (D). Individual cells were scored for nuclear or cytoplasmic PRR14L localization. Total cell numbers are indicated above the respective bars. *n* = 3 independent experiments.

The PRR14L proximome reveals an interaction with chromatin and transcription related factors

To investigate the role of PRR14L in the nucleus, we performed an APEX2- (ascorbate peroxidase 2) and MS-based analysis of the PRR14L proximome in HEK293FT WT cells, stably expressing FLAG-APEX2-PRR14L or PRR14L-APEX2-HA, respectively (Fig. 3A). Western blot analysis using an HRP-conjugated streptavidin antibody showed enhanced protein biotinylation upon APEX2-dependent oxidation with both biotin-phenol and H_2O_2 (Fig. S3). After validation of our approach, we performed a pull-down assay by using streptavidin beads and subsequently analyzed all biotinylated interacting proteins by MS. More than 1000 and 500 putative novel PRR14L-interacting and -proximal proteins were identified for the N- and C-terminal APEX2-PRR14L chimeric proteins, respectively (Fig. 3B and 3C; Table S2). GO (gene ontology) analysis revealed a strong enrichment of chromatin remodeling and organization-related (e.g., KAT2A, TADA2B, PBRM1) as well as positive and negative regulation of transcription-related (e.g., LDB1, ZNF318) proteins in the PRR14L proximome indicating a potential role as a transcriptional regulator (Fig. 3D and 3E).

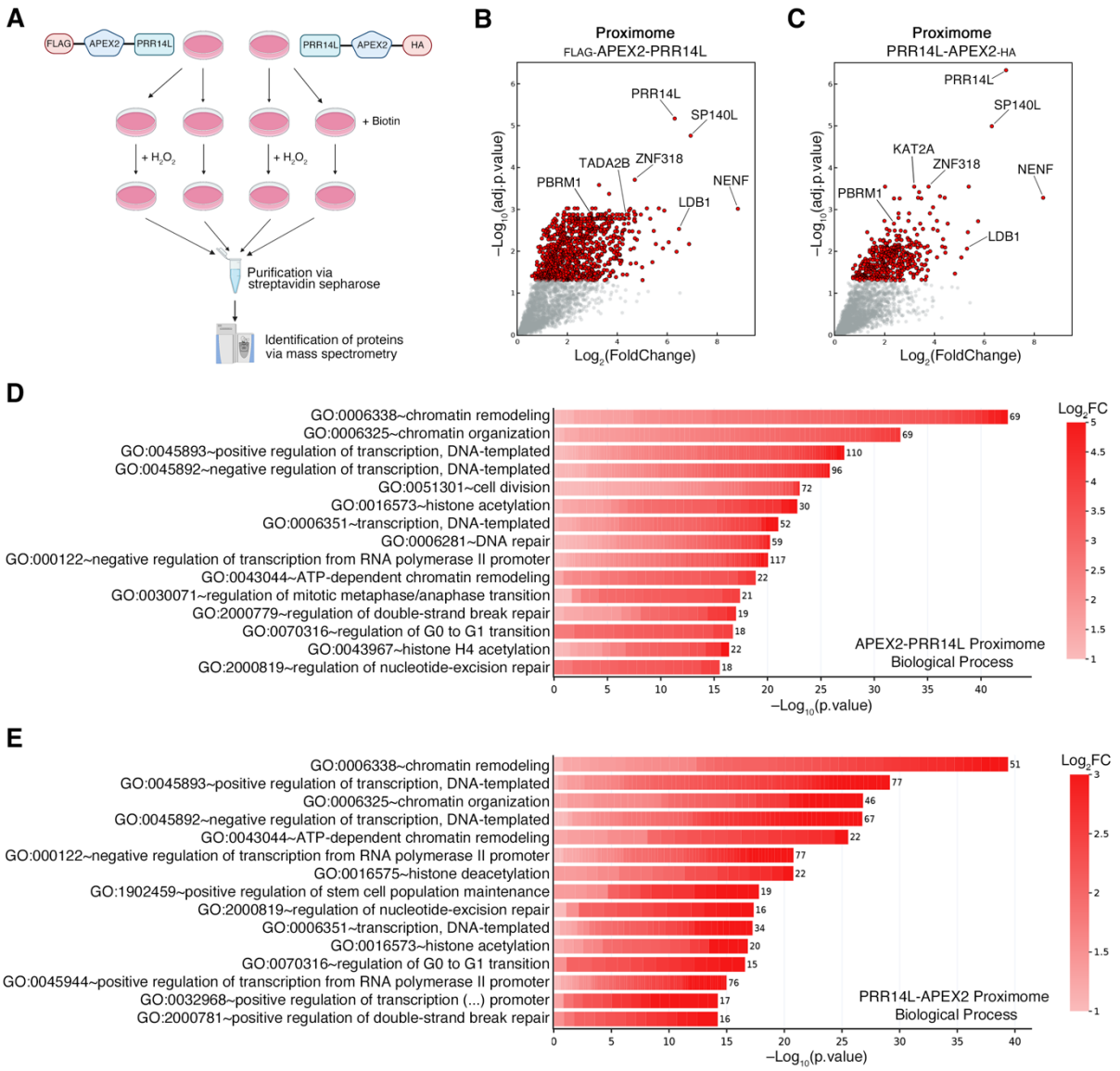

Figure 3. The PRR14L proximome reveals an interaction of PRR14L with chromatin and transcription-related factors. (A) Experimental outline of the APEX2-based PRR14L proximome assay (details in text). **(B)** Volcano plot showing all proteins identified in the PRR14L proximome of cells stably expressing FLAG-APEX2-PRR14L that show increased biotinylation and interaction with streptavidin beads compared to the control. Proteins that are specifically biotinylated ($p < 0.05$) are shown in red. Proteins that are not biotinylated ($p > 0.05$) are shown as grey dots. $n = 3$ independent experiments. **(C)** As in (B), but for cells, stably expressing PRR14L-APEX2-HA. $n = 4$ independent experiments. **(D)** Biological Process (BP) GO term analysis using protein interactions enriched in cells, stably expressing FLAG-APEX2-PRR14L. The color of each box represents fold change values for each protein. The number of proteins in the selected dataset for each term is shown on the right side of each bar. **(E)** As in (D), but for cells, stably expressing PRR14L-APEX2-HA

PRR14L affects the expression of genes implicated in the synaptic vesicle cycle

The APEX2-based proximome labeling revealed a role of PRR14L as a transcriptional regulator in the nucleus. Therefore, we knocked-down PRR14L by siRNA and performed RNA-seq analysis to investigate the effects of PRR14L KD (knock-down) on global gene expression. We detected more than 5000 genes whose expression changed significantly upon PRR14L KD (Fig. 4A and Table S3). GO term enrichment analysis, using the differentially regulated genes that are strongly down- ($Log_2FC < -1.3$) or upregulated ($Log_2FC > +0.9$), revealed a strong enrichment of synaptic signaling-related Biological Process (BP) and Cellular Compartment (CC) terms (e.g., BP:GO:0099536~synaptic signaling; CC:GO:0045202~synapse) (Fig. 4B and 4C).

We isolated RNA from HEK293FT WT cells and generated cDNA to validate a subset of the gene expression changes by RT-qPCR. *CPLX1* and *SNAP25*, genes which express proteins regulating the exocytosis of synaptic vesicles, were downregulated in HEK293FT WT cells upon PRR14L KD whereas the vesicle-associated membrane proteins *VAMP1* and *VAMP2* were upregulated (Fig. 4D) consistent with our RNA-seq results. Interestingly, three of these four genes were significantly downregulated in control conditions in FKBP52 KO cells compared to WT (Fig. 4D) suggesting that the loss of FKBP52 also affects gene expression besides the subcellular delocalization of PRR14L to the cytosol. The PRR14L-dependent changes in gene expression of *CPLX1* and *VAMP2* were also validated at the protein level by western blot analysis (Fig. 4E).

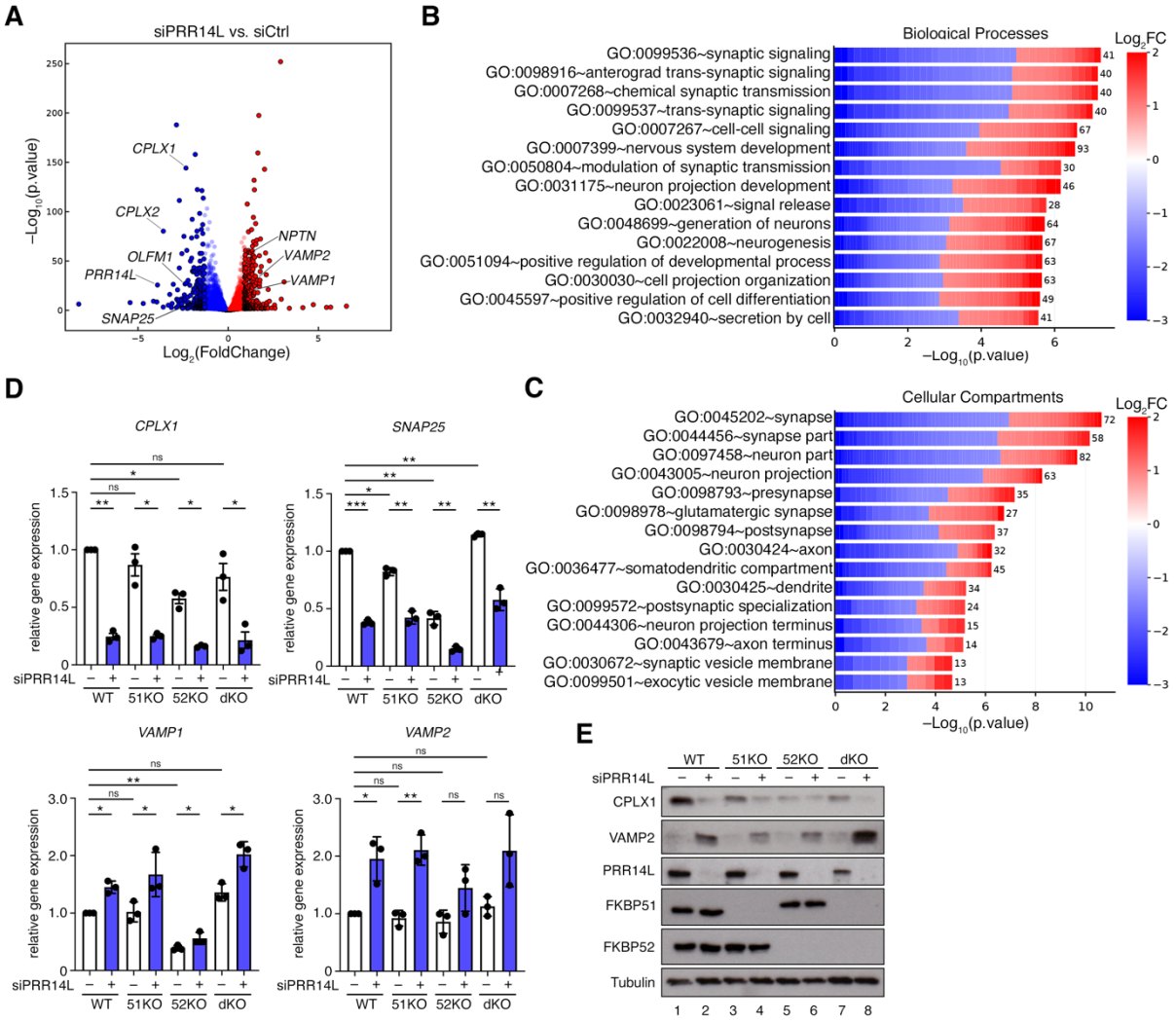

Figure 4. PRR14L affects the expression of genes implicated in the synaptic vesicle cycle. (A) Volcano plot showing changes in gene expression in HEK293FT cells using RNA-seq. Genes that are significantly ($p < 0.05$) down- or upregulated by PRR14L KD are shown in blue or red, respectively. Strongly down- ($Log_2FC < -1.3$) or upregulated (Log_2 FC > +0.9) genes are shown with black outline. Unaffected genes ($p > 0.05$) shown as grey dots. **(B)** Biological process (BP) GO term analysis using the genes that are strongly down- (blue) or upregulated (red) by PRR14L KD as described in (A). The color of each box in the cell plot represents log-transformed fold change values for each gene in siPRR14L vs. siCtrl-treated cells. The number of genes in the selected dataset for each GO term is shown on the right side of each bar. **(C)** As in (B), but for Cellular Component (CC) GO term analysis. **(D)** Expression analysis of some of the top gene hits from the GO term analysis in HEK293FT WT, FKBP51 KO, FKBP52 KO or FKBP51/52 dKO cells treated with siPRR14L or siLuc as negative control. $n = 3$ independent experiments. **(E)** Immunoblots with lysates from HEK293FT WT, FKBP51 KO, FKBP52 KO or FKBP51/52 dKO cells treated with siPRR14L or siLuc as negative control, probed with the indicated antibodies.

Discussion

Regulation of gene expression is a tightly controlled and finely-tuned process. Transcriptional regulators including transcription factors can recognize specific DNA sequences to control chromatin and transcription, forming a complex system that guides expression of the genome (Lee and Young, 2013). Here, we identified PRR14L, a novel interaction partner of FKBP51 and FKBP52, which interacts with chromatin and regulates the transcription of genes implicated in the synaptic vesicle cycle.

In an initial effort to identify mTOR-independent functions of Rapamycin, we aimed to investigate the effect of Rapamycin on the interaction of FKBPs to their client proteins. Whereas co-IP/MS analysis revealed barely any significant changes of the FKBP interactomes upon Rapamycin-treatment, we identified PRR14L as a new and poorly characterized interaction partner of FKBP51 and FKBP52. PRR14L shows no similarity to any other protein except a tantalus-like domain that spans 5% of the protein sequence, and shares homology with PRR14 and the Drosophila protein tantalus (tant) (Dietrich *et al*., 2001). The cellular role of tant is largely unknown with a tissue-specific localization pattern (Dietrich *et al*., 2001). Hence, the role of this tantalus-like domain in PRR14L function remains unclear.

FKBP51 and FKBP52 are known to shuttle between the nucleus and cytosol to regulate SHR activity (Storer *et al.*, 2011). Although it was presumed that soluble proteins move throughout the cytoplasm by simple diffusion, the discovery of a dynein/dynactin motor complex that binds steroid receptors in complex with Hsp90 and FKBP52 demonstrated a different mechanism (Galigniana *et al.*, 2010). Steroid receptors are sequestered in the cytosol by FKBP51 in the absence of hormone signals. Upon steroid hormone stimulation, FKBP51 is exchanged with FKBP52 which subsequently binds to dynein and transports the complex to the nucleus (Wochnik *et al.*, 2005). This mechanism as a “transportosome” could also be applied to the subcellular localization of PRR14L. Although PRR14L has two predicted NLS

domains which explain the observed nuclear localization, loss of FKBP52 resulted in a partial cytosolic delocalization of PRR14L. FKBP52 may be responsible to shuttle PRR14L into the nucleus upon a specific stimulus similar to the mechanism of steroid receptor activation (Storer *et al*., 2011). Loss of FKBP52 expression subsequently leads to the translocation of PRR14L from the nucleus to the cytosol where PRR14L binds FKBP51. This mechanism offers a plausible explanation for why loss of both FKBPs restored the cytoplasmic localization observed in FKBP52 KO cells back to the nuclear localization observed in control cells. In this case, the spatial regulation of PRR14L by FKBPs is abolished and the two NLS may be responsible for its nuclear localization. However, the exact mechanism of PRR14L localization in an FKBP-dependent manner has to be further investigated.

APEX2-based proximome labeling assays are a practical tool to identify proximal proteins and narrow down a possible function and localization of an uncharacterized protein. The nuclear localization of PRR14L indicates a potential role as a transcriptional regulator that binds to chromatin and affects its organization and gene expression. GO term analysis revealed that PRR14L interacts with chromatin-related proteins as for example KAT2A and TADA2B. KAT2A (also known as GCN5) is a HAT (histone acetyl transferase) that regulates leukemia cell maintenance in the context of two macromolecular complexes: ATAC (Ada two-A-containing) and SAGA (Spt-Ada-Gcn5-Acetyltransferase) (Arede *et al.*, 2022). The difference in these two complexes is a single subunit in the HAT module (TADA2A in ATAC and TADA2B in SAGA) (Spedale *et al.*, 2012). KAT2A is a genetic vulnerability in AML (acute myeloid leukemia) and its inhibition was shown to suppress growth of primary human AMLs (Tzelepis *et al.*, 2016). Previously, it was shown that mutations as well as deletions in *PRR14L* are potentially the underlying cause for CMML (chronic myelomonocytic leukemia) and myeloid neoplasms (Chase *et al.*, 2019). CMML and AML are blood and bone marrow cancers that affect the same lines of white blood cells, while CMML can develop into AML if the

number of blast cells in the blood rises above 20%. Since PRR14L interacts with KAT2A and TADA2B, and because it was previously shown that mutations in *PRR14L* can cause CMML, it is possible that PRR14L affects HAT activity by interfering with KAT2A or by directly participating in the ATAC or SAGA complexes. Further experiments will be necessary to characterize the role of PRR14L in the context of KAT2A activity and to explore its potential implications in leukemia.

In addition to a potential role in different types of leukemia, including AML and CMML, our data suggest that PRR14L may impact vesicle exocytosis. PRR14L KD resulted in alterations of gene expression of several genes associated with the synaptic vesicle cycle. Central to synaptic vesicle exocytosis is the SNARE (soluble N-ethylmaleimide-sensitive fusion protein attachment protein receptors) complex which is comprised of several proteins that are important for the docking, priming and fusion of neurotransmitter release (Ramakrishnan *et al.*, 2012). The core of the neuronal SNARE complex consists of SNAP25 (synaptosomal-associated protein 25), syntaxin and VAMPs (vesicle associated membrane proteins) with SNAP25 being the prime contributor in the complex assembly (McMahon and Südhof, 1995). Synaptic vesicle fusion is then triggered by Ca^{2+} influx that leads to the release of the inhibitory CPLX1 (complexin 1) and CPLX2 from the vesicles.

Knockdown of PRR14L affects gene expression and protein levels of some of the core components of the synaptic vesicle cycle which raises the question whether PRR14L is a positive or negative regulator of vesicle exocytosis. Upon PRR14L KD, *SNAP25* levels decrease while *VAMP1* and *VAMP2* transcription is upregulated. This suggests that the reduced expression of SNAP25 may impair the docking and fusion of vesicles with the presynaptic membrane. In response to deficient exocytosis, cells may then upregulate *VAMP1* and *VAMP2* expression to compensate for this impairment. Simultaneously, cells may downregulate *CPLX1* transcription to alleviate any inhibitory impact on vesicle exocytosis. However, it remains

unclear whether the observed effects are directly regulated by PRR14L or if they are compensatory responses of the initial transcriptional changes caused by PRR14L KD.

These findings indicate that PRR14L plays an important role in the regulation of the synaptic vesicle exocytosis in neurons. Although our work was performed in HEK293FT cells, it was shown that HEK293 cells have many properties of immature neurons suggesting a neuronal lineage (Shaw *et al.*, 2002) explaining the expression of neuronal genes in the transcriptome analysis. To further investigate the role of PRR14L in the transcriptional regulation of the genes implicated in vesicle exocytosis, ChIP-seq (chromatin-IP sequencing) analysis is necessary to be performed. This analysis will not only validate the direct binding of PRR14L to chromatin but also enable the identification of the precise DNA-binding region. By intersecting such ChIP-seq results with our RNA-seq data, it would be possible to distinguish between direct and secondary effects of PRR14L on gene expression. In addition, it may allow the identification of specific DNA sequences where PRR14L binds (assuming PRR14L binds DNA directly), or to reveal enrichment of transcription factor binding motifs that cooperate with PRR14L in the regulation of gene expression (assuming PRR14L functions as a co-factor). In sum, experiments to elucidate the precise role of PRR14L as a transcriptional regulator will require additional work in the future.

Taken together, our study identifies PRR14L as a novel interaction partner of FKBP51 and FKBP52. The nuclear localization and interaction with chromatin suggest a role as a transcriptional regulator. While PRR14L could potentially represent a genetic vulnerability associated with different types of cancers, such as AML and CMML, it might also play a more specific role in the synaptic vesicle machinery. Therefore, it will be of great interest to further study the physiological role of PRR14L and elucidate its implication in cancer and vesicle exocytosis.

Methods

Cell culture

All cell lines were grown at 37 °C, 5% CO_2. Human female embryonic kidney HEK293FT cells (#R70007, Invitrogen; RRID: CVCL_6911) were cultured in high-glucose Dulbecco's Modified Eagle Medium (DMEM) (#41965-039, Gibco) supplemented with 10% fetal bovine serum (FBS) (#F7524, Sigma, or #P30-3306, PAN Biotech) and 1% Penicillin-Streptomycin (#15140-122, Gibco).

HEK293FT cells were purchased from Invitrogen. The identity of the HEK293FT cells was validated by the Multiplex human Cell Line Authentication test (Multiplexion GmbH), which uses a single nucleotide polymorphism (SNP) typing approach, and was performed as described at www.multiplexion.de. All parental and edited cell lines were regularly tested for *Mycoplasma* contamination using a PCR-based approach and were confirmed to be *Mycoplasma*-free.

Antibodies

Antibodies against DYKDDDDK (FLAG) tag (#2368 for WB, #14793 for IF), Complexin1 (#17700), VAMP2 (#13508) were purchased from Cell Signaling Technology. Antibodies against PRR14L (#HPA062645) and Tubulin (#T9026) were purchased from Sigma. Antibodies against FKBP51 (#A301-430A) and FKBP52 (#A301-427A) were purchased from Bethyl Laboratories. Peroxidase-conjugated AffiniPure anti-rabbit and anti-mouse secondary antibodies (#711-035-152 and #715-035-151, respectively; all from Jackson ImmunoResearch) were used 1:10,000 in PBS-T (1x PBS, 0.1% Tween-20), 5% powdered milk. For immunofluorescence, all primary antibodies were used 1:200 in BBT solution (1x

PBS, 0.1% Tween-20, 0.1% BSA). Anti-rabbit Rhodamine (TRITC)-conjugated (#711-025-152, Jackson ImmunoResearch) was used 1:100 in BBT.

Plasmid constructs

The pcDNA3-FLAG-FKBP12, FKBP12.6, FKBP51, FKBP52, PRR14L plasmid constructs were generated by PCR-amplifying cDNA from HEK293FT WT cells and cloned as BamHI/Not1 into a pcDNA3-FLAG backbone using appropriate primers (Table S4). The pcDNA3-FLAG-FKBP51 ΔTPR, FKBP52 ΔTPR, PRR14L ΔNLS, PRR14L ΔΔNLS plasmid constructs were generated by cloning PCR-amplified inserts from the respective full-length plasmids described above using appropriate primers (Table S4). pcDNA3-Flag-Luc was described previously (Plescher *et al.*, 2015).

The pITR-APEX2 plasmids were generated using the NEBuilder HiFi DNA Assembly Kit (#E2621S, New England Biolab) with appropriate primers (Table S4). The N-terminal tagged pITR-FLAG-APEX2-PRR14L plasmid construct was generated by cloning two PCR-amplified inserts from the pcDNA3-FLAG-PRR14L plasmid (described above) and cloned as NheI/BamHI into a pITR-FLAG-APEX2 backbone (described in Nüchel *et al*., 2021). The C-terminal tagged pITR-PRR14L-APEX2-HA plasmid construct was generated by cloning two PCR-amplified inserts from the pcDNA3-FLAG-PRR14L plasmid and cloned as SfiI/Not1 into a pITR-APEX2-HA backbone (described in Nüchel *et al*., 2021).

All restriction enzymes were purchased from New England Biolabs. The integrity of all constructs was verified by sequencing.

Plasmid DNA transfections

Plasmid DNA transfections in HEK293FT cells were performed using Effectene transfection reagent (#301425, QIAGEN) according to the manufacturer's instructions.

Transient knock-downs with siRNA

Transient PRR14L knock-downs were performed using a pool of 4 siGENOME siRNAs (Horizon Discoveries). A RLuc duplex siRNA that targets the *R.reniformis* Luciferase gene (Horizon Discoveries) was used as a control. In brief, cells were seeded in 12-well plates at 20% confluence and the following day transfected with 20 nM of the siRNA pool using Lipofectamine RNAiMAX (#13778150, Thermo Fisher Scientific) according to manufacturer's instructions. Cells were harvested 72 h post-transfection and knock-down efficiency was verified by immunoblotting and/or RT-qPCR.

Generation of stably-expressing FLAG-tagged FKBP cell lines

For the generation of polyclonal stable lines expressing FLAG-tagged FKBPs, HEK293FT WT cells were transfected using the indicated expression vectors. Forty-eight hours post-transfection, cells were selected with 3 μg/mL puromycin (#A11138-03, gibco) for 3 days and then propagated in media containing the same puromycin concentration.

Cell lysis and immunoblotting

For standard SDS-PAGE and immunoblotting experiments, cells were treated as indicated in the figures and lysed in 250-300 μl of ice-cold Triton lysis buffer (50 mM Tris pH 7.5, 1% Triton X-100, 150 mM NaCl, 50 mM NaF, 2 mM Na-vanadate, 0.011 gr/ml beta-glycerophosphate) supplemented with 1x PhosSTOP phosphatase inhibitors (#4906837001, Roche) and 1x cOmplete protease inhibitors (#11836153001, Roche) for 10 minutes on ice.

Samples were clarified by centrifugation (15000 rpm, 10 min, 4 °C) and supernatants were boiled in 1x SDS sample buffer (5x SDS sample buffer: 350 mM Tris-HCl pH 6.8, 30% glycerol, 600 mM DTT, 12.8% SDS, 0.12% bromophenol blue). Protein samples were subjected to electrophoretic separation on SDS-PAGE and analyzed by standard Western blotting techniques. In brief, proteins were transferred to nitrocellulose membranes (#10600002 or #10600001, Amersham) and stained with 0.2% Ponceau solution (#33427-01, Serva) to confirm equal loading. Membranes were blocked with 5% skim milk powder (#42590, Serva) in PBS-T (1x PBS, 0.1% Tween-20 (#A1389, AppliChem)) for 1 hour at room temperature, washed three times for 10 min with PBS-T and incubated with primary antibodies (1:1000 in PBS-T, 5% bovine serum albumin (BSA; #10735086001, Roche)) rotating overnight at 4 °C. The next day, membranes were washed three times for 10 min with PBS-T and incubated with appropriate HRP-conjugated secondary antibodies (1:10000 in PBS-T, 5% milk) for 1 hour at room temperature. Signals were detected by enhanced chemiluminescence (ECL) using the ECL Western Blotting Substrate (#W1015, Promega) or SuperSignal West Pico PLUS (#34577, Thermo Scientific) and SuperSignal West Femto Substrate (#34095, Thermo Scientific) for weaker signals. Immunoblot images were captured on films (#28906835, GE Healthcare; #4741019289, Fujifilm).

Co-immunoprecipitation (co-IP)

For co-IP experiments, cells were transiently transfected with the indicated plasmids and lysed 36 h post-transfection in IP lysis buffer (50 mM Tris pH 7.5, 0.3% CHAPS, 150 mM NaCl, 50 mM NaF, 2 mM Na-vanadate, 0.011 g/ml β-glycerophosphate, 1x PhosSTOP phosphatase inhibitors and 1x cOmplete protease inhibitors). FLAG-tagged proteins were incubated with 30 µl pre-washed anti-FLAG M2 affinity gel (Sigma, #A2220) for 3 h at 4 °C and washed four times with IP wash buffer (50 mM Tris pH 7.5, 0.3% CHAPS, 150 mM NaCl and 50 mM NaF).

Samples were then boiled for 6 min in 1x SDS sample buffer and analysed by immunoblotting using appropriate antibodies.

Immunofluorescence and confocal microscopy

Immunofluorescence (IF) / confocal microscopy experiments were performed as previously described (Demetriades *et al.*, 2016). In brief, cells were seeded on gelatin-coated coverslips and treated as indicated in each experiment. After treatments, cells were fixed for 10 min at room temperature with 4% PFA in PBS. Samples were washed/permeabilized with PBT solution (1x PBS, 0.1% Tween-20), and blocked with BBT solution (1x PBS, 0.1% Tween-20, 0.1% BSA). Staining was performed with the indicated primary antibodies in BBT (1:200 dilution) and then with appropriate highly cross-adsorbed secondary fluorescent antibodies (1:100 in BBT for TRITC-conjugated antibodies). Finally, nuclei were stained with DAPI and cells mounted on slides using Fluoromount-G (#00-4958-02, Invitrogen). Images from single channel captures are shown in grayscale. For the merged images, TRITC is shown in red and DAPI in blue. All images were captured on a Leica confocal microscope (TCS SP8 X, Leica Microsystems) using a 40x oil objective lens and 3x digital zoom. Acquisition was done using the LAS X software (Leica Microsystems).

Subcellular localization of PRR14L was analysed by scoring cells based on the signal distribution of PRR14L, as shown in the example images in Fig. 2B. Signal was scored as nuclear (more PRR14L signal in the nucleus), cytoplasmic (more PRR14L signal in the cytoplasm), or intermediate (similar PRR14L signal between nucleus and cytoplasm). Approximately XX individual cells were scored per genotype for each experiment.

MS analysis

For the analysis of FKBP interacting proteins, cells stably expressing FLAG-tagged FKBPs were treated with 20 nM Rapamycin (#S1039, Selleckchem) for 1 hour at 37 °C and subsequently lysed for 10 min in 1 ml enriched IP lysis buffer (75 mM Tris pH 7.5, 0.45% CHAPS, 225 mM NaCl, 100 mM NaF, 4 mM Na-vanadate, 0.065 g/ml β-glycerophosphate, 2x PhosSTOP phosphatase inhibitors and 2x cOmplete protease inhibitors). Samples were incubated with 50 µl pre-washed anti-FLAG M2 affinity gel (Sigma, #A2220) for 3 h at 4 °C and washed four times with IP wash buffer (50 mM Tris pH 7.5, 0.3% CHAPS, 150 mM NaCl and 50 mM NaF) following four wash steps in 50 mM Tris pH 7.5. Bound proteins were eluted in MS elution buffer (5 ng/µl sequencing grade modified trypsin (Promega), 50 mM Tris pH 7.5, 1 mM TCEP (Tris (2-carboxyethyl) phosphine), 5 mM CAA (chloroacetamide)) for 1 h at RT. Eluates were transferred in a new tube and incubated over night at 37 °C to assure a complete tryptic digest. The next day, the digestion was stopped by adding formic acid to the final concentration of 1% and the samples were further processed for peptide cleaning.

Before samples were applied to MS analysis, peptides were concentrated and cleaned in a single step using stop-and-go-extraction tips (StageTips). For peptide clean-up, Stage-Tips were wetted by adding 200 µl methanol and centrifuged for 5 min. Then, 200 µl of 60% acetonitrile (ACN) in 0.1% FA were added just before the last remainder of methanol has left the tip to keep the C18 material wet. The tips were equilibrated with 200 µl 0.1% FA and centrifuged for 5 min. Before samples were loaded into the tip, 100 µl 0.1% FA was added to the tips and subsequently, the digest of each sample was added into the solution. Tips were centrifuged for 5 min until all solution went through the material and then washed twice with 200 µl 0.1% FA. Peptides were eluted from the material with 80 µl of 60% ACN/0.1% FA by centrifuging at 1,500 x g for 4 min. The elute was transferred into a new 0.5 ml eppi and

concentrated in a SpeedVac centrifuge at 45°C for 45 min to dryness. Samples were stored at -20°C until application to mass spectrometry.

Gene expression analysis (RNA-Seq)

To analyze gene expression changes via RNA-seq experiments, total mRNA was isolated using QIAshredder columns (#79656, QIAGEN) and the RNeasy Plus Mini Kit (#74034, QIAGEN) according to the manufacturer's instructions. RNA-seq experiments were performed by the Max Planck Genome Centre (MPGC) Cologne, Germany (https://mpgc.mpipz.mpg.de/home/). RNA quality was assessed with an Agilent Bioanalyzer (Nanochip). Library preparation was done according to NEBNext Ultra™ II Directional RNA Library Prep Kit for Illumina (#E7760L, New England Biolabs) including polyA enrichment and addition the of ERCC RNA spike-ins. Libraries were quality controlled by Agilent TapeStation or LabChip GX or GX Touch (PerkinElmer). Sequencing-by-synthesis was performed on a HiSeq 3000 (Illumina) with single read mode 1 x 150 bp.

Gene expression analysis (RT-qPCR)

For gene expression analysis, RNA was isolated with TRIzol (#15596018, Thermo Fisher Scientific) and reverse transcription was performed using the RevertAid H Minus Reverse Transcriptase kit (#EP0452, Thermo Fisher Scientific). The cDNAs were diluted 1:10 in nuclease-free H_2O and 4 µl of diluted cDNA were used per reaction, along with 5 µl of 2x Maxima SYBR Green/ROX qPCR master mix (#K0223, Thermo Fisher Scientific,) and 1 µl of primer mix (2.5 µM of forward and reverse primers, see Table S4). For each replicate experiment, reactions were set in technical triplicates in a StepOnePlus Real-Time PCR system (Applied Biosystems) and analyzed with the StepOne software (v2.2.2; Applied Biosystems).

Relative gene expression levels were calculated with the $2^{-\Delta\Delta Ct}$ method. *RPL13a* expression was used for normalization as internal control.

APEX2-based proximity biotin ligation assay (proximome)

We utilized a H_2O_2-inducible, APEX2 proximity-based biotinylation system, adapted from Kohli *et al.* (2017) to identify proteins that are in close proximity to PRR14L. This assay is based on APEX2 catalyzing the H2O2-dependent protein oxidation and can be used in combination with phenol-biotin labeling to biotinylate proximal proteins in live cells (Hung *et al.*, 2016). Although the labeling radius of APEX2 has not been determined precisely, it is estimated to be in the range of 20 nm (Martell *et al.*, 2012). Therefore, this technique allows us to interrogate not only the direct interactome but also the molecular environment of PRR14L. To describe the full set of PRR14L proximal proteins—regardless of whether these interact directly with PRR14L or not—we here use a new term, the 'proximome' (Valerius *et al.*, 2019). To determine the PRR14L proximome, we generated stable cell lines that express either N-terminally fused FLAG-PRR14L or C-terminally fused PRR14L-HA proteins to APEX2. Three and four independent biological replicates were used for FLAG-APEX2-PRR14L and PRR14l-APEX-HA, respectively, and the full dataset is provided in Table S2.

In brief, expression of the fusion proteins was induced by doxycycline treatment (20 h, 1 µg/ml). Cells were labeled by the addition of 500 µM biotin-phenol (#LS-3500, Iris Biotech) to the medium for 30 min, followed by addition of 1 mM H_2O_2 for 1 min to induce the biotinylation reaction. Cells were then washed 3x with quenching buffer (1x PBS, 10 mM sodium azide, 10 mM sodium ascorbate, 1 mM Trolox (6-hydroxy-2,5,7,8-tetramethylchroman-2-carboxylic acid) (#238813, Sigma-Aldrich)). After washes, cells were lysed in 1mL RIPA buffer (50 mM Tris pH 7.5, 150 mM NaCl, 1% Triton X-100, 0.5% sodium

deoxycholate, 0.1% SDS, pH 7.4, 1x cOmplete protease inhibitors) supplemented with 10 mM sodium azide, 10 mM sodium ascorbate and 1 mM Trolox. Lysates were incubated on ice for 15 min, and clarified by centrifugation (15 min, 10.000 x g, 4 °C). The supernatant was incubated with 80 µl streptavidin sepharose beads (GE17-5113-01, Sigma-Aldrich) for 3 hours at 4 °C. The beads were then washed 5x with 1 mL RIPA buffer and 3x with 50 mM Tris. Between washes, beads were spun down (1 min, 2000 x g, 4 °C) and wash buffer was removed. Biotinylated proteins were eluted by incubating the beads in 100 µl MS elution buffer (5 ng/µl sequencing grade modified trypsin (Promega), 50 mM Tris pH 7.5, 1 mM TCEP (Tris (2-carboxyethyl) phosphine), 5 mM CAA (chloroacetamide)) for 1 h at RT. The supernatant was transferred into a fresh 0.5 ml eppi and samples were digested over night at 37 °C. Digestion was stopped by adding 0.5% formic acid to the reaction and the peptides were subjected to StageTip purification, before injection into the mass spectrometer.

Gene Ontology analysis

Gene Ontology (GO) and pathway enrichment analysis were performed using the Database for Annotation, Visualization and Integrated Discovery (DAVID) tool (Huang *et al.*, 2009a; 2009b). For the APEX2 proximity proteome experiment, only proteins that are robustly enriched in the PRR14L proximome of cells treated with H_2O_2 were used for the DAVID GO analysis. For the RNA-seq experiment, only genes that are strongly down- ($Log_2FC < -1.3$) or upregulated ($Log_2FC > +0.9$) by PRR14L KD were used for the DAVID GO analysis.

Cellplots were generated using DAVID and the associated Flaski apps (https://flaski.app, developed and provided by the MPI-AGE Bioinformatics core facility) using the 15 most significant GO terms from each analysis. The full list of significantly changing genes and proteins, respectively, from each experiment was used for generating the Volcano plots. The

genes and proteins, respectively, used for the GO analysis (based on the selection criteria described above for each experiment) are represented by blue or red dots. Strongly down- and upregulated genes of the RNA-seq analysis are shown as blue or red dots with a black outline.

Statistics and Reproducibility

Statistical analysis and data presentation in graphs was performed using the GraphPad Prism software (v9.1.0). For all quantifications, data in the graphs are shown as mean ± SEM. Normal distribution was tested using the Shapiro-Wilk test, and correction for multiple comparisons was performed using the Tukey test. Significance was calculated using one-way ANOVA for multiple comparisons. p-values are described in the figures and figure legends (* $p<0.05$, ** $p<0.01$, *** $p<0.005$, **** $p<0.001$; ns, non-significant). Statistics source data are provided in the Numerical Source Data table.

All findings were reproducible over multiple independent experiments, within a reasonable degree of variability between replicates. The number of replicate experiments for each assay is provided in the respective figure legends. No statistical method was used to predetermine sample size, which was determined in accordance with standard practices in the field. No data were excluded from the analyses. The experiments were not randomized, and the investigators were not blinded to allocation during experiments and outcome assessment.

References

Arakawa H, Nagase H, Hayashi N, Fujiwara T, Ogawa M, Shin S, Nakamura Y. Molecular cloning and expression of a novel human gene that is highly homologous to human FK506-binding protein 12kDa (hFKBP-12) and characterization of two alternative spliced transcripts. *Biochem Biophys Res Com*. 1994. 200; 836-43.

Arede L, Foerner E, Wind S, Kulkarni R, Domingues AF, Giotopoulos G, Kleinwaechter S, Mollenhauer-Starkl M, Davison H, Chandru A, Asby R, Samarista R, Gupta S, Forte D, Curti A, Scheer E, Huntly BJP, Tora L, Pina C. KAT2A complexes ATAC and SAGA play unique roles in cell maintenance and identity in hematopoiesis and leukemia. *Blood Adv*. 2022. 6; 165-80.

Artoni F, Grützmacher N, Demetriades C. Unbiased evaluation of rapamycin's specificity as an mTOR inhibitor. *Aging Cell*. 2023. e13888.

Bonner JM, Boulianne GL. Diverse structures, functions and uses of FK506 binding proteins. *Cell Signal*. 2017. 38; 97-105.

Brown EJ, Albers MW, Shin TB, Ichikawa K, Keith CT, Lane WS, Schreiber SL. A mammalian protein targeted by G1-arresting rapamycin-receptor complex. *Nature*. 1994. 369; 756-8.

Chase A. Pellagatti A, Singh S, Score J, Tapper WJ, Lin F, Hoade Y, Bryant C, Trim N, Yip BH, Zol K, Rasi C, Forsberg LA, Dumanski JP, Boultwood J, Cross NCP. *PRR14L* mutations are associated with chromosome 22 acquired uniparental disomy, age related clonal hematopoiesis and myeloid neoplasia. *Leukemia.* 2019. 33; 1184-94.

Cheung-Flynn J, Prapapanich V, Cox MB, Riggs DL, Suarez-Quian C, Smith DF. Physiological role for the cochaperone FKBP52 in androgen receptor signalling. *Mol Endocrinol.* 2005. 19; 1654-66.

Davies TH, Sánchez ER. FKBP52. *IJBCB*. 2005. 37; 42-47.

Demetriades C, Plescher M, Teleman AA. Lysosomal recruitment of TSC2 is a universal response to cellular stress. *Nat Commun*. 2016. 7; 10662.

Dietrich BH, Moore J, Kyba M, dosSantos G, McCloskey F, Milne TA, Brock HW, Krause HM. Tantalus, a Novel ASX-Interacting Protein with Tissue-Specific Functions. *Dev Biol*. 2001.234; 441-453.

Galat A, Metcalfe SM. Peptidylproline cis/trans isomerases. *Prog Biophys Mol Biol.* 1995. 63; 67-188.

Galigniana MD, Erlejman AG, Monte M, Gomez-Sanchez C, Piwien-Pilipuk G. The hsp90-FKBP52 complex links the mineralcorticoid receptor to motor proteins and persists bound to the receptor in early nuclear events. *Mol Cell Biol*. 2010. 30; 1285-98.

Hähle A, Merz S, Meyners C, Hausch F. The Many Faces of FKBP51. *Biomolecules*. 2019. 9; 35.

Hähle A, Geiger TM, Merz S, Meyners C, Tianqi M, Kolos J, Hausch F. FKBP51 and FKBP12.6 – Novel and tight interactors of Glomulin. *PLoS ONE*. 2019. 14; e0221926.

Harikishore A, Yoon HS. Immunophilins: structures, mechanisms and ligands. *Curr Mol Pharmacol.* 2015. 9; 37-47.

Heitman J, Movva NR, Hall MN. Targets for cell cycle arrest by the immunosuppressant rapamycin in yeast. *Science*. 1991. 253; 905-9.

Huang DW, Sherman BT, Lempicki RA. Bioinformatics enrichtment tools: paths toward the comprehensive functional analysis of large gene lists. *Nucleic Acids Res*. 2009a. 37; 1-13.

Huang DW, Sherman BT, Lempicki RA. Systematic and integrative analysis of large gene lists using DAVID bioinformatics resources. *Nat Protoc*. 2009b. 4; 44-57.

Hung V, Udeshi ND, Lam SS, Loh KH, Cox KJ, Pedram K, Carr SA, Ting AY. Spatially resolved proteomic mapping in living cells with the engineered peroxidase APEX2. *Nat Protoc*. 2016. 11; 456-75.

Kohli P, Höhne M, Jüngst C, Bertsch S, Ebert LK, Schauss AC, Benzing T, Rinschen MM, Schermer B. The ciliary membrane-associated proteome reveals actin-binding proteins as key components of cilia. *EMBO Rep.* 2017. 18; 1521-35.

Lam E, Martin MM, Timerman AP, Sabers C, Fleischer S, Lukas T, Abraham RT, O`Keefe SJ, O`Neill EA, Wiederrecht GJ. A novel FK506 binding protein can mediate the immunosuppressive effects of FK506 and is associated with the cardiac ryanodine receptor. *J Biol Chem*. 1995. 270; 26511-22.

Lange A, Mills RE, Lange CJ, Stewart M, Devine SE, Corbett AH. Classical Nuclear Localization Signals: Definition, Function, and Interaction with Importin α. *J Biol Chem.* 2007. 282; 5101-05.

Lee TI, Young RA. Transcriptional Regulation and Its Misregulation in Disease. *Cell*. 2013. 152; 1237-51.

Martell JD, Deerinck TJ, Sancak Y, Poulos TL, Mootha VK, Sosinsky GE, Ellisman MH, Ting AY. Engineered ascorbate peroxidase as a genetically encoded reporter for electron microscopy. *Nat Biotechnol.* 2012. 30; 1143-8.

Martinez NJ, Chang H, de Riba Borrajo J, Gregory RI. The co-chaperones FKBP4/5 control Argonaute2 expression and facilitates RISC assembly. *RNA*. 2013. 19; 1583-1593.

März AM, Fabian AK, Kozany C, Bracher A, Hausch F. Large FK506-binding proteins shape the pharmacology of rapamycin. *Mol Cell Biol.* 2013. 33; 1357-67.

McMahon HT, Südhof TC. Synaptic core complex of synaptobrevin, syntaxin and SNAP25 forms high affinity alpha-SNAP binding site. *J Biol Chem*. 1995. 270; 2213-7.

Nüchel J, Tauber M, Nolte JL, Mörgelin M, Türk C, Eckes B, Demetriades C, Plomann M. An mTORC1-GRASP55 signaling axis controls unconventional secretion to reshape the extracellular proteome upon stress. *Mol Cell.* 2021. 81; 3275-3293.

Pirkl F, Buchner J. Functional analysis of the Hsp90-associated human peptidyl prolyl cis/trans isomerases FKBP51, FKBP52 and Cyp40. *J Mol Biol.* 2001. 308; 795-806.

Plescher M, Teleman AA, Demetriades C. TSC2 mediates hyperosmotic stress-induced inactivation of mTORC1. *Sci Rep.* 2015. 5; 13828.

Ramakrishnan NA, Drescher MJ, Drescher DG. The SNARE complex in neuronal and sensory cells. *Mol Cell Neurosci*. 2012. 50; 58-69.

Riggs DL, Roberts PJ, Chirillo SC, Cheung-Flynn J, Prapapanich V, Ratajczak T, Gaber R, Picard D, Smith DF. The Hsp90-binding peptidylprolyl isomerase FKBP52 potentiates glucocorticoid signalling in vivo. *EMBO J.* 2003. 22; 1158-67.

Shaw G, Morse S, Ararat M, Graham FL. Preferential transformation of human neuronal cells by human adenoviruses and the origin of HEK 293 cells. *FASEB Journal*. 2002. 16; 869–71.

Spedale G, Timmers HTM, Pijnappel WWMP. ATAC-king the complexity of SAGA during evolution. *Genes Dev*. 2012. 26; 527-41.

Storer CL, Dickey CA, Galigniana MD, Rein T, Cox MB. FKBP51 and FKBP52 in Signaling and Disease. *Trends Endocrinol Metab*. 2011. 22; 481-490.

Tong M, Jiang Y. FK506-Binding Proteins and Their Diverse Functions. *Curr Mol Pharma*. 2016. 9; 48-65.

Tranguch S, Cheung-Flynn J, Daikoku T, Prapapanich V, Cox MB, Xie H, Wang H, Das SK, Smith DF, Dey SK. Cochaperone immunophilin FKBP52 is critical to uterine receptivity for embryo implantation. *Proc Natl Acad Sci U S A.* 2005. 102; 14326-31.

Tzelepis K, Koike-Yusa H, De Braekeleer E, Li Y, Metzakopian E, Dovey OM, Mupo A, Grinkevich V, Li M, Mazan M, Gozdecka M, Ohnishi S, Cooper J, Patel M, McKerrell T, Chen B, Domingues AF, Gallipoli P, Teichman S, Ponstingl H, McDermott U, Saez-Rodriguez J, Huntly BJP, Iorio F, Pina C, Vassiliou GS, Yusa K. A CRISPR Dropout Screen Identifies Genetic Vulnerabilities and Therapeutic Targets in Acute Myeloid Leukemia. *Cell Rep*. 2016. 17; 1193-1205.

Valerius O, Asif AR, Beißbarth T, Bohrer R, Dihazi H, Feussner K, Jahn O, Majcherczyk A, Schmidt B, Schmitt K, Urlaub H, Lenz C. Mapping Cellular Microenvironments: Proximity Labeling and Complexome Profling (Seventh Symposium of the Göttingen Proteomics Forum). *Cells.* 2019. 8; 1992.

Van Duyne GD, Standaert RF, Karplus PA, Schreiber SL, Clardy J. Atomic structure of FKBP-FK506, an immunophilin-immunosuppressant complex. *Science*. 1991. 252; 839-42.

Wochnik GM, Rüegg J, Abel GA, Schmidt U, Holsboer F, Rein T. FK506-binding proteins 51 and 52 differentially regulate dynein interaction and nuclear translocation of the glucocorticoid receptor in mammalian cells. *J Biol Chem*. 2005. 280; 4609-16.

Supplementary Information

Figures S1-S3 and Tables S1-S7.

Supplementary Tables

Table S1. List of proteins identified in the FLAG-FKBP IP/MS analysis, related to Figure 1.
Table S2. List of proteins that bind specifically to FLAG-FKBPs identified in the IP/MS analysis, related to Figure S1.
Table S3. List of proteins identified in the FLAG-APEX2-PRR14L and PRR14L-APEX2-HA proximome analysis.
Table S4. List of proteins used for the GO analysis and associated GO terms from the secretome analysis.
Table S5. Differential gene expression analysis in HEK293FT WT cells upon PRR14L KD.
Table S6. List of proteins used for the GO analysis and associated GO terms from the RNA-seq analysis.
Table S7. List of DNA oligonucleotides used in the study.

Supplementary Figures

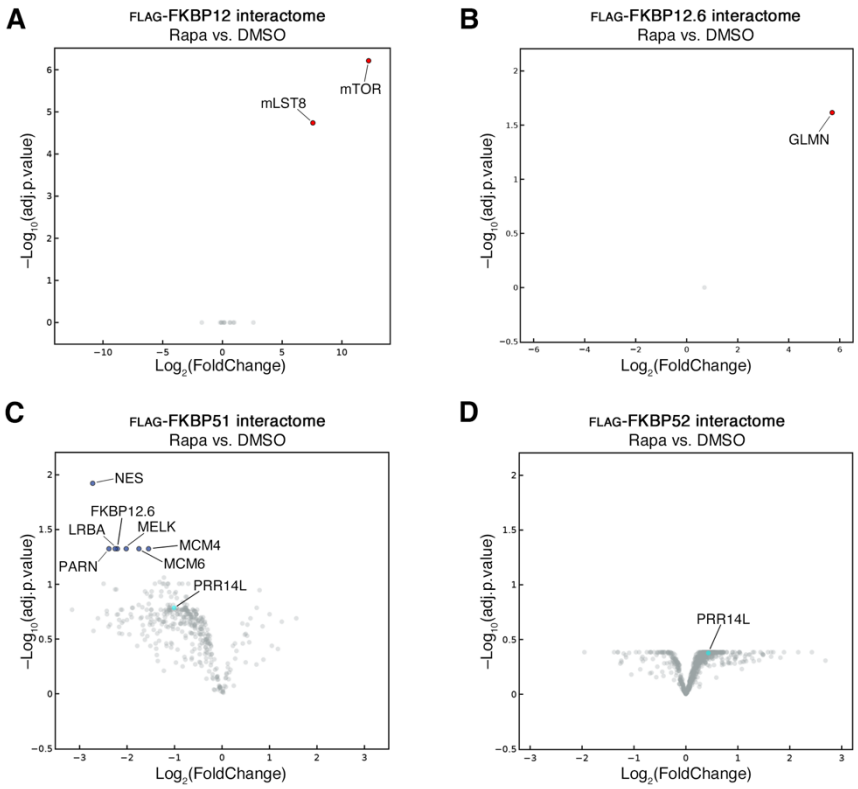

Figure S1. Interactome analysis of FLAG-tagged FKBP constructs treated with Rapamycin vs. DMSO treatment. Related to Figure 1.

(A) Interactome of HEK293FT WT cells, stably expressing FLAG-tagged FKBP12 treated with 20 nM Rapamycin for 1 h, compared to control-treated cells. Only proteins that bind specifically to FLAG-FKBP12 (in Rapamycin and DMSO conditions) are shown. Proteins that are significantly ($p < 0.05$) binding to FLAG-FKBP12 are shown in red (Log2FC > 0) or blue (Log2FC < 0), respectively. Proteins that bind insignificantly ($p > 0.05$) are shown as grey dots.

(B) As in (A), but for HEK293FT WT cells, stably expressing FLAG-tagged FKBP12.6.

(C) As in (A), but for HEK293FT WT cells, stably expressing FLAG-tagged FKBP51.

(D) As in (A), but for HEK293FT WT cells, stably expressing FLAG-tagged FKBP52

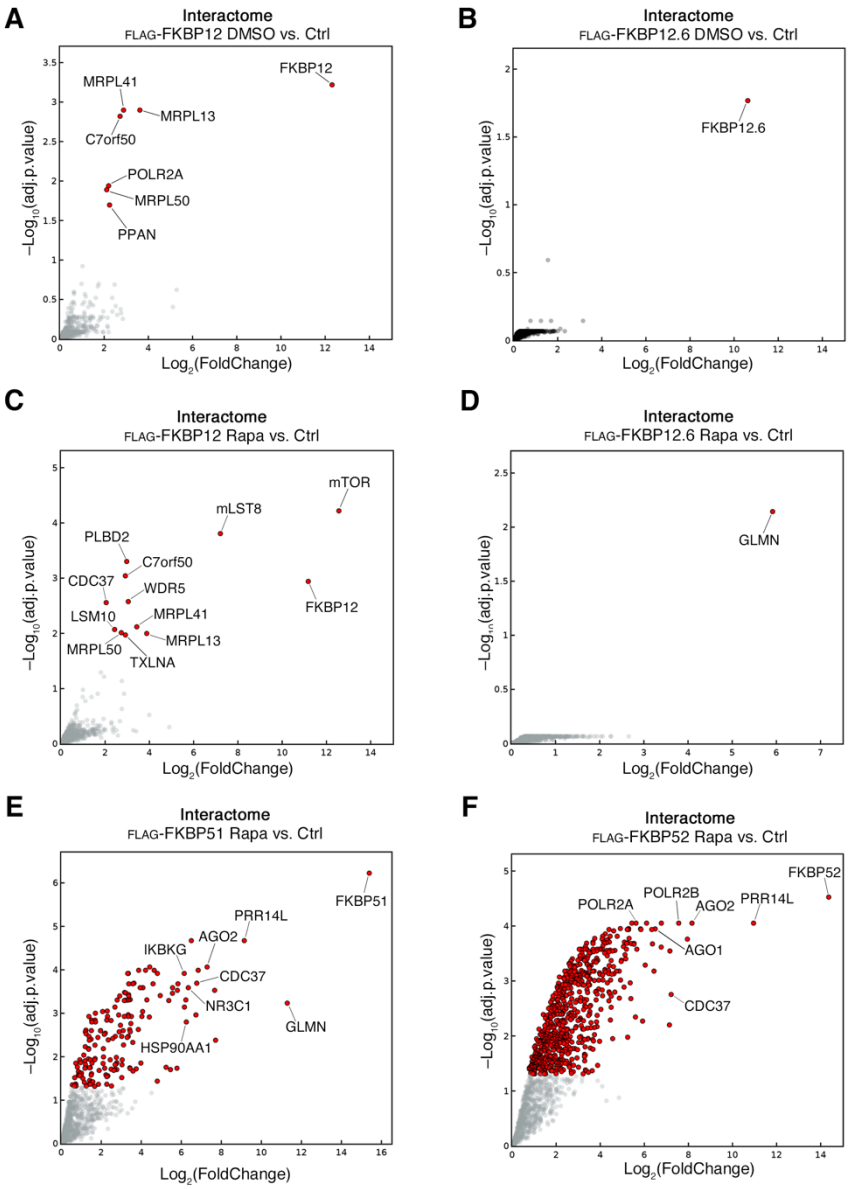

Figure S2. Additional interactome analysis of FLAG-tagged FKBP constructs compared to control cells. Related to Figure 1.

(A) Interactome of HEK293FT WT cells, stably expressing FLAG-tagged FKBP12 treated with DMSO, compared to control cells. Proteins that are significantly ($p < 0.05$) binding to FLAG-FKBP12 are shown in red. Proteins that bind insignificantly ($p > 0.05$) are shown as grey dots.

(B) As in (A), but for HEK293FT WT cells, stably expressing FLAG-tagged FKBP12.6.

(C) Interactome of HEK293FT WT cells, stably expressing FLAG-tagged FKBP12 treated with 20 nM Rapamycin for 1 h, compared to control cells. Proteins that are significantly ($p < 0.05$) binding to FLAG-FKBP12 are shown in red. Proteins that bind insignificantly ($p > 0.05$) are shown as grey dots.

(D) As in (C), but for HEK293FT WT cells, stably expressing FLAG-tagged FKBP12.6.

(E) As in (C), but for HEK293FT WT cells, stably expressing FLAG-tagged FKBP51.

(F) As in (C), but for HEK293FT WT cells, stably expressing FLAG-tagged FKBP52.

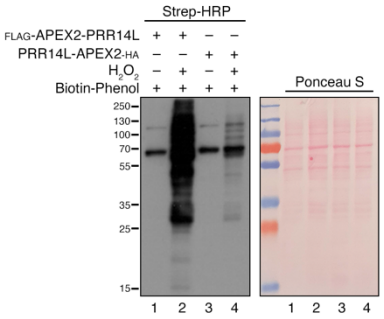

Figure S3. Validation of the APEX2 proximome biotinylation system. Related to Figure 3.

Immunoblot analysis of HEK293FT cells, stably expressing FLAG-APEX2-PRR14L or PRR14L-APEX2-HA, and activation of the biotinylation reaction with Biotin-Phenol and H_2O_2 in combination or only Biotin-Phenol as control, using an anti-Streptavidin-HRP (Strep-HRP) antibody. Equal protein loading confirmed by Ponceau S staining.

3. General Discussion

Since the discovery of mTOR in the early 1990s, a lot of work worldwide focused on unraveling the regulation of mTORC1 activity to shed light on the intricate mechanisms via which cells coordinate their response to environmental changes and maintain cellular homeostasis. mTORC1 serves as a key signaling hub that integrates information from a diverse set of upstream cues including nutrient availability, energy levels, growth factors, and stresses (Liu and Sabatini, 2020). By unraveling the complex signaling pathways involved in amino acid sensing and mTORC1 activation, we gain valuable insights into cellular metabolism, tissue development, and the maintenance of organismal homeostasis. Furthermore, Rapamycin, a potent inhibitor of mTORC1, has emerged as a crucial tool in both research and clinical settings. By selectively blocking mTORC1 signaling, Rapamycin can modulate cell growth, proliferation and autophagy, making it an attractive candidate for therapeutic interventions in various age-related diseases, including cancer, autoimmune disorders, and certain genetic conditions (Mannick and Lamming, 2023). Therefore, a thorough understanding of mTORC1 regulation by amino acids and the impact of Rapamycin treatment holds immense promise in advancing our knowledge of cellular physiology.

3.1 Regulation of mTOR by amino acids

3.1.1 The Rag GTPases are functionally different

Among the various nutrients that converge on mTORC1, amino acids play a dominant role in regulating its activity. Since the discovery of the Rag GTPases in 2008 (Sancak *et al.*, 2008; Kim *et al.*, 2008), our understanding of how amino acids regulate mTORC1 has significantly advanced with the focus on the GATOR-Rag axis. However, the Rag GTPase paralogs were previously considered functionally redundant and were used interchangeably in studies due to their high sequence homology. In my first study, I demonstrated that there are indeed functional differences between the Rag paralogs, and that, depending on the Rag that is present in the heterodimer, they confer substrate specificity as well as a varying response to amino acid starvation.

When nutrients are limited, the GATOR2 complex is inhibited and thereby releasing its inhibition from GATOR1 which results in mTORC1 inactivation (Shen *et al.*, 2018). Therefore,

nutrient availability is directly linked to the regulation of mTORC1 activity. However, I demonstrated that this is only true in cells expressing exclusively RagA since RagB, in comparison to RagA, confers insensitivity to amino acid starvation, leading to active mTORC1 even in the absence of amino acids. Although RagA and RagB share 90% of amino acid sequence homology, RagB specifically inhibits GATOR1 through two distinct mechanisms thus suppressing its inhibitory activity towards mTORC1 (Figlia *et al.*, 2022). RagB exists in two isoforms with a short isoform ($RagB^{short}$) that is expressed ubiquitously and a long isoform ($RagB^{long}$) that appears to be brain-specific (Schürmann *et al.*, 1995). Both isoforms demonstrate different approaches in conferring insensitivity to amino acid starvation. $RagB^{short}$ inhibits GATOR1 by binding to its subunit DEPDC5 sequestering GATOR1 in an inhibitory mode while $RagB^{long}$ shows low affinity for GTP and therefore, diminishes the GAP activity of GATOR1 (Figlia *et al.*, 2022). The RagB isoforms are highly expressed in neurons and specifically in the brain to maintain mTORC1 activity even during nutrient starvation. This response to the nutritional state can provide a survival mechanism. In the face of prolonged starvation, an organism has the ability to deactivate non-essential functions and enhance autophagy, enabling the recycling of substrates like nucleotides, amino acids, and lipids. These recycled substrates are then utilized to generate glucose and ketone bodies, providing the necessary energy to fuel the brain (Rabinowitz and White, 2010). Constitutively active mTORC1 in the absence of amino acids can also confer an advantage to cancer cells, promoting growth and proliferation even under nutrient-limiting conditions. This advantage becomes particularly pronounced in the core of solid tumors where nutrient availability is often limited. Additionally, many tumor cells change their relative balance of RagA/B expression favoring an increased expression of RagB over RagA to provide them with a potential growth advantage when nutrients are low (Figlia *et al.*, 2022).

In contrast to the functional differences between RagA/B, my data showed that mTORC1 differentially phosphorylates distinct substrates depending on the presence of RagC/D in the heterodimer. The current consensus in the field suggests that mTORC1 has to be on the lysosomal surface to phosphorylate its downstream targets such as S6K1, 4E-BP1, TFEB, and TFE3. However, I demonstrated that depending on the large Rag that is incorporated in the heterodimer, the localization and substrate specificity of mTORC1 are affected differently. Over the past decades, our understanding of the downstream functions regulated by mTORC1 has expanded drastically. While early discoveries identified the involvement of mTORC1 in

protein synthesis and ribosomal biogenesis (Burnett *et al.*, 1998) it has become evident that the complex also plays a dominant role in lysosomal biogenesis and autophagy (Martina *et al.*, 2012). Therefore, different substrates regulate different downstream functions of mTORC1. Rag dimers containing RagC can activate mTORC1 away from the lysosome leading to the phosphorylation of the cytosolic substrates S6K1 and 4E-BP1, which are responsible for protein synthesis and ribosomal biogenesis. On the other hand, RagD leads to the lysosomal localization of mTORC1 resulting in the additional phosphorylation of the lysosomal substrates TFEB and TFE3, preventing their translocation to the nucleus.

Constitutively-active phosphorylation of TFEB and TFE3, which is the case in cells expressing RagD, results in the inhibition of autophagosome and lysosome biogenesis (Martina *et al.*, 2012). This phenotype is characteristic of cancer cells that evade autophagy and hijack cell growth regulation by constitutively activating mTORC1 activity. I showed that in cells expressing cancer-associated RagC mutants that were previously described to cause FL (follicular lymphoma) (Okosun *et al.*, 2016), mTORC1 was unable to detach from lysosomes and constitutively inactivated the lysosomal substrates TFEB and TFE3 leading to inhibition of autophagy and lysosomal biogenesis. This highlights the importance of precise regulation and balance of RagC and RagD. Hyperactivation of RagD as well as cancer-associated RagC mutants can lead to FL whereas complete dephosphorylation of TFEB and TFE3 leads to Birt-Hogg-Dubbé syndrome (Napolitano *et al.*, 2020). This underscores the importance of precise fine-tuning and regulation of mTORC1 activity by the Rag GTPases. Interestingly, *RRAGD* itself is a transcriptional target of TFEB and hence can be upregulated in nutrient-depleted conditions when TFEB translocates to the nucleus (Di Malta *et al.*, 2017). This negative feedback loop is crucial for metabolic adaption to nutrient availability but can also support cancer metabolism and promote tumor growth when it is deregulated.

3.1.2 Amino acids are sensed through specific sensors

Amino acids signal to the Rag GTPases by binding to specific amino acid sensors. These sensors signal via the GATOR complex to the GTP/GDP-loading state of the Rag GTPases thereby activating mTORC1 under amino acid-replete conditions. Sensors for leucine (Wolfson *et al.*, 2016; Chen *et al.*, 2021), arginine (Saxton *et al.*, 2016), as well as the methionine-derived metabolite SAM (Gu et al., 2017), have been identified, all of which transmit signals through

the GATOR1/2 complexes, that act on RagA/B (Shen *et al.*, 2018). Interestingly, two distinct leucine sensors exist that both inhibit GATOR2: SAR1B and Sestrin2. Both dissociate from GATOR2 in the presence of leucine leading to mTORC1 activation. This raises the question of why multiple amino acid sensors exist for the same amino acid. One possible explanation lies in their different dissociation constants. Sestrin2 has a K_d of 20 µM (Wolfson *et al.*, 2016) whereas SAR1B has a K_d of 2 µM (Chen *et al.*, 2021). Hence, SAR1B can already detect a small pool of intracellular leucine, whereas Sestrin2 requires a higher concentration to be activated. This mechanism allows for the partial activation of mTORC1 when only a limited amount of leucine is available, while full activation occurs when sufficient leucine is present.

Furthermore, LRS and TARS2 can signal amino acid availability directly to RagC/D by sensing leucine and threonine, respectively (Han *et al.*, 2012; Kim *et al.*, 2021). Since these two sensors are tRNA-synthetases, they naturally bind their respective amino acid during translation to incorporate them into the growing peptide. Their previously identified role as amino acid sensors could add a new layer of nutrient sensing via the Rag GTPases to mTORC1. Since humans express one tRNA-synthetase for each amino acid it is possible that also other tRNA-synthetases might signal amino acid availability to mTORC1 via the Rag GTPases. Therefore, the availability of amino acids for protein translation can also be directly sensed by mTORC1.

3.1.3 Amino acids regulate mTORC1 independently of the Rag GTPases

mTORC1 can also be regulated by amino acids independently of the Rag GTPases. The small GTPase Arf1 (ADP-ribosylation factor 1) was reported to sense glutamine as well as asparagine levels directly to mTORC1 in a Rag- and LAMTOR-independent manner (Jewell *et al.*, 2015; Meng *et al.*, 2020). Arf1 is a GTPase and its guanine nucleotide cycling is important for the regulation of mTORC1 by glutamine and asparagine. Unraveling the exact mechanism will be of great interest since many cancer cell lines have increased mTORC1 activity with a high dependence on glutamine for cell growth (Jiang *et al.*, 2019). This is partially because glutamine drives the TCA cycle and therefore, cancer cells use TCA cycle intermediates as biosynthetic precursors (DeBerardinis *et al.*, 2007).

The amino acid sensing pathway via the GATOR-Rag axis, as well as the growth factor sensing pathway through the TSC-Rheb axis, have traditionally been considered independent from each other. This belief stemmed from observations that TSC2-deficient cells remained

responsive to amino availability (Smith *et al.*, 2005). However, there are indications that amino acids can indeed influence the GTP loading of Rheb, suggesting a potential regulatory mechanism of the TSC-Rheb axis in response to amino acids (Fawal *et al.*, 2015). Recent studies have demonstrated that both amino acids and growth factors affect TSC2 localization (Demetriades *et al.*, 2014; Menon et al., 2014). Notably, amino acid deprivation induced Rag GTPase-mediated lysosomal translocation of TSC2 (Demetriades *et al.*, 2014). Furthermore, arginine abundance led to the dissociation of TSC2 from the lysosome whereas arginine deprivation induced its lysosomal localization (Carroll *et al.*, 2016). Hence, amino acids have the potential to regulate mTORC1 activity not only through the GATOR-Rag axis but also via the TSC-Rheb axis.

3.2 Regulation of mTOR by Rapamycin

3.2.1 Rapamycin specifically inhibits mTOR and is used as an anti-ageing drug

Considering that hyperactive mTORC1 has been identified as the underlying cause of numerous age-related diseases, including cancer, extensive efforts have been made to the development of different mTOR inhibitors. Currently, there are three generations of mTOR inhibitors available with the initial ones including Rapamycin and its analogs. Rapamycin was discovered more than 50 years ago and is widely used for the treatment of various conditions such as renal cell carcinoma as well as preventing organ-transplant rejection (Li *et al.*, 2014). However, various hints in the literature pointed to mTOR-independent functions of Rapamycin (Goodman *et al.*, 2011; Zhang *et al.*, 2019) and therefore, I aimed to investigate if and how Rapamycin can influence cellular physiology besides the inhibition of mTOR. In the second study, I focused on the specificity of Rapamycin towards mTOR inhibition which hasn't been evaluated in detail before. My data showed that all effects of Rapamycin on a transcriptomic and proteomic level were abolished when Rapamycin was no longer able to bind to mTOR. Therefore, this detailed insight into Rapamycin's specificity as an mTOR inhibitor demonstrates that all observed effects are exclusively due to mTOR inhibition.

More than a decade ago, inhibition of mTORC1 came into the focus of anti-ageing research since genetic mutations in the mTOR pathway led to lifespan extension (Selman *et al.*, 2009). Hence, it represented the first proof of principle that a pharmaceutical agent can slow down the ageing process in mammals (Wilkinson *et al.*, 2012). However, the potential of Rapamycin

as a pro-longevity therapeutic needs to be carefully evaluated in light of its known clinical risks and potential side effects including metabolic defects such as hyperglycemia, hyperlipidemia, insulin resistance, and increased incidence of type 2 diabetes (Fraenkel *et al.*, 2008; Houde *et al.*, 2010).

In the past, many studies were conducted that used a time period of 2 to 6 weeks as "long-term" or "chronic" Rapamycin-treatment with the treated mice and rats developing severe glucose intolerance as well as hyperlipidemia (Chang *et al.*, 2009; Houde *et al.*, 2010). However, it was demonstrated that while Rapamycin treatment initially exhibited some adverse side effects during the early treatment period (2 to 6 weeks), these effects were either reversed or diminished after 20 weeks of continuous treatment, with the mice displaying better metabolic profiles than before Rapamycin administration (Fang *et al.*, 2013). It should be noted that these studies were conducted in mice, and it remains unclear if the findings can be directly translated to humans. Nevertheless, they serve as an example that prolonged Rapamycin treatment can indeed exhibit anti-ageing effects when administered over an extended period. While human clinical trials are currently ongoing, and no results are available yet, a few studies have been conducted in primates. For example, marmoset monkeys subjected to Rapamycin-treatment for 9 months showed only minor effects on clinical markers such as glucose or triglyceride levels (Sills *et al.*, 2019).

In addition to the duration of treatment, the concentration of Rapamycin also plays a crucial role. Patients who undergo Rapamycin-treatment as part of their medication for aggressive cancer types or post-organ transplantation typically receive high doses of Rapamycin, which can lead to more severe side effects. However, when aiming to extend both life- and health-span, employing a significantly lower dosage regimen may prove to be sufficient, thus potentially offering a safer and more geroprotective approach.

3.2.2 Rapamycin has no effects on the FKBP interactome

Whereas I demonstrated that Rapamycin is highly specific towards mTOR when looking at transcriptomic and proteomic changes within the cell, it can potentially affect the interactome of FKBPs. Rapamycin forms a tertiary complex with FKBPs to bind and inhibit mTORC1 (Sabers *et al.*, 1995). Although FKBP12 is the best-known member of the family, several other FKBPs were reported to bind Rapamycin and inhibit mTORC1 activity (März *et al.*, 2013). Since

Rapamycin binds to the PPIase domain of the FKBP which not only blocks the PPIase activity but can also induce conformational changes to the respective FKBPs (Storer *et al.*, 2011), in my third project I aimed to investigate, if Rapamycin affects the interactions of FKBPs with their client proteins.

The larger FKBPs, FKBP51 and FKBP52, are involved in the regulation of steroid receptor activity as for example GR (Barent *et al.*, 1998). Although these FKBPs bind Hsp90 through their TPR domains, binding of Rapamycin to their PPIase domain might affect their activity. When FKBP51 and FKBP52 bind to Hsp90, their PPIase domain interacts with GR and, therefore influences GR conformation and steroid binding affinity (Storer *et al.*, 2011). Additionally, it was shown that FKBP51 dissociates from Hsp90 to bind to an FK506 resin (Smith *et al.*, 1993). Therefore, Rapamycin could potentially affect the interaction of FKBPs to their client proteins. However, I was not able to identify any Rapamycin-induced changes in the interactome of FKBPs. Together with the data from my second study, this demonstrates that Rapamycin is indeed a specific inhibitor of mTOR and that, although it binds to FKBPs to exert its inhibition towards mTOR, it does not affect other FKBP interactions.

Although Rapamycin shows no effect on the FKBP interactome, I identified a novel FKBP interactor that binds to FKBP51 and FKBP52 via their TPR domains, called PRR14L. The physiological role of PRR14L is poorly characterized and has to be investigated further. However, given the important role of FKBP51 and FKBP52 in cellular physiology including the regulation of steroid receptor activity, it will be of great interest to further investigate the role of PRR14L as a new FKBP-interacting client protein. High expression of FKBP51 was reported to trigger adaptative changes in GR regulation and thus regulation of the stress hormone-regulating HPA (hypothalamic-pituitary-adrenal) axis (Binder *et al.*, 2004). Furthermore, FKBP51 is known to play a role in several mental health disorders such as depression and PTSD (post-traumatic stress disorder), partially due to negative feedback regulation of GR (van West *et al.*, 2006; Yehuda *et al.*, 2009). These findings demonstrate, how important it is to understand the regulation of FKBP51 and therefore also the potential impact of client proteins including PRR14L.

3.3 Future Directions

Recent discoveries have greatly contributed to our understanding of how mTORC1 is regulated by upstream stimuli, with particular emphasis on the dominant role of amino acids. Although only a small number of amino acid sensors have been identified so far, it is plausible that additional sensors may exist to detect the remaining amino acids. The Jewell lab investigated which amino acids can activate mTORC1 activity, revealing that 10 out of the 20 proteinogenic amino acids demonstrated the ability to induce mTORC1 activation (Meng *et al.*, 2020). Out of these ten amino acids, eight are suggested to signal through the Rag GTPases while the other two, glutamine and asparagine, act via a Rag-independent mechanism (Meng *et al.*, 2020). Consequently, it is conceivable that there are yet undiscovered amino acid sensors that specifically respond to the remaining amino acids. It is worthwhile investigating the potential involvement of tRNA-synthetases since LRS and TARS1B have been identified as specific amino acid sensors for leucine and threonine, respectively. Hence, the discovery of new amino acid sensors will provide a more complete understanding of how amino acids regulate mTORC1 activity.

Furthermore, my findings indicate that mTORC1 can also be active away from lysosomes phosphorylating its cytosolic substrates S6K1 and 4E-BP1. Therefore, it is possible that mTORC1 can also localize to other organelles besides lysosomes and act on different substrates. For example, it was shown previously that GRASP55 is a novel mTORC1 substrate localizing at the Golgi (Nüchel *et al.*, 2021). Additionally, mTORC1 was reported to localize to mitochondria (de la Cruz López *et al.*, 2019) or late endosomes (Flinn *et al.*, 2010). Therefore, it will be of great interest to investigate the subcellular localization of mTOR at different organelles and elucidate putative new substrates and downstream functions.

Rapamycin has been shown to extend health and lifespan in various model organisms and is nowadays a promising tool for the treatment of a variety of conditions. While my data demonstrate its specificity towards mTOR, there are still open questions regarding the dose and duration of Rapamycin administration especially in humans. Factors including half-life, metabolism, plasma protein binding and tissue distribution have to be taken into consideration when setting up a dosing regime in humans. Moreover, while low-dose Rapamycin-treatment appears to be safe, it is crucial to determine the long-term effects to ensure the safety and efficacy of the drug. Furthermore, mTOR inhibitors were shown to have sex-specific or sex-

biased benefits (Strong *et al.*, 2020) therefore it might be reasonable to have different treatment strategies for women and men. The results of the first human clinical trials that interrogate mTOR inhibition by Rapamycin and its analogs as a potential therapeutic strategy against age-related conditions, as well as in life-and health-span extension, are expected to be announced in the next few years.

3.4 Closing Remarks

Understanding the regulation of mTORC1 is of great importance due to its central role in numerous fundamental cellular processes including cell growth, proliferation, and metabolism. By comprehending the intricate mechanisms underlying mTORC1 regulation, we can gain insights into the development and progression of various diseases including cancer, metabolic disorders, and neurodegenerative conditions. Moreover, deciphering the complex signaling pathways that modulate mTORC1 activity opens up new possibilities for targeted therapeutic interventions, enabling the design of more effective treatments to restore cellular homeostasis and combat pathologies associated with dysregulated mTORC1 signaling. In essence, a comprehensive understanding of mTORC1 regulation provides a foundation for advancing biomedical research and offers promising ways for the development of innovative therapeutic strategies.

References

The following list includes all references from the general introduction and discussion.

Arakawa H, Nagase H, Hayashi N, Fujiwara T, Ogawa M, Shin S, Nakamura Y. Molecular cloning and expression of a novel human gene that is highly homologous to human FK506-binding protein 12kDa (hFKBP-12) and characterization of two alternative spliced transcripts. Biochem Biophys Res Com. 1994. 200; 836-43.

Bar-Peled L, Schweitzer LD, Zoncu R, Sabatini DM. Ragulator is a GEF for the rag GTPases that signal amino acid levels to mTORC1. Cell. 2012. 150; 1196-208.

Bar-Peled L, Chantranupong L, Cherniack AD, Chen WW, Ottina KA, Grabiner BC, Spear ED, Carter SL, Meyerson M, Sabatini DM. A Tumor Suppressor Complex with GAP Activity for the Rag GTPases That Signal Amino Acid Sufficiency to mTORC1. Science. 2013. 340; 1100-06.

Barent RL, Nair SC, Carr DC, Ruan Y, Rimerman RA, Fulton J, Zhang Y, Smith DF. Analysis of FKBP51/FKBP52 chimeras and mutants for Hsp90 binding and association with progesterone receptor complexes. Mol Endocrinol. 1998. 12; 342-54.

Ben-Sahra I, Howell JJ, Asara JM, Manning BD. Stimulation of de novo pyrimidine synthesis by growth signaling through mTOR and S6K1. Science. 2013. 339; 1323-8.

Ben-Sahra I, Hoxhaj G, Ricoult SJH, Asara JM, Manning BD. mTORC1 induces purine synthesis through control of the mitochondrial tetrahydrofolate cycle. Science. 2016. 351; 728-33.

Benjamin D, Colombi M, Moroni C, Hall MN. Rapamycin passes the torch: a new generation of mTOR inhibitors. Nat Rev Drug Discov. 2011. 10; 868-80.

Binder EB, Salyakina D, Lichtner P, Wochnik GM, Ising M, Pütz B, Papiol S, Seaman S, Lucae S, Kohli MA, Nickel T, Künzel HE, Fuchs B, Majer M, Pfennig A, Kern N, Brunner J, Modell S, Baghai T, Deiml T, Zill P, Bondy B, Rupprecht R, Messer T, Köhnlein O, Dabitz H, Brückl T, Müller N, Pfister H, Lieb R, Mueller JC, Löhmussaar E, Strom TM, Bettecken T, Meitinger T, Uhr M, Rein T, Holsboer F, Müller-Myhsol B. Polymorphisms in FKBP5 are associated with increased recurrence of depressive episodes and rapid response to antidepressant treatment. Nat Genet. 2004. 36; 1319-25.

Bonner JM, Boulianne GL. Diverse structures, functions and uses of FK506 binding proteins. Cell Signal. 2017. 38; 97-105.

Bosotti R, Isacchi A, Sonnhammer EL. FAT: a novel domain in PIK-related kinases. Trends Biochem Sci. 2000. 25; 225-7.

Brandt C, Hillmann P, Noack A, Römermann K, Öhler LA, Rageot D, Beaufils F, Melone A, Sele AM, Wymann MP, Fabbro D, Löscher W. The novel, catalytic mTORC1/2 inhibitor PQR620 and PI3K/mTORC1/2 inhibitor PQR530 effectively cross the blood-brain barrier and increase seizure threshold in a mouse model of chronic epilepsy. Neuropharmacology. 2018. 140; 107-20.

Brown EJ, Albers MW, Shin TB, Ichikawa K, Keith CT, Lane WS, Schreiber SL. A mammalian protein targeted by G1-arresting rapamycin-receptor complex. Nature. 1994. 369; 756-8.

Brugarolas J, Lei K, Hurley RL, Manning BD, Reiling JH, Hafen E, Witters LA, Ellisen LW, Kaelin Jr WG. Regulation of mTOR function in response to hypoxia by REDD1 and the TSC1/TSC2 tumor suppressor complex. Genes Dev. 2004. 18; 2893-904.

Brunn GJ, Hudson CC, Sekulic A, Williams JM, Hosoi H, Houghton PJ, Lawrence Jr JC, Abraham RT. Phosphorylation of the translational repressor PHAS-I by the mammalian target of rapamycin. Science. 1997. 277; 99-101.

Burnett PE, Barrow RK, Cohen NA, Snyder SH, Sabatini DM. RAFT1 phosphorylation of the translational regulators p70 S6 kinase and 4E-BP1. Proc Natl Acad Sci U S A. 1998. 95; 1432-7.

Carracedo A, Ma L, Teruya-Feldstein J, Rojo F, Salmena L, Alimonti A, Egia A, Sasaki AT, Thomas G, Kozma S, Papa A, Nardella C, Cantley LC, Baselga J, Pandolfi PP. Inhibition of mTORC1 leads to MAPK pathway activation through a PI3K-dependent feedback loop in human cancer. J Clin Invest. 2008. 118; 3065-74.

Chang G, Wu Y, Chiu Y, Chen W, Liao J, Hsu H, Chao T, Hung S, Mao FC. Long-term administration of rapamycin reduces adiposity, but impairs glucose tolerance in high-fat diet-fed KK/H1J mice. Basic Clin Pharmacol Toxicol. 2009. 105; 188-98.

Chen J, Zheng XF, Brown EJ, Schreiber SL. Identification of an 11-kDa FKBP12-rapamycin-binding domain within the 289-kDa FKBP12-rapamycin-associated protein and characterization of a critical serine residue. Proc Natl Acad Sci U S A. 1995. 92; 4947-51.

Chen C, Liu Y, Liu Y, Zheng P. mTOR regulation and therapeutic rejuvenation of aging hematopoietic stem cells. Sci Signal. 2009. 2:ra75.

Chen J, Ou Y, Luo R, Wang J, Wang D, Guan J, Li Y, Xia P, Chen PR, Liu Y. SAR1B senses leucine levels to regulate mTORC1 signalling. Nature. 2021. 596; 281-4.

Choi J, Chen J, Schreiber SL, Clardy J. Structure of the FKBP12-rapamycin complex interacting with the binding domain of FRAP. Science. 1996. 273; 239-42.

Choi B, Feng L, Yoon HS. FKBP38 protects Bcl-2 from caspase-dependent degradation. J Biol Chem. 2010. 285; 9770-9.

Chung J, Kuo CJ, Crabtree GR, Blenis J. Rapamycin-FKBP specifically blocks growth-dependent activation of and signaling by the 70 kd S6 protein kinase. Cell. 1992. 69; 1227-36.

Cruzat V, Rogero MM, Keane KN, Curi R, Newsholme P. Glutamine: Metabolism and immune function, supplementation and clinical translation. Nutrients. 2018. 10; 1564.

Davies TH, Ning Y, Sánchez ER. A new first step in activation of steroid receptors: hormone-induced switching of FKBP51 and FKBP52 immunophilins. J Biol Chem. 2002. 277; 4597-600.

De la Cruz López KG, Guzmán MET, Sánchez EO, Carrancá AG. mTORC1 as a Regulator of Mitochondrial Functions and a Therapeutic Target in Cancer. Front Oncol. 2019. 9; 1373.

DeBerardinis RJ, Mancuso A, Daikhin E, Nissim I, Yudkoff M, Wehrli S, Thompson CB. Beyond aerobic glycolysis: transformed cells can engage in glutamine metabolism that exceeds the requirement for protein and nucleotide synthesis. Proc Natl Acad Sci U S A. 2007. 104; 19345-50.

Demetriades C, Doumpas N, Teleman AA. Regulation of TORC1 in response to amino acid starvation via lysosomal recruitment of TSC2. Cell. 2014. 156; 786-99.

DeYoung MP, Horak P, Sofer A, Sgroi D, Ellisen LW. Hypoxia regulates TSC1/2-mTOR signaling and tumor suppression through REDD1-mediated 14-3-3 shuttling. Genes Dev. 2008. 22; 239-51.

Di Malta C, Siciliano D, Calcagni A, Monfregola J, Punzi S, Pastore N, Eastes AN, Davis O, de Cegli R, Zampelli A, Di Giovannantonio LG, Nusco E, Platt N, Guida A, Ogmundsdottir MH, Lanfrancone L, Perera RM, Zoncu R, Pelicci PG, Settembre C, Ballabio A. Transcriptional activation of RagD GTPase controls mTORC1 and promotes cancer growth. Science. 2017. 356; 1188-92.

Dibble CC, Elis W, Menon S, Qin W, Klekota J, Asara JM, Finan PM, Kwiatkowski DJ, Murphy LO, Manning BD. TBC1D7 is a third subunit of the TSC1-TSC2 complex upstream of mTORC1. Mol Cell. 2012. 47; 535-46.

Dolinski K, Muir S, Cardenas M, Heitman J. All cyclophilins and FK506 binding proteins are, individually and collectively, dispensable for viability in Saccharomyces cerevisae. Proc Natl Acad Sci USA. 1997. 94; 13093-8.

Eng CP, Sehgal SN, Vézina C. Activity of rapamycin (AY-22,989) against transplanted tumors. J Antibiot. 1984. 37; 1231-7.

Erlejman AG, De Leo SA, Mazaira GI, Molinari AM, Camisay MF, Fontana V, Cox MB, Piwien-Pilipuk G, Galigniana MD. NF-kB transcriptional activity is modulated by FK506-binding proteins FKBP51 and FKBp52: a role for peptidyl-prolyl isomerase activity. J Biol Chem. 2014. 289; 26263-76.

Fang Y, Westbrook R, Hill C, Boparai RK, Arum O, Spong A, Wang F, Javors MA, Chen J, Sun LY, Bartke A. Duration of rapamycin treatment has differential effects on metabolism in mice. Cell Metab. 2013. 17; 456-62.

Feng M, Gu C, Ma S, Wang Y, Liu H, Han R, Gao J, Long Y, Mi H. Mouse FKBP23 mediates conformer-specific functions of BiP by catalyzing Pro117 cis/trans isomerization. Biochem Biophys Res Commun. 2011. 408; 537-40.

Figlia G, Müller S, Hagenston AM, Kleber S, Roiuk M, Quast J, Bosch NT, Ibanez DC, Mauceri D, Martin-Villalba A, Teleman AA. Brain-enriched RagB isoforms regulate the dynamics of mTORC1 activity through GATOR1 inhibition. Nat Cell Biol. 2022. 24; 1407-21.

Flinn RJ, Yan Y, Goswami S, Parker PJ, Backer JM. The late endosome is essential for mTORC1 signaling. Mol Biol Cell. 2010. 21; 833-41.

Flynn JM, O'Leary MN, Zambataro CA, Academia EC, Presley MP, Garrett BJ, Zykovich A, Mooney SD, Strong R, Rosen CJ, Kapahi P, Nelson MD, Kennedy BK, Melov S. Late-life rapamycin treatment reverses age-related heart dysfunction. Aging Cell. 2013. 12; 851-62.

Fraenkel M, Ketzinel-Gilad M, Ariav Y, Pappo O, Karaca M, Castel J, Berthault M, Magnan C, Cerasi E, Kaiser N, Leibowitz G. mTOR inhibition by rapamycin prevents beta-cell adaptation to hyperglycemia and exacerbates the metabolic state in type 2 diabetes. Diabetes. 2008. 57; 945-57.

Galat A. Sequence diversification of the FK506-binding proteins in several different genomes. Eur J Biochem. 2000. 267; 4945-59.

Galigniana MD, Radanyi C, Renoir J, Housley PR, Pratt WB. Evidence That the Peptidylprolyl Isomerase Domain of the hsp90-binding Immunophilin FKBP52 Is Involved in Both Dynein Interaction and Glucocorticoid Receptor Movement to the Nucleus. J Biol Chem. 2001. 276; 14884-9.

Goodman CA, Frey JW, Mabrey DM, Jacobs BL, Lincoln HC, You J, Hornberger TA. The role of skeletal muscle mTOR in the regulation of mechanical load-induced growth. J Physiol. 2011. 589; 5485-501.

Grove TZ, Cortajarena AL, Regan L. Ligand binding by repeat proteins: natural and designed. Curr Opin Struct Biol. 2008. 18; 507-15.

Gu X, Orozco JM, Saxton RA, Condon KJ, Liu GY, Krawczyk PA, Scaria SM, Harper JW, Gygi SP, Sabatini DM. SAMTOR is an *S*-adenosylmethionine sensor for the mTORC1 pathway. Science. 2017. 358; 813-8.

Gwinn DM, Shackelford DB, Egan DF, Mihaylova MM, Mery A, Vasquez DS, Turk BE, Shaw RJ. AMPK phosphorylation of raptor mediates a metabolic checkpoint. Mol Cell. 2008. 30; 214-26.

Halloran J, Hussong SA, Burbank R, Podlutskaya N, Fischer KE, Sloane LB, Austad SN, Strong R, Richardson A, Hart MJ, Galvan V. Chronic inhibition of mammalian target of rapamycin by rapamycin modulates cognitive and non-cognitive components of behaviour throughout lifespan in mice. Neuroscience. 2012. 223; 102-13.

Han JM, Jeong SJ, Park MC, Kim G, Kwon NH, Kim HK, Ha SH, Ryu SH, Kim S. Leucyl-tRNA synthetase is an intracellular leucine sensor for the mTORC1-signaling pathway. Cell. 2012. 149; 410-24.

Harding MW, Galat A, Uehling DE, Schreiber SL. A receptor for the immune-suppressant FK506 is a cis-trans peptidyl-prolyl isomerase. Nature. 341; 758-60.

Harikishore A and Yoon HS. Immunophilins: Structures, Mechanisms and Ligands. Curr Mol Pharmacol. 2015. 9; 37-47.

Heitman J, Movva NR, Hall MN. Targets of cell cycle arrest by the immunosuppressant rapamycin in yeast. Science. 1991. 253; 905-9.

Holz MK, Ballif BA, Gygi SP, Blenis J. mTOR and S6K1 mediate assembly of the translation preinitiation complex through dynamic protein interchange and ordered phosphorylation events. Cell. 2005. 123; 569-80.

Houde VP, Brulé S, Festuccia WT, Blanchard P, Bellmann K, Deshaies Y, Marette A. Chronic rapamycin treatment causes glucose intolerance and hyperlipidemia by upregulating hepatic gluconeogenesis and impairing lipid deposition in adipose tissue. Diabetes. 2010. 59; 1338-48.

Hunold A, Haueisen J, Ahtam B, Doshi C, Harini C, Camposano S, Warfield SK, Grant PE, Okada Y, Papadelis C. Localization of the Epileptogenic Foci in Tuberous Sclerosis Complex: A Pediatric Case Report. Front Hum Neurosci. 2014. 8; 175.

Ingle GR, Sievers TM, Holt CD. Sirolimus: continuing the evolution of transplant immunosuppression. Ann Pharmacother. 2000. 34; 1044-55.

Inoki K, Li Y, Xu T, Guan K. Rheb GTPase is a direct target of TSC2 GAP activity and regulates mTOR signaling. Genes Dev. 2003. 17; 1829-34.

Jacinto E, Loewith R, Schmidt A, Lin S, Rüegg MA, Hall A, Hall MN. Mammalian TOR complex 2 controls the actin cytoskeleton and is rapamycin insensitive. Nat Cell Biol. 2004. 6; 1122-8.

Jacinto E, Facchinetti V, Liu D, Soto N, Wei S, Jung SY, Huang Q, Qin J, Su B, SIN1/MIP1 maintains rictor-mTOR complex integrity and regulates Akt phosphorylation and substrate specificity. Cell. 2006. 127; 125-37.

Jain J, McCaffrey PG, Miner Z, Kerppola TK, Lambert JN, Verdine GL, Curran T, Rao A. The T-cell transcription factor NFATp is a substrate for calcineurin and interacts with Fos and Jun. Nature. 1993. 365; 352-5.

Jayaraman T, Brillantes AM, Timerman AP, Fleischer S, Erdjument-Bromage H, Tempst P, Marks AR. FK506 binding protein associated with the calcium release channel (ryanodine receptor). J Biol Chem. 1992. 267; 9474-7.

Jiang J, Srivastava S, Zhang J. Starve Cancer Cells of Glutamine: Break the Spell or Make a Hungry Monster? Cancers (Basel). 2019. 11; 804.

Jewell JL, Kim YC, Russell RC, Yu FX, Park HW, Plouffe SW, Tagliabracci VS, Guan KL. Differential regulation of mTORC1 by leucine and glutamine. Science. 2015. 347; 194-8.

Kaeberlein M, Powers 3rd RW, Steffen KK, Westman EA, Hu D, Dang N, Kerr EO, Kirkland KT, Fields S, Kennedy BK. Regulation of yeast replicative life span by TOR and Sch9 in response to nutrients. Science. 2005. 310; 1193-6.

Kapahi P, Zid BM, Harper T, Koslover D, Sapin V, Benzer S. Regulation of lifespan in Drosophila by modulation of genes in the TOR signaling pathway. Curr Biol. 2004. 14; 885-90.

Keith CT, Schreiber SL. PIK-Related Kinases: DNA Repair, Recombination, and Cell Cycle Checkpoints. Science. 1995. 270; 50.

Kim DH, Sarbassov DD, Ali SM, King JE, Latek RR, Erdjument-Bromage H, Tempst P, Sabatini DM. mTOR interacts with raptor to form a nutrient-sensitive complex that signals to the cell growth machinery. Cell. 2002. 110; 163-75.

Kim E, Goraksha-Hicks P, Li L, Neufeld TP, Guan K. Regulation of TORC1 by Rag GTPases in nutrient response. Nat Cell Bio. 2008. 10; 935-45.

Kim J, Kundu M, Viollet B, Guan K. AMPK and mTOR regulate autophagy through direct phosphorylation of Ulk1. Nat Cell Biol. 2011. 13; 132-141.

Kim S, Choi J, Wang P, Go CD, Hesketh GG, Gingras A, Jafarnejad SM, Sonenberg N. Mitochondrial Threonyl-tRNA Synthetase TARS2 Is Required for Threonine-Sensitive mTORC1 Activation. Mol Cell. 2021. 81; 38-407.

Lang K, Schmid FX, Fischer G. Catalysis of protein folding by prolyl isomerase. Nature. 1987. 329; 268-70.

Lebwohl D, Anak O, Sakmoud T, Klimovsky J, Elmroth I, Haas T, Posluszny J, Saletan S, Berg W. Development of everolismus, a novel oral mTOR inhibitor, across a spectrum of diseases. Ann N Y Acad Sci. 2013. 1291; 14-32.

Li J, Kim SG, Blenis J. Rapamycin: one drug, many effects. Cell Metab. 2014. 19; 373-9.

Liu J, Farmer Jr JD, Lane WS, Friedman J, Weissman I, Schreiber SL. Calcineurin is a common target of cyclophilin-cyclosporin A and FKBP-FK506 complexes. Cell. 1991. 66; 807-15.

Liu Q, Kang SA, Thoreen CC, Hur W, Wang J, Chang JW, Markhard A, Zhang J, Sim T, Sabatini DM, Gray NS. Development of ATP-competitive mTOR inhibitors. Methods Mol Biol. 2012. 821; 447-60.

Liu GY, Sabatini DM. mTOR at the nexus of nutrition, growth, ageing and disease. Nat Rev Mol Cell Bio. 2020. 21; 183-203.

Ma D, Bai X, Zou H, Lai Y, Jiang Y. Rheb GTPase controls apoptosis by regulating interaction of FKBP38 with Bcl-2 and Bcl-XL. J Biol Chem. 2010. 285; 8621-7.

Mannick JB, Lamming DW. Targeting the biology of aging with mTOR inhibitors. Nat Aging. 2023.

Martel RR, Klicius J, Galet S. Inhibition of the immune response by rapamycin, a new antifungal antibiotic. Can J Physiol Pharmacol. 1977. 55; 48-51.

Martina JA, Chen Y, Gucek M, Puertollano R. MTORC1 functions as a transcriptional regulator of autophagy by preventing nuclear transport of TFEB. Autophagy. 2012. 8; 903-14.

Martina JA, Diab HI, Li H, Puertollano R. Novel roles for the MiTF/TFE family of transcription factors in organelle biogenesis, nutrient sensing, and energy homeostasis. Cell Mol Life Sci. 2014. 71; 2483-97.

März AM, Fabian A, Kozany C, Bracher A, Hausch F. Large FK506-binding proteins shape the pharmacology of rapamycin. Mol Cell Biol. 2013. 33; 1357-67.

Meng D, Yang Q, Wang H, Melick CH, Navlani R, Frank AR, Jewell JL. Glutamine and asparagine activate mTORC1 independently of Rag GTPases. J Biol Chem. 2020. 295; 2890-99.

Menon S, Manning BD. Common corruption of the mTOR signaling network in human tumors. Oncogene. 2008. 27; S43-51.

Menon S, Dibble CC, Talbott G, Hoxhaj G, Valvezan AJ, Takahashi H, Cantley LC, Manning BD. Spatial control of the TSC complex integrates insulin and nutrient regulation of mTORC1 at the lysosome. Cell. 2014. 156; 771-85.

Nada S, Hondo A, Kasai A, Koike M, Saito K, Uchiyama Y, Okada M. The novel lipid raft adaptor p18 controls endosome dynamics by anchoring the MEK-ERK pathway to late endosomes. EMBO J. 2009. 28; 477-89.

Napolitano G, Di Malta C, Esposito A, de Araujo MEG, Pece S, Bertalot G, Matarese M, Benedetti V, Zampelli A, Stasyk T, Siciliano D, Venuta A, Cesana M, Vilardo C, Nusco E, Monfregola J, Calcagni A, Di Fiore PP, Huber LA, Ballabio A. A substrate-specific mTORC1 pathway underlie Birt-Hogg-Dubé syndrome. Nature. 2020. 585; 597-602.

Nickerson ML, Warren MB, Toro JR, Matrosova V, Glenn G, Turner ML, Duray P, Merino M, Choyke P, Pavlovich CP, Sharma N, Walther M, Munroe D, Hill R, Maher E, Greenberg C, Lerman MI, Linehan WM, Zbar B, Schmidt LS. Mutations in a novel gene lead to kidney tumors, lung wall defects, and benign tumors of the hair follicle in patients with the Birt-Hogg-Dubé syndrome. Cancer Cell. 2002. 2; 157-64.

Nojima H, Tokunaga C, Egushi S, Oshiro N, Hidayat S, Yoshino K, Hara K, Tanaka N, Avruch J, Yonezawa K. The mammalian target of rapamycin (mTOR) partner, raptor, binds the mTOR substrate p70 S6 kinase and 4E-BP1 through their TOR signaling (TOS) motif. J Biol Chem. 2003. 278; 15461-4.

Nüchel J, Tauber M, Nolte JL, Mörgelin M, Türk C, Eckes B, Demetriades C, Plomann M. An mTORC1-GRASp55 signaling axis controls unconventional secretion to reshape the extracellular proteome upon stress. Mol Cell. 2021. 81; 3275-93.

Okosun J, Wolfson RL, Wang J, Araf S, Wilkins L, Castellano BM, Escudero-Ibarz L, Al Seraihi AH, Richter J, Bernhart SH, Efeyan A, Iqbal S, Matthews J, Clear A, Guerra-Assuncao JA, Bödör, Quentmeier H, Mansbridge C, Johnson P, Davies A, Strefford JC, Packham G, Barrans S, Jack A, Du M, Calaminici M, Lister TA, Auer R, Montoto S, Gribben JG, Siebert R, Chelala C, Zoncu R, Sabatini DM, Fitzgibbon J. Recurrent mTORC1-activating RRAGC mutations in follicular lymphoma. Nat Genet. 2016. 48; 183-8.

Oshiro N, Yoshino K, Hidayat S, Tokunaga C, Hara K, Eguchi S, Avruch J, Yonezawa K. Dissociation of raptor from mTOR is a mechanism of rapamycin-induced inhibition of mTOR function. Genes Cells. 2004. 9; 359-66.

Peterson TR, Laplante M, Thoreen CC, Sancak Y, Kang A, Kuehl WM, Gray NS, Sabatini DM. DEPTOR is an mTOR inhibitor frequently overexpressed in multiple myeloma cells and required for their survival. Cell. 2009. 137; 873-86.

Porstmann T, Santos CR, Griffiths B, Cully M, Wu M, Leevers S, Griffiths JR, Chung Y, Schulze A. SREBP activity is regulated by mTORC1 and contributes to Akt-dependent cell growth. Cell Metab. 2008. 8; 224-36.

Punt CJ, Boni J, Bruntsch U, Peters M, Thielert C. Phase I and pharmacokinetic study of CCI-779, a novel cytostatic cell-cycle inhibitor, in combination with 5-fluorouracil and leucovorin in patients with advanced solid tumors. Ann Oncol. 2003. 14; 931-7.

Rabinowitz JD, White E. Autophagy and metabolism. 2010. Science. 330; 1344-8.

Rawson RB. The SREBP pathway—insights from Insigs and insects. Nat Rev Mol Cell Biol. 2003. 4; 631-40.

Rebsamen M, Pochini L, Stasyk T, de Araújo MEG, Galluccio M, Kandasamy RK, Snijder B, Fauster A, Rudashevskaya EL, Bruckner M, Scorzoni S, Filipek PA, Huber KVM, Bigenzahn J, Heinz LX, Kraft C, Bennett KL, Indiveri C, Huber LA, Superti-Furga G. SLC38A9 is a component of the lysosomal amino acid-sensing machinery that controls mTORC1. Nature. 2015. 519; 477-81.

Rodrik-Outmezguine VS, Okaniwa M, Yao Z, Novotny CJ, McWhirter C, Banaji A, Won H, Wong W, Berger M, de Stanchina E, Barratt DG, Cosulich S, Klinowska T, Rosen N, Shokat KM. Overcoming mTOR Resistance Mutations with a New Generation mTOR Inhibitor. Nature. 2016. 534; 272-6.

Sabatini DM, Erdjument-Bromage H, Lui M, Tempst P, Snyder SH. RAFT1: a mammalian protein that binds to FKBP12 in a rapamycin-dependent fashion and is homologous to yeast TORs. Cell. 1994. 78; 35-43.

Sabers CJ, Martin MM, Brunn GJ, Williams JM, Dumont FJ, Wiederrecht G, Abraham RT. Isolation of a protein target of the FKBP12-rapamycin complex in mammalian cells. J Biol Chem. 1995. 270; 815-22.

Sancak Y, Thoreen CC, Peterson TR, Lindquist RA, Kang SA, Spooner E, Carr SA, Sabatini DM. PRAS40 is an insulin-regulated inhibitor of the mTORC1 protein kinase. Mol Cell. 2007. 25; 903-15.

Sancak Y, Peterson TR, Shaul YD, Lindquist RA, Thoreen CC, Bar-Peled L, Sabatini DM. The Rag GTPases bind raptor and mediate amino acid signaling to mTORC1. Science. 2008. 320; 1496-501.

Sancak Y, Bar-Peled L, Zoncu R, Markhard AL, Nada S, Sabatini DM. Ragulator-Rag complex targets mTORC1 to the lysosomal surface and is necessary for its activation by amino acids. Cell. 2010. 141; 290-303.

Sarbassov DD, Ali SM, Kim D, Guertin DA, Latek RR, Erdjument-Bromage H, Tempst P, Sabatini DM. Rictor, a novel binding partner of mTOR, defines a rapamycin-insensitive and raptor-independent pathway that regulates the cytoskeleton. Curr Biol. 2004. 14; 1296-302.

Sarbassov DD, Guertin DA, Ali SM, Sabatini DM. Phosphorylation and regulation of Akt/PKB by the rictor-mTOR complex. Science. 2005. 307; 1098-101.

Sarbassov DD, Ali SM, Sengupta S, Sheen JH, Hsu PP, Bagley AF, Markhard AL, Sabatini DM. Prolonged rapamycin treatment inhibits mTORC2 assembly and Akt/PKB. Mol Cell. 2006. 22; 159-68.

Saxton RA, Chantranupong L, Knockenhauer KE, Schwartz TU, Sabatini DM. Mechanism of arginine sensing by CASTOR1 upstream of mTORC1. Nature. 2016. 536; 229-33.

Saxton RA, Sabatini DM. mTOR Signaling in Growth, Metabolism, and Disease. Cell. 2017. 169; 361-371.

Schaeffer HJ, Catling AD, Eblen ST, Collier LS, Krauss A, Weber MJ. MP1: a MEK binding partner that enhances enzymatic activation of the MAP kinase cascade. Science. 1998. 281; 1668-71.

Schmelzle T, Hall MN. TOR, a Central Controller of Cell Growth. Cell. 2000. 103; 253-62.

Schürmann A, Brauers A, Massmann S, Becker W, Joost HG. Cloning of a novel family of mammalian GTP-binding proteins (RagA, RagBs, RagB1) with remote similarity to the Ras-related GTPases. J Biol Chem. 1995. 270; 28982-8.

Selman C, Tullet JMA, Wieser D, Irvine E, Lingard SJ, Choudhury AI, Claret M, Al-Qassab H, Carmignac D, Ramadani F, Woods A, Robinson ICA, Schuster E, Batterham RL, Kozma SC, Thoms G, Carling D, Okkenhaug K, Thornton JM, Partridge L, Gems D, Withers DJ. Ribosomal protein S6 kinase 1 signaling regulates mammalian life span. Science. 2009. 326; 140-4.

Shen K, Choe A, Sabatini DM. Intersubunit Crosstalk in the Rag GTPase Heterodimer Enables mTORC1 to Respond Rapidly to Amino Acid Availability. Mol Cell. 2017. 68; 552-65.7

Shen K, Huang RK, Brignole EJ, Condon KJ, Valenstein ML, Chantranupong L, Bomaliyamu A, Choe A, Hong C, Yu Z, Sabatini D. Architecture of the human GATOR1 and GATOR2-Rag GTPases complexes. Nature. 2018. 556; 64-69.

Shirane M, Nakayama K. Inherent calcineurin inhibitor FKBP38 targets Bcl-2 to mitochondria and inhibits apoptosis. Nat Cell Biol. 2003. 5; 28-37.

Siekierka JJ, Hung SHY, Poe M, Lin CS, Sigal NH. A cytosolic binding protein for the immunosuppressant FK506 has peptidyl-prolyl isomerase activity but is distinct from cyclophilin. Nature. 1989. 341; 755-57.

Sills AM, Artavia JM, DeRosa BD, Ross CN, Salmon AB. Long-term treatment with the mTOR inhibitor rapamycin has minor effect on clinical laboratory markers in middle-aged marmosets. Am J Primatol. 2019. 81; e22927.

Smith DF, Albers MW, Schreiber SL, Leach KL, Deibel Jr MR. FKBP54, a novel FK506-binding protein in avian progesterone receptor complexes and HeLa extracts. J Biol Chem. 1993. 268; 24270-3.

Son SM, Park SJ, Lee H, Siffigi F, Lee JE, Menzies FM, Rubinsztein DC. Leucine Signals to mTORC1 via Its Metabolite Acetyl-Coenzyme A. Cell Metab. 2019. 29; 192-201.

Storer CL, Dickey CA, Galigniana MD, Rein T, Cox MB. FKBP51 and FKBP52 in signaling and disease. Trends Endocrinol Metab. 2011. 22; 481-90.

Strong R, Miller RA, Bogue M, Fernandez E, Javors MA, Libert S, Marinez PA, Murphy MP, Musi N, Nelson JF, Petrascheck M, Reifsnyder P, Richardson A, Salmon AB, Macchiarini F, Harrison DE. Rapamycin-mediated mouse lifespan extension: Late-life dosage regimes with sex-specific effects. Aging Cell. 2020. 19; e13269.

Timerman AP, Ogunbumni E, Freund E, Wiederrecht G, Marks AR, Fleischer S. The calcium release channel of sarcoplasmic reticulum is modulated by FK-506-binding protein. Dissociation and reconstitution of FKBP-12 to the calcium release channel of skeletal muscle sarcoplasmic reticulum. J Biol Chem. 1993. 268; 22992-9.

Tsun Y, Bar-Peled L, Chantranupong L, Zoncu R, Wang T, Kim C, Spooner E, Sabatini DM. The folliculin tumor suppressor is a GAP for the RagC/D GTPases that signal amino acid levels to mTORC1. Mol Cell. 2013. 52; 495-505.

Van West D, Van Den Eede F, Del-Favero J, Souery D, Norrback K, Van Duijn C, Sluijs S, Adolfsson R, Mendlewicz J, Deboutte D, Van Broeckhoven C, Claes S. Glucocorticoid receptor gene-based SNP analysis in patients with recurrent major depression. Neuropsychopharmacology. 2006. 31; 620-7.

Vellai T, Takacs-Vellai K, Zhang Y, Kovacs AL, Orosz L, Müller F. Influence of TOR kinase on lifespan in C.elegans. Nature. 2003. 426; 620.

Vézina C, Kudelski A, Sehgal SN. Rapamycin (AY-22,989), a new antifungal antibiotic. I. Taxonomy of the producing streptomycete and isolation of the active principle. J Antibiot. 1975. 28; 721-6.

Wang T, Donahoe PK, Zervos AS. Specific interaction of type I receptors of the TGF-beta family with the immunophilin FKBP-12. Science. 1994. 265; 674-6.

Wang HQ, Nakaya Y, Du Z, Yamane T, Shirane M, Kudo T, Takeda M, Takebayashi K, Noda Y, Nakayama KI, Nishimura M. Interaction of presenilins with FKBP38 promotes apoptosis by reducing mitochondrial Bcl-2. Hum Mol Genet. 2005. 14; 1889-902.

Wang Y, Han R, Wu D, Li J, Chen C, Ma H, Mi H. The binding of FKBP23 to BiP modulates BiP's ATPase activity with ist PPiase activity. Biochem Biophys Res Commun. 2007. 354; 315-20.

Weichhart T. mTOR as Regulator of Lifespan, Aging, and Cellular Senescence: A Mini-Review. Gerontology. 2017. 64; 127-34.

Wilkinson JE, Burmeister L, Brooks SV, Chan C, Friedline S, Harrison DE, Hejtmancik JF, Nadon N, Strong R, Wood LK, Woodward MA, Miller RA. Rapamycin slows aging in mice. Aging Cell. 2012. 11; 675-82.

Wochnik GM, Rüegg J, Abel GA, Schmidt U, Holsboer F, Rein T. FK506-binding proteins 51 and 52 differentially regulate dynein interaction and nuclear translocaton of the glucocorticoid receptor in mammalian cells. J Biol Chem. 2005. 280; 4609-16.

Wolfson RL, Chantranupong L, Saxton RA, Shen K, Scaria SM, Cantor JR, Sabatini DM. Sestrin2 is a leucine sensor for the mTORC1 pathway. Science. 2016. 351; 43-8.

Wu JJ, Liu J, Chen EB, Wang JJ, Cao L, Narayan N, Fergusson MM, Rovira II, Allen M, Springer DA, Lago CU, Zhang S, DuBois W, Ward T, deCabo R, Gavrilova O, Mock B, Finkel T. Increases mammalian lifespan and a segmental and tissue-specific slowing of aging after genetic reduction of mTOR expression. Cell Rep. 2013. 4; 913-20.

Wullschleger S, Loewith R, Oppliger W, Hall MN. Molecular organization of target of rapamycin complex 2. J Biol Chem. 2005. 280; 30697-704.

Wunderlich W, Teis FD, Alpi A, Pfeifer A, Parton RG, Lottspeich F, Huber LA. A novel 14-kilodalton protein interacts with the mitogen-activated protein kinase scaffold mp1 on a late endosomal/lysosomal compartment. J Cell Bio. 2001. 152; 765-76.

Wyant GA, Abu-Remaileh M, Wolfson RL, Chen WW, Freinkman E, Danai LV, van der Heiden MG, Sabatini DM. mTORC1 Activator SLC38A9 Is Required to Efflux Essential Amino Acids from Lysosomes and Use Protein as a Nutrient. Cell. 2017. 171; 642-54.

Yang S, Lee HY, Young DM, Tien A, Rowson-Baldwin A, Shu YY, Jan YN, Jan LY. Rapamycin induces glucose intolerance in mice by reducing islet mass, insulin content, and insulin sensitivity. J Mol Med. 2012. 90; 575-85.

Yang H, Rudge DG, Koos JD, Vaidialingam B, Yang HJ, Pavletich NP. mTOR kinase structure, mechanism and regulation. Nature. 2013. 497; 217-23.

Yehuda R, Cai G, Golier JA, Sarapas C, Galea S, Ising M, Rein T, Schmeidler J, Müller-Myhsok B, Holsboer F, Buxbaum JD. Gene expression patterns associated with posttraumatic stress disorder following exposure to the World Trade Center attacks. Biol Psychiatry. 2009. 66; 708-11.

Zgajnar NR, De Leo SA, Lotufo CM, Erlejman AG, Piwien-Pilipuk G, Galigniana MD. Biological Actions of the Hsp90-binding Immunophilins FKBP51 and FKBP52. Biomolecules. 2019. 9; 52.

Zhang X, Chen W, Gao Q, Yang J, Yan X, Zhao H, Su L, Yang M, Gao C, Yao Y, Inoki K, Li D, Shao R, Wang S, Sahoo N, Kudo F, Eguchi T, Ruan B, Xu H. Rapamycin directly activates lysosomal mucolipin TRP channels independent of mTOR. PLoS Biol. 2019. 17; e3000252.

Zheng XF, Florentino D, Chen J, Crabtree GR; Schreiber SL. TOR kinase domains are required for two distinct functions, only one of which is inhibited by rapamycin. Cell. 1995. 82; 121-30.

Acknowledgements

First of all, I would like to thank my supervisor Dr. Constantinos Demetriades. You gave me the chance to learn how to work independently and how to become a strong and empowered scientist. Although the path was not always easy, you always supported me to keep going. I am happy that I chose your lab for my master's thesis back in 2017 and that I could stay to pursue my PhD.

I also want to thank Prof. Dr. Jan Riemer for your advice and scientific input as part of my thesis advisory committee but also to agree on being my second reviewer of this thesis.

Likewise, I am grateful to Prof. Dr. Marius Lemberg for kindly agreeing to be the head of my thesis committee as well as Dr. Julian Nüchel to be the minutes taker in my disputation.

I want to thank all current and former members of the Demetriades lab for your constant scientific input in all meetings and presentations as well as the many collaborations that have happened in the last couple of years. Some of them were successful so that we even got a publication out of it. Here, I want to thank especially Peter Gollwitzer and Filippo Artoni for working together and putting together some nice science.

Especially I want to thank the Girls Club for all the funny lunch times, long coffee dates, many small breaks with lots of sweets but also all the moments we had outside of the lab. We traveled to several countries and cities together and immersed ourselves in all kinds of different cultures. Everyone that knows me will understand how much I appreciated that and how happy it made me throughout the years.

I also want to thank my friends and family who always have been there for me. It was always nice to have people outside of the scientific universe to relax and calm down after long and stressful lab days. Thank you for making me feel normal when I felt nerdy and geeky.

Finally, I want to thank my superhuman. Thank you for constantly pushing me to strive to be the best version of myself. Thank you for believing in me and what I am able to achieve. Without you I wouldn’t be where I am today and for sure I wouldn’t be the person I am today.

Eidesstattliche Erklärung

„Hiermit versichere ich an Eides statt, dass ich die vorliegende Dissertation selbstständig und ohne die Benutzung anderer als der angegebenen Hilfsmittel und Literatur angefertigt habe. Alle Stellen, die wörtlich oder sinngemäß aus veröffentlichten und nicht veröffentlichten Werken dem Wortlaut oder dem Sinn nach entnommen wurden, sind als solche kenntlich gemacht. Ich versichere an Eides statt, dass diese Dissertation noch keiner anderen Fakultät oder Universität zur Prüfung vorgelegen hat; dass sie - abgesehen von unten angegebenen Teilpublikationen und eingebundenen Artikeln und Manuskripten - noch nicht veröffentlicht worden ist sowie, dass ich eine Veröffentlichung der Dissertation vor Abschluss der Promotion nicht ohne Genehmigung des Promotionsausschusses vornehmen werde. Die Bestimmungen dieser Ordnung sind mir bekannt. Darüber hinaus erkläre ich hiermit, dass ich die Ordnung zur Sicherung guter wissenschaftlicher Praxis und zum Umgang mit wissenschaftlichem Fehlverhalten der Universität zu Köln gelesen und sie bei der Durchführung der Dissertation zugrundeliegenden Arbeiten und der schriftlich verfassten Dissertation beachtet habe und verpflichte mich hiermit, die dort genannten Vorgaben bei allen wissenschaftlichen Tätigkeiten zu beachten und umzusetzen. Ich versichere, dass die eingereichte elektronische Fassung der eingereichten Druckfassung vollständig entspricht.“

Teilpublikationen:

Gollwitzer P*, **Grützmacher N***, Wilhelm S, Kümmel D, Demetriades C (2022). A Rag GTPase dimer code defines the regulation of mTORC1 by amino acids. *Nat Cell Bio* 24; 1394-1406. *equal contribution
doi:10.1038/s41556-022-00976-y

Artoni F, **Grützmacher N**, Demetriades C. Unbiased evaluation of rapamycin’s specificity as an mTOR Inhibitor. *Aging Cell*. e13888.
doi:10.1111/acel.13888

Köln, den 18. Juni 2023

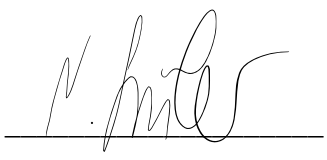

Nina Grützmacher